In-Field Performance of Geosynthetics Used To Reinforce Roadway Base Layers; Phase I: Instrumentation Selection and Verification

Final Report

Prepared for the
STATE OF MONTANA
DEPARTMENT OF TRANSPORTATION
RESEARCH, DEVELOPMENT AND TECHNOLOGY TRANSFER PROGRAM
in cooperation with the
U.S. DEPARTMENT OF TRANSPORTATION
FEDERAL HIGHWAY ADMINISTRATION

September 30, 1996

Prepared by
Dr. Steven W. Perkins
Assistant Professor
&
Joseph A. Lapeyre
Graduate Research Assistant

Department of Civil Engineering
Montana State University
Bozeman, Montana 59717
Office Telephone: 406-994-6119
Fax: 406-994-6105
E-Mail: stevep@ce.montana.edu

TECHNICAL REPORT STANDARD PAGE

1. Report No.	2. Government Accession No.	3. Recipient's Catalog No.
FHWA/MT-96/8126		

4. Title and Subtitle	5. Report Date
In-Field Performance of Geosynthetics Used to Reinforce Roadway Base Layers; Phase I: Instrumentation Selection and Verification	September 30, 1996
	6. Performing Organization Code
7. Author(s) Steven W. Perkins, Ph.D., P.E. Joseph A. Lapeyre	8. Performing Organization Report No.
9. Performing Organization Name and Address Department of Civil Engineering Montana State University Bozeman, Montana 59717	10. Work Unit No.
	11. Contract or Grant No. 8126
12. Sponsoring Agency Name and Address Montana Department of Transportation 2701 Prospect Avenue P.O. Box 201001 Helena, Montana 59620-1001	13. Type of Report and Period Covered Final May 1, 1995 - September 30, 1996
	14. Sponsoring Agency Code 5401

15. Supplementary Notes
Preparation in cooperation with the U.S. Department of Transportation, Federal Highway Administration

16. Abstract

Geosynthetics have been proposed and used on a limited basis to reinforce the base course layer of flexible pavements for the purpose of reducing base course thickness. A review of the literature shows conflicting results regarding the level of performance improvement offered by placing geosynthetics in the base course layer. It appears that the mechanisms of base course reinforcement in flexible pavements are poorly understood, making it difficult to estimate the improvement in performance given a particular set of site conditions. Indeed, a comprehensive design solution for the problem has not been proposed.

Research has been initiated by the Montana Department of Transportation to understand if and how geosynthetics can be used to reinforce roadway base course layers. This research, as currently planned, may involve the construction and monitoring of geosynthetically reinforced full-scale field test sections subject to real traffic loading. Stress, strain, moisture content and temperature sensors would be used to monitor performance of the test sections. The research is being conducted in phases. Initially, a literature review was conducted to establish a need for further research. With this need identified, the first phase of the research was initiated. This final report discusses the work performed under Phase I of the project. The objective of the Phase I research was to examine instrumentation proposed for use in the field test sections to be constructed under a subsequent phase of the project. This objective was accomplished by constructing a pilot test section with certain instruments placed on the geosynthetics and within the base course and asphalt concrete layers. These instruments were monitored for a 4 month period. Laboratory wide-width tension tests were performed on the geosynthetics used in the pilot test section for the purpose of comparing the measured strain from the instrument to the global strain experienced by the material. From this work, conclusions are made regarding the appropriateness of certain instruments and installation techniques for use in field test sections. Conclusions are also made regarding the manner in which the local strain from the instruments attached to the geosynthetics relates to the global strain experienced by the material.

17. Key Words	18. Distribution Statement
Pavement, Highway, Geogrid, Geotextile, Geosynthetic, Reinforcement, Base Course	Unrestricted. This document is available through the National Technical Information Service, Springfield, VA 21161.

19. Security Classif. (of this report)	20. Security Classif. (of this page)	21. No. of Pages	22. Price
Unclassified	Unclassified	160	

DISCLAIMER STATEMENT

The information reported herein was sponsored by the Montana Department of Transportation in conjunction with the Federal Highway Administration. The opinions, findings and conclusions expressed in this publication are those of the author and not necessarily those of the Montana Department of Transportation or the Federal Highway Administration.

ALTERNATIVE FORMAT STATEMENT

MDT attempts to provide reasonable accommodations for any disability that may interfere with a person participating in any service, program, or activity of the Department. Alternative accessible formats of this document will be provided upon request. For further information, call (406) 444-6269 or TDD (406) 444-7696.

A color copy of Appendix A may be obtained from the Montana Department of Transportation, Research, Development and Technology Transfer Program for the cost of reproduction

ACKNOWLEDGMENTS

The site used for the Phase I pilot test section, along with the base course and asphalt concrete materials and workmanship, was generously provided by the JTL Group, Incorporated of Belgrade, Montana. Amoco fabrics and the Tensar Corporation provided geosynthetic materials used in the study. Bridge Diagnostics, Incorporated of Boulder, Colorado was retained as an instrumentation contractor for the project.

TABLE OF CONTENTS

LIST OF TABLES

LIST OF FIGURES

CONVERSION FACTORS

The following conversion factors are required for interpretation of results contained in the appendices. Within the text of the report, SI units are used with English units listed in parenthesis.

1 kN/m = 68.6 lb/ft

1m = 3.28 ft

1mm = 0.0394 in

1 kN = 0.112 ton = 225 lb

1 MPa = 145 psi

SUMMARY

Geosynthetics have been proposed and used on a limited basis to reinforce the base course layer of flexible pavements for the purpose of reducing base course thickness. A review of the literature shows conflicting results regarding the level of performance improvement offered by placing geosynthetics in the base course layer. It appears that the mechanisms of base course reinforcement in flexible pavements are poorly understood, making it difficult to estimate the improvement in performance given a particular set of site conditions. Indeed, a comprehensive design solution for the problem has not been proposed.

Research has been initiated by the Montana Department of Transportation to understand if and how geosynthetics can be used to reinforce roadway base course layers. This research, as currently planned, may involve the construction and monitoring of geosynthetically reinforced full-scale field test sections subject to real traffic loading. Stress, strain, moisture content and temperature sensors would be used to monitor performance of the test sections. The research is being conducted in phases. Initially, a literature review was conducted to establish a need for further research. With this need identified, the first phase of the research was initiated. This final report discusses the work performed under a subsequent phase of the project. The objective of the Phase I research was to examine instrumentation proposed for use in the field test sections to be constructed under Phase II of the project. This objective was accomplished by constructing a pilot test section with certain instruments placed on the geosynthetics and within the base course and asphalt concrete layers. These instruments were monitored for a 4 month period. Laboratory wide-width tension tests were performed on the geosynthetics used in the pilot test section for the purpose of comparing the measured strain from the instrument to the global strain experienced by the material. From this work, conclusions are made regarding the appropriateness of certain instruments and installation techniques for use in field test sections. Conclusions are also made regarding the manner in which the local strain from the instruments attached to the geosynthetics relates to the global strain experienced by the material.

INTRODUCTION

In recent years, geosynthetics (including geogrids and geotextiles) have been proposed and used for the reinforcement of the base course layer of flexible pavements for the purpose of reducing base course thickness. The attractiveness of such a construction technique is great in areas where quality gravel sources are scarce and associated haul costs are prohibitive. This condition exists in the eastern half of Montana, as well as many other areas of the nation. Many large urban areas are experiencing similar problems as gravel sources become depleted. The possibility of adding geosynthetics to the base course layer for the purpose of extending the life of the roadway may also be an attractive design alternative when life-cycle costs are considered.

The literature indicates that the mechanisms associated with geosynthetic base course reinforcement of flexible pavements are appreciably different from other soil reinforcement applications and are poorly understood. Existing studies present conflicting results regarding the level of improvement in performance offered by placing geosynthetics in the base course of flexible pavements. These studies tend to cast doubt on simplistic design charts developed for all possible site conditions which specify a reduction in base course thickness for a given thickness of unreinforced base course when using a particular geosynthetic product.

The work described in this report represents one phase of a multiphase project designed to investigate the performance improvement of roadways whose base course layer is reinforced with geosynthetics. Initially, a literature review was conducted to establish a need for further research. With this need identified, the first phase of the research was initiated. This final report discusses the work performed under Phase I of the project. The objective of the Phase I research was to examine instrumentation proposed for use in the field test sections to be constructed under Phase II of the project. This objective was accomplished by constructing a pilot test section with certain instruments placed on the geosynthetics and within the base course and asphalt concrete layers. These instruments measured strain on the geosynthetics and within the base course and asphalt layers. The instruments were monitored for a 4 month period. Laboratory wide-width tension tests were performed on the geosynthetics used in the pilot test section for the purpose of comparing the measured strain from the instrument to the global strain experienced by the material. From this work, conclusions are made regarding the appropriateness of certain instruments and installation techniques for use in field test sections. Conclusions are also made regarding the manner in which

the local strain from the instruments attached to the geosynthetics relates to the global strain experienced by the material.

INSTRUMENTATION USED IN STUDY

The purpose of this section is to describe the electronic sensors and associated data logging equipment used in the Phase I study. All the instruments described below were used in the pilot test section. The instruments mounted to the geosynthetics were also used in the laboratory for the in-air tension tests.

INSTRUMENTATION MOUNTED ON THE GEOSYNTHETICS

Vibrating Wire Strain Gage

The vibrating wire strain gages used in the study were a Geokon (Lebanon, NH) model VSM-4000 strain gage. This gage is shown in Figure A1.1 (all figures noted in this section are found in Appendix A.1). The gage has a range of 0.3 % strain (3000 micro strain) with a sensitivity of 0.0001 % strain (1 micro strain) and a nominal active gage length of 150 mm (5.9 in). As discussed later, the mounting plates for certain gages could be oriented differently, thereby resulting in different effective gage lengths. These gages were employed to measure strains on the geosynthetic in the event that the strain magnitude was small. The vibrating wire strain gage measures strain by determining the lengthening of a steel wire running through the center rod of the instrument. The steel wire is initially tensioned when the gage is manufactured. As the two ends of the instrument separate or contract, the tension in the wire changes. The level of tensile force in the wire is measured by electronically plucking the wire and measuring its resonant frequency of vibration using an electromagnetic coil. The frequency of the wire is related to the tension force in the wire and is in turn related to the amount of displacement between the ends of the instrument, which provides a measure of strain over the gage length of the instrument. The advantage of the vibrating wire gage over more conventional electrical resistance (or semiconductor) types lies mainly in the use of a frequency, rather than a voltage, as the output signal from the gage. Frequencies may be transmitted over long cable lengths without appreciable degradation caused by variations in cable resistance,

contact resistance, or leakage to ground. Vibrating wire gages also have much better long-term zero stability (i.e. little drift). The principal disadvantage with vibrating wire gages is the low frequency of response. In general, several seconds of sampling time are required to pluck and measure the frequency of the instrument, making dynamic measurements impractical.

The VW strain gage was attached to the geosynthetics through rectangular mounting plates measuring 89 by 57 mm (3.5 by 2.24 in). Each end of the mounting plate arrangement consisted of two plates which were used to sandwich the geosynthetic. Six bolts were used to fasten the plates together. The ends of the VW strain gage were fastened to the end plates with a collar through which the cylindrical end of the gage rested. The gage was fixed in place by securing a set screw extending through the collar and resting against the cylindrical end of the gage. The long dimension of the mounting plate was oriented and fixed in the direction of the strain measurement (i.e. along the axis of the gage). The axis of the gage was approximately 14 mm (0.55 in) above the surface of the geosynthetic.

Vibrating Wire Displacement Gage

The vibrating wire displacement gage was designed to measure larger strains. A Geokon model 4420 vibrating wire crackmeter was used (shown in Figure A1.2). This gage has a range of 25.4 mm (1.0 in) with a sensitivity of 0.025 mm (0.001 in). Given the 280 mm (11.0 in) nominal gage length of the instrument, this corresponds to a strain range of 9 % and a sensitivity of 0.009 %. The vibrating wire displacement gage operates on the same principle as the vibrating wire strain gage, the only difference being that the wire is connected in series to an extendable spring allowing greater deformations to be measured without snapping the wire. Due to their stability and slow response time, the vibrating wire gages were used to measure long-term displacements/strains.

The VW displacement gage was attached to the geosynthetics in a similar way as the VW strain gage. The ends of the gage were attached to rectangular mounting plates measuring 89 by 57 mm (3.5 by 2.24 in). Each end of the mounting plate arrangement consisted of two plates which were used to sandwich the geosynthetic. Six bolts were used to fasten the plates together. The ends of the VW displacement gage were fastened to the end plates through a ball pivot point. In this way, the end plates could be rotated to any orientation. The axis of the gage was approximately 25 mm (1.0 in) above the surface of the geosynthetic.

LVDT Displacement Gage

The Linear Variable Differential Transducer (LVDT) displacement gage was a RDP Electronics (Pottstown, PA), submersible, miniature AC, model D5/200W LVDT with a range of +/- 5.1 mm (+/- 0.20 in) and a sensitivity of +/- 0.015 mm (0.00059 in) and is shown in Figure A1.3. Given the 50 mm (1.97 in) nominal gage length of the instrument, this corresponds to a strain range of +/- 10 % and a sensitivity of +/- 0.03 %. The LVDT consists of a movable magnetic core passing through one primary and two secondary coils. An AC voltage is applied to the primary coil, thereby inducing an AC voltage in each secondary coil, with a magnitude that depends on the proximity between the magnetic core and each secondary coil. The secondary voltages are connected in series opposition, so that the net output of the LVDT is the difference between these two voltages. When the core is at its mid-position, the net output voltage is zero. When the core moves off center, the net output voltage increases linearly in magnitude with a polarity depending on the direction of core displacement. The LVDT gages were used to measure both long-term displacements/strains and displacement/strain due to short-term dynamic loads. Due to the possibility of electronic drift, the LVDT's are generally thought to be more appropriate for short-term measurements. The results of the study, however, tend to show that electronic drift was insignificant.

The LVDT displacement gage used relatively small rectangular mounting plates measuring 30 mm by 12 mm (1.18 by 0.5 in). The short dimension of the mounting plates was oriented and fixed in the direction of the displacement measurement. The axis of the gage was approximately 14 mm (0.55 in) above the surface of the geosynthetic.

Foil Strain Gage

Kyowa (Soltec Corp., San Fernando, CA) high elongation strain gages (KFE-5-120-C1) were used both for the pilot test section and the in-air tension experiments and were mounted only to the geogrid specimen. Figure A2.10 shows a photograph of a foil strain gage mounted to a geogrid specimen. These gages have a range of approximately 10 % strain. All strain gages were installed along the flat faces of the geogrid ribs. Two different surface preparation and strain gage bonding techniques were used for the in-air tension tests and the pilot test section.

For the in-air tension tests, the following procedure was used. The area of the rib to receive the gage was sanded with 320-A sand paper. Sanding took place along the length of the rib as well as across the rib. The rib was sanded until the shiny surface was dulled. Care was taken not to raise

fibers along the rib. When the sanding was complete, the surface was roughened, yet flat and free of raised fibers. The rib was then cleaned with a lint-free cotton swab soaked with acetone.

A surface treatment agent (Kyowa S-8) was then applied to the rib. The agent was applied with a lint-free cotton swab and then dried with a blow dryer for 15 seconds. The surface treatment step was repeated and allowed to dry for approximately 5 minutes.

Strain gage cement (Kyowa CC-33A Strain Gage Cement) was applied to the rib. The foil strain gage was grasped with tweezers and placed on the rib. Once the gage was properly oriented on the rib, a polyethylene sheet (included with the foil strain gages) was placed over the foil strain gage. Finger pressure was applied lightly to the sheet for approximately 60 seconds. At this point, the gage was firmly bonded to the geogrid rib. MicroMeasurements (Raleigh, NC) M-Coat A was applied as a protector over the length of the foil strain gage. The coating dries in approximately ½ hour and provides physical protection to the foil strain gage. The majority of the specimens tested contained a duplicate gage mounted on the opposite side of the first gage. The procedure described above was simply repeated for the opposite side of the rib. For cases where two gages were mounted, the gages were connected through a half-bridge arrangement. This arrangement eliminated any bending effects from the measured results. Specimens were also tested with only one gage mounted on the rib. A quarter-bridge arrangement was used for this case.

For the pilot test section, 600 grit paper was used to prepare the surface. The rib was then etched with MicroMeasurements Tetra-Etch (TEC-1). The surface was then rinsed with water and allowed to dry. A single gage was attached to the upper side of the geogrid using MicroMeasurements M-Bond AE-10. An additional gage was attached to a small, detached sample of the geogrid. The two gages were attached by a full wheatstone bridge circuit and connected to 2-pair, twisted pairs, overall shielded, 22 gage cable. The gage attached to the unstressed sample provided for temperature compensation. The bonding procedure described above appeared to be adequate for the strains observed in the field. Additional laboratory tension tests, however, indicated that gage debonding occurred between 1-3 % strain.

Environmental protection of the gages was provided by sandwiching the geogrid area between sheets of MicroMeasurements M-Coat F Butyl rubber sealant and M-Coat F neoprene. Additional protection was provided by sandwiching this area between sheets of clear plastic with liberal amounts of silicone used between the sheets, particularly around the cable entry. Four gages were attached to the geogrid specimen in the pilot test section.

INSTRUMENTATION CONTAINED IN BASE AND AC

Three different sensor types were used to measure strain in the base course of the pilot test section. The sensors were placed in an orientation to measure strain in a lateral direction perpendicular to the direction of traffic.

Vibrating Wire Embedment Strain Gage

The vibrating wire embedment strain gage consisted of a Geokon model VCE 4200 vibrating wire embedment type strain gage mounted between two circular plates (Figure A1.4). This gage operates on the same principal as the vibrating wire strain gage used on the geosynthetics. The plates were 76 mm (3 in) in diameter. The inside distance between the plates was 161 mm (6.34 in). This gage has a range of 0.3% strain (3000 micro strain) with a sensitivity of 0.0001% strain (1 micro strain). These gages were employed to measure strains in the base in the event that the strain magnitude was small.

Vibrating Wire Embedment Displacement Gage

The vibrating wire embedment displacement gage was designed to measure larger strains. Two different displacement gages were used. Initially, it was planned to use two Geokon model 4430 vibrating wire borehole deformation meters. These gages were mounted between two circular plates (Figure A1.5). These plates were 101 mm (4 in) in diameter with a inside distance between the plates of 317 mm (12.5 in). This gage has a range of 25.4 mm (1 in) with a sensitivity of 0.025 mm (0.001in). For the gage length of these instruments, this corresponds to a strain range of 8 % and a sensitivity of 0.008 %. During the installation of the base course, one of the Geokon model 4430 gages was found to be inoperable. In its place, a Geokon model 4420 vibrating wire crackmeter was used. This gage has the same specifications as the 4430 gage. The 4430 gage operates in the same way as the 4420 gage. The vibrating wire gages were used to measure long-term displacements/strains.

LVDT Embedment Displacement Gage

A RDP Electronics, submersible, miniature AC, model D5/400W LVDT with a range of +/- 10.2 mm (0.402 in) and a sensitivity of +/- 0.03 mm (+/- 0.00118 in) was mounted between circular

plates measuring 39 mm (1.54 in) in diameter and 81 mm (3.19 in) between the plates (Figure A1.6). For the gage length of these instruments, this corresponds to a strain range of +/- 13 % and a sensitivity of +/- 0.04 %. The LVDT operates on the same principle as those used on the geosynthetic. The LVDT gages were used to measure both long-term displacement/strain and displacement/strain due to short-term dynamic loads.

Vibrating Wire Embedment AC Strain Gage

Geokon model VCE-4200-HT (high temperature) vibrating wire embedment type strain gages were used to measure strain in the asphalt concrete in a direction perpendicular to the direction of traffic (Figure A1.7). A high temperature Teflon cable was used with these transducers. This gage has a range of 0.3% strain (3000 micro strain) with a sensitivity of 0.0001% strain (1 micro strain). This gage operates on the same principle as the vibrating strain gage used on the geosynthetic. The gage has an active gage length of 150 mm (5.9 in).

DATA LOGGING SYSTEM

The data logging system used to monitor the instruments attached to the geosynthetics was the same system used in the field for the Phase I test section. A Campbell Scientific (Logan, UT) Data Logger, Model CR-10 was used to monitor all the vibrating wire instruments. This logger is also capable of logging the non-vibrating wire instruments. Accessories included with the logger were 2 AM-416 16 channel mulitplexers (all 16 channels of a multiplexer are routed into one channel of the logger), one AVW1 Vibrating Wire Interface (provides excitation for all VW gages), PS12LA Power Supply (12VDC and battery), SC32A RS-232 Interface (allows communication directly through a PC serial port), and a DC112 Modem (1200 baud modem for remote access to data). The CR-10 is designed for stand-alone field data acquisition and storage at relatively slow rates. It can interface to all types of sensors including VW gages, sensors with DC outputs, and all types of temperature sensors.

An IOTech (Cleveland, OH) Daqbook 100 was used to monitor the non-vibrating wire instruments. This logger included a DBK40 BNC Analog Interface (16 channel box that allows BNC connections to be made). The Daqbook is basically an A/D converter that can communicate with a PC. It allows data to be collected and stored at various speeds. In the Phase I test sections, this

logger is used for dynamic testing of the non-vibrating wire instruments.

Signal conditioning is provided for the LVDT's through a RDP Electrosense S7-AC signal conditioner which provides an AC excitation and a +/-10V DC output. This output can be read by both the logger and Daqbook. The foil strain gages used a RDP Electrosense S7-DC signal conditioner with an excitation voltage of 5 VDC and set to a gain of 260.

IN-AIR GEOSYNTHETIC TENSION TESTING

PURPOSE

A large, wide-width tension test frame was constructed to perform tension tests on geosynthetics used in the Phase I pilot test section. This apparatus will also be used to test the geosynthetics used in the Phase II test sections. The tension test frame was designed and constructed to accomplish three objectives. First, it is necessary to understand how the local strain (i.e. the strain over a relatively small gage length) in a geosynthetic compares to the global strain (as measured over the entire test specimen length) when a uniform load, and presumably a uniform strain, is applied uniaxially to the geosynthetic. This information is needed to verify that the strain measured in the field using instruments with a relatively short gage length is an accurate representation of that which the geosynthetic experiences. The second reason for these tests was to examine the transducer fastening technique planned for use in the field to ensure that the fasteners perform as required. As demonstrated below, the fastening technique influences the measured strain and is related to the first objective. The third reason for tensile testing is to confirm the stress strain response supplied by the manufacturer, or to supplement this information if necessary. Calibration information generated by comparing the strain from a particular sensor to the global strain is used to adjust the field data from the Phase I pilot test section.

LOADING FRAME

The loading frame for in-air tensile testing of geosynthetics consists of an upper and lower holding frame. These parts are shown schematically in Figure B1 (Appendix B) with a photograph

of the load frame with a geogrid specimen mounted shown in Figure A2.1 (Appendix A2). The loading frame accommodates a specimen with maximum dimensions of 1.83 m (6.00 ft) in width by 0.914 m (3.00 ft) in height. This size specimen is much larger than that used in most wide-width tensile tests, where specimens measure 0.2 m (7.87 in) by 0.1 m (3.94 in). The large width was necessary to accommodate the different instruments placed on the specimen, while the 2:1 ratio was maintained such that a condition of zero lateral strain could be achieved over the majority of the central region of the specimen.

The upper and lower holding frames contain 178 mm (7.00 in) diameter steel cylinders around which the geosynthetic is wrapped and gripped. The upper steel cylinder is rigidly attached to two vertical supports which connect to an I-beam which in turn rests on the top of a load cell. The steel cylinder located on the lower holding frame contains a central axle such that the drum can be rotated. The lower cylinder is attached to short vertical supports which are attached to an I-beam. The I-beam is bolted to the bottom load platen of a Baldwin load frame. The Baldwin operates by driving the top load platen, and therefore the upper holding frame, upwards. The geosynthetic is initially placed on the upper steel cylinder. To prevent excessive slip of the geosynthetic around the cylinder, a piece of strip steel measuring 20 mm (0.787 in) by 5 mm (0.197 in) in cross section is placed atop the leading end (or edge) of the geosynthetic and bolted to the steel cylinder. The bolt hole spacing is 100 mm (3.94 in). In addition, a thin strip of rubber is placed between the geosynthetic and the steel strip. The geosynthetic is then wrapped around the cylinder 2 ½ times such that the geosynthetic leaves the drum on the opposite side of the steel holding strip. The steel holding strip is slightly wider than the width of the geosynthetic specimen. The geosynthetic is then wrapped a half-turn around the lower steel cylinder with a steel holding strip fastening the specimen to the drum in the same manner as used for the upper cylinder. The cylinder is then rotated to provide 2 ½ wraps of specimen around the cylinder, with the cylinder then bolted to the vertical supports to prevent further rotation. The cross-head of the loading frame is then raised to remove slack in the specimen.

During loading of the specimen, the geosynthetic will slip a small amount around the cylinder. In addition, the material contained in the wrap will strain and deform. This makes it difficult to define a gage length necessary to calculate an average strain for the specimen. To overcome this problem, it was necessary to monitor the absolute displacement of two extreme points on the specimen, one close to the top of the specimen and one close to the bottom. This allowed the

relative displacement between these two points to be calculated. Knowing the length between the two points allowed for the average strain across the specimen to be determined. This procedure was provided for two lateral positions along the specimen, such that the average strain could be determined along two vertical lines. Celesco (Canoga Park, CA) position transducers (PT-101) with a 255 mm (10 in.) range were used to monitor the absolute displacement of each of the four points. The transducer operates by a cable extending from a spool within a rectangular box. Additional cable was attached to this cable to allow for connections to the top of the specimen. The boxes were clamped to the fixed bottom platen on the Baldwin load frame. Figure A2.2 shows the cables from the position transducers mounted to the geotextile. The mounts for the cable ends consisted of a bolt and washer arrangement with the cable attachment point being held as closely as possible to the face of the geotextile.

A Computer Boards (Mansfield, MA) data collection board (CIO-DAS08-PGM) was mounted to a 386 PC with Computer Boards Control-CB software used to operate the board. A terminal board (CIO-MINI37) and 10V power supply were used to power and connect to the load cell and the four Celesco position transducers. The Control-CB software allowed for the data (as well as mathematically manipulated data) to be monitored and plotted real time on the screen of the PC. This feature was used to monitor the strain rate associated with the applied load during a test. The loading rate was adjusted to maintain a strain rate of approximately 10 % strain per minute.

Several tests were performed on the geotextile and the geogrid with each material placed in both the machine and transverse directions while manually measuring the applied load with an electronic readout box. The machine direction corresponds to the direction in which the geosynthetic emerges from the manufacturing machine, while the transverse direction, or cross-machine direction, refers to the direction perpendicular to the machine direction. This step was performed to assess the performance of the load frame system. Approximately 36 kN (5400 lb) [24 kN/m (900 lb/ft) of material] was applied to the geotextile with the geotextile's machine direction oriented in the direction of loading. The machine direction corresponds to the direction in which the material proceeds from the textile mill, while the transverse direction corresponds to the orthogonal direction. During this load application, the geotextile strained appreciably, but did not rupture. It was also observed that the geotextile did not tear in the vicinity of the steel strip used to fasten the geotextile to the drum. Five tests on different geogrid specimens were performed. Three tests were performed in the machine direction and two tests were performed in the transverse direction. The geogrid was

loaded to the point of rupture. The geogrid was seen to rupture by splitting through the mid-cord of a longitudinal fiber. For the material oriented in the machine direction, the rupture load ranged from 14.5 to 11.0 kN/m (543 to 412 lb/ft), with the material oriented in the transverse direction ranging from 21.5 to 19.7 kN/m (805 to 738 lb/ft).

SENSORS USED FOR LOCAL STRAIN MEASUREMENTS

The sensors used in the Phase I pilot test section were mounted on geosynthetic specimens tested in the load frame described above. The sensor types used are listed below.

1. Vibrating wire strain gages
2. Vibrating wire displacement gages
3. LVDT displacement gages
4. Foil strain gages

A description of these instruments was given in the section *Instrumentation Used In Study*. Photographs of the VW strain, VW displacement and LVDT gages attached to the geotextile are shown in Figures A2.3, A2.4 and A2.5, respectively. The entire suite of instruments attached to the geotextile is shown in Figure A2.6. Holes were pre-drilled in the geotextile to allow the bolts for the mounting plates to pass. The dimensional positions of the instruments is shown in Figure B2. The length of the instrument shown in Figure B2 corresponds to the distance from the centers of the mounting plates (i.e. the nominal gage length of the instrument). The instruments attached to the geogrid specimen are shown mounted to the geogrid in Figures A2.7-A2.11. The dimensional placement of the instruments on the geogrid was similar to that of the geotextile.

TESTS PERFORMED

In general, experiments were performed with VW strain gages, VW displacement gages and LVDT displacement gages attached to the geotextile specimens. For the geogrid specimens, the same suite of gages was used with the addition of foil strain gages. Celesco position transducers were mounted to the specimens to measure global strain.

The following variables were included in the test program:

1. Geosynthetic type: Tensar BX1100 geogrid (Atlanta, GA) and Amoco 2006 geotextile (Atlanta, GA).
2. Direction of load with respect to geosynthetic orientation: Machine or transverse direction.
3. Arrangement of mounting brackets.

The two geosynthetics tested were mounted in the test frame such that the load was applied in either the machine direction or in the transverse direction. In general, the strength and stiffness of geosynthetics is different in the two directions. In addition, the manner in which the mounting plates grip the geogrid specimen is different in the two directions due to the difference in aperture opening size. The majority of the tests were performed by applying two unloading-reloading cycles during the course of loading.

Various mounting techniques were examined for the VW strain gages and the VW displacement gages. The purpose of these tests was to examine the effect of the mounting brackets on the strain measured by the gage. Mounting the end plates in different orientations was expected to influence the effective gage length of the sensor, thereby influencing the calculated strain measurement. For the VW strain gages, tests were performed with all six bolts on a given end-plate secured, with four of the six bolts on the extreme ends of the plates secured and with two of the six bolts on the extreme ends secured (see Figure A2.3). The end plates for the VW displacement gages were oriented with the long dimension of the plate in the direction of the strain measurement and with the short dimension of the plate in the direction of the strain measurement. VW displacement gages were mounted back-to-back on a geogrid and geotextile specimen to evaluate the influence of bending in the material. Tests were performed with the foil strain gages to evaluate the influence of the strain gage cement and the environmental protection layers used to protect the gages in the field application.

RESULTS

Global strain was measured by a set of two Celesco position transducers at two points across the specimen. Figures B3-B6 show the results from the two sets of Celesco position transducers for geogrid and geotextile specimens oriented in the machine and transverse directions. From this data,

it is seen that minor differences exist in the measured strain from one side of the geosynthetic to the other, indicating that the load frame assembly and geosynthetic mounting procedure provided for a uniform load and strain application. For each test conducted, the comparison of the global strain response from each set of Celesco position transducers indicated the quality or acceptableness of the test. If the two responses were seen to be significantly different, the test results were discarded. Figures B7-B10 show the global strain, averaged from the two sets of Celesco position transducer readings, from two different tests for geogrid and geotextile specimens oriented in the machine and transverse directions. These results show that the repeatability of the test results is good.

Comparison of Global Strain To Manufacturer's Data

The global strain measurement from the Celesco position transducers was compared to data provided by the geosynthetic manufacturers. The manufacturers data is considered to represent typical values. In Figures B11-B14, the average global strain for the geosynthetics in the machine and transverse directions is compared to the manufacturer's data. The behavior measured in this study appears to be reasonably close, but not identical, to the response reported by the manufacturers.

Strain Response - Vibrating Wire Strain Gages

Experiments were performed with two vibrating wire strain gages attached to the geosynthetic specimens. Due to the low strain range of these gages, experiments were carried out only to relatively low load levels. Figures B15-B18 show the comparison of the strain measured from the vibrating wire strain gages and the global strain for the geogrid and geotextile oriented in the machine and transverse directions. The vibrating wire strain response is the average of the measurements taken from two gages located on the specimen. The global strain response is also the average from the two sets of measurements.

From Figures B15-B18, it is seen that the measured strain from the vibrating wire strain gages is much lower than the global strain. This result can be explained by examining the mounting plates used for the vibrating wire strain gages. The relatively large size of these plates left 62 mm (2.44 in) of unclamped geosynthetic between the inside ends of the plates. For the geotextile, it is expected that clamping the mounting plates together would prevent the geosynthetic from straining within the confines of the plates, leaving only 62 mm (2.44 in) of material which will experience strain. The strain experienced by this 62 mm (2.44 in) of material results in a given displacement

that is sensed by the gage. This displacement is divided by the gage length of the sensor (150 mm, 5.9 in) to produce the output strain plotted in Figures B15-B18. The true strain experienced by the unclamped material, should then be equal to the measured strain multiplied by the ratio of 150 mm (5.9 in) to 62 mm (2.44 in) (i.e. a multiplication factor of 2.4). It is this true strain, which is being measured by the Celesco position transducers, which needs to be compared to the global strain measured. For the geogrid, the situation is complicated by the fact that the material is not continuous between the clamps. It is expected that the multiplication factor would depend on the number of free ribs contained within the unclamped region.

The raw vibrating wire strain gage data shown in Figures B15-B18 has been experimentally calibrated such that it matches the global strain measured. This has been accomplished by evaluating multiplication factors (i.e. the ratio of the global strain to the local strain from the vibrating wire strain gage) at different load levels. From the discussion above, it is expected that this multiplication factor would be equal to 2.4 for all levels of load. Figures B19-B20 show the calibrated vibrating wire strain gage measurements plotted with the global strain measurements for geogrid specimens oriented in the machine and transverse direction. A best-fit multiplication factor of 2.8 was found to produce the best match to the global measure. Figures B21-B22 show the calibrated vibrating wire strain gage measurements for the geotextiles in the machine and transverse directions. A constant multiplication factor of 5 produced the fit seen in Figure B21 for the geotextile in the machine direction while a factor of 2.4 produced the fit seen in Figure B22 for the geotextile in the transverse direction.

The importance of the mounting bracket arrangement and the corresponding unclamped region on the strain response is further illustrated in Figure B23, where results are seen from tests where only four and two bolts on the ends of the mounting plates were fastened. It is seen that as the number of bolts used decreases (i.e. as the unclamped material increases in length) the measured strain approaches the global strain.

Strain Response - Vibrating Wire Displacement Gages

In principle, it is expected that the VW displacement gages would yield a trend similar to the VW strain gages, since the gage clamps a portion of the material contained between its nominal gage length. The nominal gage length is 280 mm (11.0 in), whereas the distance between the mounting plates is 185 mm (7.28 in). It would then be expected that the measured strain from the gage would

be less than the global strain by a factor of 1.5. The response of the VW displacement gages was complicated, however, by the way in which the gage and mounting plate assembly caused the material to initially bow between the mounting plates. A combination of the weight and tension force in the instrument's spring, coupled with the ability of the mounting plates to rotate appeared to be sufficient to cause an initial bow in the material. This was true for both the geogrid and the geotextile. As load was applied to the specimen, the slack in the material caused by the bow between the mounting plates was slowly removed. The displacement seen by the gage was consequently larger than expected during initial loading. Physical observations of the tests indicated that the bow was not completely removed until nearly 4 kN/m (150 lb/ft) of load was applied to the specimen. This led to a strain versus load curve that was concaved until the bow was removed. This also led to strains from the VW displacement gages being typically greater than the global strain, which negated the response expected.

A certain amount of the initial concaved response was removed from the data presented in Figures B24-B27, which shows the measured response from the vibrating wire displacement gages compared to the global strain for the geosynthetics in the machine and transverse directions. From these figures, it is seen that the majority of the tests show a strain from the VW displacement gages which exceeds the global strain. Experiments were also performed with the mounting plates rotated by 90° such that the short dimension of the mounting plate was in the direction of the instrument. This arrangement increased the unclamped portion of the material between the plates. This arrangement also caused less bowing of the material between the plates. In general, the results from these tests were seen to be closer to the global strain as compared to the results seen in Figures B24-B27.

Experiments were performed with two vibrating wire displacement gages mounted together (back-to-back) on opposite sides of the material. Originally, these tests were performed to assess effects of bending in the material. Since the strain response from either gage was seen to be nearly identical, it was concluded that bending in a uniaxial tension test for geosynthetic materials is insignificant. The tests provided more useful information due to opposite pairs of gages negating the bowing effect created by a single gage. The response of the gage in this configuration is thought to be more characteristic of a single gage in the ground due to the confining effect of the soil surrounding the gage, which would prevent bowing of the geosynthetic in the vicinity of the gage. Figures B28-B31 show the calibrated results of tests performed on the geosynthetics in the machine

and transverse directions. The response of the VW displacement gage is the response averaged from the two gages mounted back-to-back and with an appropriate calibration factor applied to achieve a match to the global strain. The response from the two back-to-back gages were always seen to be very close to each other. With the exception of the gages mounted to the geotextile in the transverse direction, the raw strain response of the VW displacement gages was seen to be slightly less than the global strain. This result coincides with the trend observed from the VW strain gages. The calibration factors used for the geogrid in the machine and transverse direction were 1.1 and 1.05, respectively, while for the geotextile, factor of 1.08 and 1.00 were used in each respective direction.

Strain Response - LVDT Displacement Gages

The response of the LVDT displacement gages followed the same trend as that described for the VW strain gages. The length of the unclamped material between the mounting plates was 39 mm 1.54 in). The nominal gage length was 50 mm (1.97 in). With these dimensions, it would be expected that a multiplication factor of 1.28 would be required to correct the strain measured by the LVDT gages. Figures B32-B35 show the results on the geosynthetics in the machine and transverse directions. With the exception of the geogrid in the transverse direction, the strain from the LVDT gages was less than the global strain. The LVDT response for the geogrid in the machine direction was calibrated to match the global strain by multiplying the response by a constant factor of 1.15, with the result shown in Figure B36. Calibration of the LVDT response for the geogrid in the transverse direction was not necessary. The LVDT response for the geotextile in the machine direction was calibrated by multiplying the response by a constant factor of 1.1, with the result shown in Figure B37. For the geotextile in the transverse direction, a best-fit was achieved by using a power expression, where the multiplication factor was calculated as

$$M.F. = 1.2\epsilon^{-0.138}$$

where M.F. is the multiplication factor applied to the LVDT strain response for a strain level given by a magnitude ε in percent. This equation gives multiplication factors ranging from 1.4 to 1.05 for strain ranging from 0.2 to 2.5 % strain. The corrected response is shown in Figure B38.

Strain Response - Foil Strain Gages

Foil strain gages were mounted only to geogrid specimens. Figures B39 and B40 illustrate results from a specimen loaded in the machine and transverse direction, respectively. The global strain is the average of the two sets of Celesco position transducer readings. The local strain is the strain directly measured from a set of strain gages mounted on opposite sides of a geogrid rib connected in a half-bridge arrangement. From Figures B39 and B40, it is seen that the local strain exceeds the global strain. The foil strain gage response has been calibrated by multiplying the raw response by a constant factor of 0.8 and 0.625 for the geogrid specimen in the machine and transverse direction, respectively. The calibrated response is shown in Figures B41 and B42.

From Figures B39-B42 it appears that the measured local strain exceeds the global strain by a constant multiplier for monotonically increasing loads. In other words, for monotonic loading situations, it appears that the global strain of the material can be estimated reasonably well by dividing the local measured strain by a constant factor. The response seen during unloading and reloading, however, is different. It appears that the global and local response is nearly one to one during unloading-reloading cycles. This is illustrated in Figure B43 where the second unloading-reloading cycle from the transverse loading test (Figure B40) is plotted by simply shifting the local response curve back over atop the global response curve. The local strain was not multiplied by the factor 0.625 for the curve shown in Figure B43. From Figure B43, it is seen that the raw local response matches the global response nearly one for one. This suggests that, to assess the global response of geogrids in field applications, it is necessary to duplicate the types of loads anticipated in the field, in the laboratory, for the purpose of relating the measured local strain to the global strain. As with the other instruments, the results indicate that calibration factors differ between the transverse and machine directions. This implies that calibration factors will be specific to the type of geogrid material and procedure used to manufacture the material.

Figure B44 illustrates results from a test in the machine direction where a single strain gage was attached to one side of a geogrid rib. The local response in Figure B44 has been plotted by taking the measured response and multiplying it by the constant factor of 0.8 used to produce the local response curve in Figure B41. Comparing Figure B44 to Figure B41 it appears that a single strain gage in a quarter-bridge arrangement produces nearly the same type of response as two strain gages attached in a half-bridge arrangement. These results suggest two conclusions. First, there appears to be very little local bending in a pure tension type of loading. Second, it appears that the

gage and its bonding cement does little to induce unwanted stiffening of the geogrid rib.

The influence of the environmental protection used in the field application was examined by conducting tests with a single gage on one side of a geogrid specimen with the butyl rubber and neoprene applied around the gage. The results from these tests are shown in Figures B45 and B46. The response from the foil strain gage appears to match quite closely the global strain curve for the specimen in the machine direction. This implies that the strain from the foil strain gage with the environmental protection is less than that with no environmental protection, meaning that the protection layers provide some stiffening to the area of the gage, or act to distribute the strain around the area of the gage. A correction factor of 0.8 was necessary without the environmental protection. The same appears to hold true for the geogrid in the transverse direction. In Figure B46, a correction factor of 0.87 has been applied to the foil strain gage data. A factor of 0.625 was required without the environmental protection. The results from the field application have used calibration factors of 1.00 and 0.87.

SUMMARY

From the in-air tension tests described above, the following findings were made:

1. The tension apparatus designed as part of this project is capable of applying a uniform, uniaxial strain across the specimen. The apparatus is seen to produce repeatable results.
2. The results from this apparatus show a response which is close, but by no means identical, to that supplied by the manufacturer.
3. All results show the importance of accounting for the geosynthetic material contained in the mounting plate clamping area. As the ratio of the unclamped length between the mounting plates to the nominal gage length of the instrument decreases, so does the strain measured by the instrument in comparison to the global strain. This ratio, or multiplication factor used to calibrate the measured strain, is dependent on the geosynthetic type and the direction of loading. A summary of the multiplication factors used to calibrate the strain response of the instruments used in this study is given in Table 1. The factors given in Table 1 correspond to results most indicative of the manner in which the gage would perform in the field.
4. The mounting bracket arrangement used for the vibrating wire displacement gages was seen

to produce a significant bowing of the material at the beginning and well into the initial loading of the specimen. This occurrence caused the strain measured from the gage to be greater than the global strain and created problems in interpreting the data. Mounting these gages back-to-back eliminated this effect and produced a result more in line with the conclusion made above in item 3.

5. The response of foil strain gages mounted to a geogrid rib was seen to be greater than the global strain. The results showed that the strain could be corrected to the global response by multiplying the strain by a constant factor for the monotonically increasing loading portion of the curve. For unloading-reloading behavior, however, the raw response of the foil strain gage appeared to match the global response. This indicates that if this measurement is being generated from cyclic dynamic data, a correction to the response is not required. This would not be true for monotonically applied loads. The strain gage cement was not seen to have an influence on the response of the material. Local bending in the rib was also not observed. The environmental protection layers used to protect the gages in the field test sections was seen to have a stiffening effect on the measured response. Calibration factors applied to the raw data appeared to produce a reasonable match for both monotonic loading and cyclic loading for overall strain levels less than approximately 2 %.
6. Calibration of measured data from the VW and LVDT displacement gages appeared suitable for both the monotonic and cyclic loading portions of the curves.

The results indicate the importance of evaluating particular gages with their associated mounting brackets for specific geosynthetic materials loaded in a specific direction. While the trends in the data for the different gages and geosynthetic materials are common, the magnitude of these trends is different for the different materials and gages used and must be evaluated on a case-by-case basis.

Table 1: Multiplication Factors Applied To Sensors On The Geosynthetics

Geosynthetic	Direction	Sensor Type			
		VW Strain	VW Displ.	LVDT	Foil Strain
Geogrid	Machine	2.8	1.1	1.15	1.00
Geogrid	Transverse	2.8	1.05	None	0.87
Geotextile	Machine	5	1.08	1.1	–
Geotextile	Transverse	2.4	1.00	$1.2\varepsilon^{-0.138}$	–

PHASE I PILOT TEST SECTION CONSTRUCTION AND MONITORING

The Phase I test section was constructed in a local contractor's gravel quarry located between Bozeman and Belgrade. The contractor, JTL Inc., allowed for the construction of the test section along a truck travel path leading from the gravel pit to the weigh scale. The travel path was covered by a layer of deteriorating asphalt. JTL Inc. donated the raw materials (gravel base and asphalt concrete) and the equipment and labor necessary to construct the test section. Construction of the test section began on 13 July and was completed on 1 August, 1995.

PURPOSE

The purpose of the pilot test section was to evaluate instrumentation that was thought to be suitable for use in the Phase II test sections and whose likelihood for success was uncertain. The pilot test section was not chosen with the aim of duplicating the types of subgrade and layer thickness and preparation conditions anticipated in the Phase II test sections. While this would have been a desirable feature to incorporate in the pilot test section, cost and time limitations did not allow for such action.

TEST SECTION CONSTRUCTION OVERVIEW

The test section was constructed by excavating the existing asphalt and subgrade along a straight section measuring 42.7 m (140 ft) in length by 4.6 m (15 ft) in width. The existing asphalt was 10 to 40 mm (0.4-1.6 in) in thickness. The existing subgrade consisted of a dry to moist, silty, sandy gravel with cobbles. The subgrade appeared to be at a relative density of 75-85 %. The excavation extended to approximately 267 mm (10.5 in) below the top of the existing asphalt grade. Approximately 100 mm (4 in) of the subgrade was scarified and recompacted with a vibratory steel drum roller. A thin layer of base course material was placed and spread to level the bottom of the excavation. This layer was not compacted and ranged in thickness from 10 to 50 mm (0.4-2 in). Views of the test section at the completion of this stage are shown in Figure A3.1. Figure A3.1a is a view looking to the Northeast. The weigh scale office can be seen in the extreme upper left hand side of the photograph. The scale is on the east side of the building. Figure A3.1b shows a view looking to the Southwest. The entrance to the gravel pit is immediately to the right (west) of the end of the test section. When completed, trucks enter the pit along the existing travel way to the west of the test section and return by entering onto the test section when coming out of the pit and traveling towards the weigh scale. In this way, the test section only sees loaded trucks whose weights are recorded at the scales.

A 16.7 m (55 ft) section of geogrid (Tensar BX1100) was placed within the extreme Northeast end of the test section. A 13.8 m (45 ft) section of geotextile (Amoco 2006) was placed immediately to the Southwest of the geogrid section. The remaining 12.2 m (40 ft) of the test section to the Southwest was left as an unreinforced control section. A view of the test section with the geogrid and geotextile in place is shown in Figure A3.2.

As seen in Figure A3.2, instrumentation was then attached to the geosynthetics. The manner in which this instrumentation was fixed and protected is described in a later section. Approximately 200 mm (8 in) of base course was then placed and spread throughout the test section. This base course was a gravel with sand and silt, with particles no larger than 76 mm (3 in). Instruments were installed in the base as it was placed. These instruments and installation procedures are described later in this section. The base course was placed with a large front-end loader and spread with a small skid-steer loader, as shown in Figure A3.3. The base course was hand-spread in the areas of instruments embedded in the base. The resulting section prior to compaction is shown in Figure

A3.4. The base course was compacted with a vibratory steel-drum roller. Additional base course was placed and spread level with a grader and recompacted with the same roller (Figure A3.5). Approximately 64 mm (2.5 in) of asphalt concrete was then placed with a bottom-dump truck, spread level with a grader (Figure A3.6) and then compacted with a steel-drum vibratory roller (Figure A3.7).

INSTRUMENTATION LAYOUT

Twenty four instruments were placed in the Phase I pilot test section. These instruments were attached to the geosynthetics, embedded in the base course and embedded in the asphalt concrete. These instruments are listed below.

Instruments on geosynthetics

1. Vibrating wire (VW) strain gage (2)
2. Vibrating wire displacement gage (2)
3. LVDT displacement gage (4)
4. Foil strain gage (4)

Instruments in base course

1. Vibrating wire embedment strain gage (2)
2. Vibrating wire embedment displacement gage (2)
3. LVDT embedment displacement gage (4)

Instruments in asphalt concrete

1. Vibrating wire embedment strain gage (4)

The instruments described above were placed in the locations shown in Figure C1.1 (Appendix C.1). The dashed lines running the length of the test section were designed to correspond to anticipated truck wheel paths. The embedment strain and displacement gages in the base and asphalt concrete were placed as close as possible to the bottom of the respective layers. A summary of the gages used in the Phase I test section, their gage lengths, strain range and strain sensitivity, is given in Table 2.

Table 2: Instrumentation Specifications

Instrument Location	Instrument Type	Gage Length mm (in)	Strain Range (%)	Strain Sensitivity (%)
Geosyn.	VW Strain Gage	150 (5.90)	0.3	0.0001
Geosyn.	VW Displacement	280 (11.0)	9	0.009
Geosyn.	LVDT Displacement	50 (1.97)	+/- 10	+/- 0.03
Geosyn.	Foil Strain Gage	5 (0.197)	10	---
Base	VW Embedment Strain	161 (6.34)	0.3	0.0001
Base	VW Embedment Displ.	317 (12.4)	8	0.008
Base	LVDT Embed. Displ.	81 (3.19)	+/- 13	+/- 0.04
AC	VW Embed. Strain	153 (6.02)	0.3	0.0001

INSTRUMENTATION INSTALLATION

Instruments Attached To Geosynthetics

The instruments on the geosynthetics were attached in a manner identical to that described in the section on in-air tension testing. All instruments were oriented to measure strains in the lateral direction of the roadway (i.e. in the transverse direction of the geosynthetics). Figures A4.1 and A4.2 show the vibrating wire displacement gage and vibrating wire strain gage, and the two LVDT's attached to the geotextile, respectively. It is seen that very little slack exists between the mounting plates of the transducers. Figures A4.3, A4.4 and A4.5 show the vibrating wire displacement gage, vibrating wire strain gage, and LVDT attached to the geogrid, respectively. As seen in Figure A4.5, the LVDT mounting bracket straddled one rib of the geogrid. As seen in Figures A4.3-A4.5, a protective layer of medium sand, approximately 5 mm (0.2 in) in thickness, was placed below each of the instruments attached to the geogrid. In addition, a small piece of the geotextile was placed beneath the footprint of the instrument to prevent the instrument from binding with the aggregate base course material. The sand cushion beneath the geogrid was continued along the length of the cables attached to the instruments and deepened to approximately 10 mm (0.4 in) to prevent base course aggregate from puncturing the cables. The cables were also fastened to the geogrid strands with plastic zip ties. The sand pack was not used beneath the geotextile as it was with the geogrid.

Three strategies were employed for permanently covering and protecting the transducers located on the geosynthetics prior to the placement of base course aggregate. The first option consisted of covering the instrument with a half section of PVC pipe. The ends of the pipe were packed with sand to prevent base course from entering the pipe. This cover option is shown in Figure A4.6. The second option consisted of covering the transducer with medium sand and then covering the sand mound with a layer of geotextile (Figure A4.7). The third option consisted of covering the instrument with a medium sand and placing a half section of PVC pipe over the sand pack such that the entire pipe cavity was filled with sand. This option is illustrated in Figure A4.8. The options used for the instruments attached to the geosynthetics are listed in Table 3. Due to limited number of VW displacement and VW strain gages, not all cover options could be used for these sensors. It is noted that the PVC pipe used for instrument #1 was significantly more flexible than the other PVC pipes. All cables extending across the top surface of the geosynthetics were also covered with a sand pack to prevent cable damage from the aggregate base.

The foil strain gages, attached to the geogrid as described in the section on in-air tension testing, were covered with protective layers in the laboratory prior to transporting the geogrid to the field (Figure A4.9). This was done to prevent water damage as well as abrasion damage to the gage. The covering consisted of the following steps.

1. The gage installation area was sandwiched between sheets of M-Coat F butyl rubber sealant and M-Coat F neoprene.
2. The entire area was then sandwiched between sheets of clear plastic with liberal amounts of silicone used between sheets, particularly around the area of cable entry.
3. The entire area was then sandwiched again between sheets of geosynthetic fabric, again with liberal amounts of silicone applied.

Due to the manufactured packing around the foil strain gages, additional covering in the field consisted only of a thin layer of sand mounded atop the gage locations. With the above precautions taken, the instruments on the geosynthetics were ready for base course to be placed.

Table 3: Geosynthetic Instrument Cover Options

Instrument Number	Geosynthetic Instrument Type	Cover Option
1	VW Displacement Gage	3
2	VW Displacement Gage	2
5	VW Strain Gage	1
9	VW Strain Gage	2
29	LVDT Displacement Gage	2
30	LVDT Displacement Gage	3
31	LVDT Displacement Gage	1
32	LVDT Displacement Gage	3

Instruments Embedded In Base Course

Prior to the placement of the aggregate base course, temporary covers were placed around the gages to be embedded in the base to protect them from damage during compaction. Three types of covers were used to accommodate the different sizes of the instruments and to explore different methods. A large irrigation control box with the bottom removed was placed around the vibrating wire embedment displacement gages (Figure A4.10). A layer of sand was placed in the bottom of the container and along the length of the cable extending from the container. A similar arrangement was used for the LVDT embedment gages (Figure A4.11) with a sand pack also being used. Both of these containers were rigid. A flexible tube (Figure A4.12) was used to encase the vibrating wire embedment strain gages. With these containers in place, base course material was placed and spread as previously described. Hand spreading was necessary in the vicinity of the embedment gages. Aggregate base was mounded around the outside of the two rigid containers such that the base course extended above the top of the container. This was necessary to prevent the container from being pushed down by subsequent compaction. The flexible container was allowed to extend above the base course grade such that the base course could be spread directly adjacent to the container. The flexibility of the container allowed for the compaction equipment to compress both the container and the base as the compacter rolled over the location. Observing the compaction operation showed that both techniques worked quite well and that no physical differences in the base course material

existed between material adjacent to the containers and that lying far away.

Once the base was compacted, as described above, the containers were pulled from the ground. The flexible container had to be slit to be removed while the other containers pulled from the ground more easily due to their sloped sides. Aggregate base material was then compacted around the instruments to backfill the cavities left by the containers. This was accomplished with the use of a short length of wooden stake and a hammer. The stake allowed for the base to be compacted well within areas interior to the plates of the gages. The base was compacted to the greatest density possible. This technique also allowed for the gages to be positioned within the middle of their range. This was accomplished by monitoring the instruments in real time while gently tapping on the base course either in the interior or exterior areas of the end plates. The remaining base necessary to fill the cavity was placed in the same fashion. As described previously, additional base course was added to level the test section and additional compaction was provided. This compaction took place without any protection of the instruments.

Instruments Embedded in Asphalt Concrete

The embedment strain gages in the asphalt concrete were placed by precompacting asphalt concrete around the gage. This was accomplished by placing the gage in an open wooden mold (Figure A4.13) and compacting asphalt around the gage with a wooden stake and hammer. For one of the gages (#10, over the geogrid under a wheel path), the asphalt was allowed to cool and set-up over night. For the other three gages (11, 9 and 12), the asphalt was compacted approximately an hour before placement of the asphalt layer. These two approaches were taken to examine the effect of curing time on the compatibility of the AC brick with the surrounding AC. Using the AC brick compacted a day in advance, it was feared that the AC contained in the brick would not be sufficiently heated by the surrounding AC such that the brick did not bond well with the adjacent material. It was speculated that this problem would be avoided by compacting the brick immediately before AC placement. One of the specimens cooled overnight is shown in Figure A4.14. The AC bricks were oriented in the transverse direction of the roadway. The asphalt was placed as described previously with care taken to avoid driving over the gages during the initial dumping of the asphalt.

LONG TERM MONITORING PROGRAM

The instruments described above were monitored using the Cambell data logger. The components associated with this logger have been described earlier in this report. The logger was programmed to record data every hour for 24 hours per day. The data recorded for each hour was data averaged over a 10 minute period prior to the time of recording. The logger is capable of cycling through the 24 channels every 30 seconds, meaning that for the 10 minute data collection period, 20 samples per instrument are taken and averaged. The data was stored in the data logger and could be downloaded from a remote computer using a telephone modem as often as needed.

The data logger was turned on and began recording data on July 22, 1995 at 2:00 P.M. On this date, the aggregate base had been placed and spread but not compacted. The only transducers recording meaningful data were those attached to the geosynthetics. The first compaction of the base took place on July 24th at approximately 7:00 A.M. The data logger was turned off at this point such that the transducers could be monitored real-time to ensure that damage was not occurring during compaction. On July 25th, aggregate base was compacted around the embedment transducers. Following compaction, three truck pass tests were conducted. By July 25th at 3:00 P.M. the data logger was turned back on. At this point, the only transducers not providing meaningful data were the embedment strain gages for the asphalt concrete. On July 31st the MDT non-destructive division performed Road Rater tests on the unsurfaced test sections. In addition, two truck pass tests were conducted. These tests are described in the section below. On August 1st at approximately 7:00 A.M. the base course layer was leveled and compacted for a second time. The asphalt concrete was placed shortly thereafter with the embedment gages placed in the AC. The asphalt was allowed to cure for several hours with the section being opened to truck traffic at 1:00 P.M. It is noted that the unsurfaced section was closed to traffic up until the time that the asphalt was placed. The Cambell data logger was inoperable between August 3, 12:00 P.M. to September 7, 12:00 P.M. Any stored data was lost during this period. During this period, the logger was returned to the manufacturer for service. The malfunction was due to a bad diode which was replaced. During this time, dynamic data could still be collected. A truck pass test was performed on August 29. Additional Road Rater tests were performed on the surfaced test section on September 21st. Two additional truck pass tests were performed on the AC surfaced section on October 19. The logger was disconnected on October 26. The test section was dismantled in early November and all instruments, with the exception of

the AC embedment gages, were retrieved. Table 4 lists the above described events.

Table 4: Chronological Order of Events For Construction and Testing and Reference Times

Date	Time	Event	Reference Times (hours)
July 22	2:00 P.M.	Cambell data logger turned on, uncompacted base in place.	--
July 24	7:00 A.M.	Base course compacted.	0
July 25	7 A.M. - 2 P.M.	Base course transducers set, truck pass tests 1-4.	22-29
July 25	3:00 P.M.	Logger turned back on.	31
July 31	10:00 A.M.	Road rater and truck pass tests 5 & 6 on unsurfaced section.	170
Aug. 1	7:00 A.M.	Base leveled & recompacted, AC placed and compacted.	191
Aug. 1	1:00 P.M.	Section open to traffic.	197
Aug.3-Sept. 6	12:00 P.M. 12:00 P.M.	Cambell data logger inoperable	242-1083
Aug, 29	8:00 A.M.	Truck pass test 7	864
Sept. 21	9:00 A.M.	Road rater tests	1441
Oct. 19	8:00 A.M.	Truck pass tests 8 and 9	2112
Oct. 26	5:00 P.M.	Logger disconnected	2289

Long Term Truck Traffic Loading

Daily traffic loading consisted of gravel trucks ranging from approximately 400 to 27 kN (45 to 3 tons) in weight. Truck weights were recorded at the scales. During the 14 weeks of monitoring, 7550 trucks passed over the sections for a total vehicle weight of 1490 MN (167,000 tons), giving an average daily traffic of 82 trucks at approximately 200 kN (22 tons) per truck. Figure C1.2 shows the daily and weekly truck traffic expressed in terms of a total truck weight per day or week.

From this figure, it is seen that the daily traffic can fluctuate by a factor of 5 while the weekly traffic is more consistent.

Strain in Geosynthetics

Long term results from the instruments mounted to the geogrid and the geotextile are given in Figures C1.3-C1.10 (Appendix C1). In these figures the strain determined from each instrument is plotted against time, where time zero corresponds to July 24, 7:00 A.M. (see Table 4). At this point in time, the base course had been placed and spread, but not compacted. A base line reading of the instruments was taken prior to the placement of the base. This base line reading was compared to readings after the logger was turned on. It was seen that very little strain developed in the geosynthetics as a result of placement without compaction of the base. The results shown in Figures C1.3-C1.10 have been corrected with the multiplication factors given in Table 1 arising from the in-air tension tests. The strains are positive in extension.

Vibrating Wire Displacement Gages

Figure C1.3 shows the long term response of VW displacement gage 2 located on the geogrid. The gage was located on the proposed truck wheel path for the section. The results show that approximately 0.4 % strain was induced in the geogrid due to the initial compaction of the base course. The deformation of the geogrid appeared to be permanent. An additional 0.15 % strain appeared to be induced when the base course was leveled and compacted for a second time and during the first 50 hours when the section was opened to traffic after the AC was placed. At this time the data logger became inoperable and was not fixed until hour 1083. During this time, the strain increased by approximately 0.025 %. Readings beyond this point show spikes of up to 0.5 % strain. It is believed that these spikes are due to erroneous instrument readings and not to instantaneous traffic loading. This type of data is only seen for the VW displacement gage, which has been reported to exhibit spikes of this nature. From hour 1083 to the end of the record, the strain appears to gradually increase by approximately 0.05 %. During this period, several shorter periods of increased strain can be noted. These periods appear to be around hours 1400, 1750 and 2000. The second set of Road Rater tests corresponds to the first period around hour 1400. As noted later, increased periods of strain are also noted at hours 1400 and 1750 for some of the other instruments. Examination of Figure C1.2 does not, however, indicate that these hours correspond to elevated

periods of traffic loading.

Figure C1.4 shows the response of the VW displacement gage attached to the geotextile. This response indicates that very little strain is seen during base placement and compaction and that small amounts of permanent strain is seen towards the end of the reading period. The spike occurring around the time when the section was opened to traffic (0.5 %) appears to be as large as that seen for the geogrid and is most likely due to erroneous instrument readings. In general, however, the strain seen with this instrument is less than that for the same gage attached to the geogrid. This gage, however, was located off the wheel path whereas the gage on the geogrid was directly below the wheel path.

Vibrating Wire Strain Gages

Figure C1.5 shows the response of the VW strain gage located on the geogrid. The sporadic strain readings are well beyond the range of the instrument (0.3 % strain), indicating that the instrument was over strained during the initial placement of base and produced only erroneous or inaccurate readings.

Figure C1.6 shows the response of the VW strain gage on the geotextile. This gage was located below the wheel path and shows more strain than the VW displacement gage on the geotextile in an off-path location. This gage also shows more strain than the VW displacement gage on the geogrid, which was also below the wheel path. The trend of the curve is similar to the VW displacement gage on the geogrid. The instrument shows 0.325 % strain induced during initial compaction of the base. An additional 0.5 % strain occurred at the time of the second compaction and opening of the section to traffic after the placement of the AC layer. Unlike the VW displacement gage on the geogrid, the strain is seen to decrease by approximately 0.05 % while the logger was inoperable. Over the course of the life of the section, the strain increases again by 0.03%. Periods of increased strain are observed around hours 1400 and 1750, like those observed for the geogrid. The increased strain around hour 2000 is not observed as it was for the geogrid. As noted at the beginning of this section, the strain from the instrument was multiplied by the factor listed in Table 1 (a factor of 2.4 for this particular gage). This explains why the strain plotted in Figure C1.6 is beyond the 0.3 % strain range of the instrument.

LVDT Displacement Gages

Figures C1.7 and C1.8 show the response of the LVDT displacement gages attached to the geogrid. Each of these figures contains three diagrams. The upper most diagram is the data taken directly from the gage. The other two diagrams pertain to data generated to account for temperature effects on the gages and are explained in more detail below. LVDT 31 (Figure C1.7) is more in line with the anticipated truck wheel path as compared to LVDT 32 (Figure C1.8). These gages indicate a response during the first 40 hours, corresponding to placement and compaction of the base, that compares closely to that from the VW displacement gage (Figure C1.3). The spikes corresponding to times when the section was just opened to traffic appear to be more extreme than those shown in Figure C1.3, although they are seen only during this period of time and not throughout the life of the section. The raw data from the LVDT's did not show accumulated permanent strain with increasing time and traffic as did the VW displacement gage. It is possible that the small mounts used for the LVDT were not sufficient to grip the grid and slipped and relaxed over time. It is interesting to note that the LVDT under the wheel path (LVDT 31) showed more accumulated permanent strain than did the LVDT off the wheel path.

The raw data shows fluctuations with a 24 hour period. It was suspected that these cycles were due to temperature effects on the voltage output of the gage. To investigate this effect, data was investigated for each gage during periods when temperature fluctuated and little traffic was seen at the site. This data was taken typically from 8 P.M. to 6 A.M. From this data there was seen to be a strain response of the instrument with changes in temperature. Since the LVDT's did not contain a thermistor, temperature data from the closest vibrating wire gage contained in the same layer was used. Typically, these gages were only 1.5 m (4.9 ft) from the LVDT. The data showed that strain decreased as temperature decreased. The peak in the strain response lead the peak in the temperature response by anywhere from 2 to 10 hours.

An attempt was made to correct the raw data for temperature effects. This was accomplished by first generating a strain versus temperature factor from data from the different gages. As mentioned above, this data was taken from 8 P.M to 6 A.M. when little to no traffic existed. Coefficients ranging from 0.0108 to 0.0144 % strain per °c (0.006 to 0.008 % strain per° F) were used for the four LVDT's on the geosynthetics. Strain corrections were calculated based on a temperature record from a nearby vibrating wire gage. The strain correction record is the middle diagram of each LVDT figure. Due to the uncertainty with the time shift exiting between the peak

strain and peak temperature with each cycle, no correction was attempted by shifting the strain correction record. The strain correction record was subtracted from the raw data to obtain the strain record corrected for temperature effects shown as the bottom diagram in each figure. The corrected strain record shows a gradual increase in strain with time, which would not have been observed from the uncorrected record. The corrected record for gage #32 also shows a moderate increase in strain around hours 1400 and 1750, as did the vibrating wire gages. The corrected record, however, still shows daily fluctuations. It is believed that these daily fluctuations are due to the time shift between the gage response and the calculated temperature induced strain response.

Figures C1.9 and C1.10 show the response of the LVDT displacement gages attached to the geotextile. These plots are comparable to those for the geogrid (Figures C1.7 and C1.8) in that the LVDT under the wheel path (#29) shows more strain than the off-path LVDT (#30) and that the corrected strain gradually increases with time. Moderate increases in strain are also observed around hours 1400 and 1750. Examining the temperature correction diagrams, it is also seen that the temperature corrected strain, and hence the temperature itself, changes most dramatically before hours 1400 and 1750. It is not clear if the temperature has an effect on the response of the pavement system, as measured through the instrumentation, or if the temperature has a universal effect on the instruments themselves.

Foil Strain Gages

Long term data was collected from the foil strain gages and was seen to be of poor quality. This result is not surprising since these gages were intended only for use in dynamic measurements. In general, the long term response of these gages was quite small and erratic with respect to the results seen for the other gages.

Strain in Base Course

Figures C1.11-C1.18 show the response of the embedment gages located in the base course. The zero time for these plots corresponds to the same time as that for the gages on the geosynthetics (i.e. July 24, 7:00 A.M.). Between hour 0 and 170, the instruments had been set and only the traffic corresponding to truck pass tests 1-4 had passed over the section. The strains are positive in extension and negative in compression.

Vibrating Wire Embedment Displacement Gages

Figure C1.11 shows the response of the VW embedment displacement gage located in the base above the geogrid and along an off-wheel path. The record shows a number of excessive spikes which may indicate a faulty gage. The long term response of the gage indicates that the base course compressed by approximately 0.3 % strain. Figure C1.12 shows the response of a similar gage located in the base in the non-reinforced section on a wheel-path. The results show that approximately 1.5 % strain (extension) occurred during compaction and placement of the AC. The strain appears to increase slightly over time. Unlike the VW embedment displacement gage located in the base above the geogrid, this VW gage shows much more moderate strain spikes and strains which are permanent.

Vibrating Wire Embedment Strain Gages

Figure C1.13 shows the response of the VW embedment strain gage located above the geogrid along a wheel path. This gage shows strains both in compression (-) and extension (+) during base initial testing and compaction, with these strain spikes being no greater than +0.2 %. The later portion of the data indicates that a small extensional strain has accumulated and that the periodic response of the gage due to daily truck traffic can be either compressional or extensional. This variation is most likely due to trucks passing over the section along slightly different wheel paths.

Figure C1.14 shows the response of the VW embedment strain gage located in the base above the geotextile. Unlike the gage above the geogrid, this gage shows permanent strain (0.2 %) resulting from the compaction process. There appears to be an overall decrease in this permanent strain for later times.

LVDT Embedment Displacement Gages

Figures C1.15 and C1.16 show the response of the LVDT embedment displacement gages (27 and 28) located in the base above the geogrid. Three diagrams are shown for each of the figures. These diagrams correspond to the raw data, a strain correction record accounting for gage changes with changes in temperature, and the strain record corrected for temperature changes. The strain correction record was determined by the same technique described above for the LVDT's on the geosynthetic.

Gage 27 is in an off-path location while gage 28 is located below the wheel path. Both gages are seen to experience extensional strains during initial testing and compaction in the range of 0.15 - 1.7 %, and are seen to result in permanent deformations. Once the section was opened to traffic a small amount of extensional accumulated permanent strain (0.1-0.2 %) is seen to result. The corrected record shows a gradual increase in extensional strain with increased time.

Figure C1.17 shows the response of the LVDT embedment gage located in the base above the geotextile. This gage shows a similar response to the LVDT gages located in the base above the geogrid. Figures C1.18 shows the response of the LVDT embedment displacement gage located in the base of the non-reinforced section. The gage shows 2.25 % strain during the base leveling and recompaction.

Figures C1.15 - C1.18 show the significance of correcting for temperature effects on the gages. It is seen that an uncorrected strain record showing no significant change in strain with time will show an increase in extensional strain when the temperature correction record is applied. The method used to develop the temperature record involves a number of assumptions. In light of these assumptions, it is not clear if the corrected record is an accurate representation of the material response.

Strain in AC

Figures C1.19-C1.22 show the response of the four VW embedment strain gages located in the asphalt concrete. The top plot in each figure corresponds to the raw data obtained from the instrument. The four gages each showed a relatively dramatic cycle of response during the first 48 hours of operation after the gages were set in the AC layer (at which point the logger became inoperable). This data has not been presented due to its erratic nature. Once the logger was repaired, the data shows daily cycles of strain. The vibrating wire instruments are designed to be very stable with respect to the sensor's electronics with changes in temperature. It is necessary to correct the strain readings for changes in the tension of the vibrating wire due to changes in length with corresponding temperature changes. This correction is insignificant for the temperature variations seen. This then indicates that the cyclical response seen is due either to expansion and contraction of the AC or due to mechanical loading.

To assess the contribution due to thermal expansion and contraction of the AC, a strain versus time response due to thermal expansion/contraction was predicted using a representative

coefficient of thermal expansion for asphalt concrete and the temperature record from the instrument. The coefficient of thermal expansion was estimated by examining the records of strain versus temperature for the four AC sensors for times when traffic was not present (i.e. approximately 8 P.M. to 6 A.M.). The records produced coefficients ranging from $5.4x10^{-4}$ to $1.1x10^{-3}$ % strain per °c ($3x10^{-4}$ to $6x10^{-4}$ % strain per °F). An average coefficient of $7.2x10^{-4}$ % strain per °c ($4x10^{-4}$ % strain per °F) was used to predict the strain versus time records shown as the middle plot in Figures C1.19-C1.22. This strain record was then subtracted from the raw data to produce the bottom plot shown in these figures. This bottom plot represents the strain in the AC due to mechanical loading and any permanent effects of thermal cycles. From these figures it is seen that the mechanical strain also appears to be periodic with an amplitude of approximately 0.01 %.

DYNAMIC MONITORING PROGRAM

The dynamic testing program consisted of loaded truck pass tests and Road Rater tests conducted by the Non-Destructive Testing Unit of the MDT. The dynamic data logger, described earlier in this report, was used to collect data from the non-vibrating wire instruments during these tests. During the second Road Rater test performed on September 21st, data monitoring programs were downloaded to the Cambell logger to enable the logger to cycle through one channel at a time, such that the Road Rater could be placed in the vicinity of a vibrating wire instrument with data from this instrument being taken at a rate of approximately 1 sample every second. The multiplication factors given in Table 1 were used to correct data from the instruments attached to the geosynthetics. Temperature correction of the gages was not necessary due to the short sampling interval.

Truck Pass Tests

The non-vibrating wire instruments were monitored as trucks were allowed to slowly pass over the test section. The trucks typically traveled at a speed of 2.2 m/s (5 mph). Tests were performed prior and after the placement of the AC layer. Four types of trucks were used for the nine truck pass tests listed in Table 4. Truck pass tests 1 and 2 used a 2-axle pickup truck weighing approximately 15 kN (1.7 tons). An empty belly dump truck weighing 156 kN (17.5 tons) was used for truck pass 3. This truck is shown in Figure A5.1. A single unit dump truck with a pup trailer (shown in Figure A5.2) was used for truck pass 4. Both the truck and pup were full with gravel. A

weight of each unit was not obtained. A full single unit dump truck with a pup trailer was used for truck pass tests 5 and 6. The entire vehicle weighed 423 and 406 kN (47.6 and 45.6 tons) for tests 5 and 6, respectively. Tests 1-6 were performed on the unsurfaced test section. The record of the truck used for test 7 was not available. A full belly dump truck weighing 414 and 429 kN (46.6 and 48.2 tons) was used for truck pass tests 8 and 9, respectively. Tests 7-9 were performed on the surfaced test section. A summary of the truck data for the different tests is given in Table 5.

Table 5: Vehicles Used For Truck Pass Tests

Test #	Date	Truck Type	Weight, kN (tons)	Surfacing
1	July 25	Pickup	15 (1.7)	Unsurfaced
2	July 25	Pickup	15 (1.7)	Unsurfaced
3	July 25	Belly Dump (empty)	156 (17.5)	Unsurfaced
4	July 25	Single Unit With Pup	not known	Unsurfaced
5	July 31	Single Unit With Pup	423 (47.6)	Unsurfaced
6	July 31	Single Unit With Pup	406 (45.6)	Unsurfaced
7	Aug. 29	Unknown	not known	Surfaced
8	Oct. 19	Belly Dump	414 (46.6)	Surfaced
9	Oct. 19	Belly Dump	429 (48.2)	Surfaced

Foil Strain Gages on Geogrid

Figures C2.1-C2.23 give results from the foil strain gages for truck pass tests 1-9. Each of the three operable foil strain gages were monitored during each test. Only those gages producing a significant response are plotted in Figures C2.1-C2.23. Foil strain gage #36 was located along a wheel path on the west side of the section. Gage #35 was located in the centerline of the section, while gage #34 was located along a wheel path on the east side of the section. The strain response was zeroed with respect to the reading at the beginning of the test. Negative strains do not mean that the geogrid went into compression, but mean that the tension existing in the grid at that time was reduced by the amount shown for the test. Figures C2.1-C2.4 show the response of gages 35 and 36 for truck pass tests 1 and 2. It is seen that only for gage 36, test 2, did the strain increase in tension

due to the truck pass. Figures C2.5-C2.7 show the results for truck pass test 3. All six axles are seen for gage #36, where the strains are in tension for the first three axles and become negative for the last three axles. Negative strains are seen for the other gages. Similar results are seen for test 4 in Figures C2.8-C2.10, however the load from the pup trailer is not seen. The results seen in Figures C2.11-C2.13 for test 5 and Figures C2.14-C2.16 for test 6 are also similar, where the loads from the three axle and two axle pup trailer for tests 5 and 6, respectively, are seen. From these figures, it is seen that maximum positive strains increase from approximately 0.007 % to 0.025 % and maximum negative strains decrease from -0.002 % to -0.05 % as the truck weight increases.

Figures C2.19-C2.23 provide results from tests 7-9 conducted on the surfaced section. The results appear to be somewhat more erratic than those on the unsurfaced test section, but show similar trends. Maximum positive and negative strains from these tests are approximately 0.007 % and -0.01 %.

Each sensor location contained only one gage on the upper side of the geogrid. It is not clear if local bending in the area of the gage had an effect on its response. With the small deflections seen, it is felt that this effect is minor.

LVDT Displacement Gages on Geosynthetics

The response of the LVDT displacement gages mounted to the geosynthetics is not as good as that seen with the foil strain gages. Figures C2.24-C2.29 show these results. As with the foil strain gages, results are provided only for those traces that produced a significant response. In general, a response was seen only for tests 4, 5 and 6, which corresponds to a combination of the heaviest vehicles and an unsurfaced section. These figures do not show the sharp response of each axle like those for the foil strain gages. Figure C2.28 is the response which best shows each truck axle. The strains seen from the LVDT are also different in that permanent strains are typically observed and the magnitude of these strains are typically 10-20 times those seen for the foil strain gages. These results are most likely due to the high profile and small mounting area associated with the gage. These results cannot be explained by differences in behavior seen in the in-air tension tests. The importance and the need for close examination of such an instrument before use in a field application is apparent from these results.

LVDT Embedment Displacement Gages in Base Course

Figures C2.30-C2.37 show the results of the LVDT embedment displacement gages located in the base course above the geogrid. Like the LVDT's mounted to the geotextile, sharp responses to each truck axle is, in general, not observed. In general, the gage located off the wheel path showed compressional strains, while the gage located below the wheel path showed dilational strains. Compressional strains were as great as -0.25 %, while dilational strains were as great as 0.35%. In only one case was a response observed for a test on the surfaced section.

Figures C2.38-C2.44 show results for the LVDT embedment displacement gage located in the base course above the geotextile and below a wheel path. The majority of the strains are dilational, with values as great as 1.2 %. Like the gages located above the geogrid, only one response was observed for the tests performed on the surfaced sections.

Figures C2.45-C2.50 show results for the LVDT embedment displacement gage located in the base course of the non-reinforced section and below a wheel path. Both compressional and dilational strains are observed for these results. The magnitude of these strains vary from -0.15 % to 1.2%.

Road Rater Tests

Road Rater tests were performed for the purpose of evaluating the ability of the instruments to respond to the dynamic surface load. The tests were also conducted for the purpose of determining whether this was a suitable means of providing dynamic response data for use in the Phase II test sections. Although not a primary objective, the Road Rater tests were also used to back-calculate elastic moduli for the various pavement layers.

The first series of Road Rater tests on July 31st were performed on the unsurfaced test section after the base was initially placed, spread and compacted and after base material was compacted around the embedment transducers. A model 2000 Road Rater (Foundation Mechanics, Inc., El Segundo, CA) machine was used for these tests and consisted of a circular plate, 305 mm (12 in) in diameter, through which a dynamic load was applied over a period of time at a given frequency. Dynamic displacement transducers monitored the vertical deformation of the ground surface at points extending radially from the applied load. Dynamic displacement was measured at points 0, 203, 305, 608, 912 and 1216 mm (0, 8, 12, 24, 36 and 48 in) from the center of the applied load. The load frequency was 25 Hz with the instrument sampling frequency set at 20 Hz. For the tests

performed on July 31st, five multi-level force values were applied within a given load cycle, with this load cycle repeated 5 times for the majority of the test locations. The dynamic force levels were 6.67, 8.90, 11.1 and 13.3 kN (1500, 2000, 2500 and 3000 lb.). Each load in the load cycle was applied for approximately 3-5 seconds, with the next load in the cycle applied immediately thereafter. For each test, the Road Rater loading plates was set on the ground surface directly above the instrument to be monitored.

Figures C3.1-C3.3 present results from the July 31st Road Rater tests. Figures C3.1-C3.3 show the response of foil strain gages 34, 35 and 36. The response of foil strain gages 34 and 35 clearly show the five separate load cycles. This distinction is not quite as evident for foil strain gage 36. The results indicate that an average tensile strain of 0.002% has been induced in the geogrid due to the Road Rater loading. The gage response does not show the effect of increasing load within a given load cycle, while the results appear to indicate a slight relaxing of the geogrid with increasing load cycle (i.e. the level of tensile strain appears to decrease with increasing load cycle). Very little permanent strain is seen to be induced by the Road Rater. The LVDT's attached to the geogrid and geotextile were also monitored during the tests. The results showed strain values well below the sensitivity of the instrument. Similar results were seen for the LVDT embedment displacement gages in the base.

The second series of Road Rater tests performed on September 21st were similar to the first series. The loading sequence consisted of four cycles of incrementing loads, where the loads were set at 11.1, 13.3, 15.6 and 17.8 kN (2500, 3000, 3500 and 4000 lb.). The frequency of loading was reduced from 25 Hz to 20 Hz with the instrument sampling rate increased from 20 Hz to 60 Hz in an attempt to capture the response for a given load application. Figures C3.4-C3.6 present results from the September 21st Road Rater tests. Figures C3.4-C3.6 show the response of the foil strain gages 34, 35 and 36. The response of foil strain gages is similar to the earlier Road Rater tests. The additional asphalt on the section and the higher load levels appears to have induced a strain in the geogrid which is comparable to the earlier tests (approximately 0.002 %). The curves are not quite as distinct as compared to the earlier tests due to the increased sampling rate. These curves do tend to show the effect of increasing load level during a given load cycle. The response of the LVDT gages on the geosynthetics and in the base course was similar to the July 31st tests.

For the September 21st Road Rater tests, the Road Rater was also used to apply load atop the vibrating wire instruments. This was done to assess the possibility of using these instruments for

dynamic measurements, provided the sampling rate could be sufficiently high. Individual programs were downloaded to the Cambell logger allowing for one vibrating wire instrument to be sampled and monitored. This increased the sampling time to approximately 1 Hz. The Road Rater was configured to apply four cycles of the same load (17.8 kN, 4000 lb) such that a near constant dynamic load could be applied to the instrument. The loading frequency was increased to 50 Hz in an attempt to make this load appear even more constant. Six of the twelve vibrating wire instruments were successfully tested. The 17.8 kN (4000 lb) load was applied for approximately 100 seconds to each instrument. Figures C3.7-C3.12 show the results of these tests. Figure C3.7 shows the results from VW displacement gage 2 located on the geogrid. A compressive strain of approximately 0.03 % is induced in the geogrid with approximately 0.01 % of this strain appearing to be permanent at the end of loading. Figure C3.8 shows the response of VW strain gage 5 on the geotextile. This gage shows a tensile strain of 0.002 % with approximately half this strain being permanent at the end of loading.

Figure C3.9 shows the results from VW embedment displacement gage 3 located in the base above the geogrid. The response indicates that the base experienced 0.06 % of compressional strain which was all permanent. Figure C3.10 shows the response of VW embedment strain gage 7 located in the base above the geotextile. Approximately 0.008 % tensile strain was induced in the base with 0.003 % being permanent. Figure C3.11 shows the response of VW embedment strain gage 9 located in the AC above the geotextile. Approximately 0.0002 % tensile strain was induced in the AC with approximately half of this strain being permanent at the end of loading.

The MDT NDT unit analyzed the Road Rater data to back-calculate elastic moduli for the various pavement layers. From the July 21st tests, corresponding to an unsurfaced section, the unreinforced section showed the largest moduli values for the base, followed by the geogrid and geotextile sections. The geogrid section showed the largest moduli values for the subgrade, followed by the unreinforced section and the geotextile section. Results from these tests are shown in Figure C3.12. Each data point was averaged from Road Rater tests at one location for four different force application values. Average values of resilient moduls for each test section from the July 21st tests are given in Figure C3.13. Results from the September 21st tests, corresponding to a surfaced section, are shown in Figures C3.14 - C3.17. Figure C3.14 shows resilient modulus values for the AC layer. Figure C3.15 provides results for the base and subgrade layers. Average values for each test section are given in Figures C3.16 and C3.17. The results tend to show somewhat lower moduli

values for the base and subgrade for the geotextile section in comparison to the geogrid section. It is difficult to compare these results to the control section since only one test was performed in this section, while the results from the other sections indicate a significant degree of scatter. Given the lack of quality control regarding the section thicknesses and compaction, the reader is discouraged from making conclusions regarding support characteristics of the various sections due to the inclusion of the geosynthetics.

FINDINGS AND CONCLUSIONS

The primary objective of this project was to evaluate and assess instrumentation that might be used in the construction of test sections under the second phase of this project. The purpose of this project was not to evaluate the performance of specific geosynthetic products. Although certain trends might indicate the relative performance of the products used, the reader is discouraged from making any conclusions along these lines from the data arising from the pilot test section. Quality control was not emphasized during the construction of the pilot test section. As a result, the thickness of the base and AC layers varied from one end of the section to the other. In addition, instruments were only located by approximate means. The proximity of loading with respect to the instrument location is, therefore, not precisely known.

To accomplish the objective of the project, it was first necessary to understand the manner in which the measured strain from the instruments attached to the geosynthetics compared to the global strain applied across the material. This was accomplished by constructing a large, wide-width tension device. The results from this device indicate that the apparatus is capable of applying a uniform, uniaxial strain across the specimen. Comparison of results to those available from the manufacturer shows a close, but not an exact correspondence.

The in-air tension test results show the importance of accounting for the geosynthetic material contained in the mounting plate clamping area. As the ratio of the unclamped length between the mounting plates to the nominal gage length of the instrument decreases, so does the strain measured by the instrument in comparison to the global strain. This ratio, or multiplication factor used to calibrate the measured strain, is dependent on the geosynthetic type and the direction of loading. A summary of the multiplication factors used to calibrate the strain response of the

instruments used in this study was given in Table 1.

The mounting bracket arrangement used for the vibrating wire displacement gages was seen to produce a significant bowing of the material at the beginning and well into the initial loading of the specimen. This occurrence caused the strain measured from the gage to be greater than the global strain and created problems in interpreting the data. Mounting these gages back-to-back eliminated this effect and produced a result more in line with the conclusion made for the other gages.

The response of foil strain gages mounted to a geogrid rib was seen to be greater than the global strain. The results showed that the strain could be corrected to the global response by multiplying the strain by a constant factor for the monotonically increasing loading portion of the curve. For unloading-reloading behavior, however, the raw response of the foil strain gage appeared to match the global response. This indicates that if this measurement is being generated from cyclic dynamic data, a correction to the response is not required. This would not be true for monotonically applied loads. The strain gage cement was not seen to have an influence on the response of the material. Local bending in the rib was also not observed. The environmental protection layers used to protect the gages in the field test sections was seen to have a stiffening effect on the measured response. Calibration factors were still necessary for the foil strain gages with the environmental protection applied. Calibration of measured data from the VW and LVDT displacement gages appeared suitable for both the monotonic and cyclic loading portions of the curves.

The results indicate the importance of evaluating particular gages with their associated mounting brackets for specific geosynthetics loaded in a specific direction. While the trends in the data for the different gages and geosynthetic materials are common, the magnitude of these trends is different for the different materials and gages used and must be evaluated on a case-by-case basis.

The results from the pilot test section indicate that an understanding of the response of instruments attached to the geosynthetics in a laboratory tension device is not sufficient for understanding the manner in which these same sensors act in a field condition. For instance, the LVDT's were seen to work very well in the lab, yet their response in the field was not comparable to the response of other instruments. In particular, the LVDT's did not show an initial build up of strain due to compaction of the base course as did the vibrating wire gages. This indicates the need for conducting laboratory scale experiments with the sensors proposed for use and involving materials and loading comparable to that which might be seen in the field.

The vibrating wire strain gages attached to the geosynthetic and embedded in the base course

appeared to work well with the exception of the range of the instrument. The range was seen to be too small for the application. The vibrating wire displacement gage attached to the geosynthetic appeared to work well and provided a response which appears reasonable. It is felt that the bowing problem seen in the lab tests is not a factor in the field due to the surrounding confinement of the soil. Dynamic Road Rater tests on the instrument indicated that the gage may be capable of measuring a dynamic response if the sampling frequency could be increased. The manufacturer is currently investigating this possibility, however it appears that this technology will not be ready by the time the Phase II test sections are built.

The LVDT displacement gages attached to the geosynthetics did not appear to work as well as the other gages for both long-term and dynamic loading. The problem is believed to lie with the mounting plates used for the sensor. It is felt that the gage was too short and blocky in its current configuration, with the mounting plate area being too small. The dynamic response of the gage was somewhat sluggish and gave a magnitude well in excess of that seen by the foil strain gages. This was most likely due to the mounting problems noted above. This also indicates the need for close examination of these gages in a controlled laboratory setting. The gages and their cables were also seen to be influenced by temperature. The methods used for accounting for this temperature effect need to be verified by placing dummy sensors beside the active sensor such that the effect can be directly measured. Otherwise, the LVDT did not appear to have any appreciable drift with time. Plans are currently being developed to build a mount for the LVDT's that allow for a longer gage length and allows the body of the sensor to be closer to the geosynthetic. The foil strain gages appeared to work exceptionally well for dynamic measurements on the geogrid. Only one of the four gages was lost during construction. The remaining 3 were seen to survive the entire 4 months that the section was open.

Each of the three sensors embedded in the base course were seen to work reasonably well and give comparable results. It appears that the manner used to place the gages in the base course provided for a minimal inclusion effect. Laboratory scale tests are also needed to verify the behavior seen in the field.

The vibrating wire strain gages placed in the AC appeared to have bonded well with the AC. The gages showed very clearly the thermal strains taking place in the AC layer. The method of accounting for thermal strains, such that the strain due to mechanical effects could be extracted from the results, appears to have worked well.

The VW displacement and strain gages and the LVDT displacement gages on the geosynthetics and the LVDT embedment gages in the base showed an increase in strain around hours 1400 and 1750. Immediately preceeding these times, the temperature in the pavement was seen to decrease significantly. These results were seen for the LVDT's when they had been corrected for temperature induced strains due to temperature effects on the sensor's electronics. Increased levels of strain were not observed for the temperature corrected results from the VW strain gages in the AC layer. It is tempting to attribute these increased periods of strain to additional temperature effects on the instruments themselves not accounted for in the correction procedures described earlier. This effect, however, was observed for all the different instrument types. Since there is no reason for this effect to be seen for the VW sensors, and these times do not appear to correspond to periods of increased traffic loading, it is believed that the temperature has an effect on the pavement system response which is being detected by the sensors. This effect needs to be examined more closely in a controlled environment.

The work performed under this phase of the project has indicated the need to perform additional experiments to aid in understanding how the instrumentation responds in the field. The data from the Phase I pilot test section has indicated an uncertainty in the measurements and the effects of temperature on some of these measurements. Controlled laboratory experiments are needed to calibrate the instruments for the types of loads anticipated in the field.

IMPLEMENTATION PLAN

In light of the findings noted above, it is believed that an insufficient degree of knowledge and confidence exists in the instrumentation package to proceed directly to field test sections. This indicates the need to perform laboratory experiments under well-controlled conditions to examine the response of specific instruments. These experiments will allow for the examination of various mounting and installation techniques. These experiments also present the opportunity to perform the research in a manner which has a greater assurance of success with respect to the objective of the project, that being to develop a design methodology for reinforced flexible pavements.

The next phase of the project should consist of laboratory experiments on geosynthetic reinforced pavement sections for the purpose of developing a prototype analytical model and design

tool for reinforced roads. These experiments will also be used to evaluate instrument performance. This approach allows the research team to proceed through the same steps (i.e. design and construction of test sections, interpretation of results, development of an analytical model, development of a design tool) as those intended for use with field test sections, yet in an environment that is more controlled. This environment allows for the correction of unanticipated problems and the study of important variables influencing the problem. Perhaps most important, the research methodology can be throughly scrutinized prior to committing a large amount of funds to the construction of field test sections. The end product of this second phase will be a prototype design tool which will serve as the basis for the design tool ultimately developed for field loading conditions.

This revised Phase II should then be followed by the construction of field test sections (Phase III). Using the data generated in this phase, the model and design tool developed as part of Phase II would be extended to match field conditions. Two options exist for this approach. One option would be to construct field test sections along an existing or newly constructed section of roadway in Montana, as was planned for the original Phase II. A second option would be to construct "field" test sections at the U.S. Army Corp of Engineers Cold Regions Research and Engineering Laboratory (CRREL) in a state-of-the-art facility known as the Frost Effects Research Facility (FERF). Advantages to using the FERF include more controlled construction and loading conditions and a more controlled temperature and moisture environment. In addition, tests in the FERF could be performed more quickly and for less money. The product of Phase III would be a design tool which would match conditions experienced in the field. A possible Phase IV might be pursued, which would consist of the construction of uninstrumented demonstration test sections along various sections of roadway in Montana.

This new scope of work provides for a more segmented research approach allowing for changes in direction as phases of the project are completed. The original goal of the project (to provide MDT with a practical design tool) remains an integral part of each phase. This new approach is more sound than the previous approach and has a greater likelihood of success.

APPENDIX A
PHOTOGRAPHS

A color copy of Appendix A may be obtained from the Montana Department of Transportation, Research, Development and Technology Transfer program for the cost of reproduction.

APPENDIX A1
ELECTRONIC INSTRUMENTATION

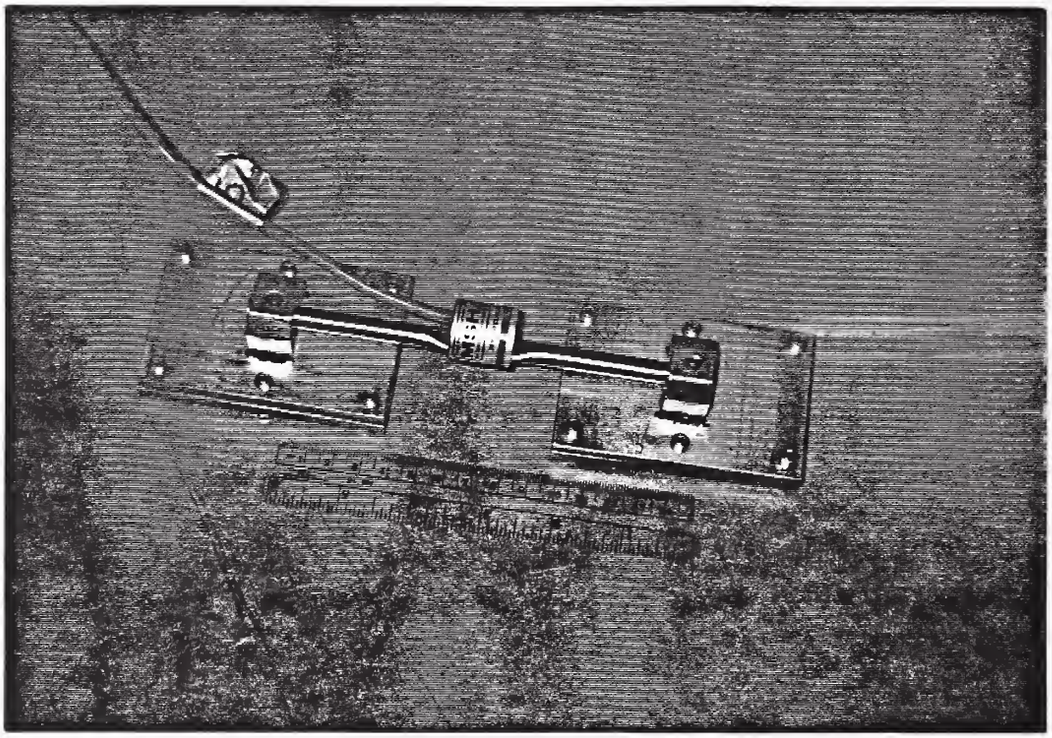

Figure A1.1: Vibrating Wire Strain Gage (Geokon Model VSM-4000)

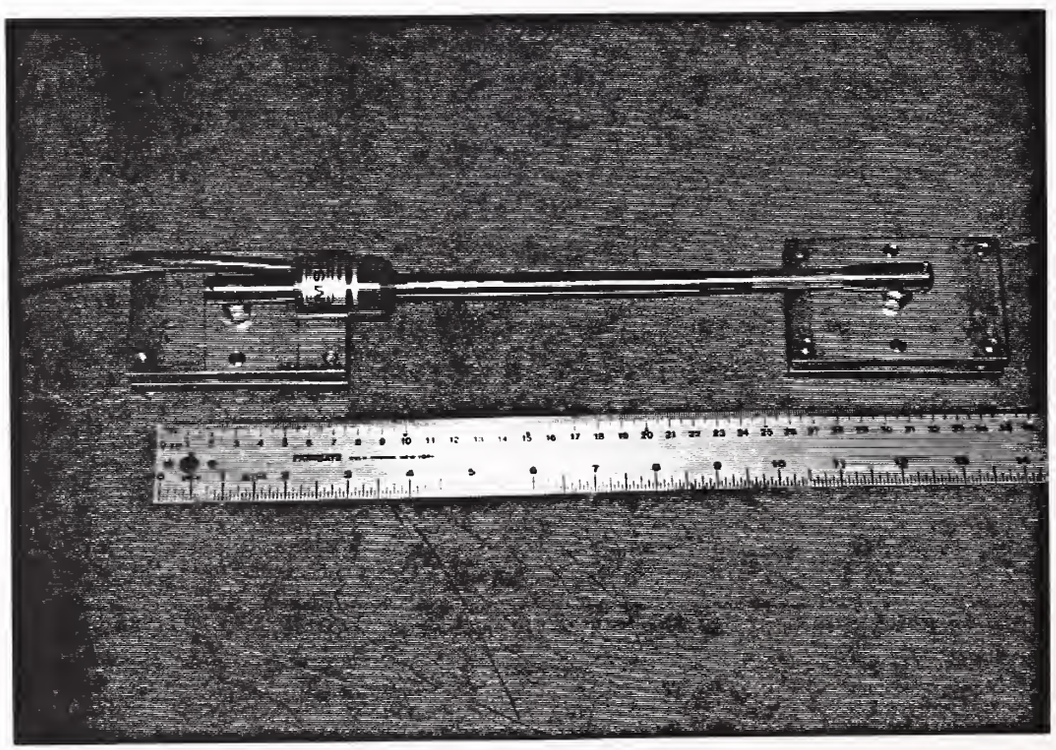

Figure A1.2:Vibrating Wire Displacement Gage (Geokon Model 4420)

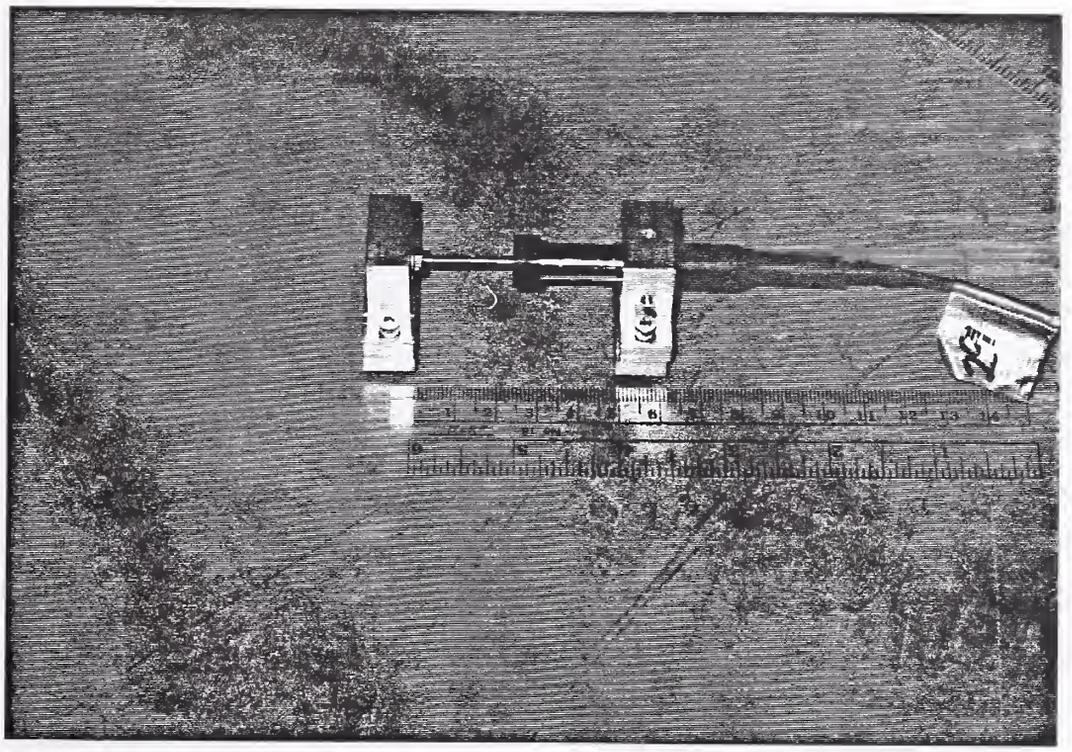

Figure A1.3: LVDT Displacement Gage (RDP Electronics Model D5/200W)

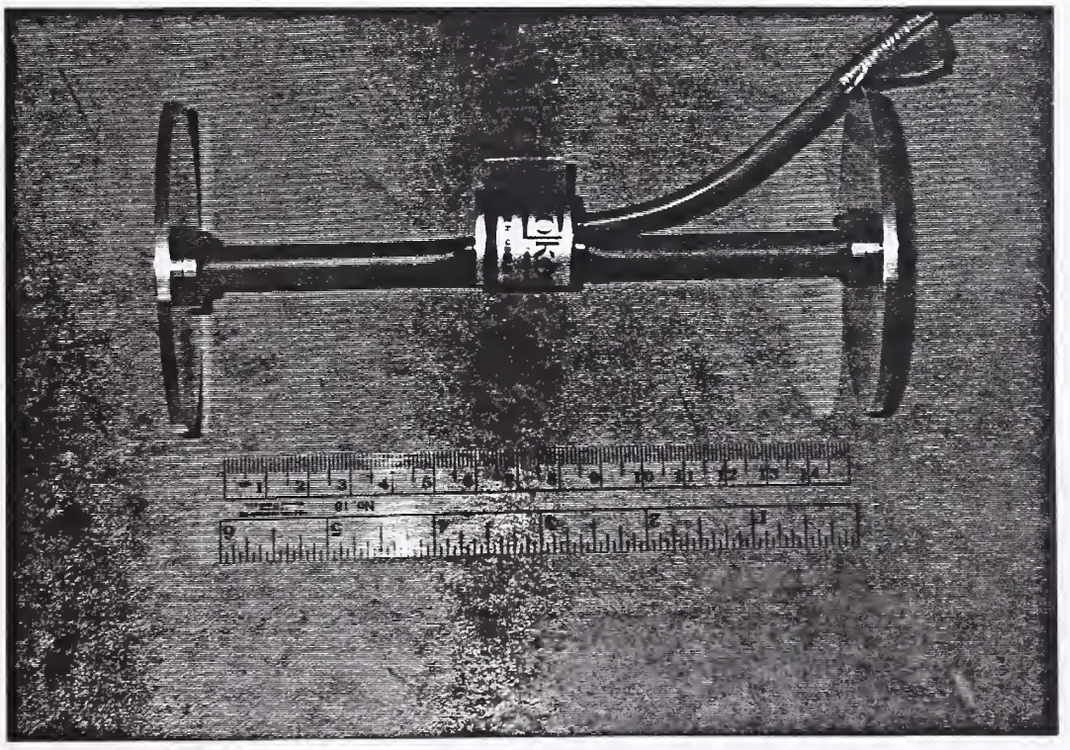

Figure A1.4: Vibrating Wire Embedment Strain Gage (Geokon Model VCE-4200)

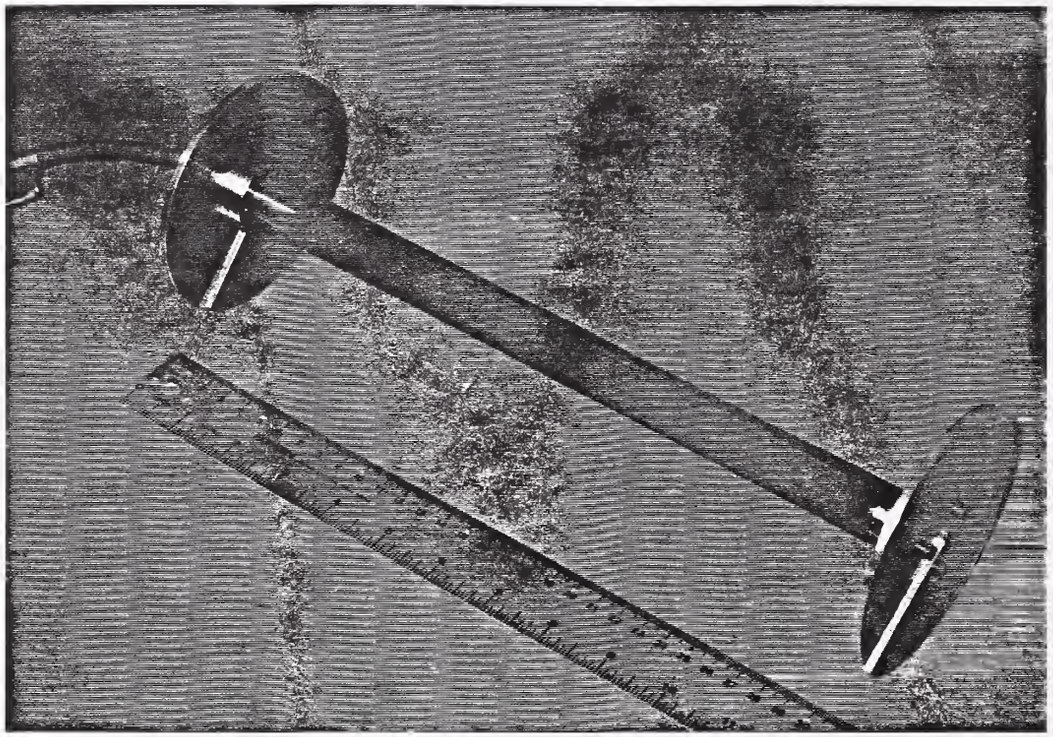

Figure A1.5: Vibrating Wire Embedment Displacement Gage (Geokon Model 4430)

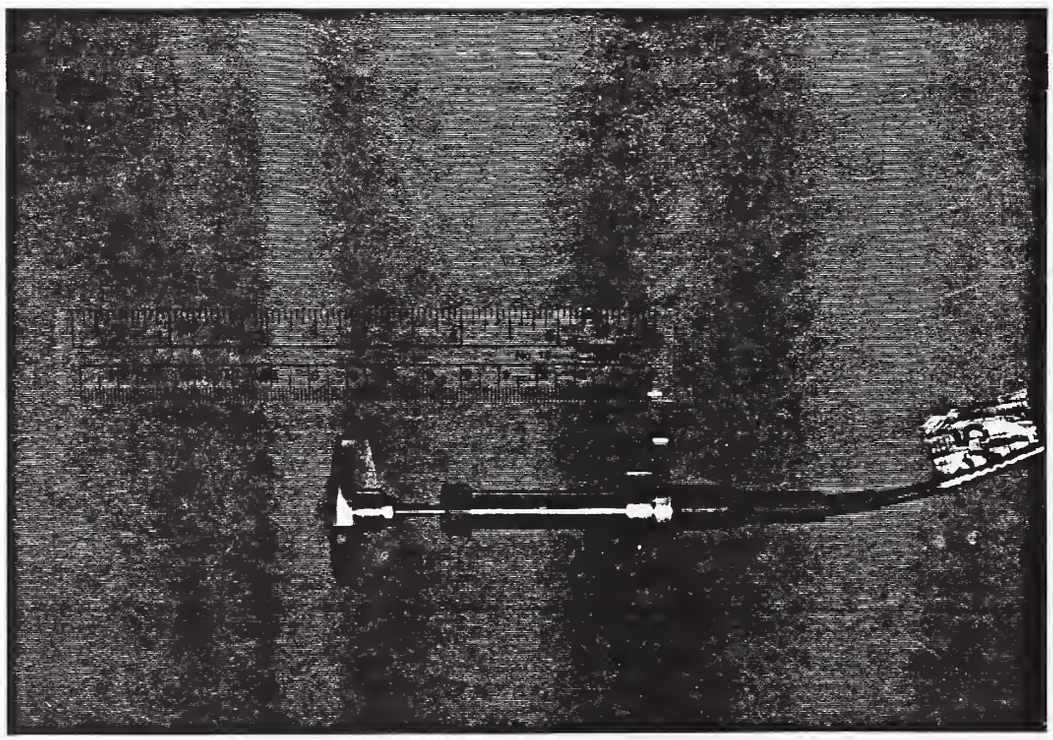

Figure A1.6: LVDT Embedment Displacement Gage (RDP Electronics Model D5/400W)

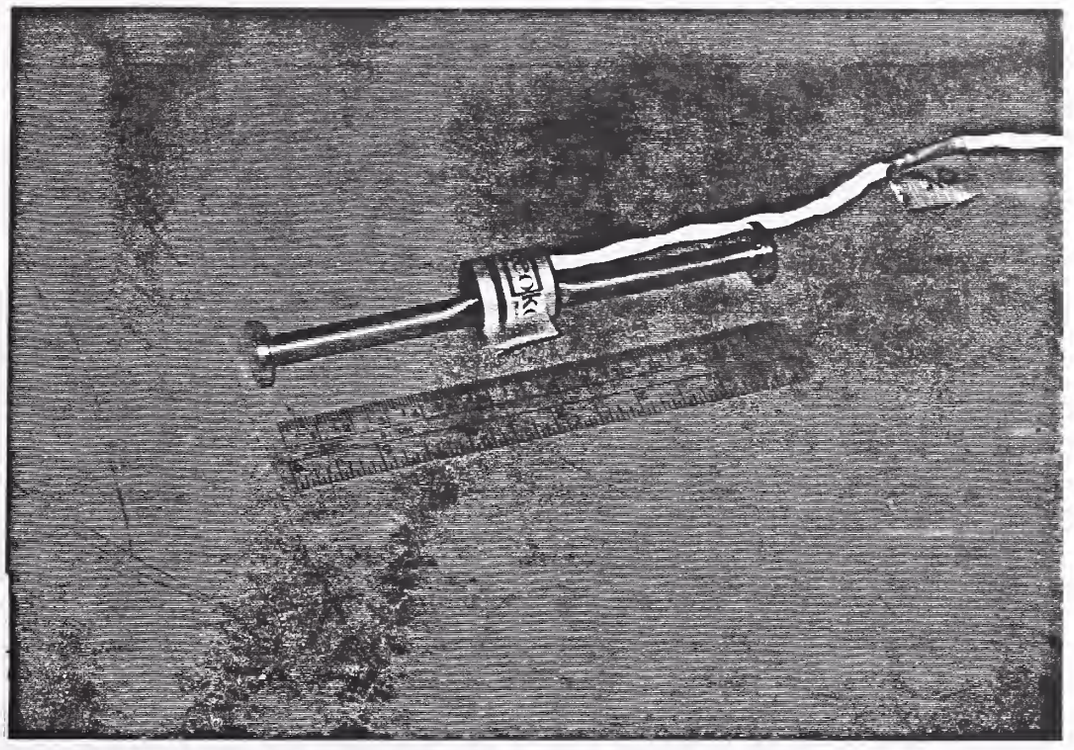

Figure A1.7: Vibrating Wire Embedment AC Strain Gage (Geokon Model VCE-4200-HT)

APPENDIX A2
IN-AIR TENSION TESTS-PHOTOGRAPHS

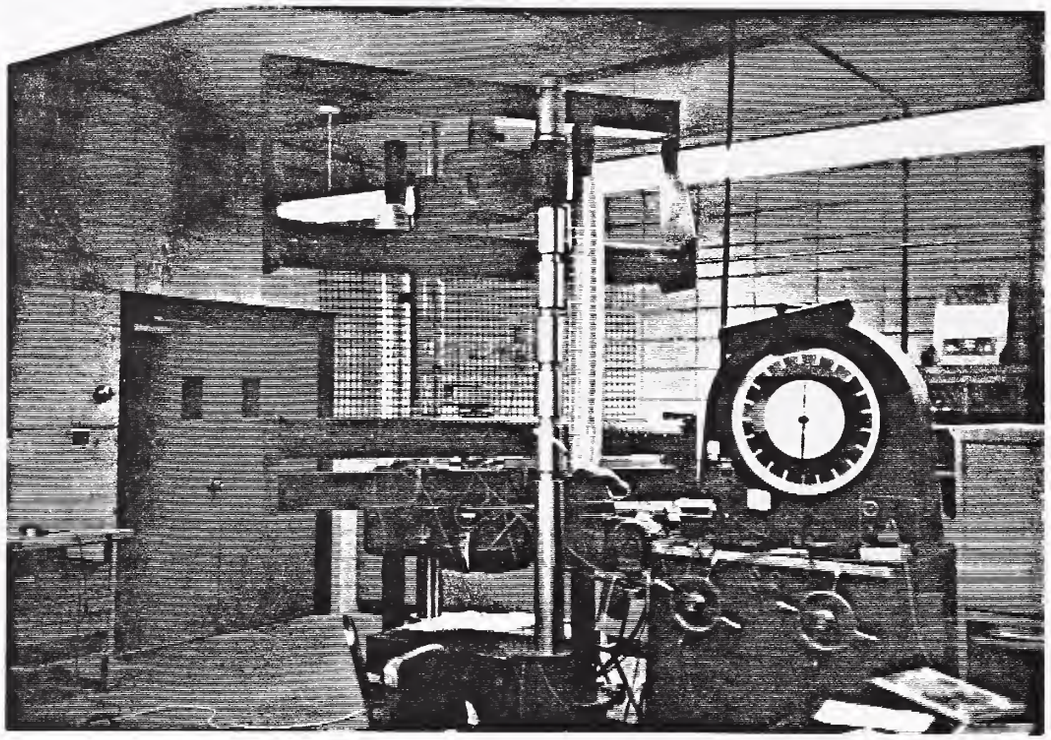

Figure A2.1: In-Air Tension Load Frame

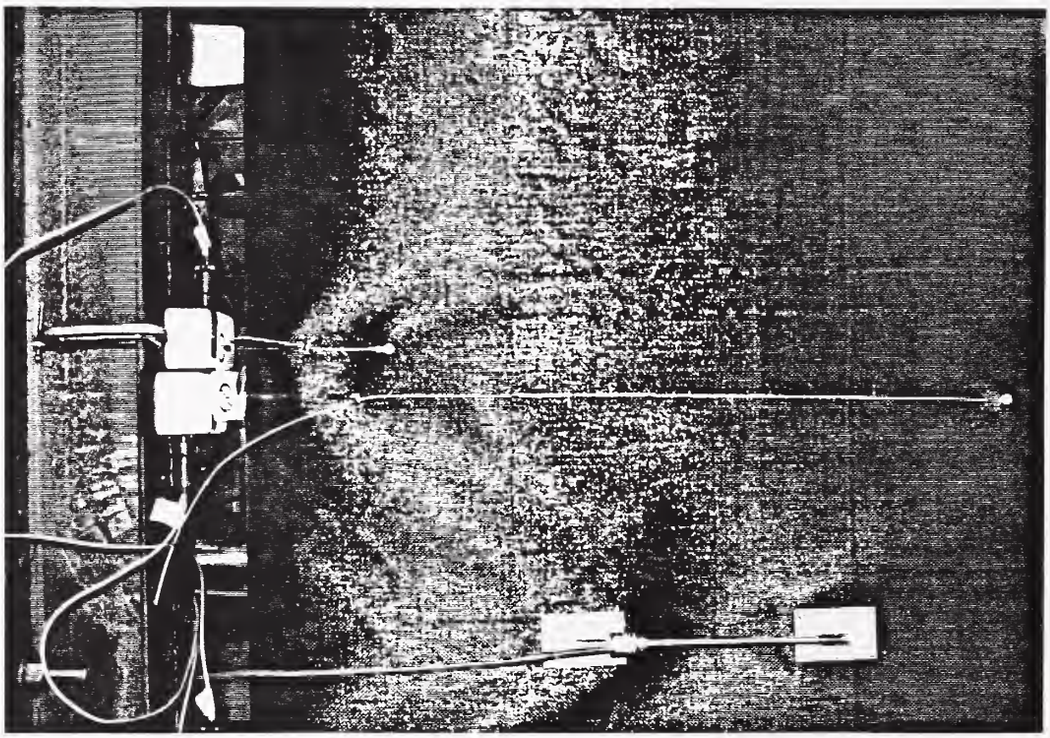

Figure A2.2: Displacement Transducers For Global Strain (Celesco Model PT-101)

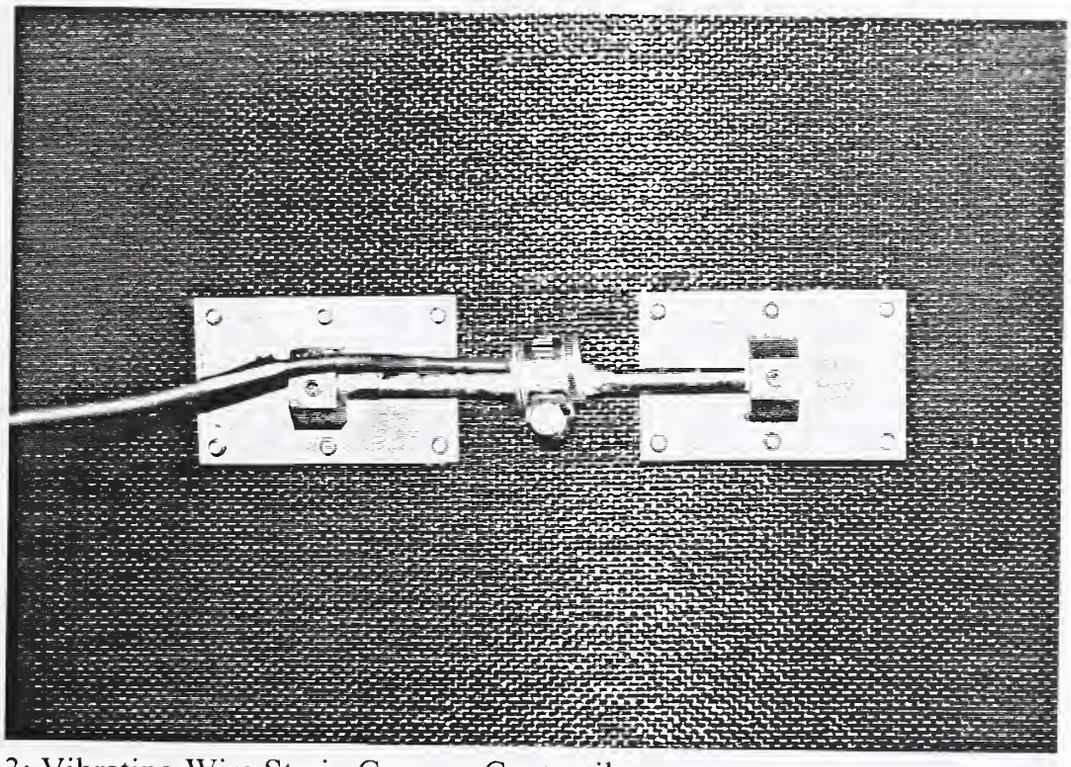

Figure A2.3: Vibrating Wire Strain Gage on Geotextile

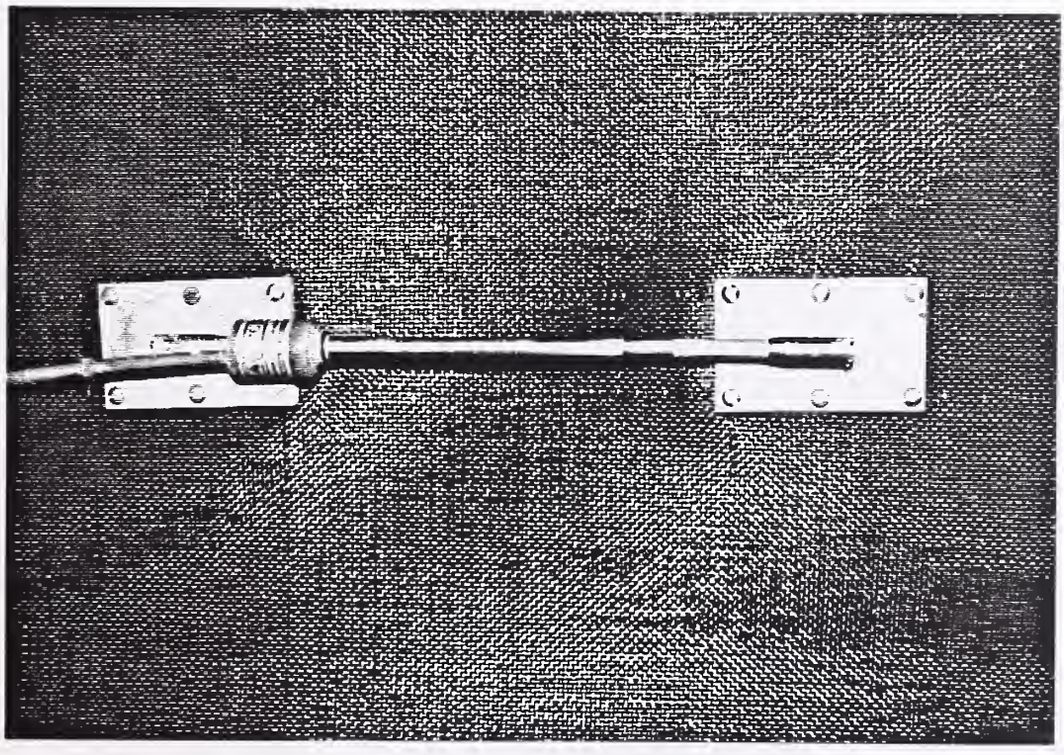

Figure A2.4: Vibrating Wire Displacement Gage on Geotextile

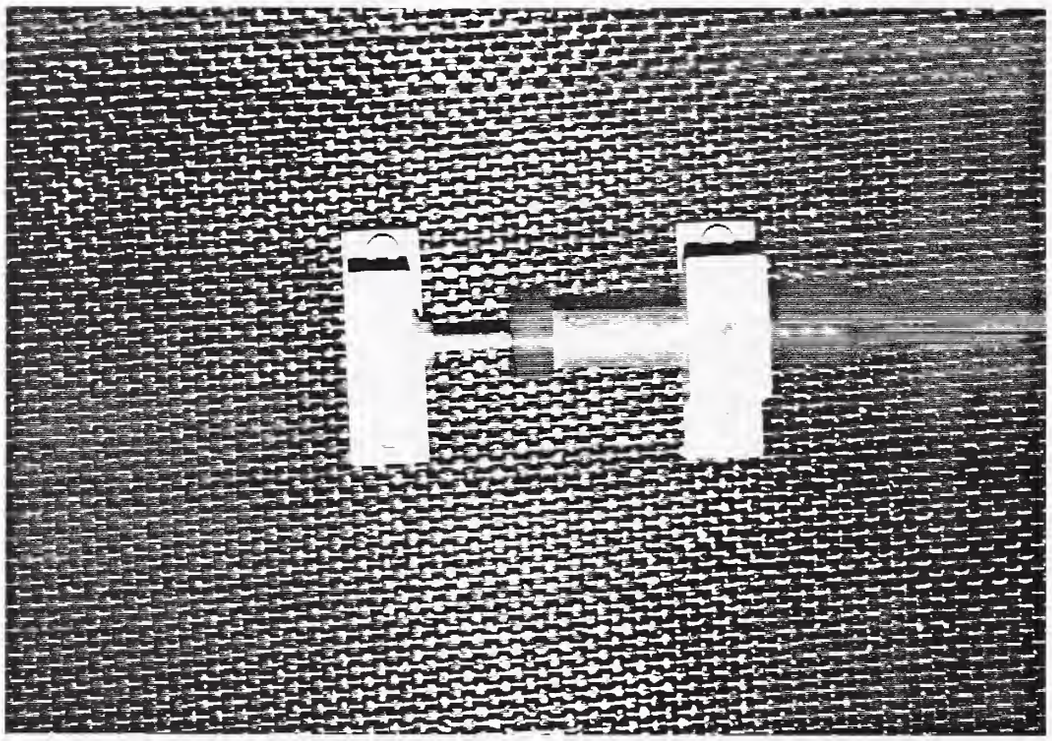

Figure A2.5: LVDT Displacement Gage on Geotextile

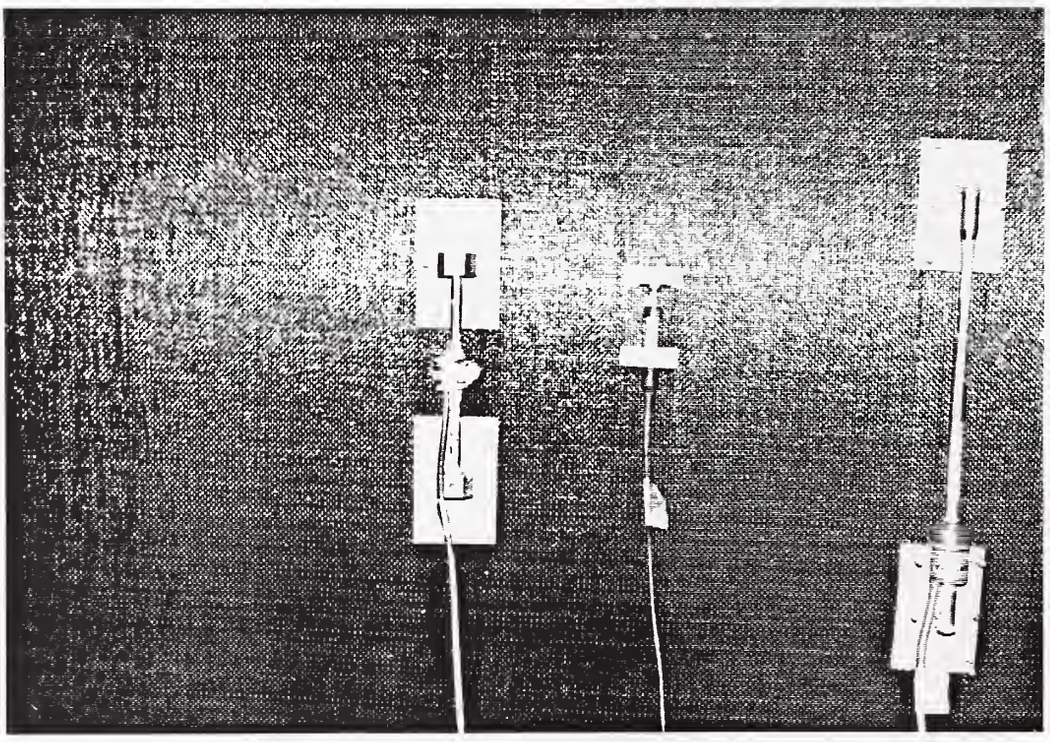

Figure A2.6: All Instruments on Geotextile

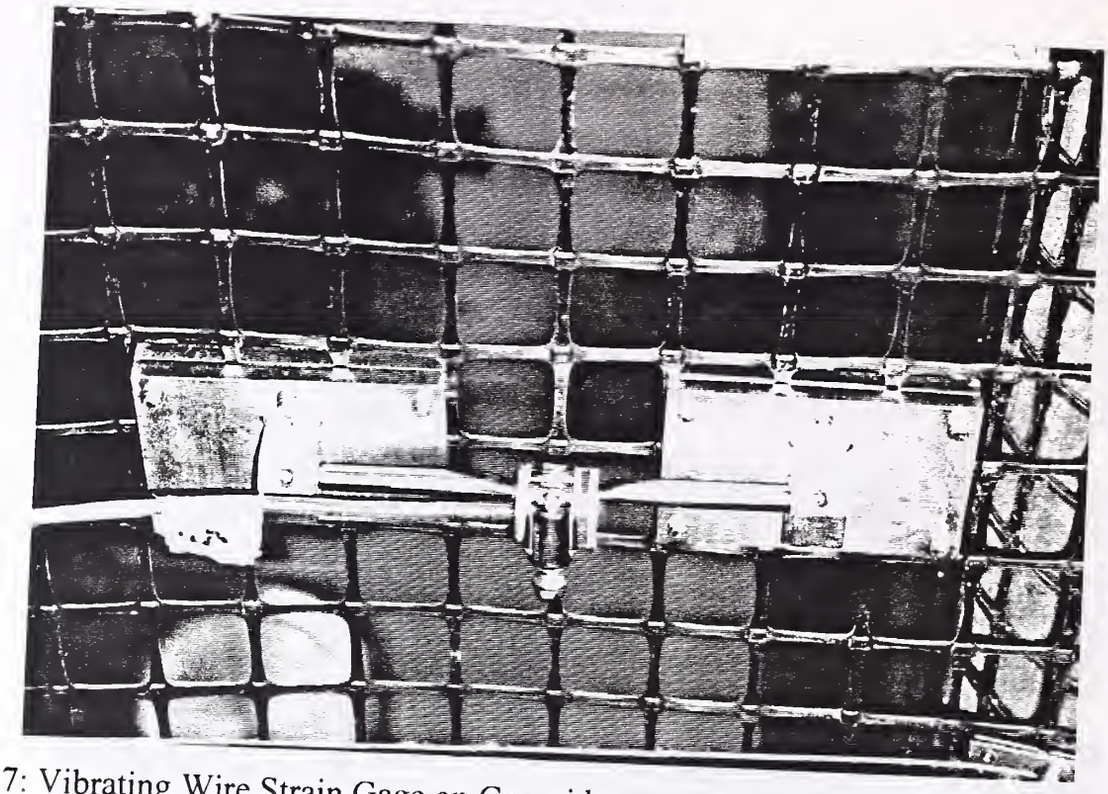

Figure A2.7: Vibrating Wire Strain Gage on Geogrid

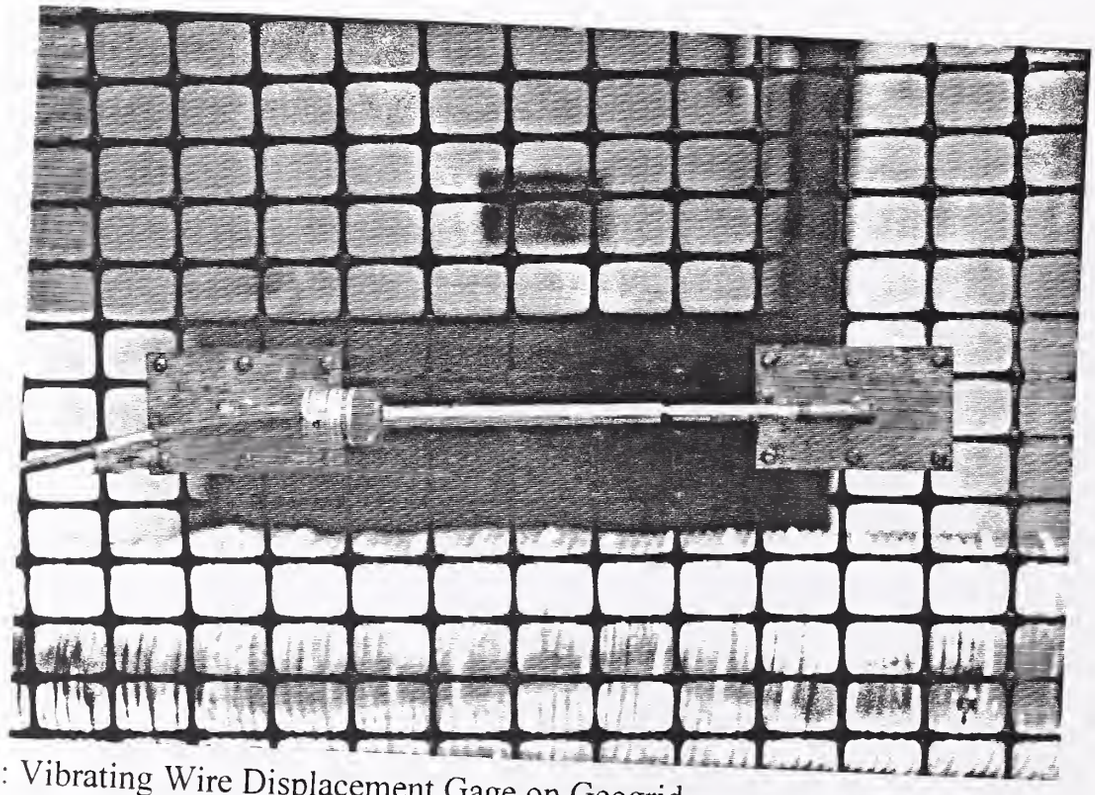

Figure A2.8: Vibrating Wire Displacement Gage on Geogrid

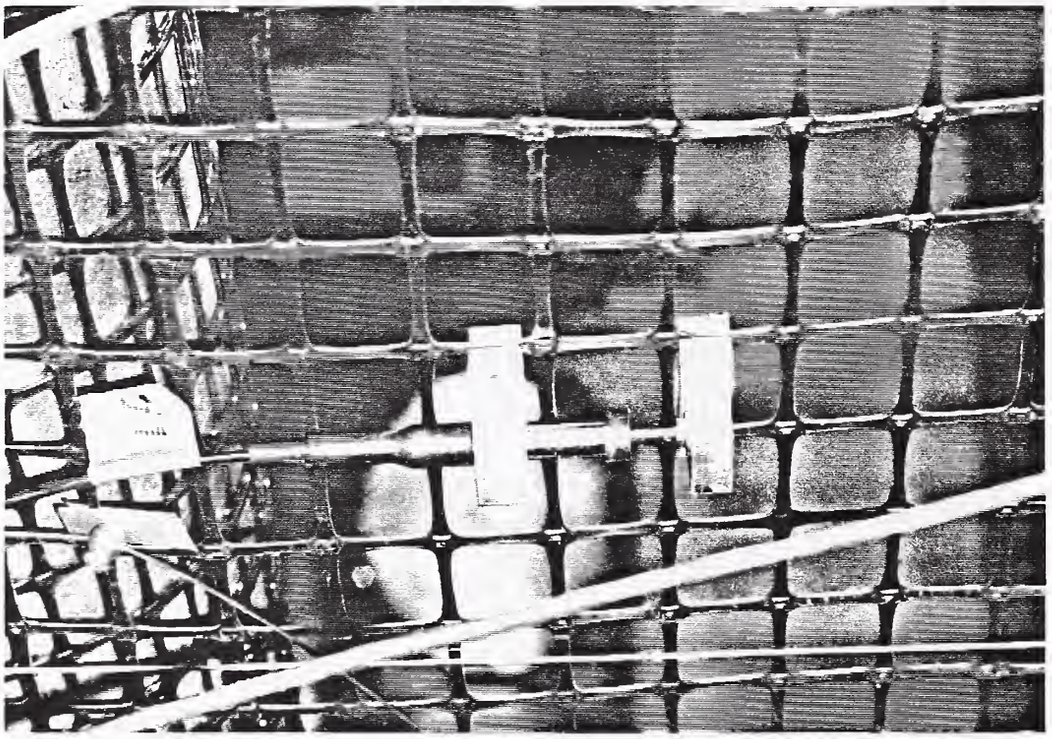

Figure A2.9: LVDT Displacement Gage on Geogrid

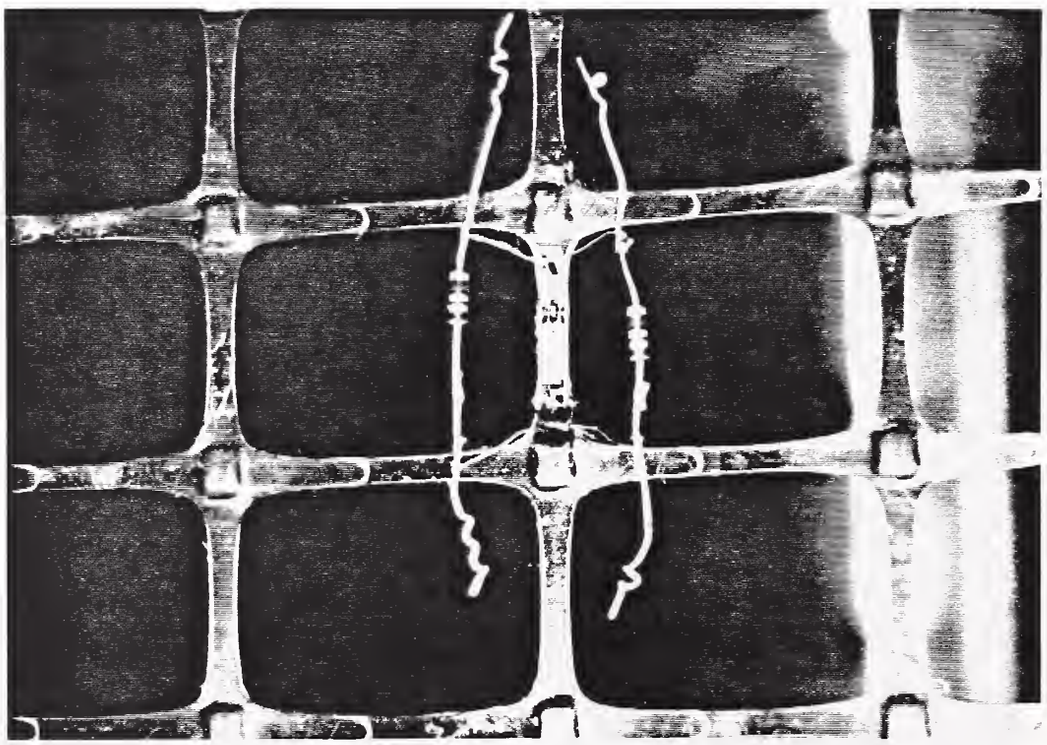

Figure A2.10: Foil Strain Gage on Geogrid

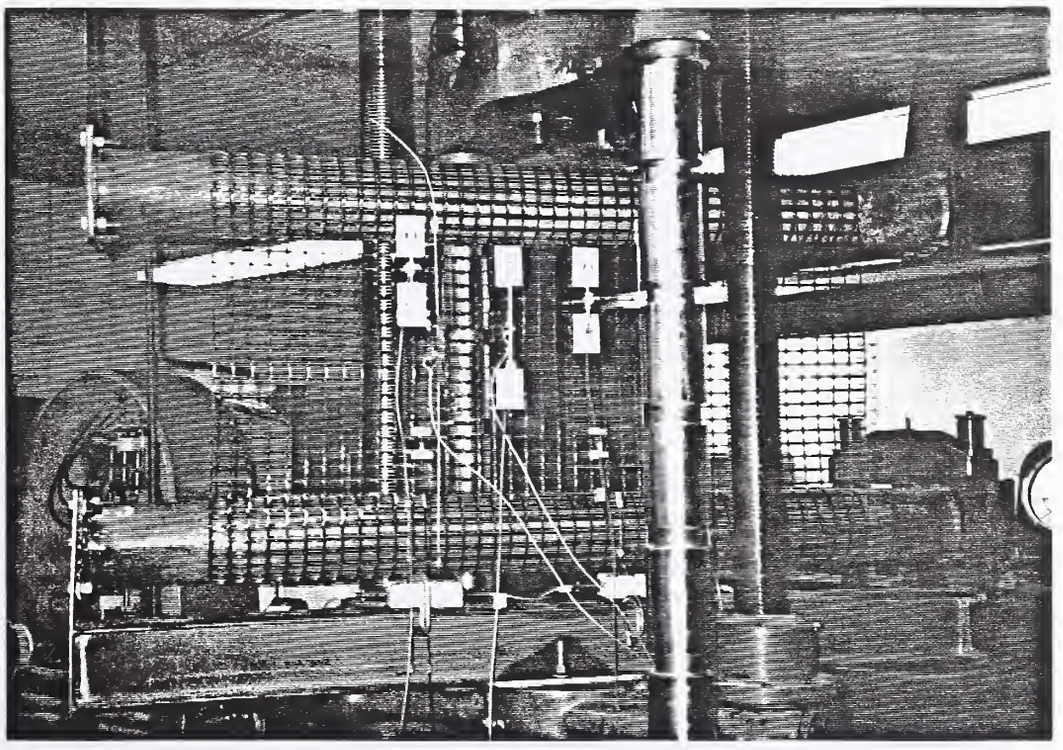

Figure A2.11: All Instruments on Geogrid

APPENDIX A3
TEST SECTION CONSTRUCTION

a)

b)

Figure A3.1: Excavated Test Section Prior to Placement of Geosynthetics, a) looking Northeast, b) looking Southwest.

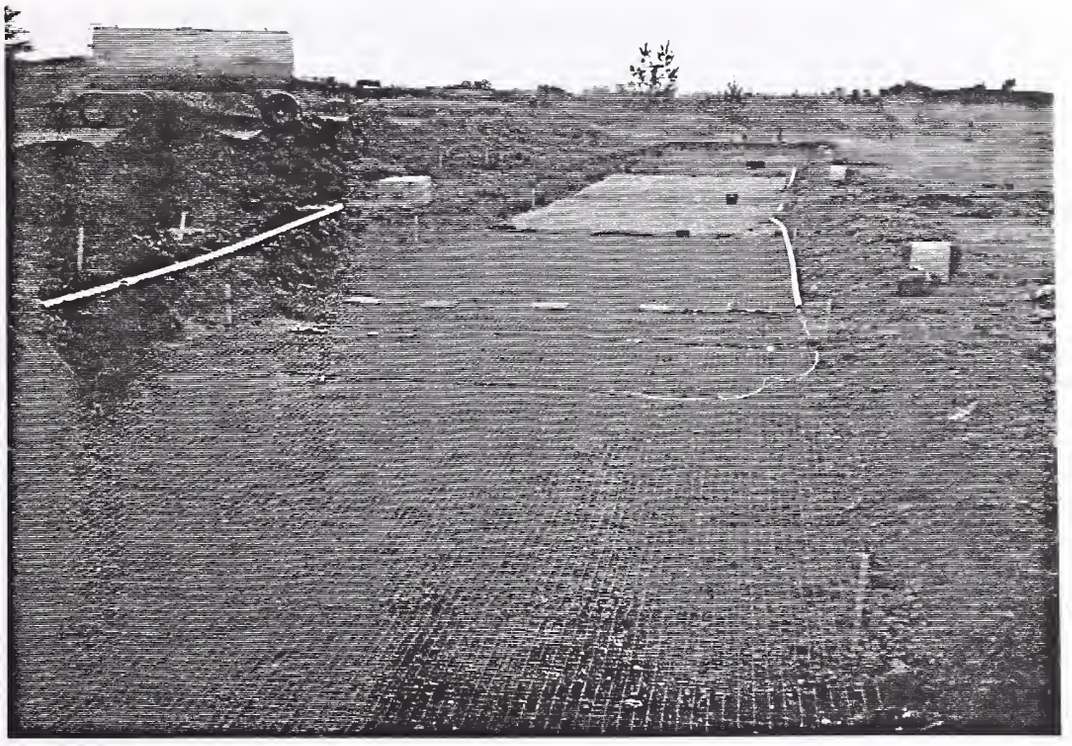

Figure A3.2: Test Section Showing Geogrid and Geotextile Prior to Placement of Base Course

Figure A3.3: Placement of Base Course

Figure A3.4: Test Section After Placement of Base and Prior to Compaction

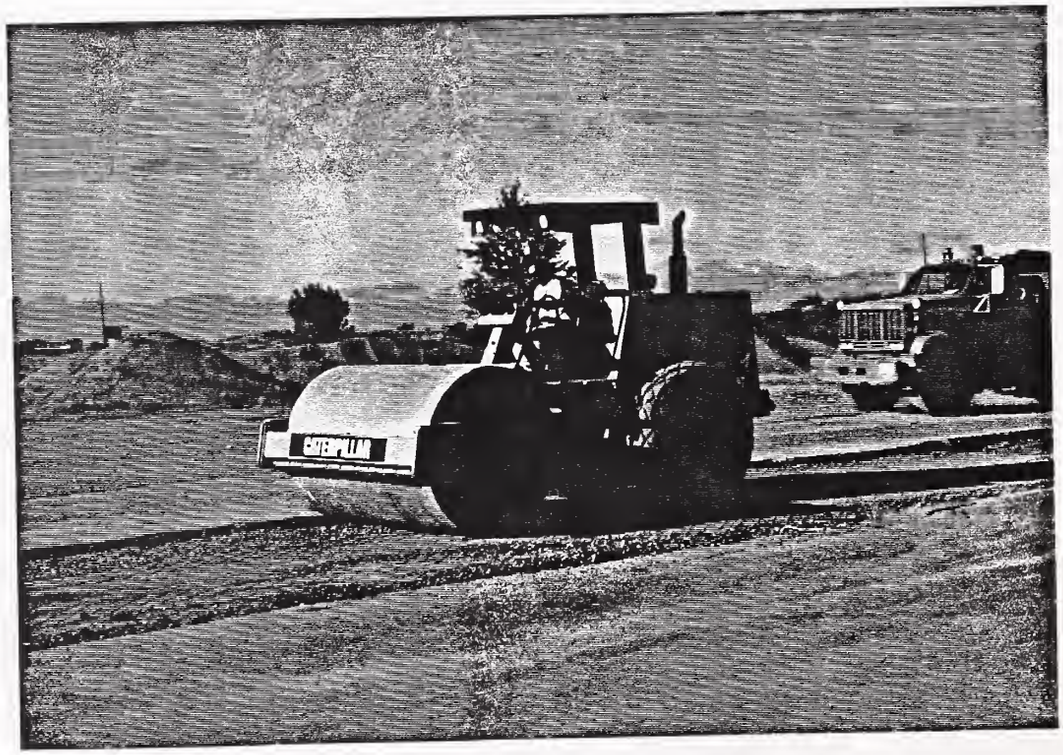

Figure A3.5: Final Grading and Compaction of Base Course

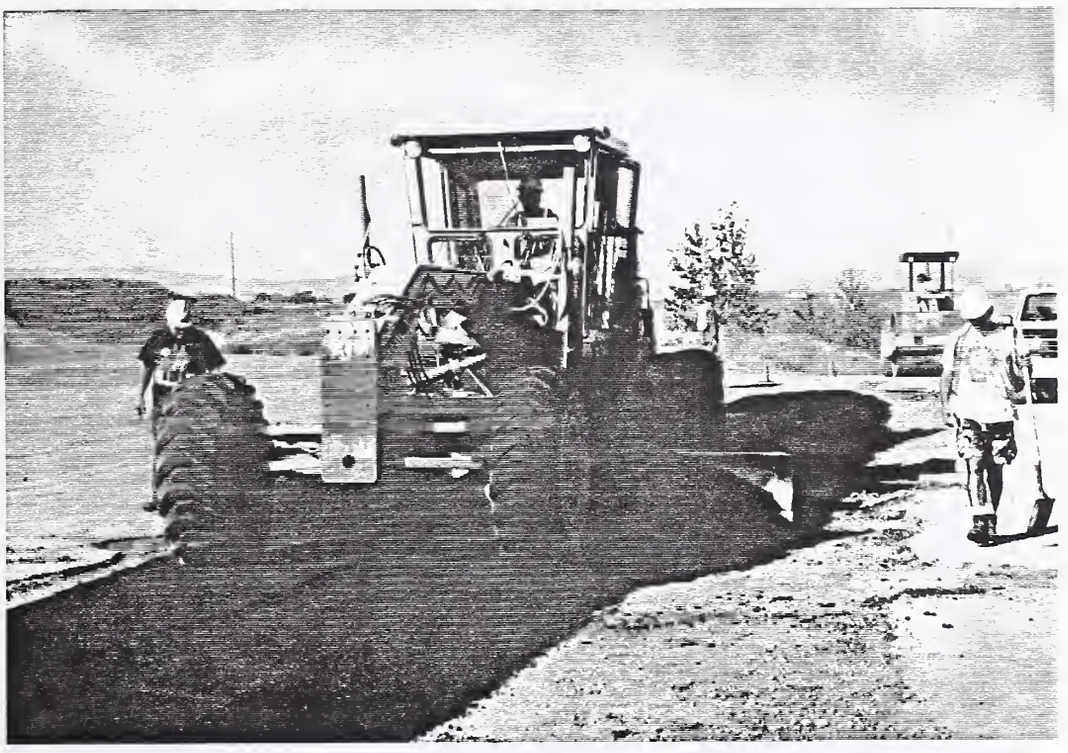

Figure A3.6: Spreading of Asphalt

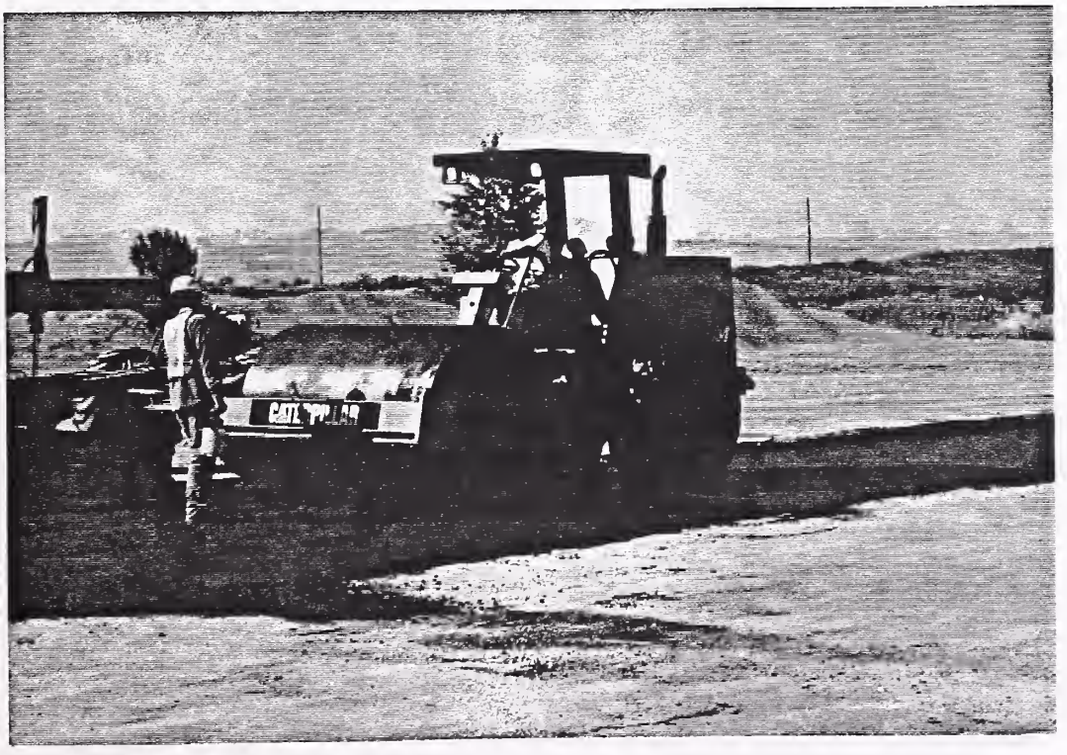

Figure A3.7: Compaction of Asphalt

APPENDIX A4
INSTRUMENTATION INSTALLATION

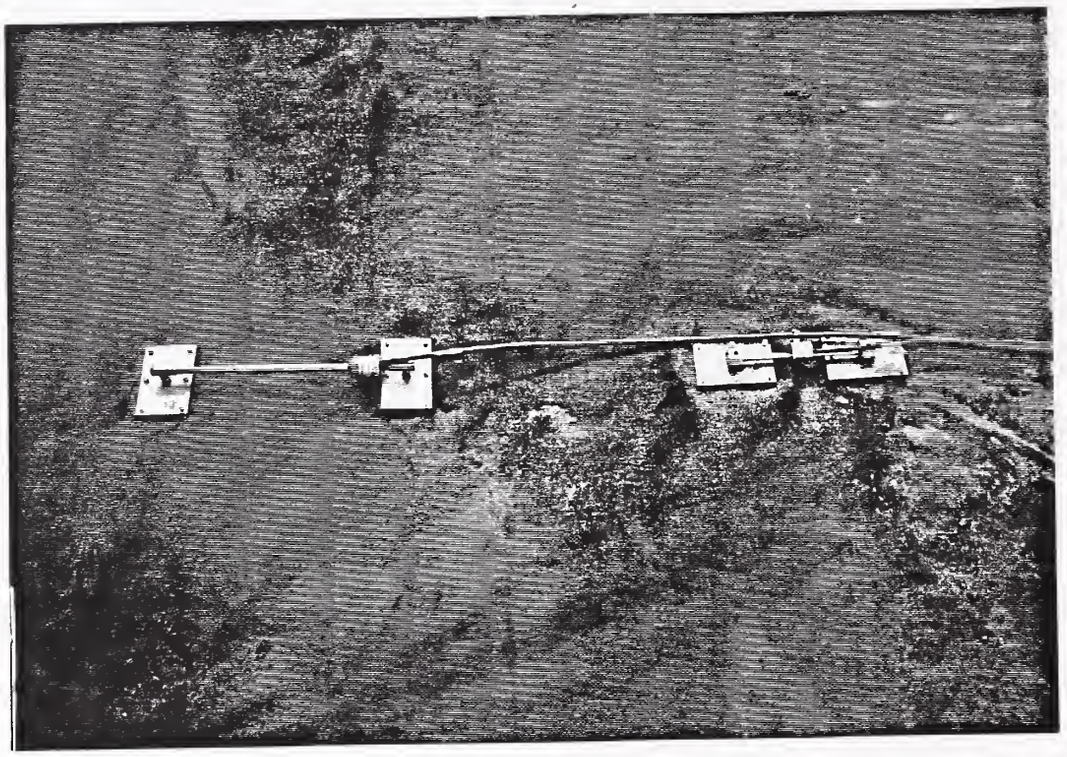

Figure A4.1: VW Displacement and VW Strain Gages Attached to Geotextile

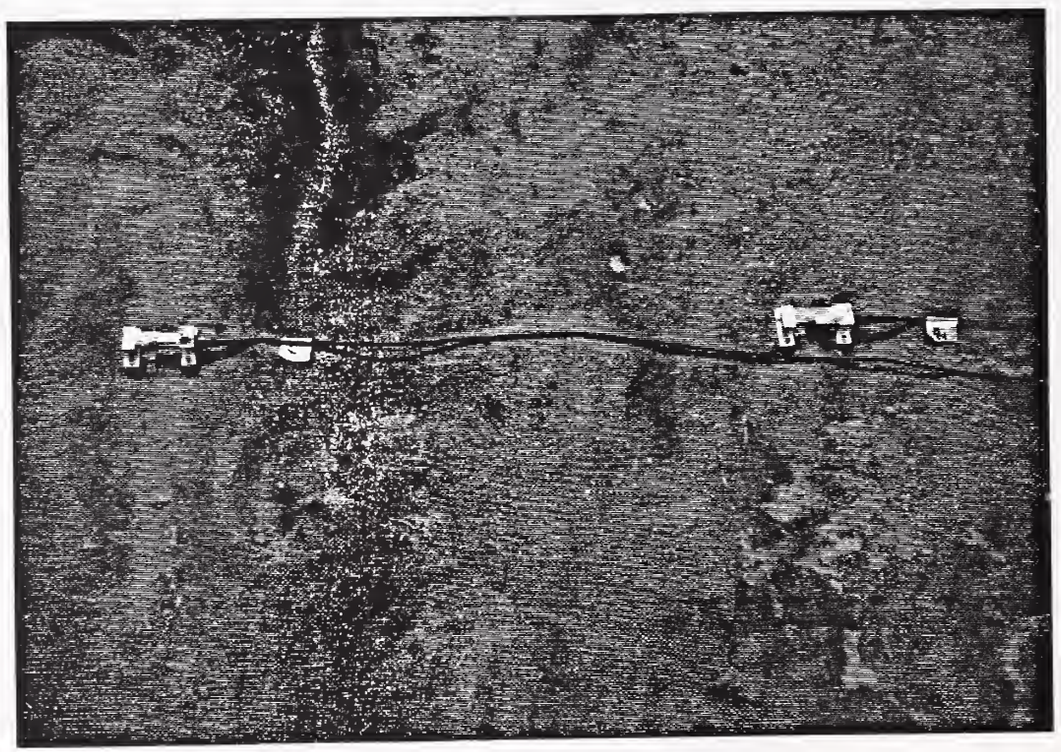

Figure A4.2: LVDT Displacement Gages Attached to Geotextile

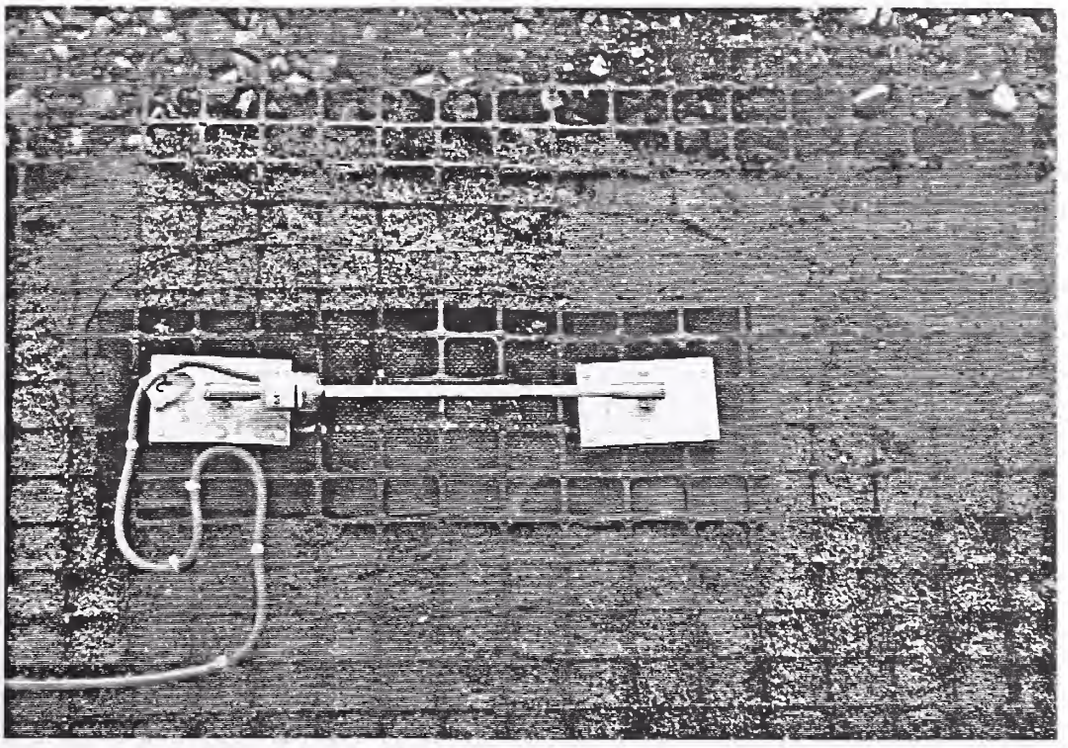

Figure A4.3: VW Displacement Gage Attached to Geogrid

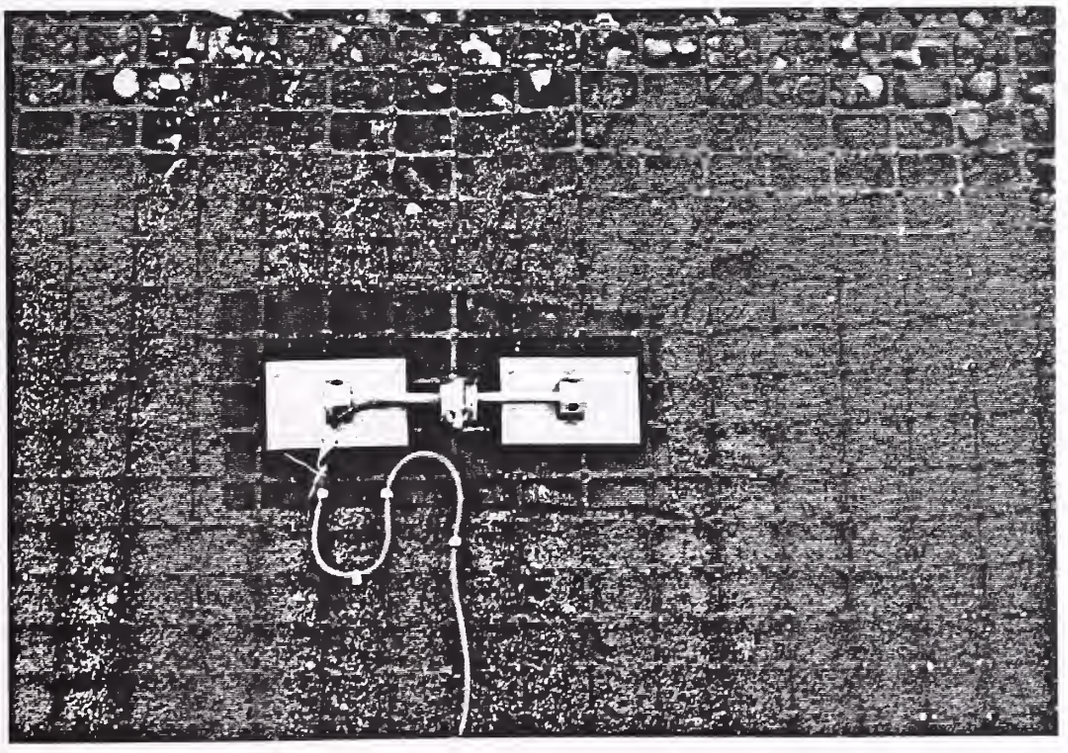

Figure A4.4: VW Strain Gage Attached to Geogrid

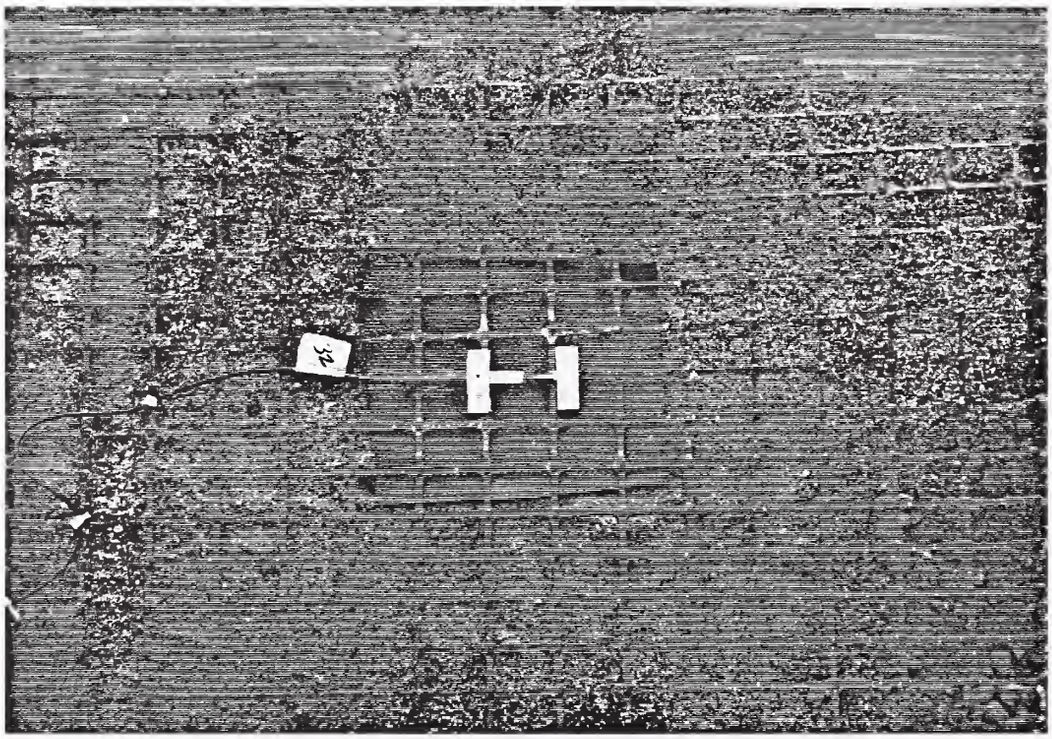

Figure A4.5: LVDT Displacement Gage Attached to Geogrid

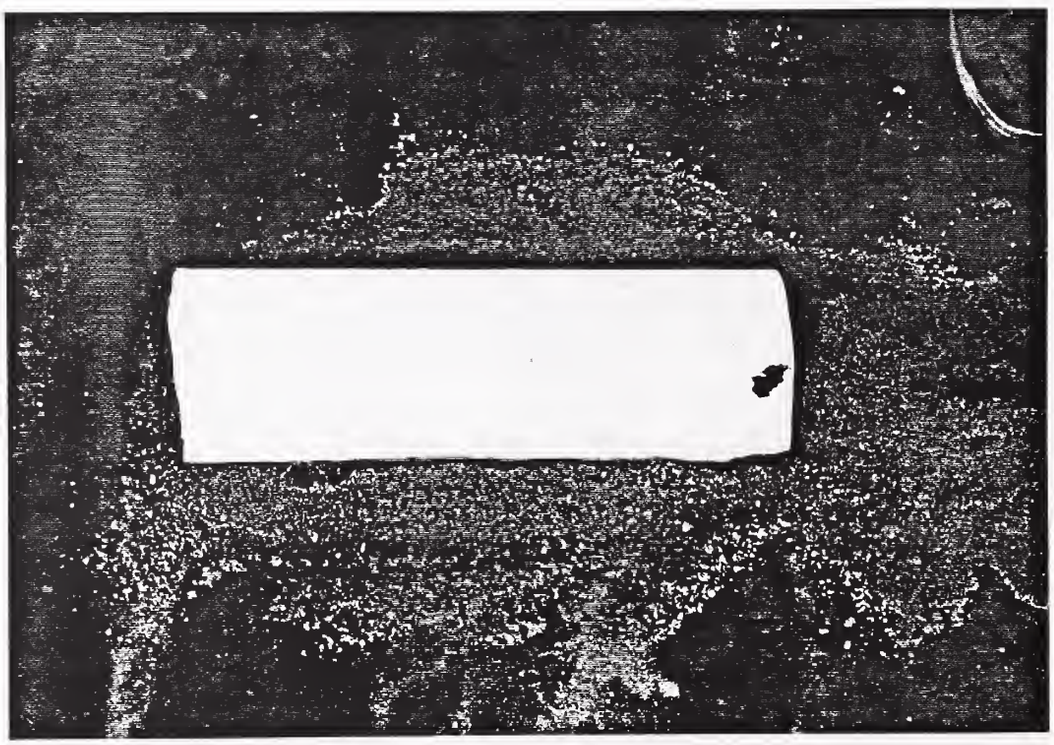

Figure A4.6: Half PVC Pipe With No Interior Sand Cover Option

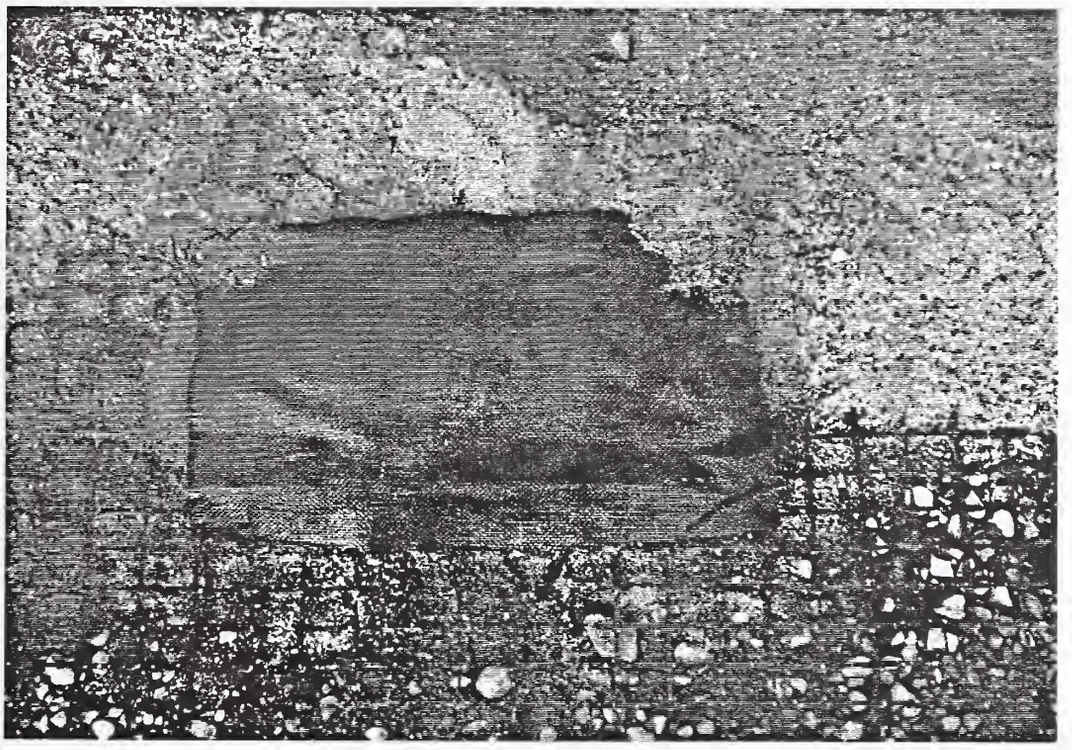

Figure A4.7: Sand and Geotextile Cover Option

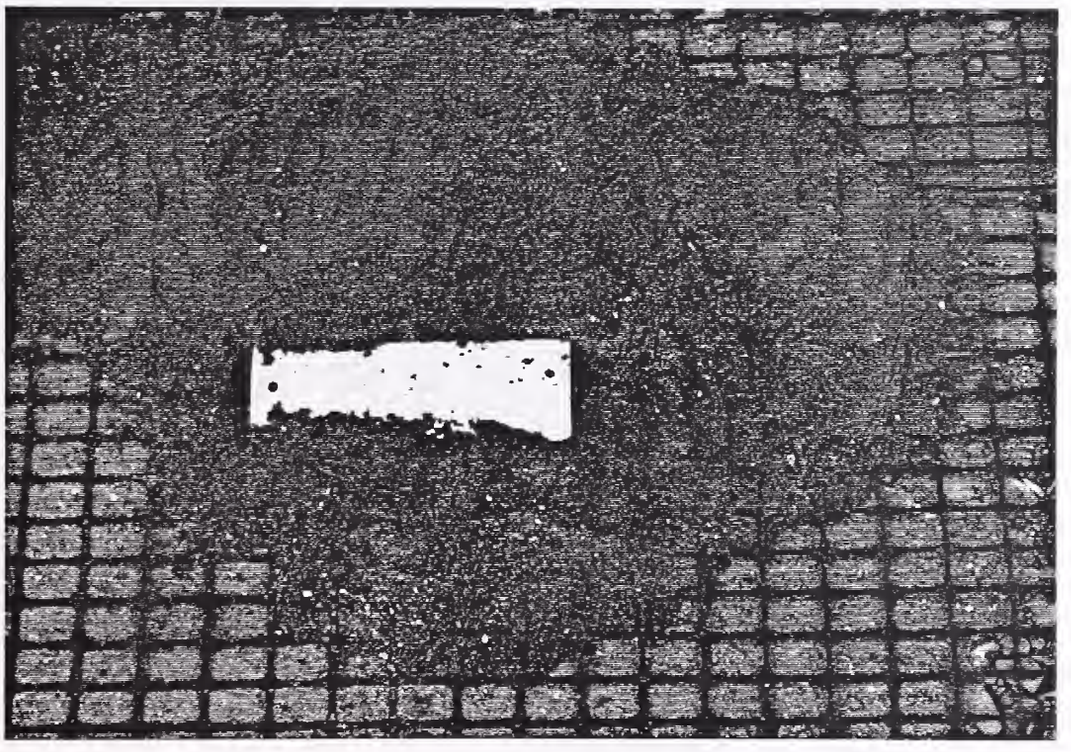

Figure A4.8: Half PVC Pipe With Interior Sand Cover Option

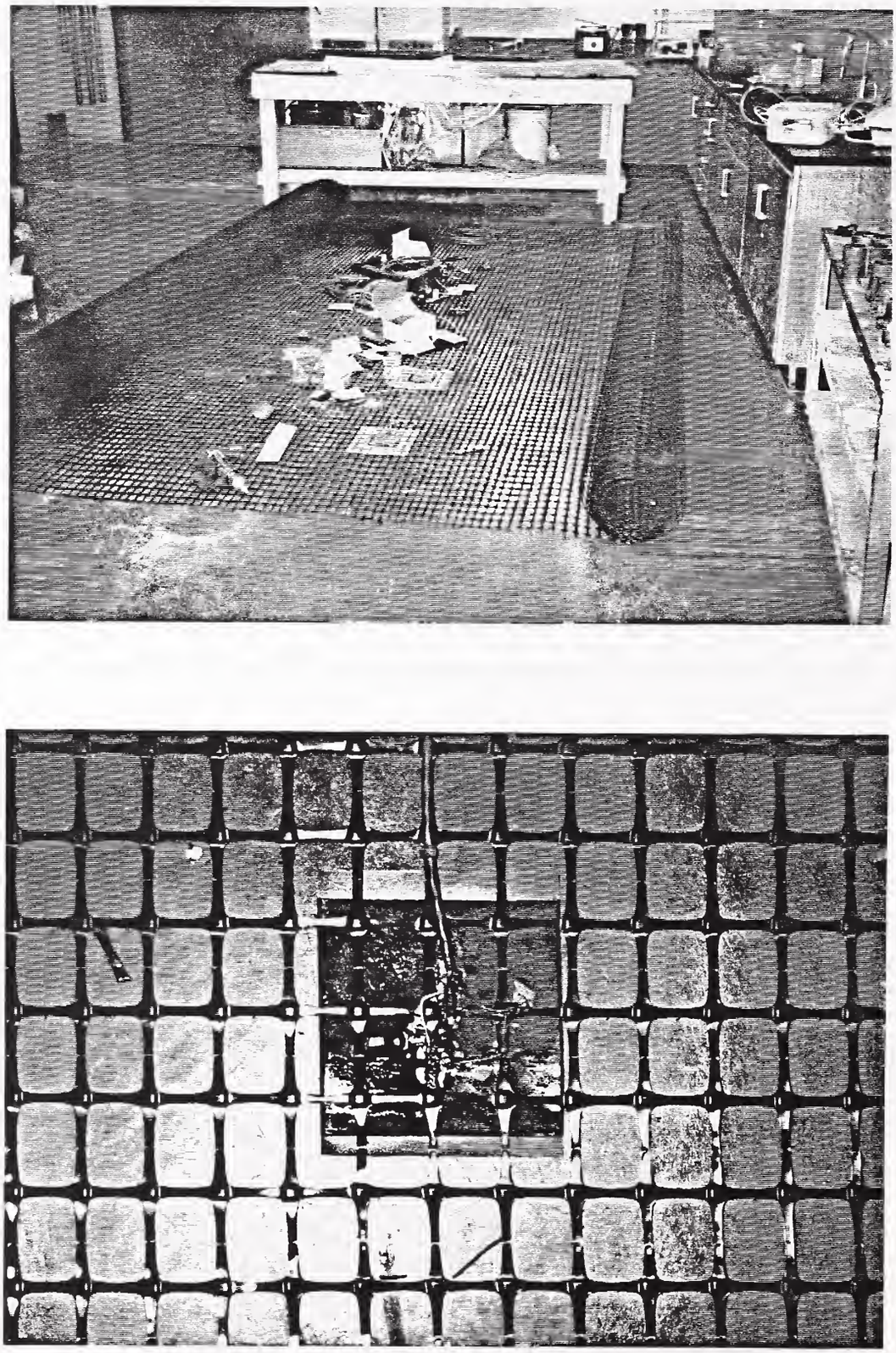

Figure A4.9: Protective Covers for Foil Strain Gages (first 2 of 3 photos)

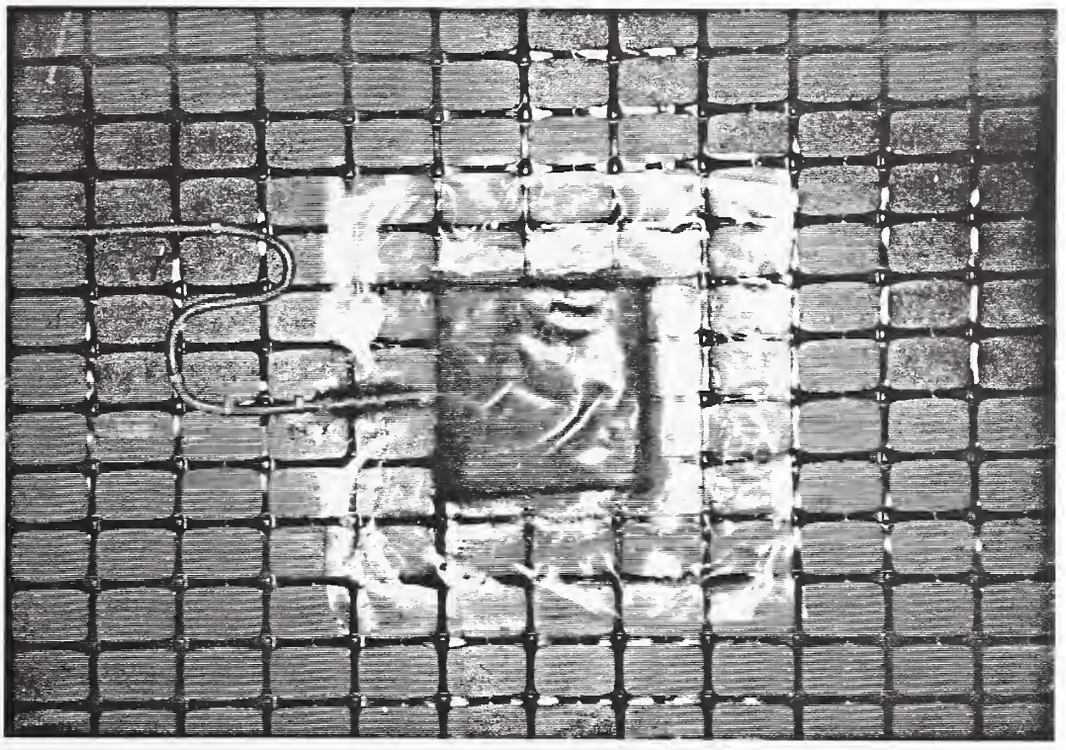

Figure A4.9: Protective Covers for Foil Strain Gages (third of 3 photos)

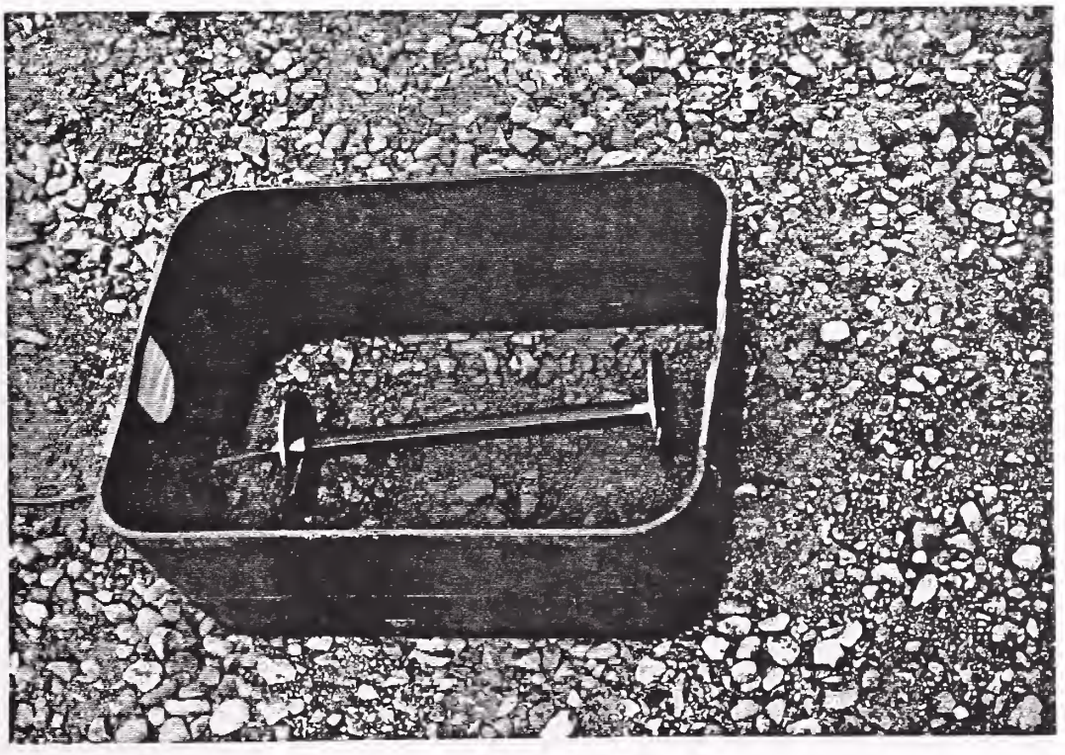

Figure A4.10: Temporary Protection Box for VW Embedment Displacement Gage

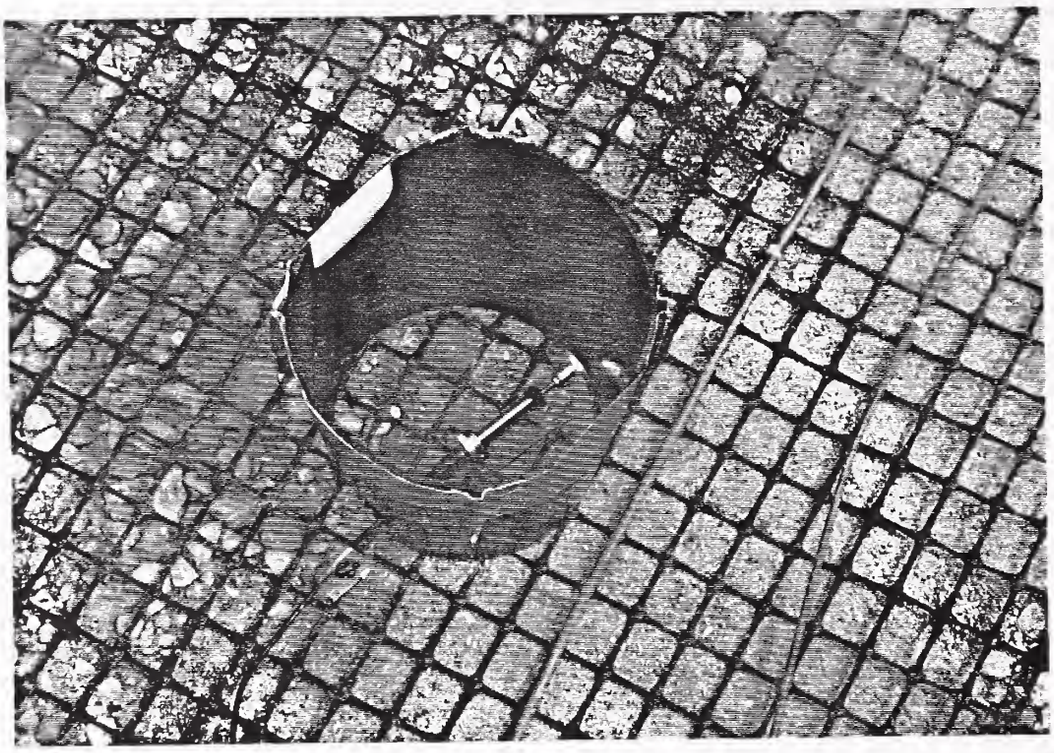

Figure A4.11: Temporary Protection Container for LVDT Embedment Displacement Gage

Figure A4.12: Temporary Protection Container for VW Embedment Strain Gage

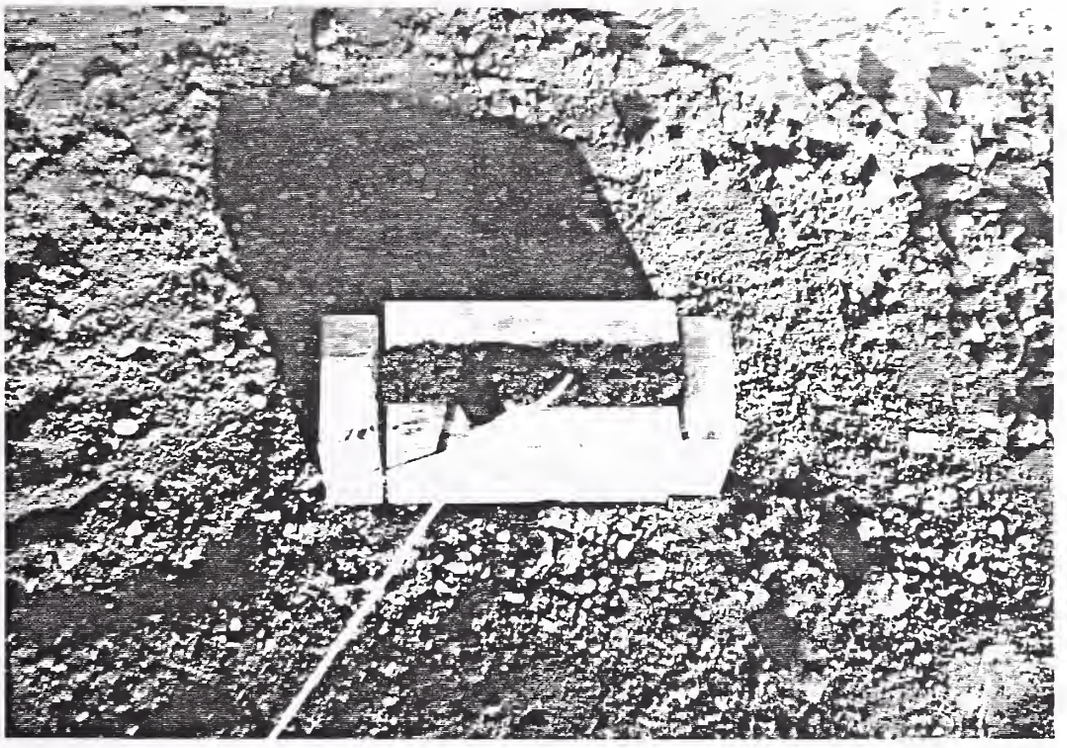

Figure A4.13: Precompaction of VW Embedment AC Strain Gage

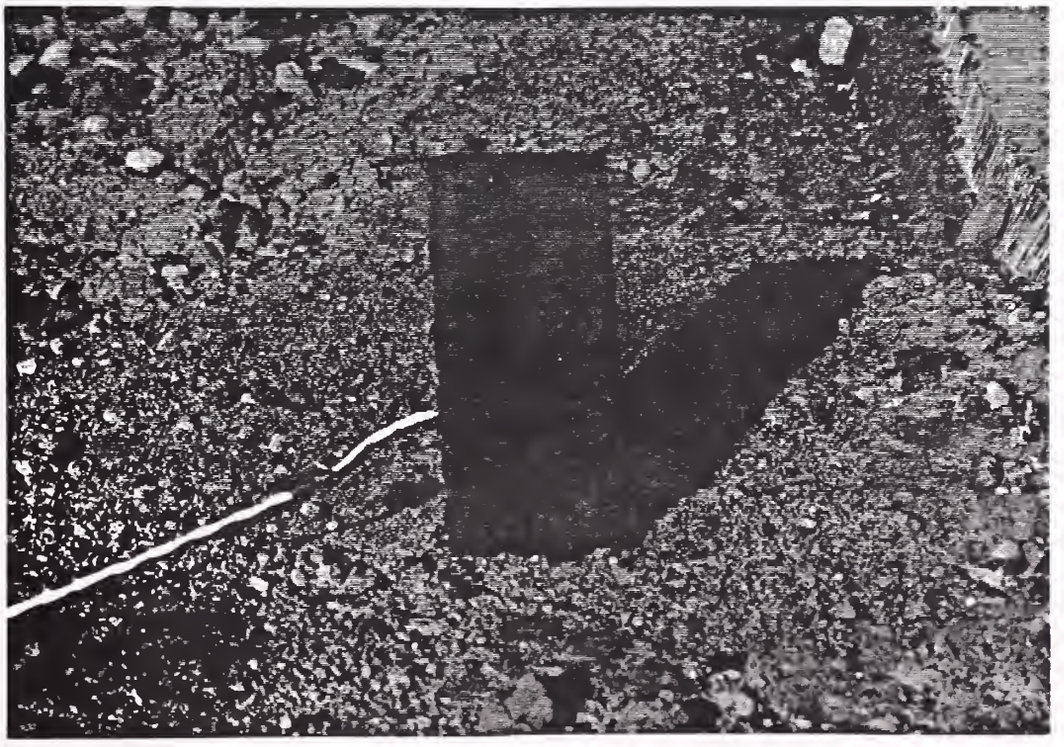

Figure A4.14: Cooled AC Brick With VW Embedment AC Strain Gage

APPENDIX A5
TRUCK PASS TEST VEHICLES

Figure A5.1: Belly Dump Truck

Figure A5.2: Single Unit Truck With Pup Trailer

APPENDIX B
IN-AIR TENSION TEST FIGURES

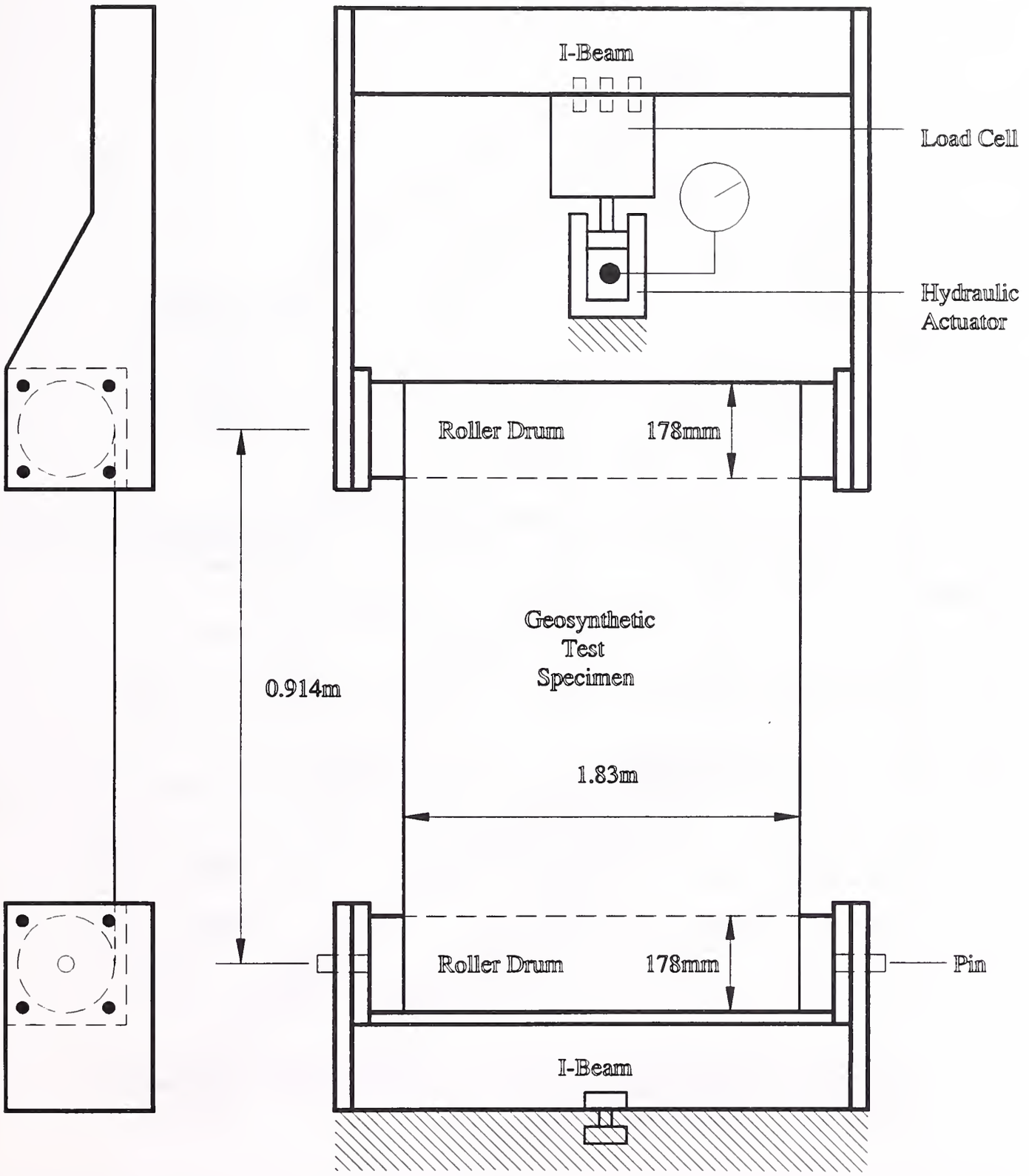

Figure B1: Schematic of In-Air Tension Load Frame

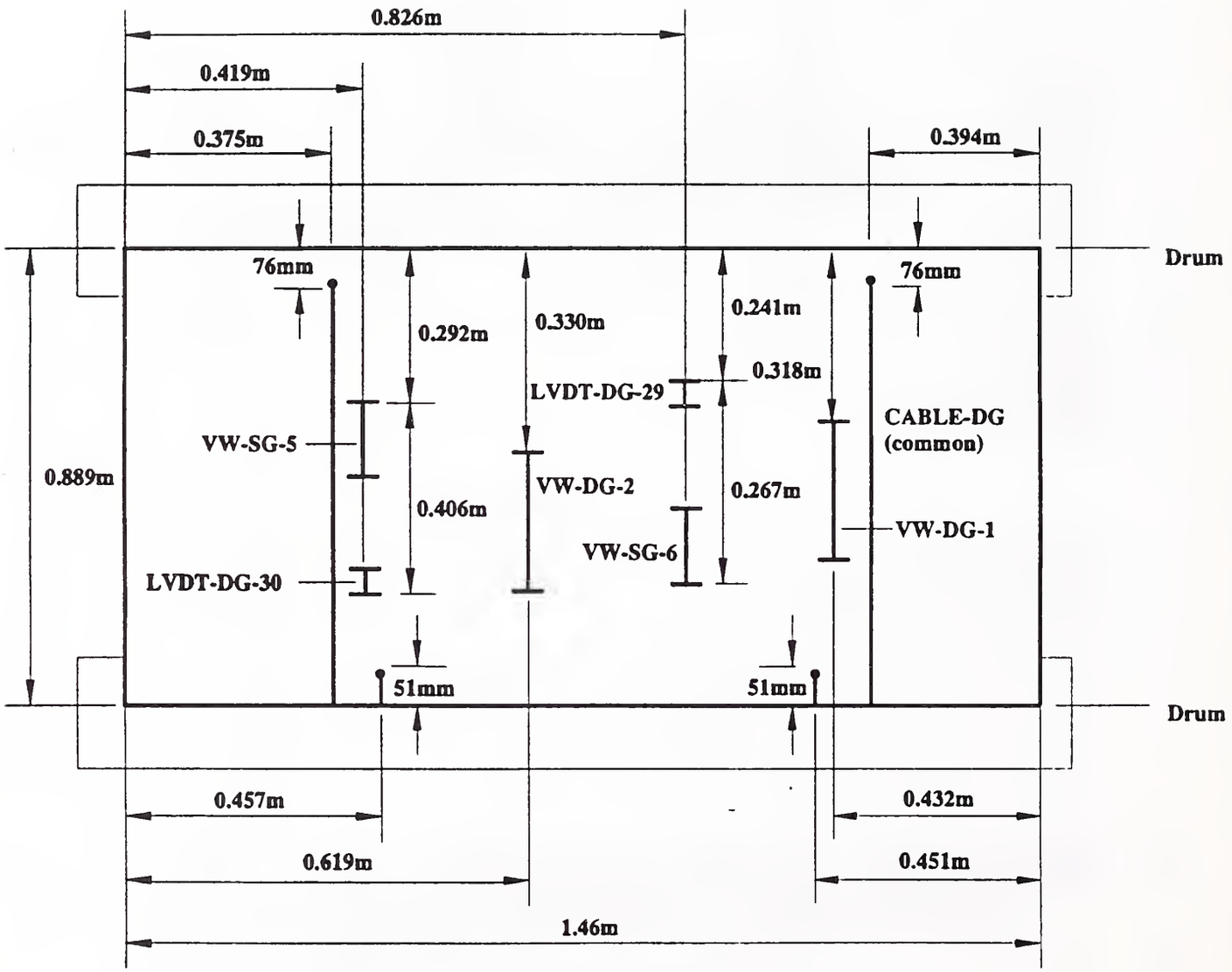

Figure B2: Dimensional Placement of Instruments on a Geosynthetic Specimen

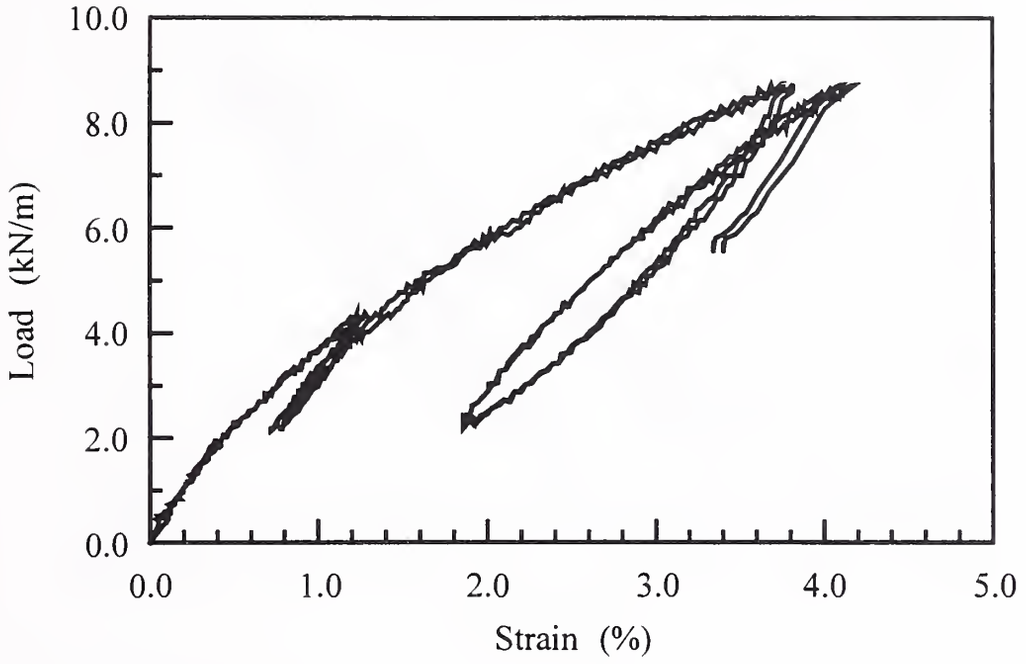

Figure B3: Global Strain From Two Sets of Celesco Gages: Geogrid, Machine Direction

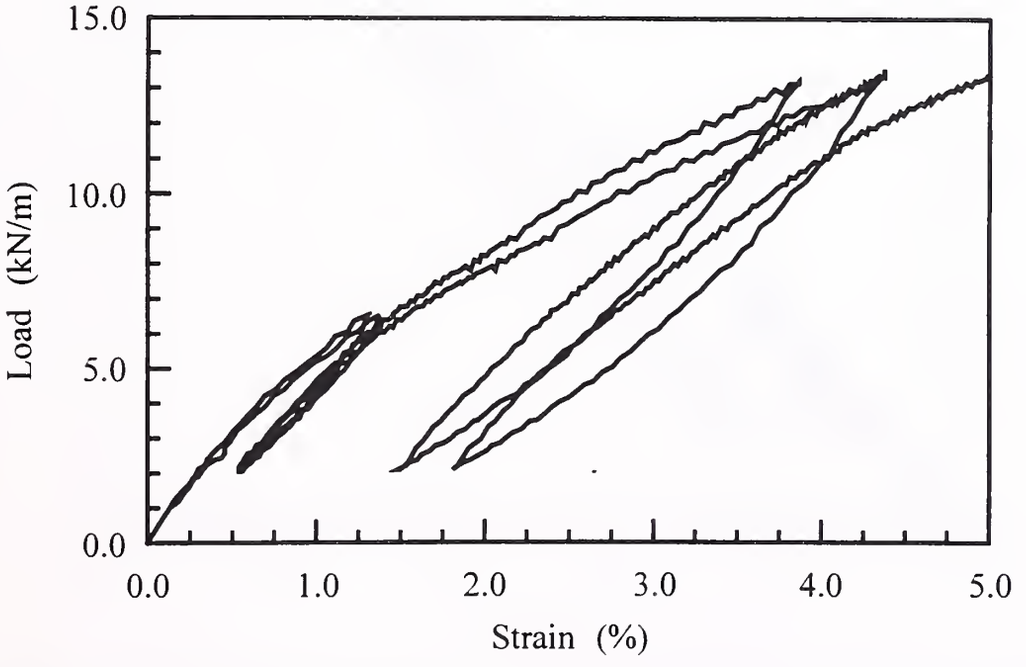

Figure B4: Global Strain From Two Sets of Celesco Gages: Geogrid, Transverse Direction

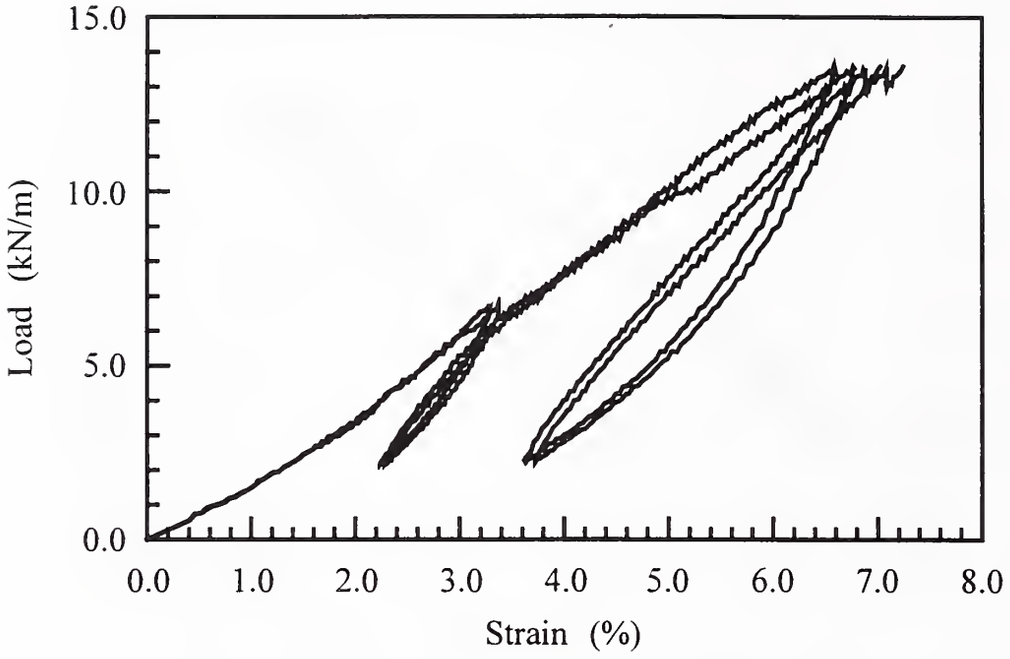

Figure B5: Global Strain From Two Sets of Celesco Gages: Geotextile, Machine Direction

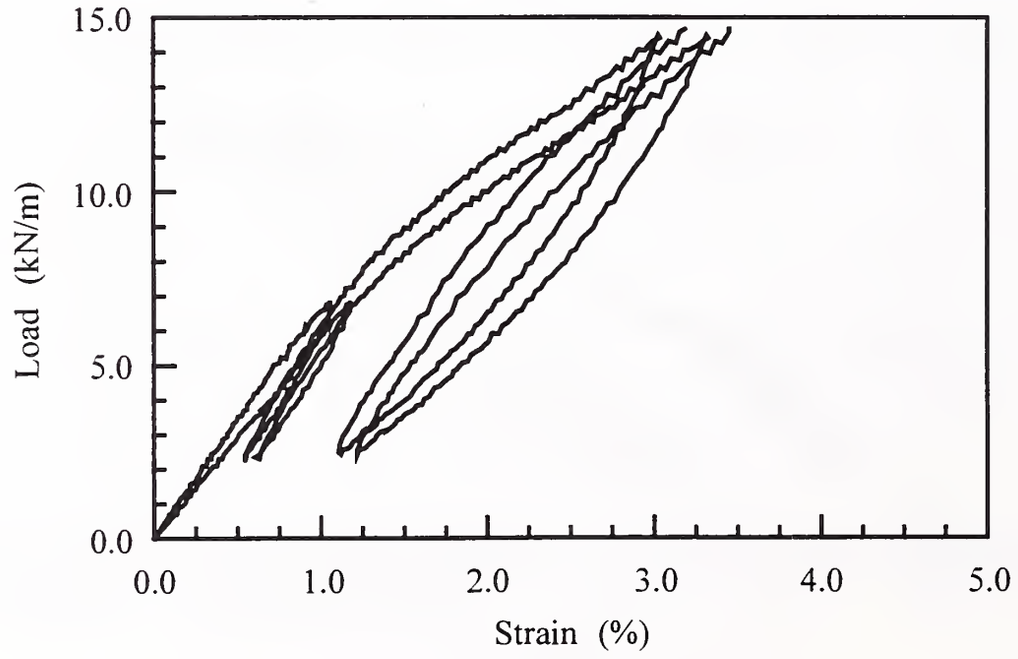

Figure B6: Global Strain From Two Sets of Celesco Gages: Geotextile, Transverse Direction

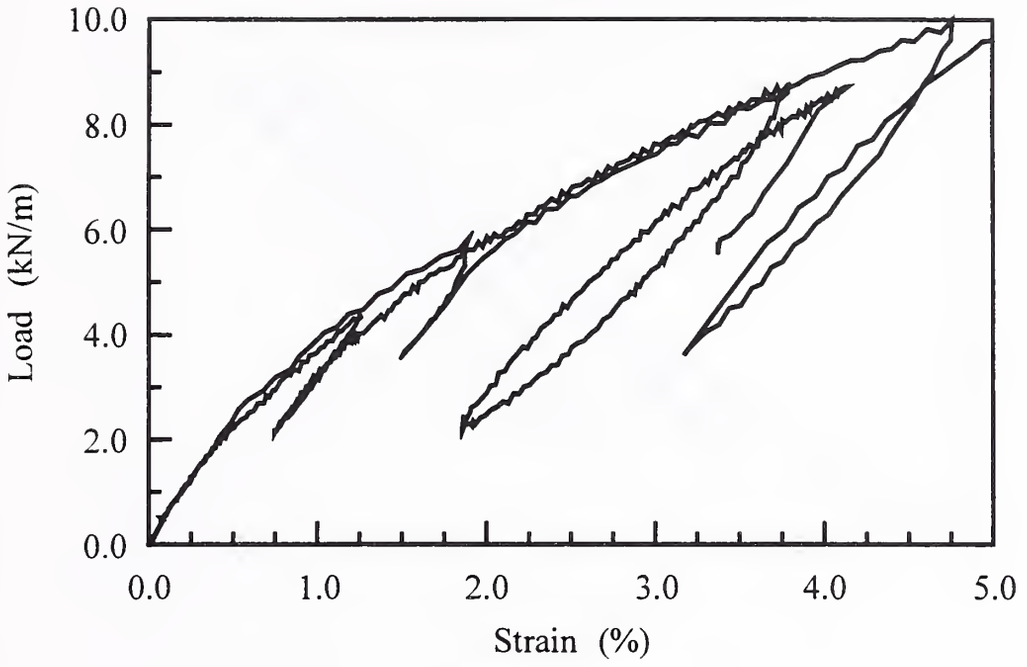

Figure B7: Global Strain From Two Tests: Geogrid, Machine Direction

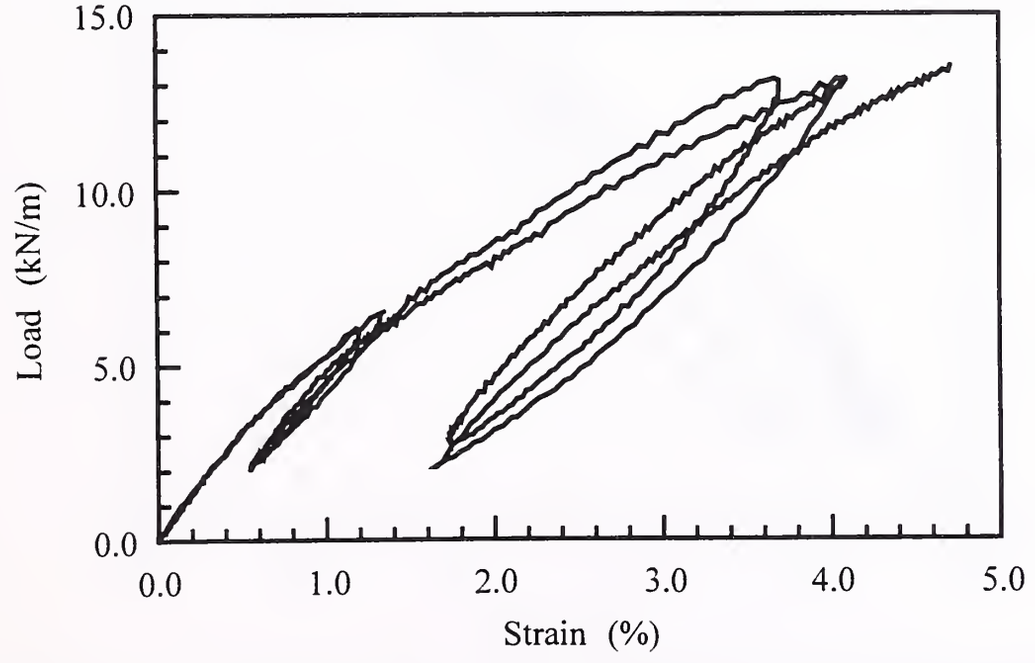

Figure B8: Global Strain From Two Tests: Geogrid, Transverse Direction

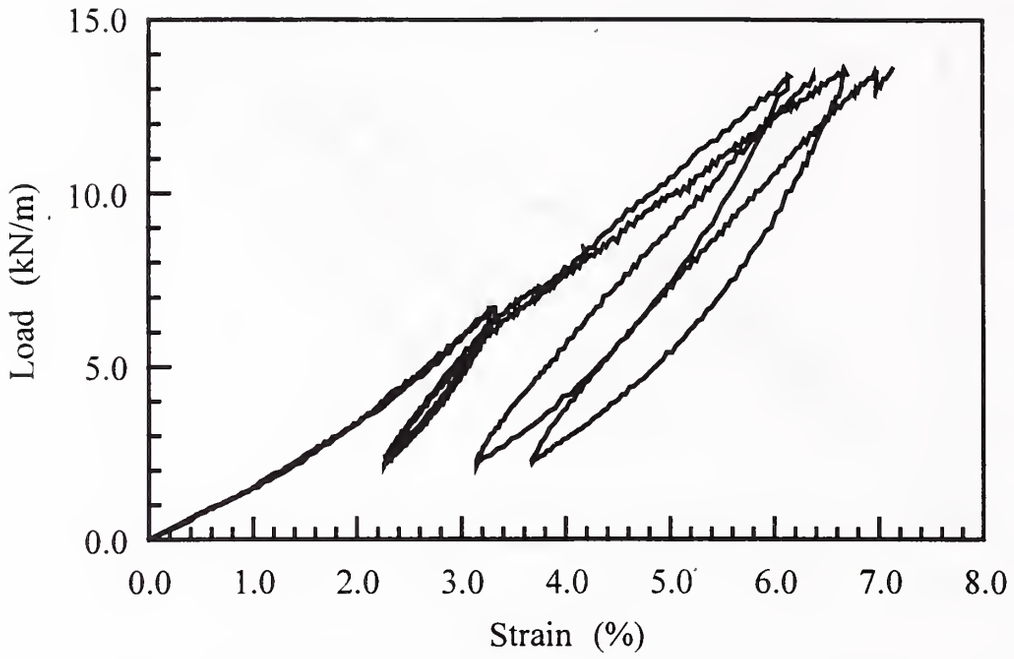

Figure B9: Global Strain From Two Tests: Geotextile, Machine Direction

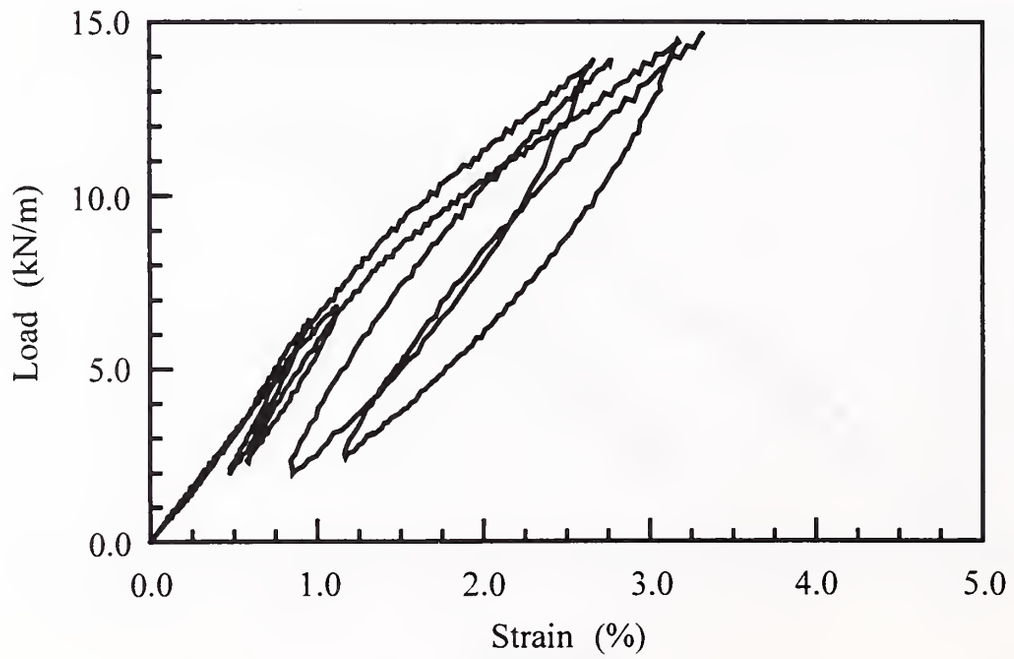

Figure B10: Global Strain From Two Tests: Geotextile, Transverse Direction

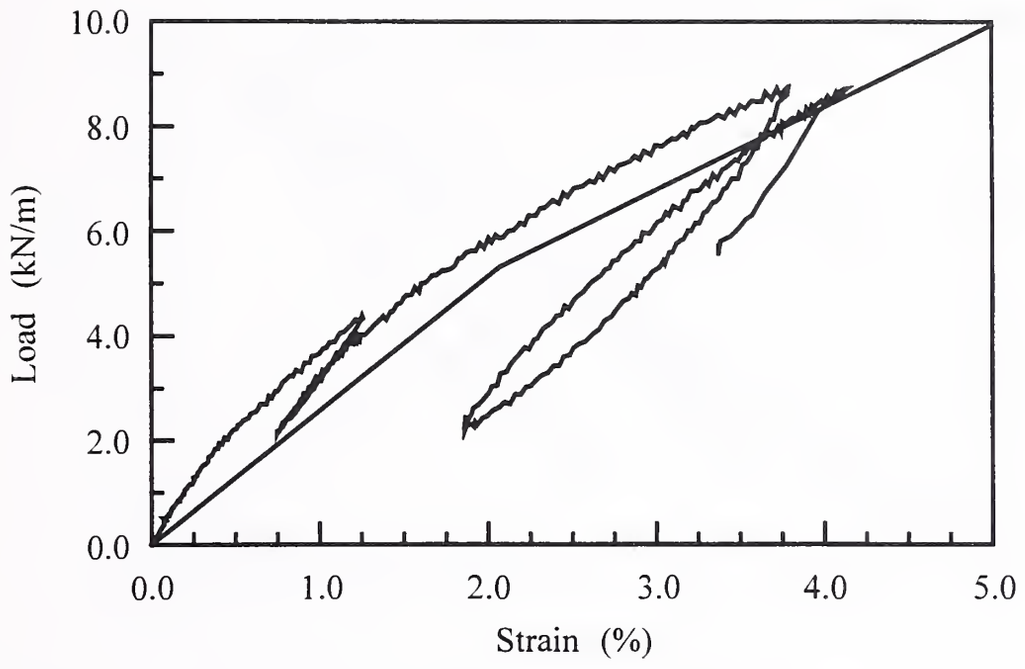

Figure B11: Comparison of Results to Manufacturer's Data: Geogrid, Machine Direction

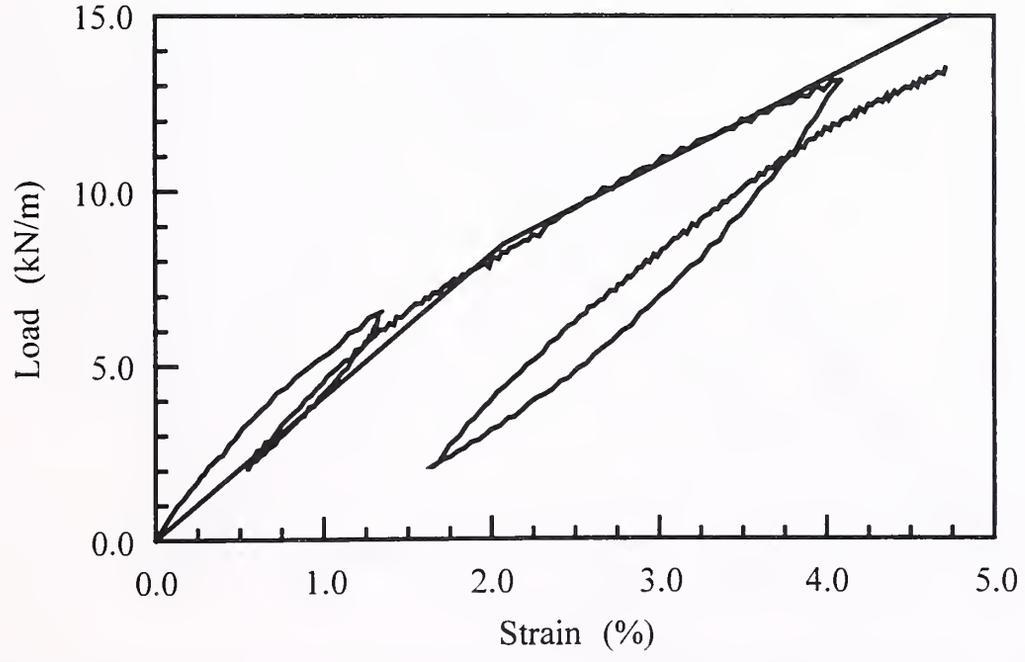

Figure B12: Comparison of Results to Manufacturer's Data: Geogrid, Transverse Direction

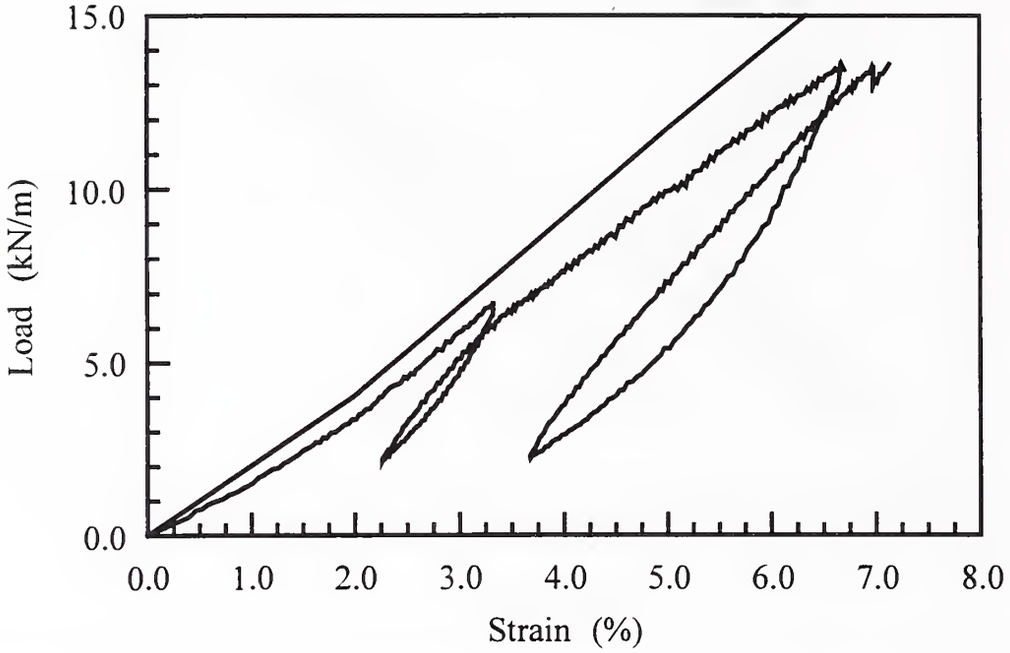

Figure B13: Comparison of Results to Manufacturer's Data: Geotextile, Machine Direction

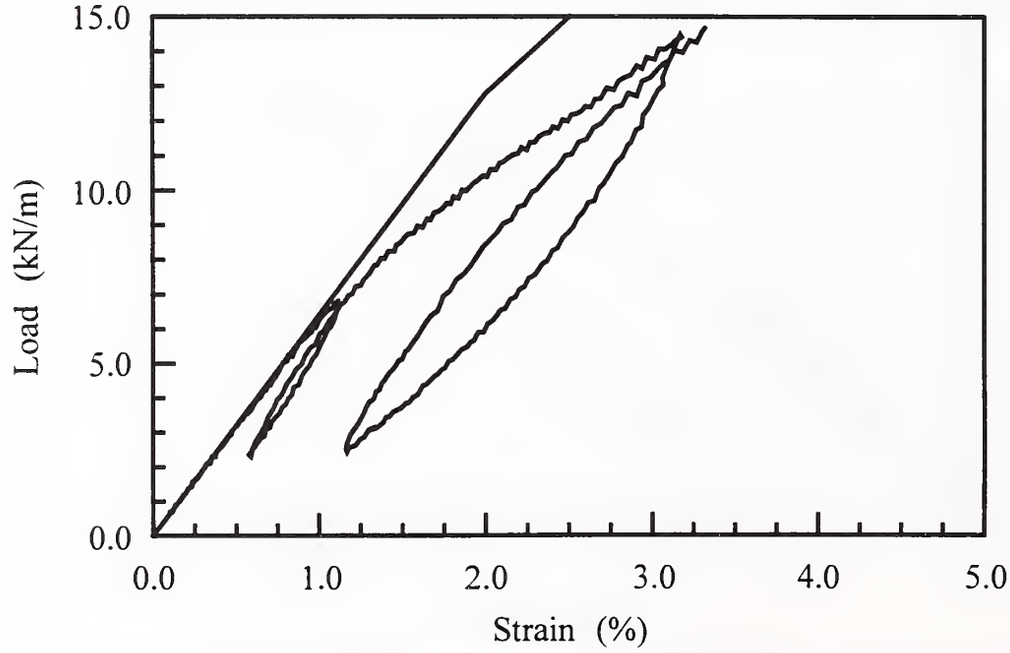

Figure B14: Comparison of Results to Manufacturer's Data: Geotextile, Transverse Direction

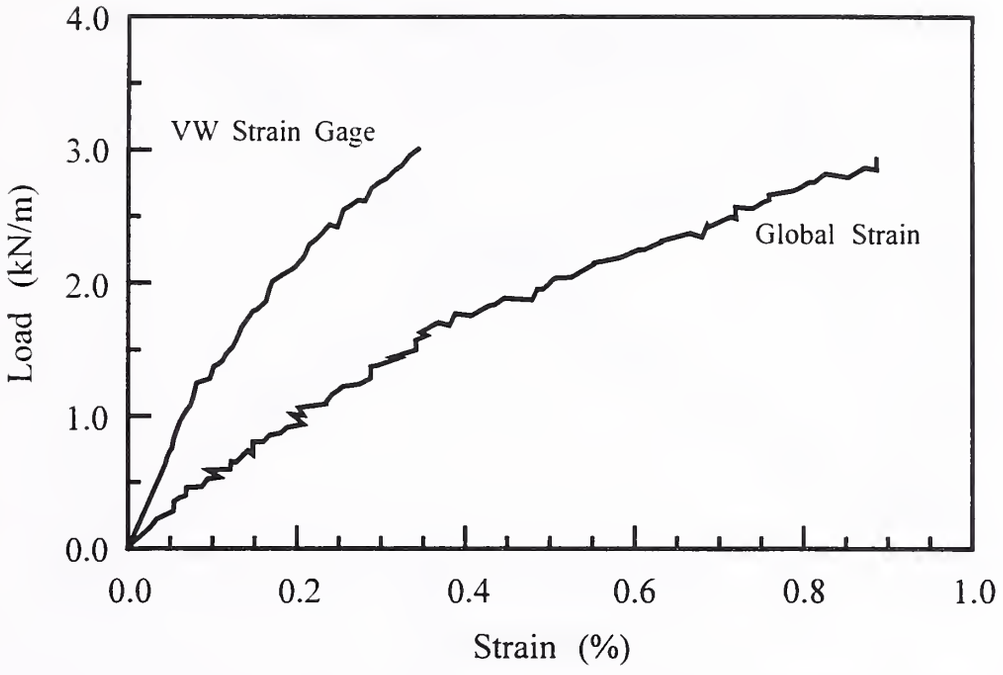

Figure B15: Vibrating Wire Strain Gage: Geogrid, Machine Direction

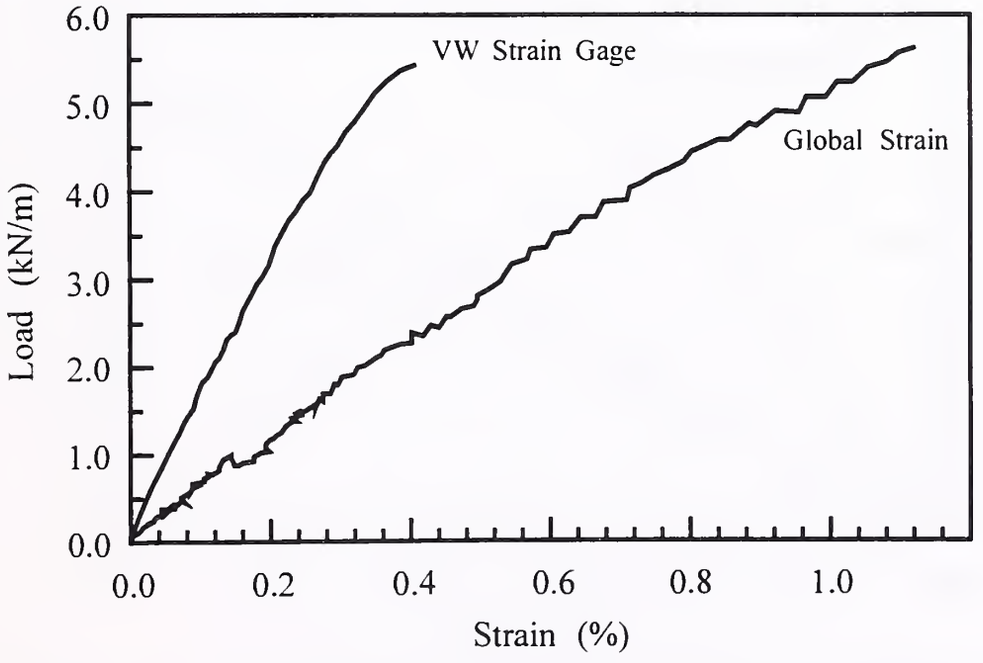

Figure B16: Vibrating Wire Strain Gage: Geogrid, Transverse Direction

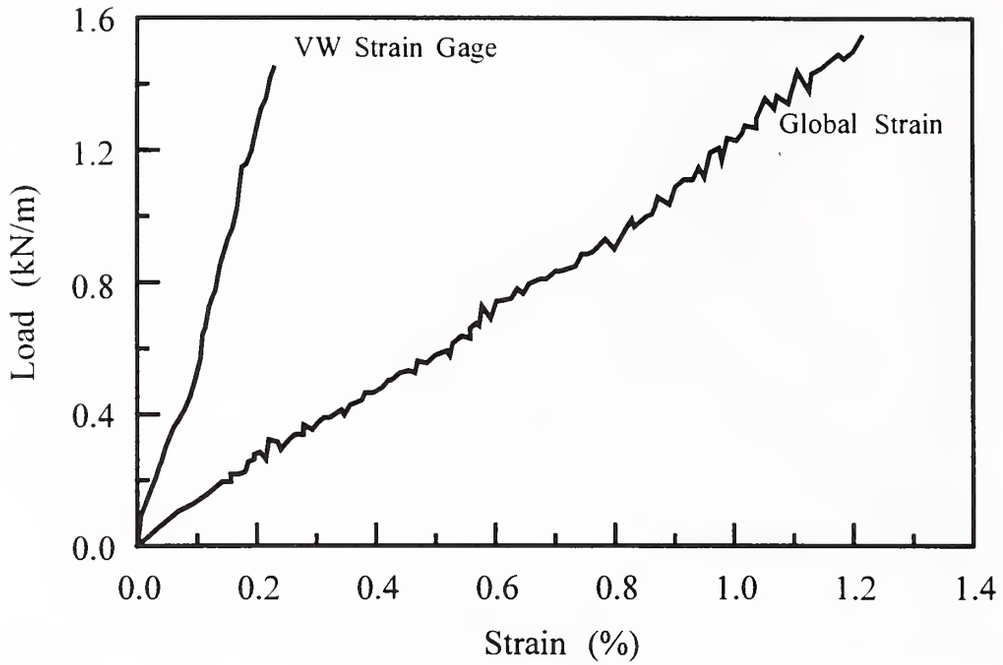

Figure B17: Vibrating Wire Strain Gage: Geotextile, Machine Direction

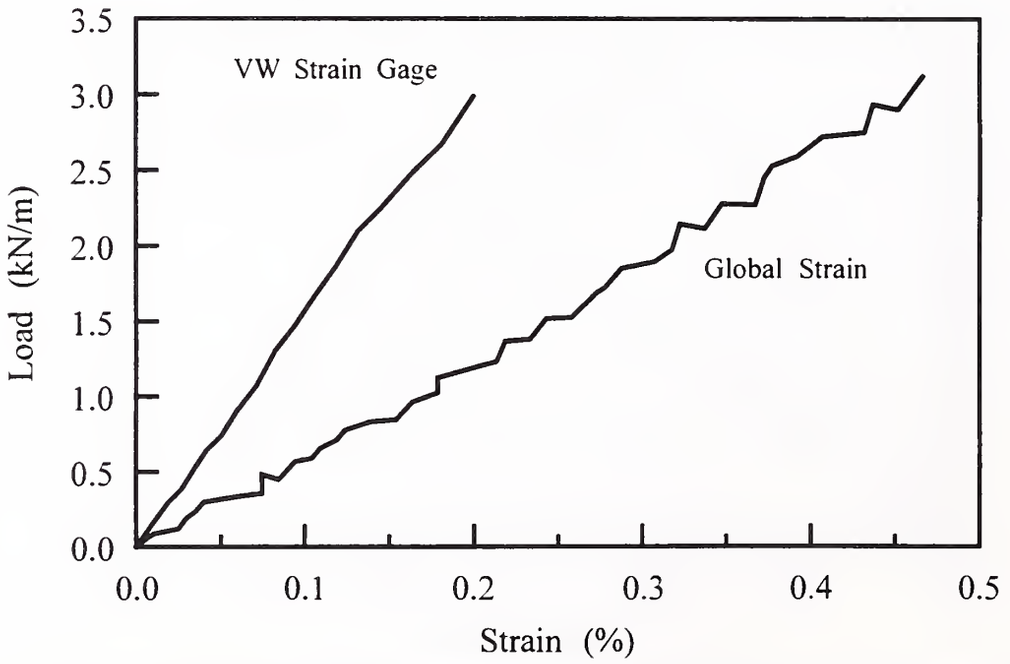

Figure B18: Vibrating Wire Strain Gage: Geotextile, Transverse Direction

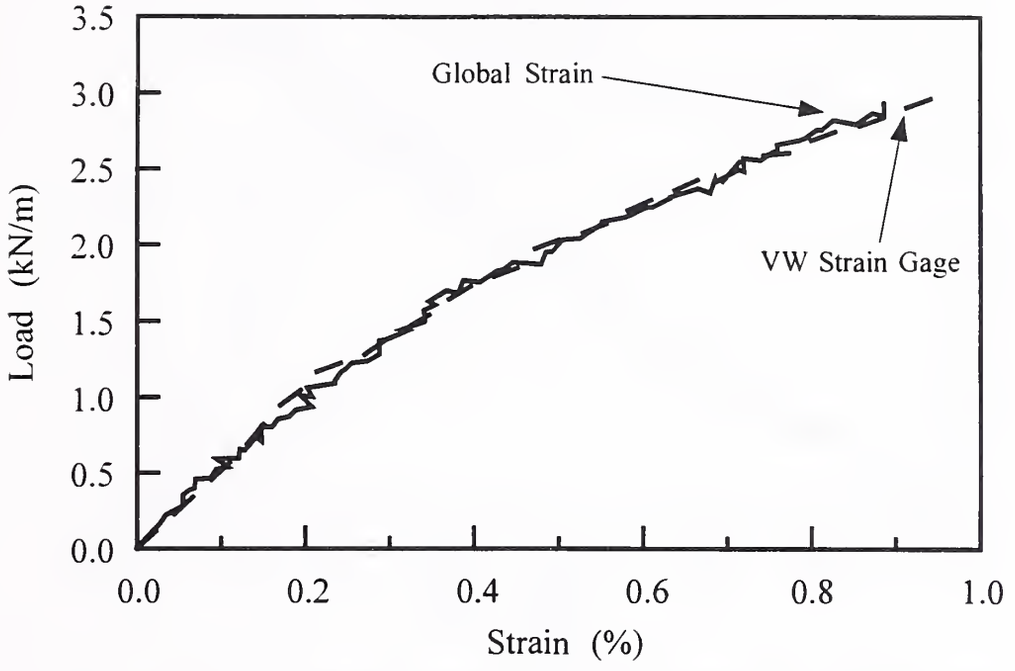

Figure B19: Calibrated Vibrating Wire Strain Gage: Geogrid, Machine Direction

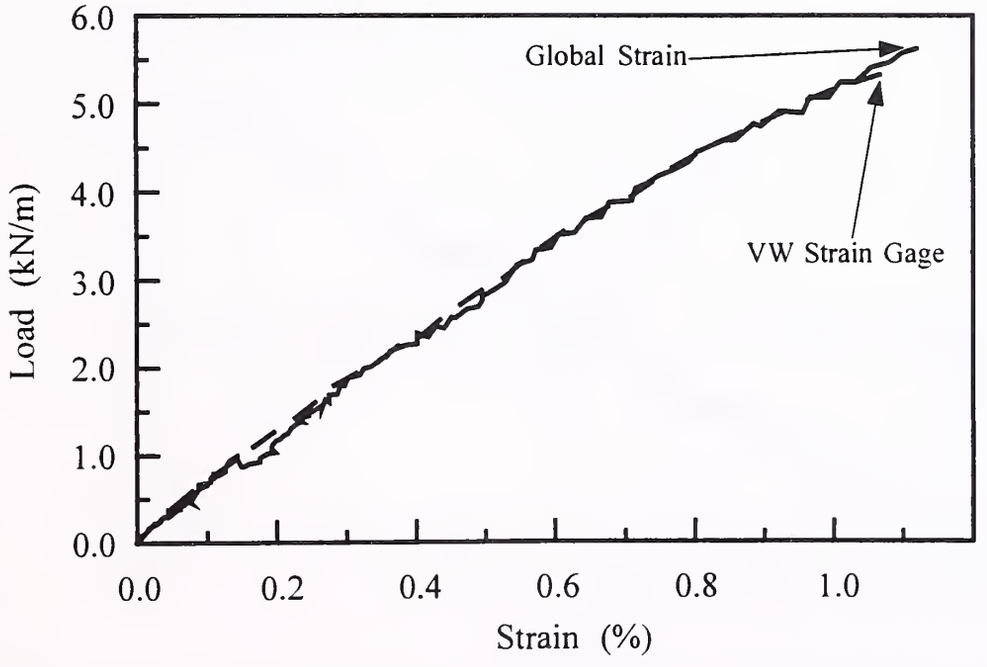

Figure B20: Calibrated Vibrating Wire Strain Gage: Geogrid, Transverse Direction

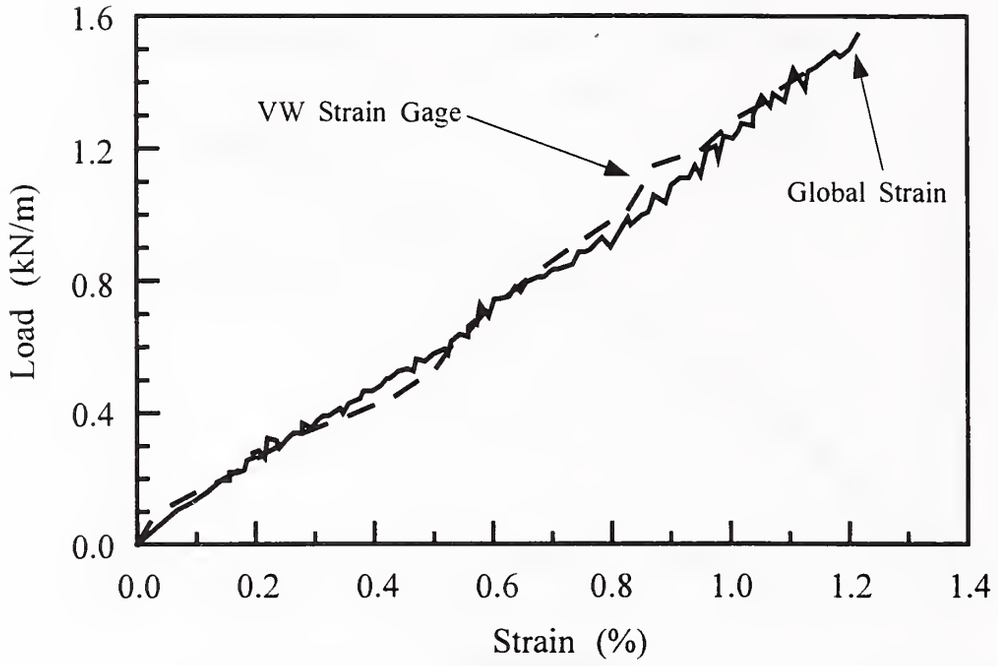

Figure B21: Calibrated Vibrating Wire Strain Gage: Geotextile, Machine Direction

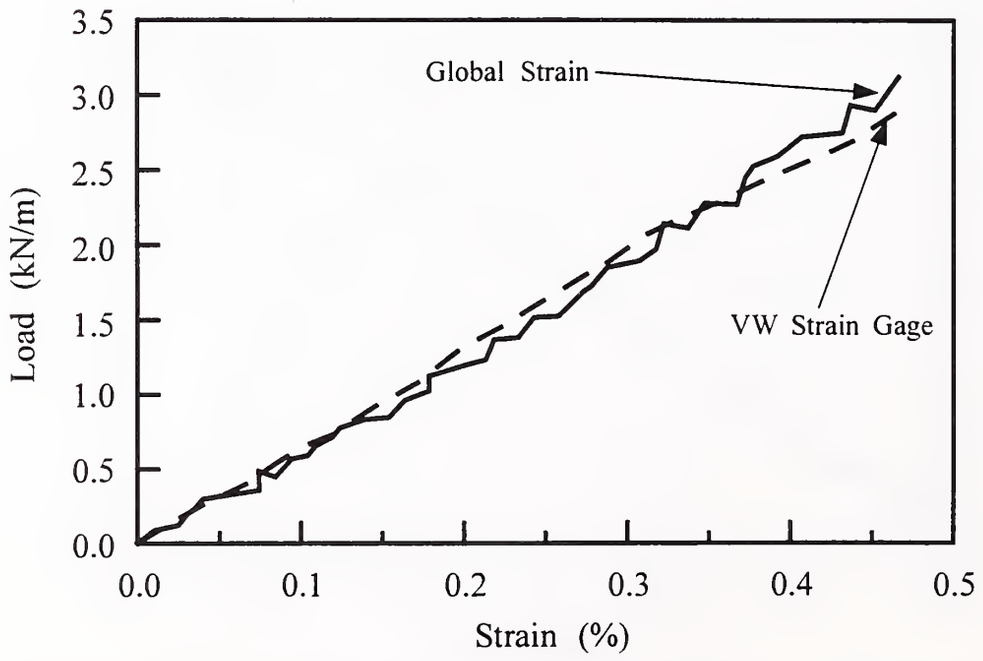

Figure B22: Calibrated Vibrating Wire Strain Gage: Geotextile, Transverse Direction

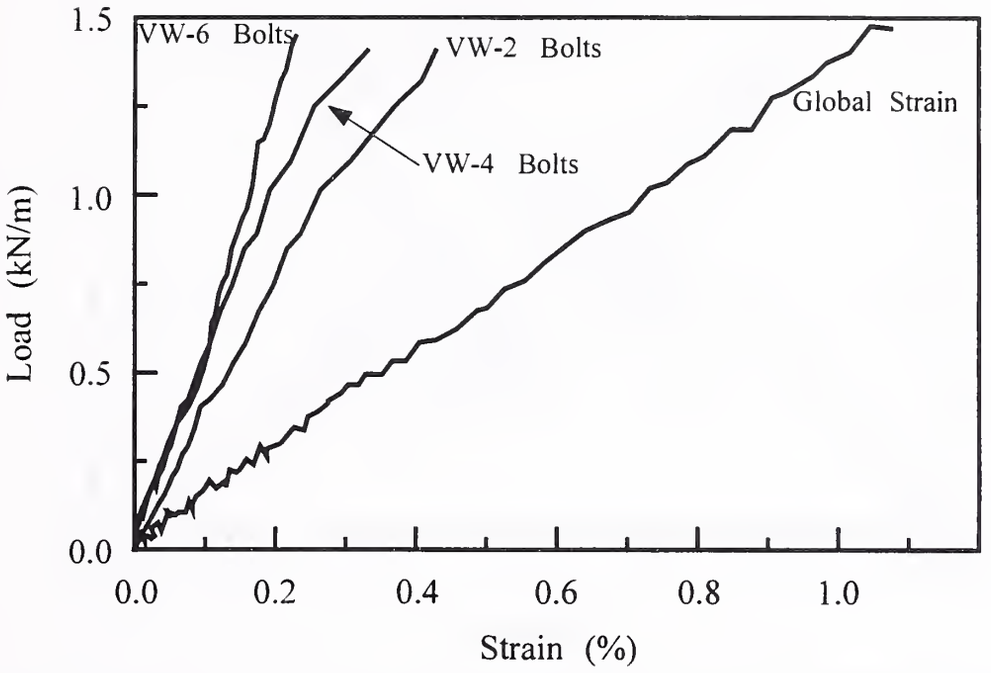

Figure B23: Comparison of Vibrating Wire Strain Gage With 6, 4 and 2 Bolts Fastened

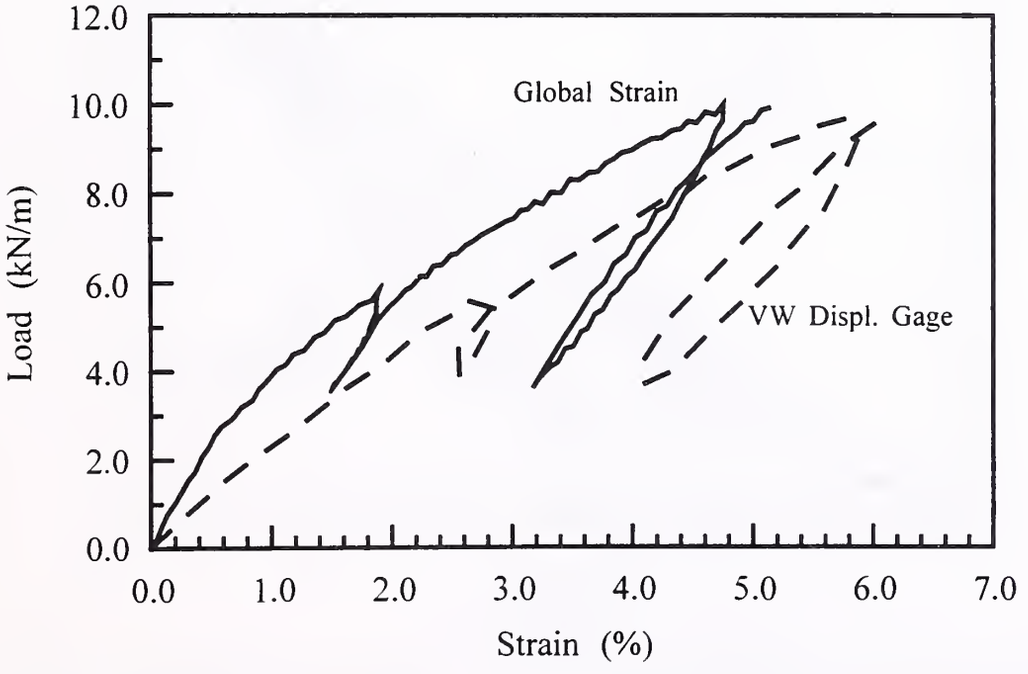

Figure B24: Vibrating Wire Displacement Gage: Geogrid, Machine Direction

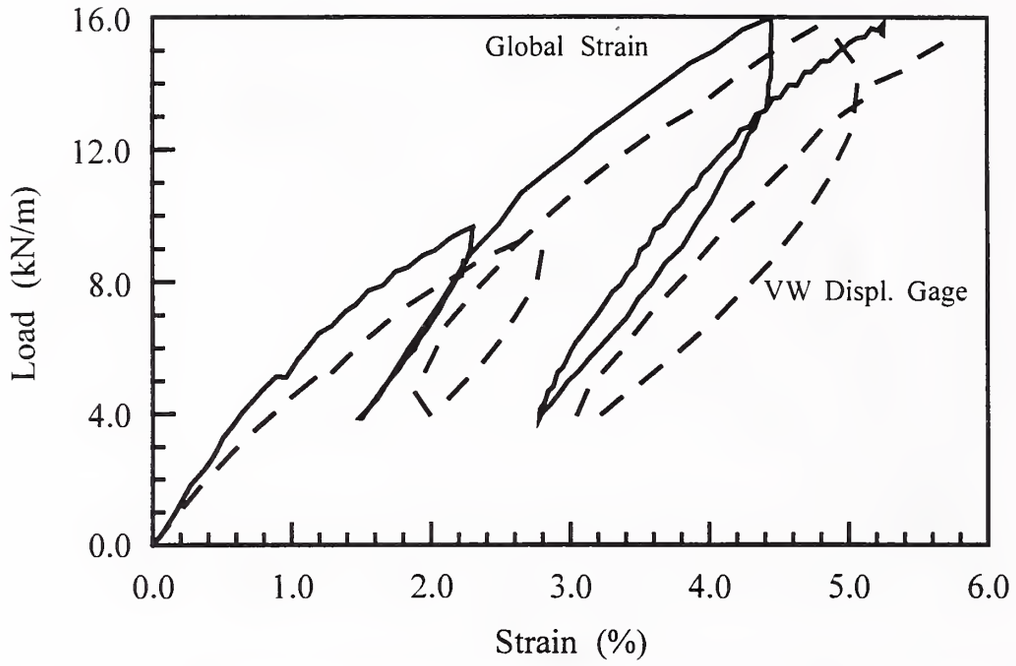

Figure B25: Vibrating Wire Displacement Gage: Geogrid, Transverse Direction

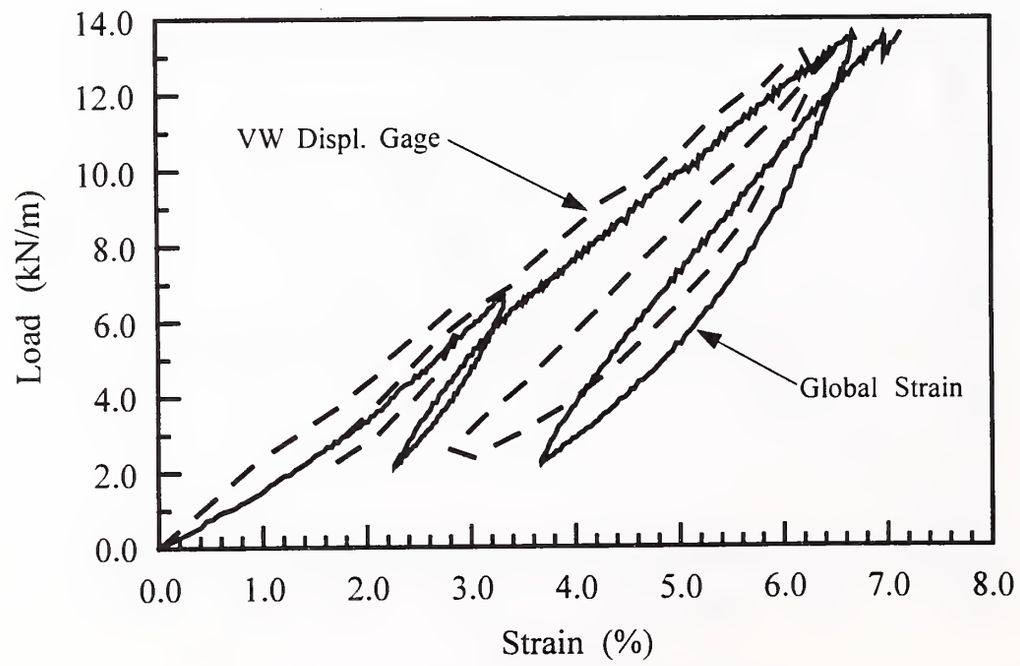

Figure B26: Vibrating Wire Displacement Gage: Geotextile, Machine Direction

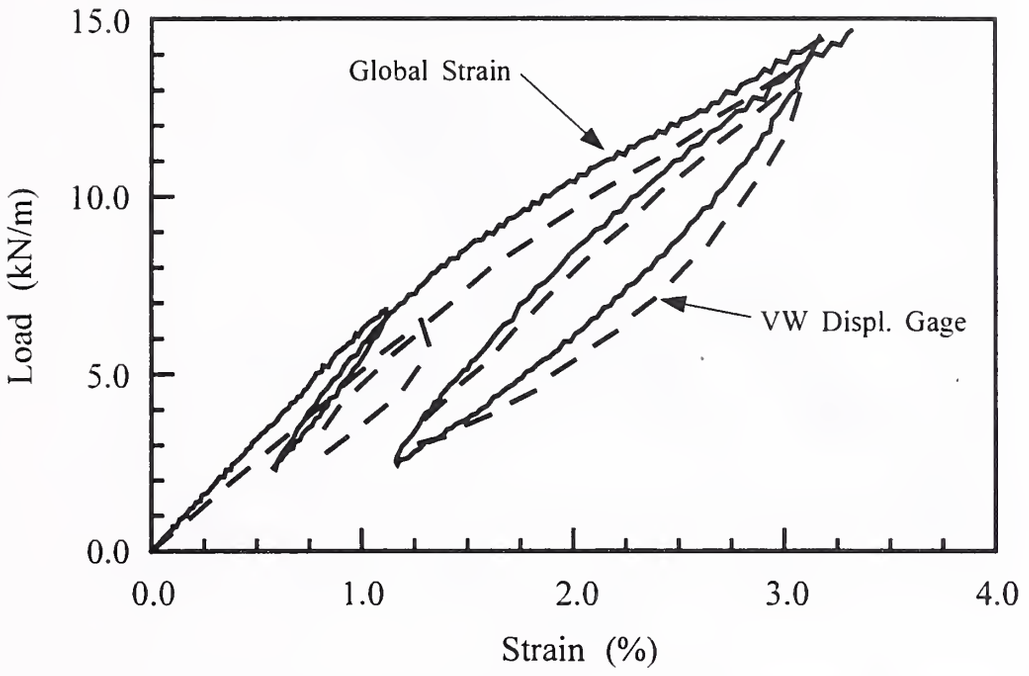

Figure B27: Vibrating Wire Displacement Gage: Geotextile, Transverse Direction

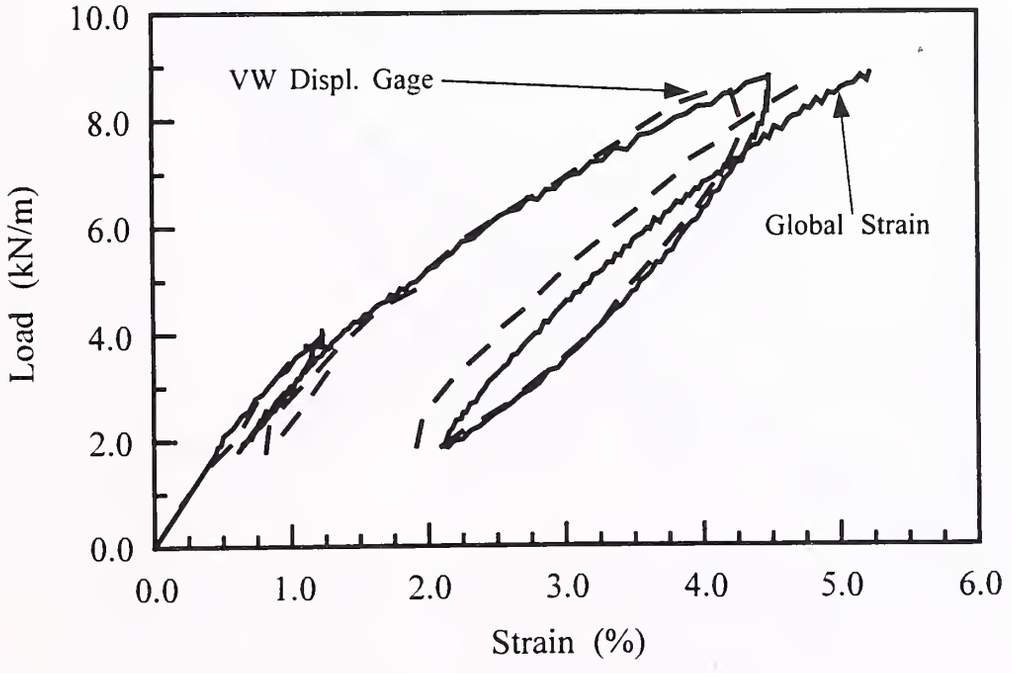

Figure B28: Calibrated Back-to-Back Vibrating Wire Displacement Gage: Geogrid, Machine Direction

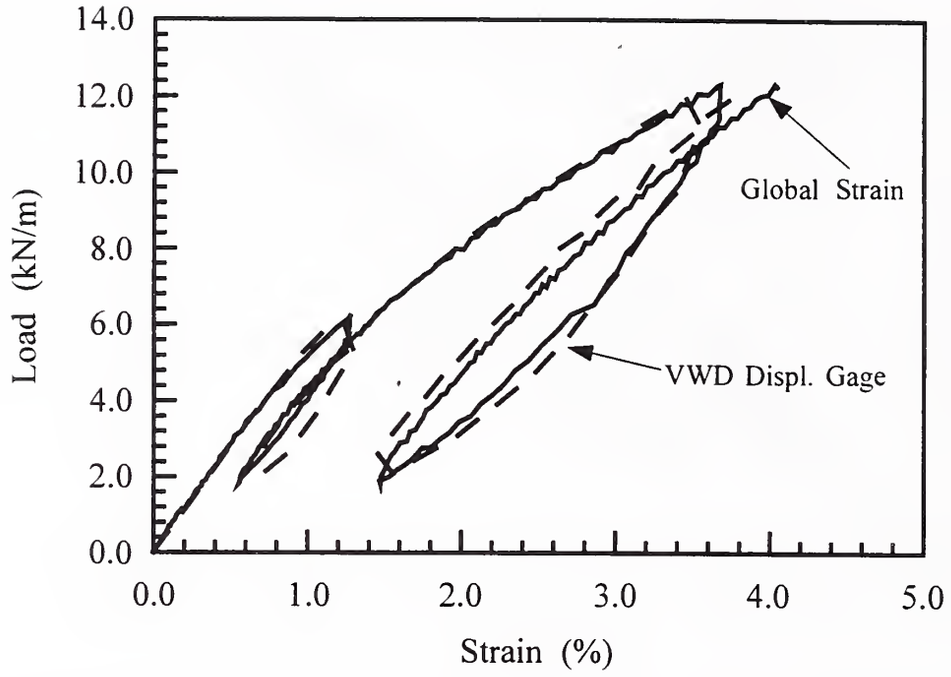

Figure B29: Calibrated Back-to-Back Vibrating Wire Displacement Gage: Geogrid, Transverse Direction

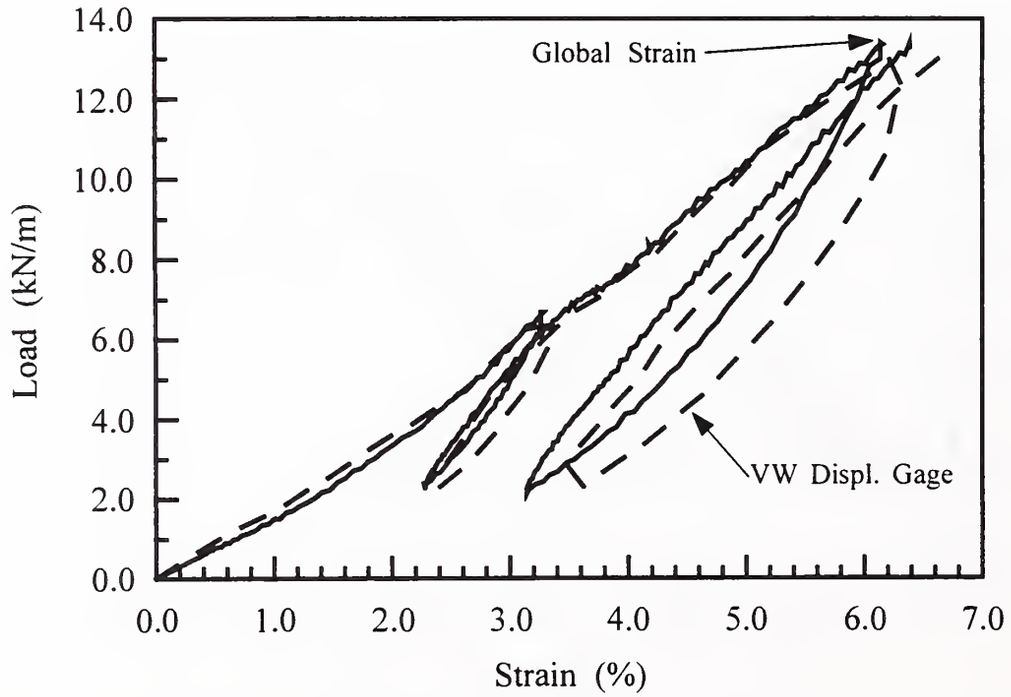

Figure B30: Calibrated Back-to-Back Vibrating Wire Displacement Gage: Geotextile, Machine Direction

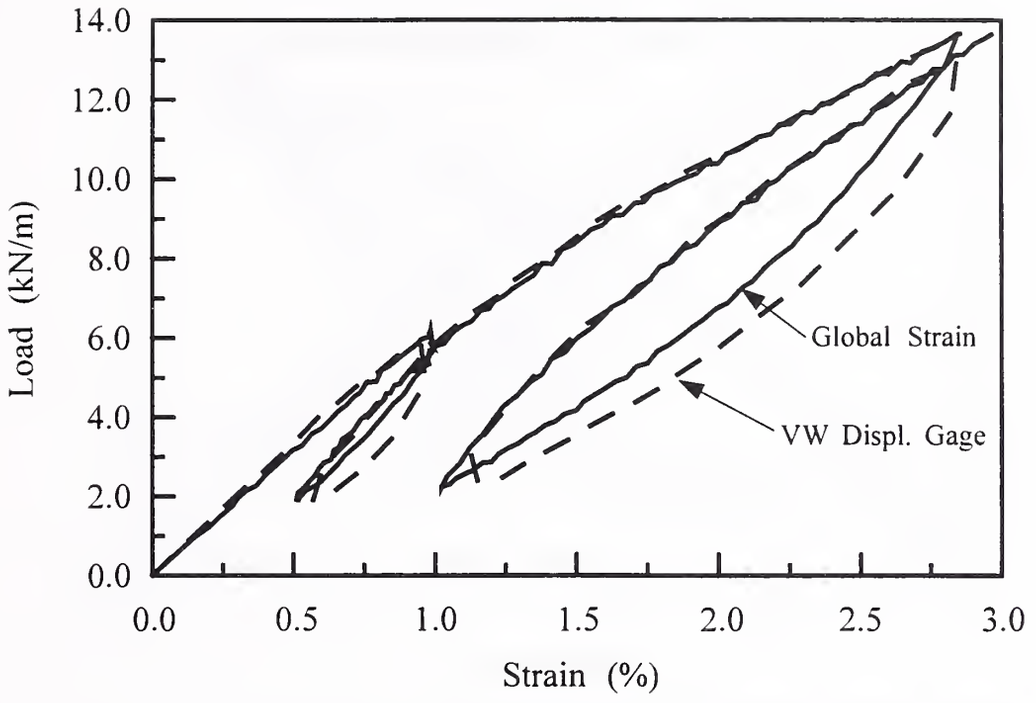

Figure B31: Calibrated Back-to-Back Vibrating Wire Displacement Gage: Geotextile, Transverse Direction

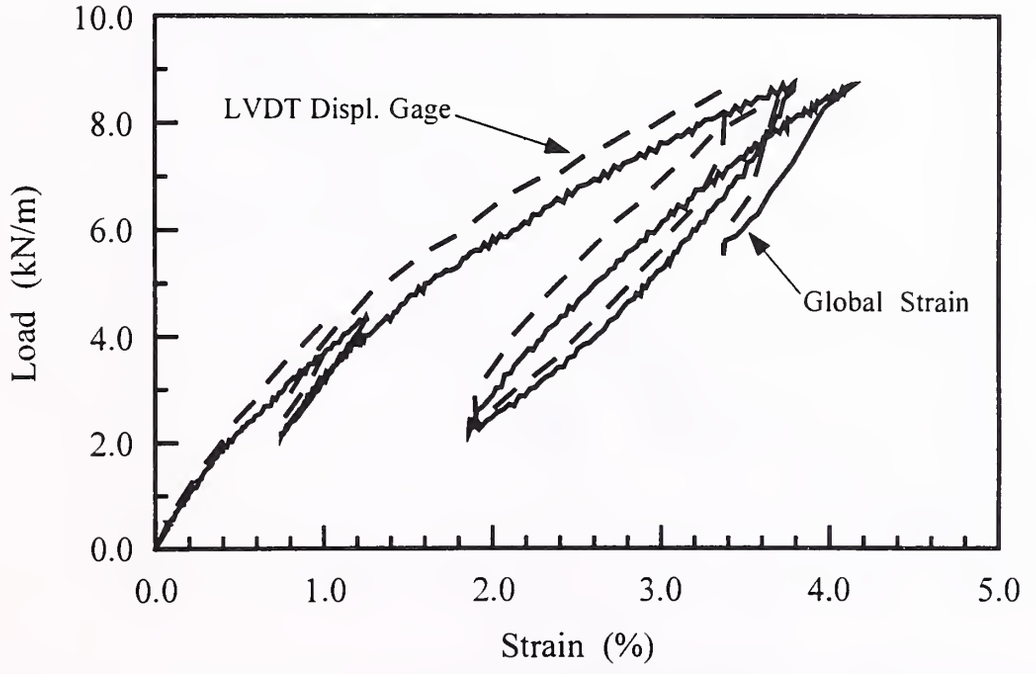

Figure B32: LVDT Displacement Gage: Geogrid, Machine Direction

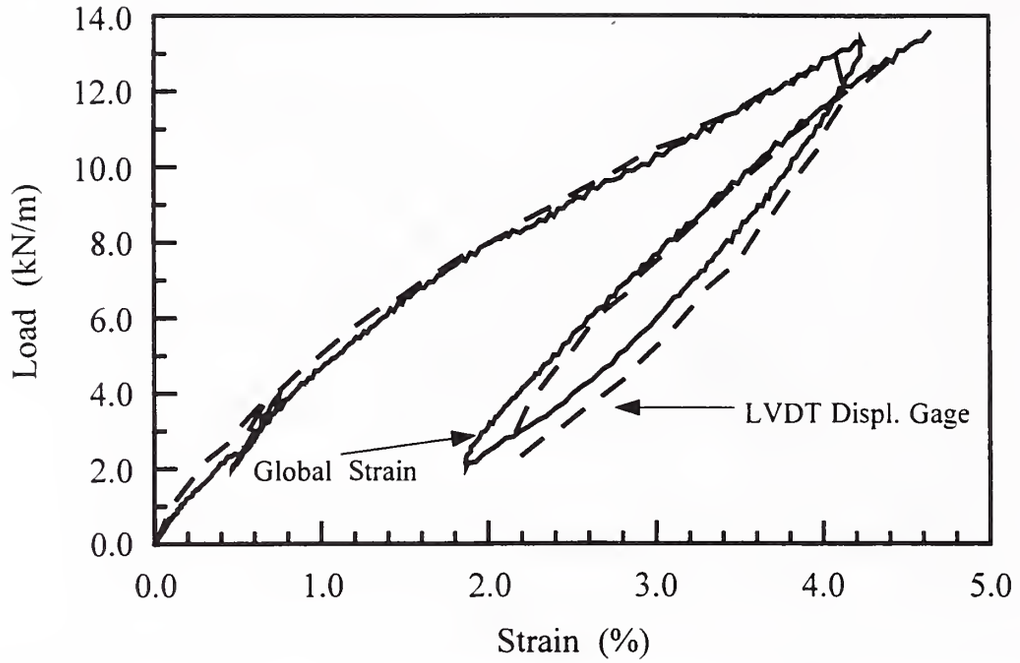

Figure B33: LVDT Displacement Gage: Geogrid, Transverse Direction

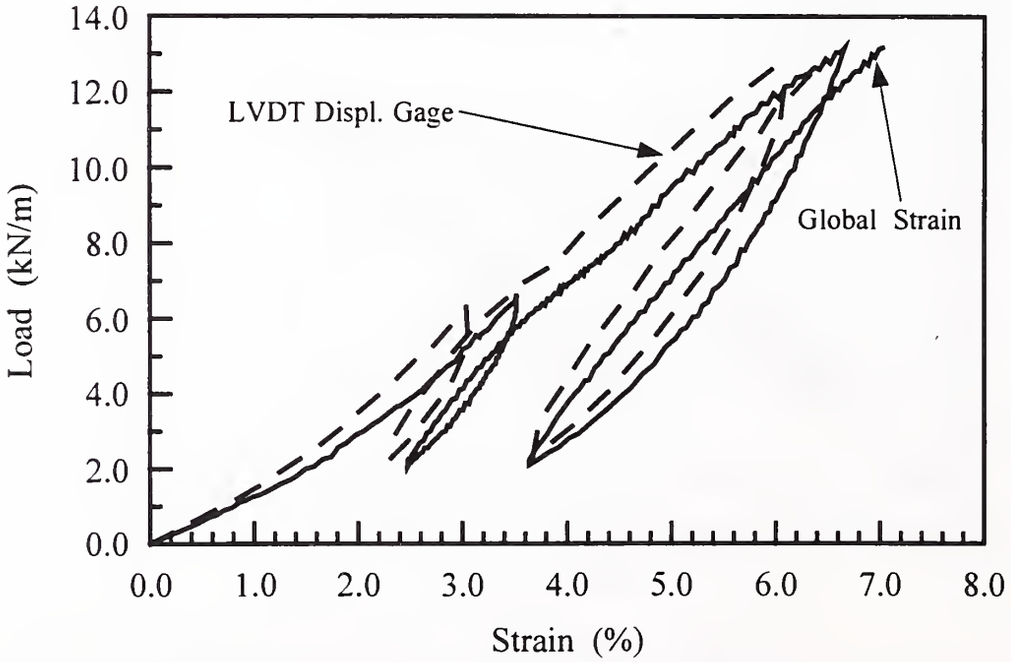

Figure B34: LVDT Displacement Gage: Geotextile, Machine Direction

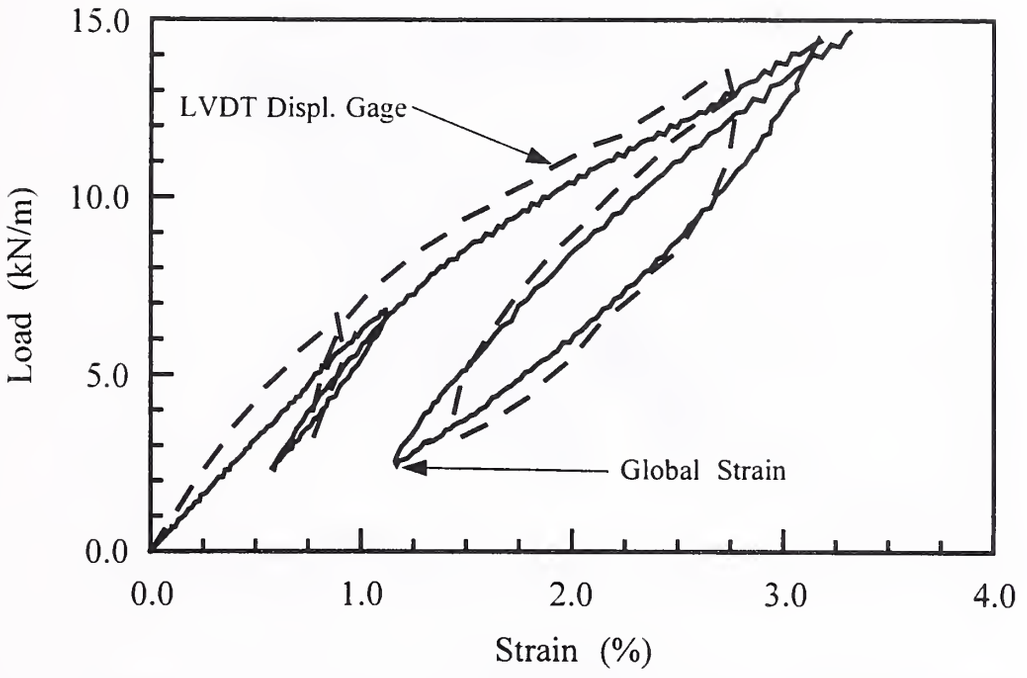

Figure B35: LVDT Displacement Gage: Geotextile, Transverse Direction

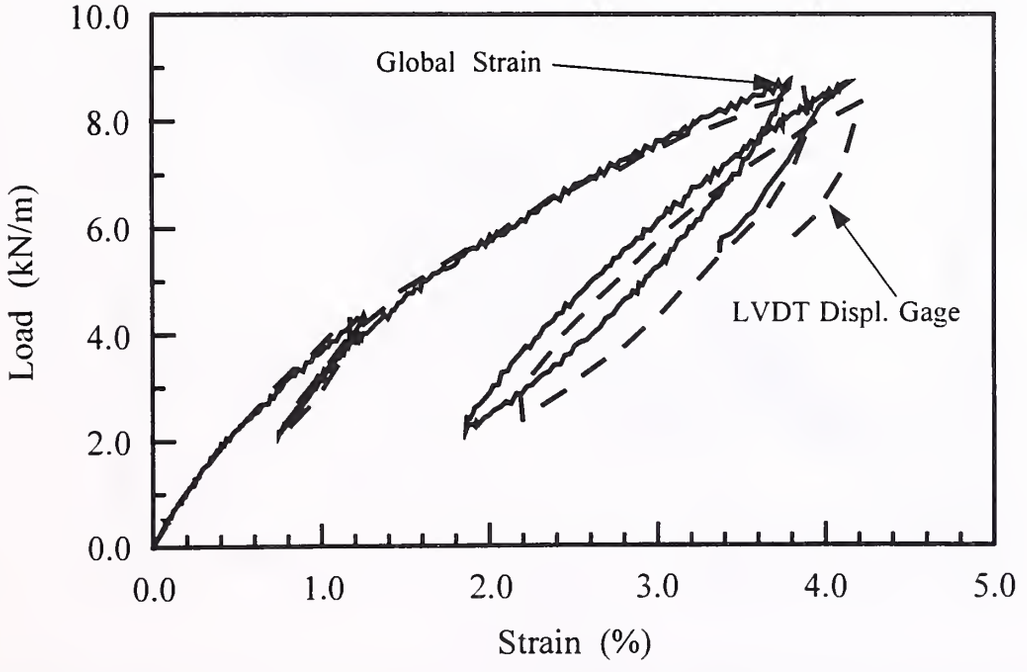

Figure B36: Calibrated LVDT Displacement Gage: Geogrid, Machine Direction

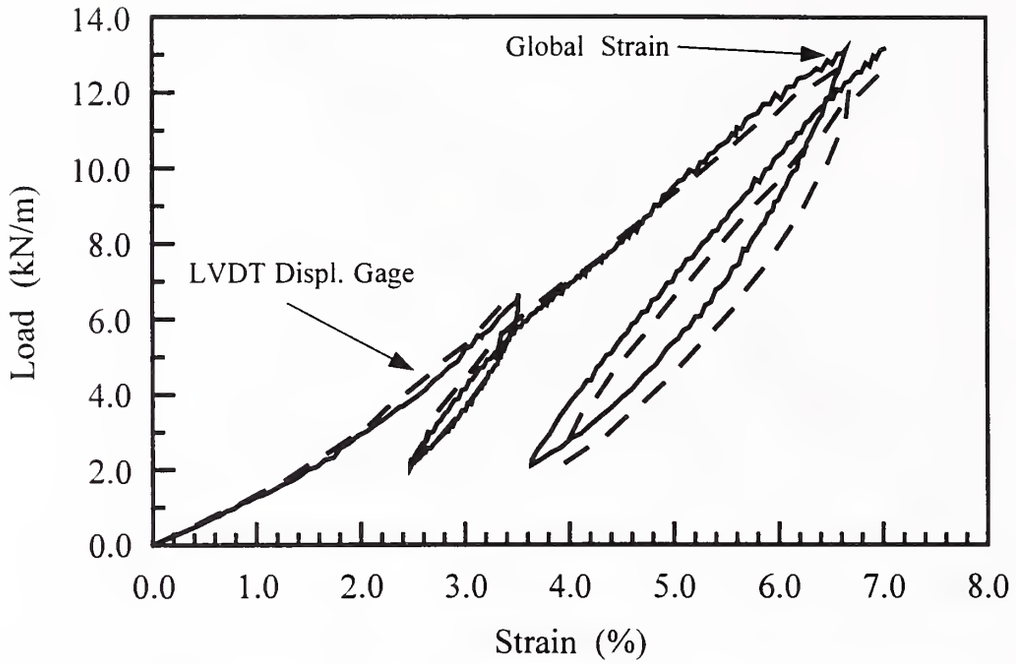

Figure B37: Calibrated LVDT Displacement Gage: Geotextile, Machine Direction

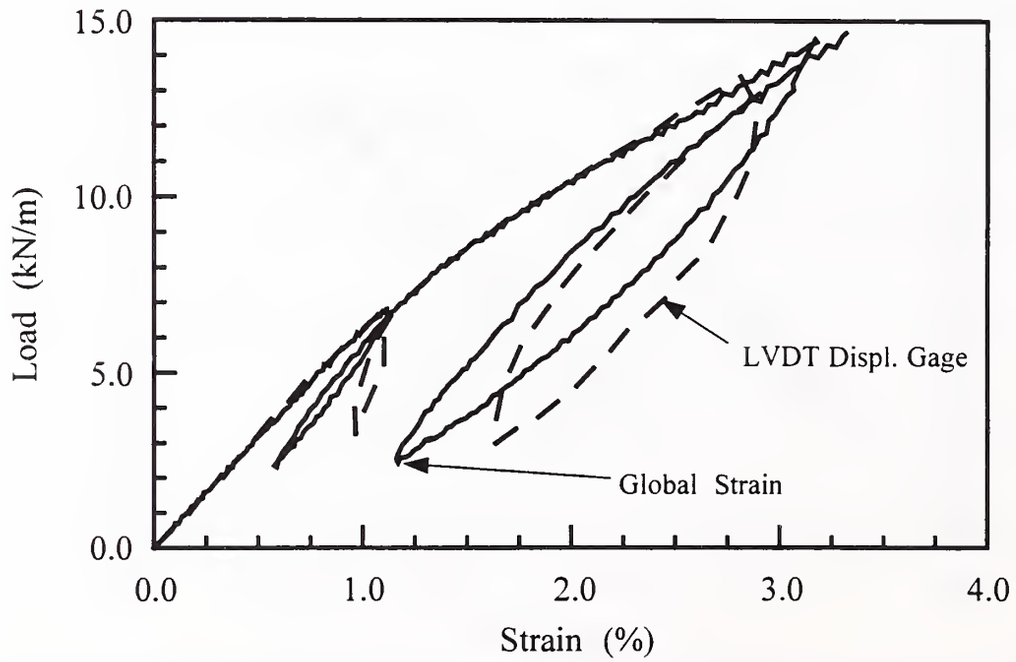

Figure B38: Calibrated LVDT Displacement Gage: Geotextile, Transverse Direction

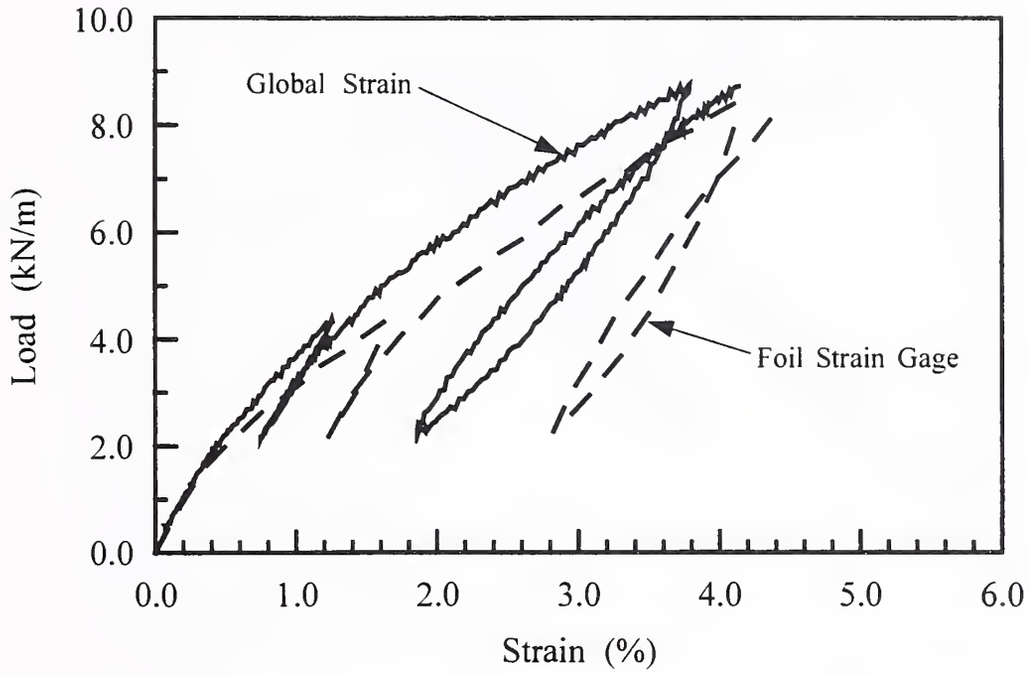

Figure B39: Foil Strain Gage: Geogrid, Machine Direction

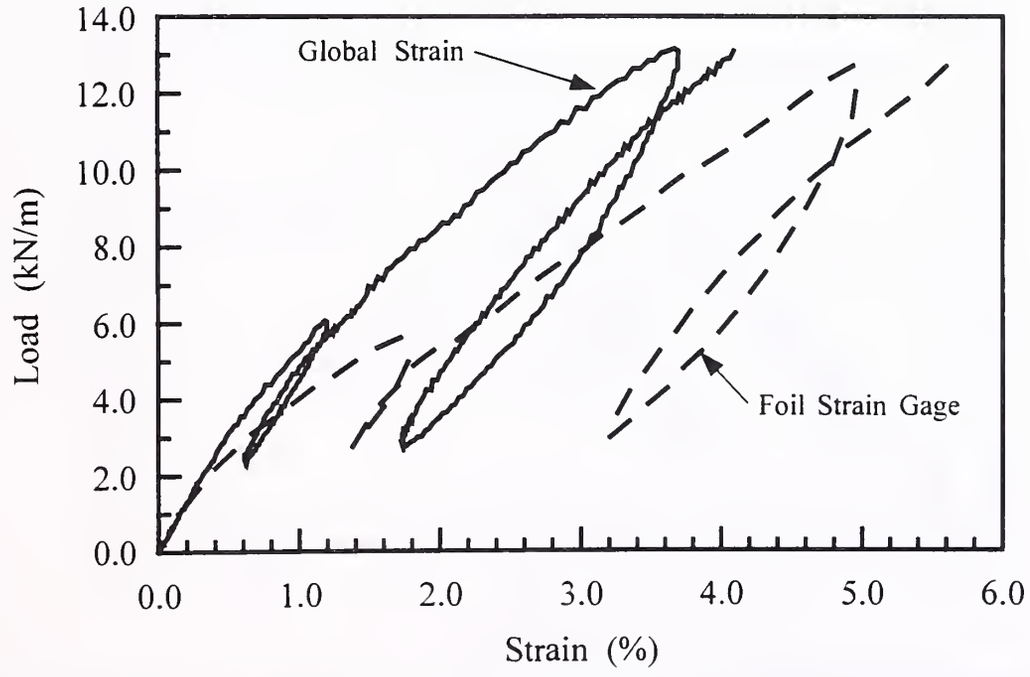

Figure B40: Foil Strain Gage: Geogrid, Transverse Direction

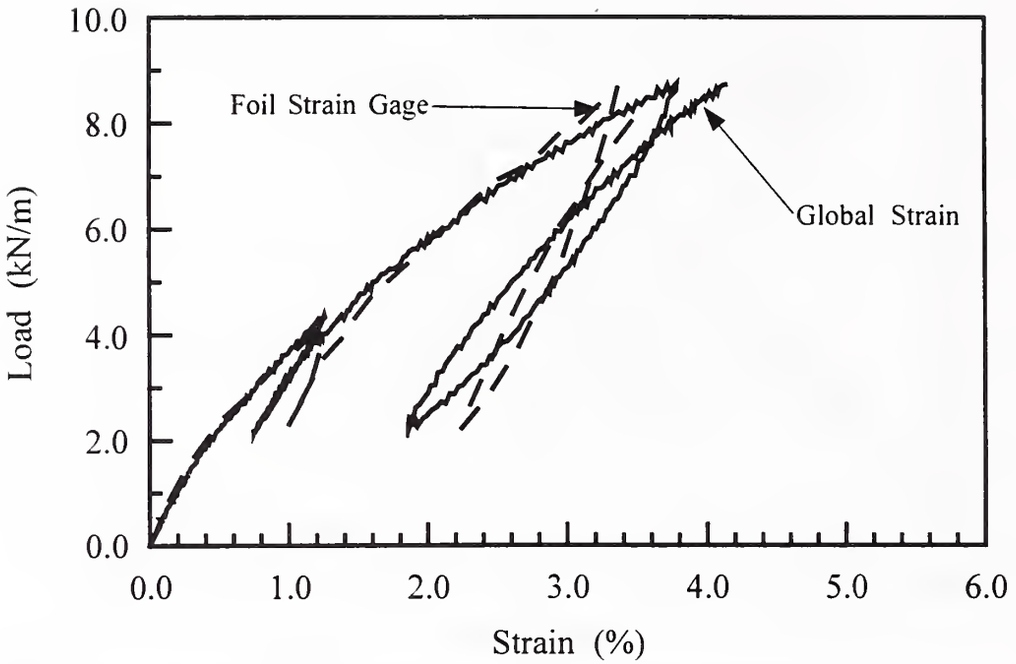

Figure B41: Calibrated Foil Strain Gage: Geogrid, Machine Direction

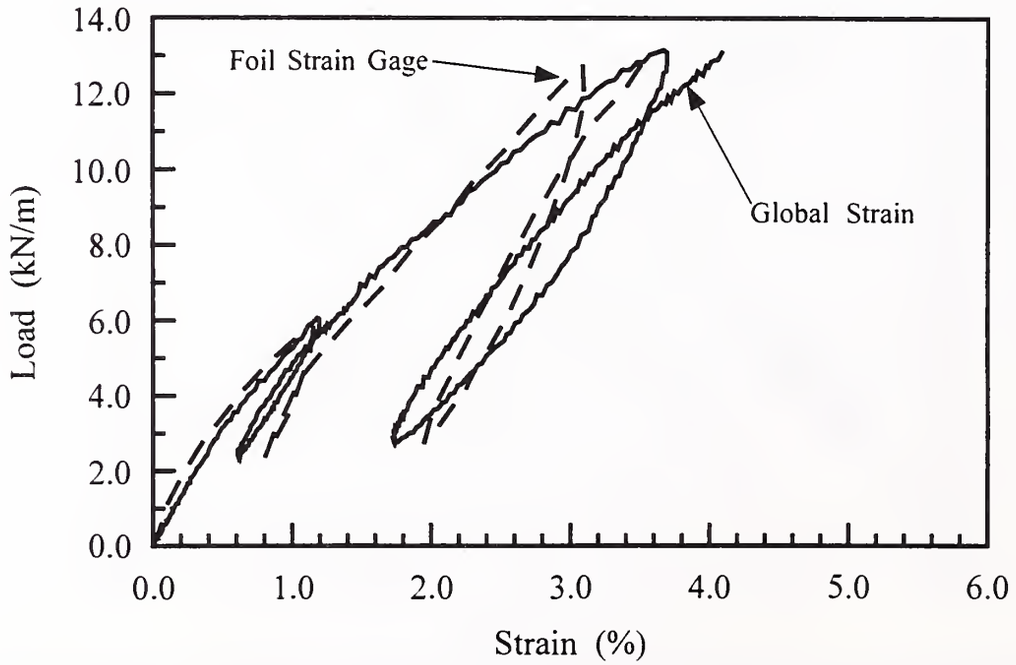

Figure B42: Calibrated Foil Strain Gage: Geogrid, Transverse Direction

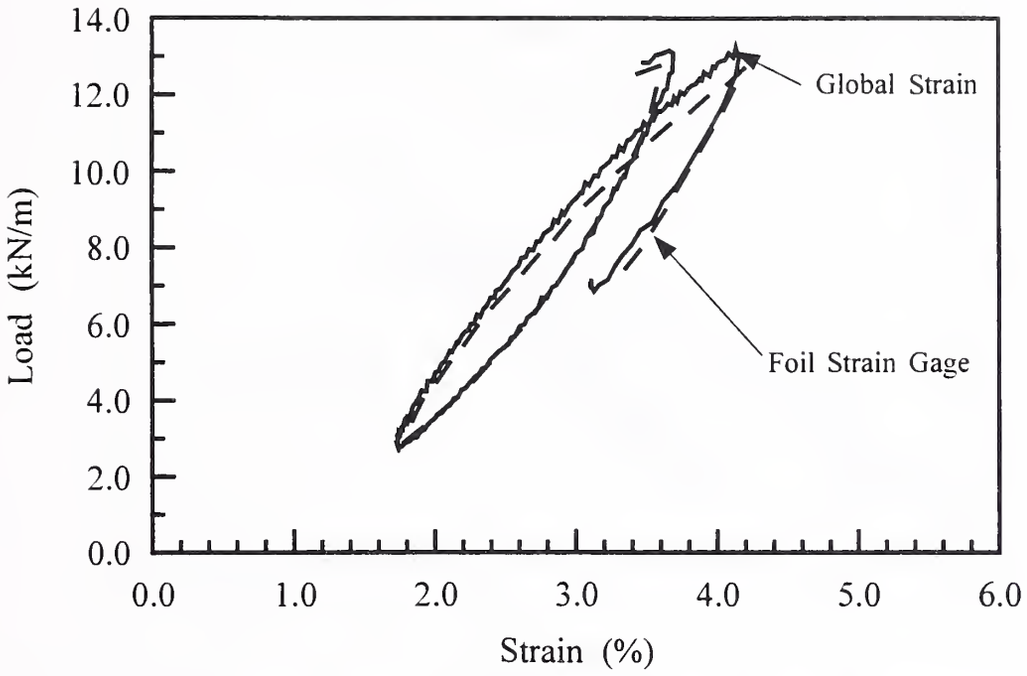

Figure B43: Unloading-Reloading Response From Foil Strain Gage: Geogrid, Transverse Direction

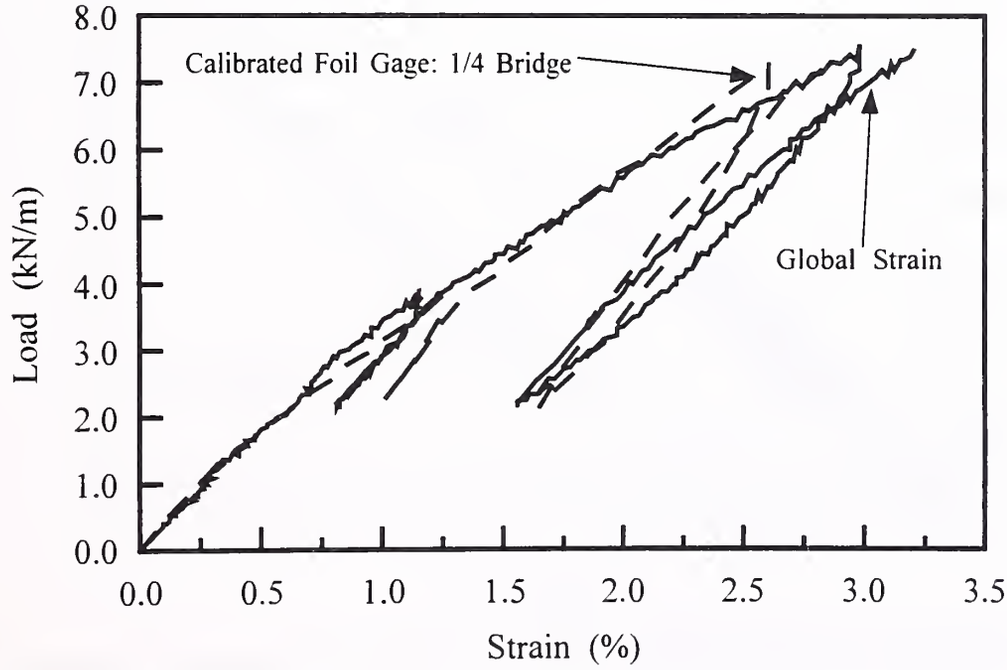

Figure B44: Calibrated 1/4 Bridge Foil Strain Gage: Geogrid, Machine Direction

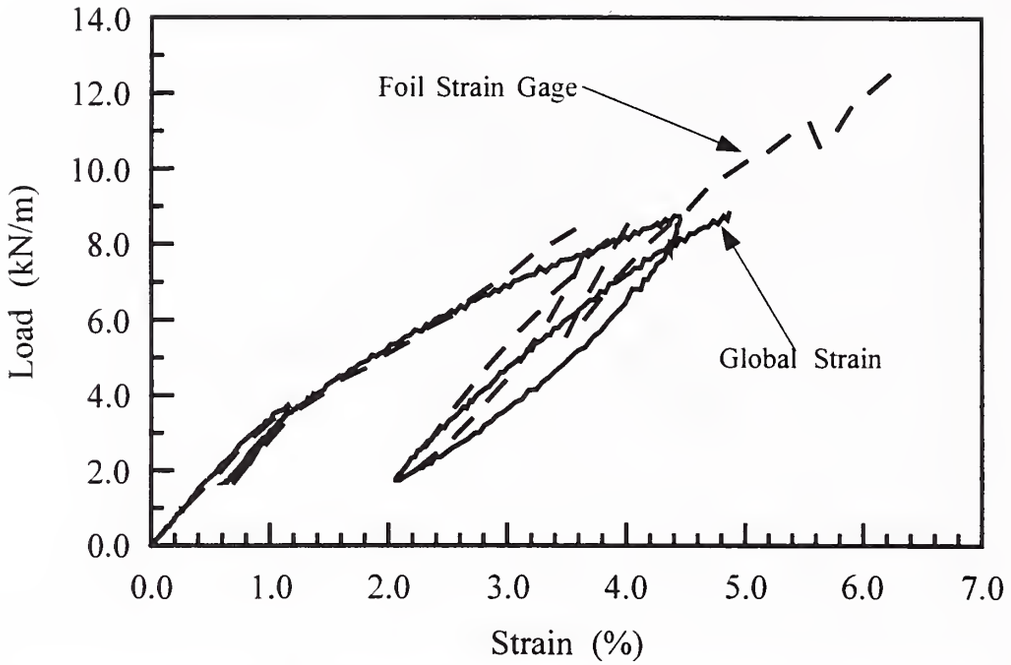

Figure B45: Calibrated Foil Strain Gage With Environmental Protection: Geogrid, Machine Direction

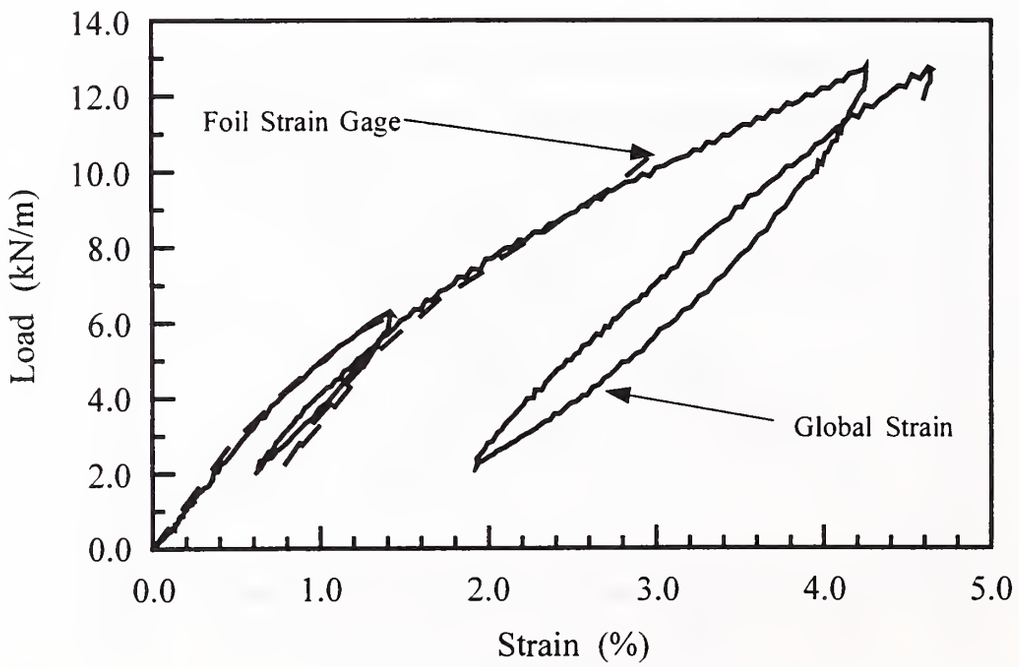

Figure B46: Calibrated Foil Strain Gage With Environmental Protection: Geogrid, Transverse Direction

APPENDIX C
TEST SECTION DATA

APPENDIX C1
LONG TERM MONITORING RESULTS

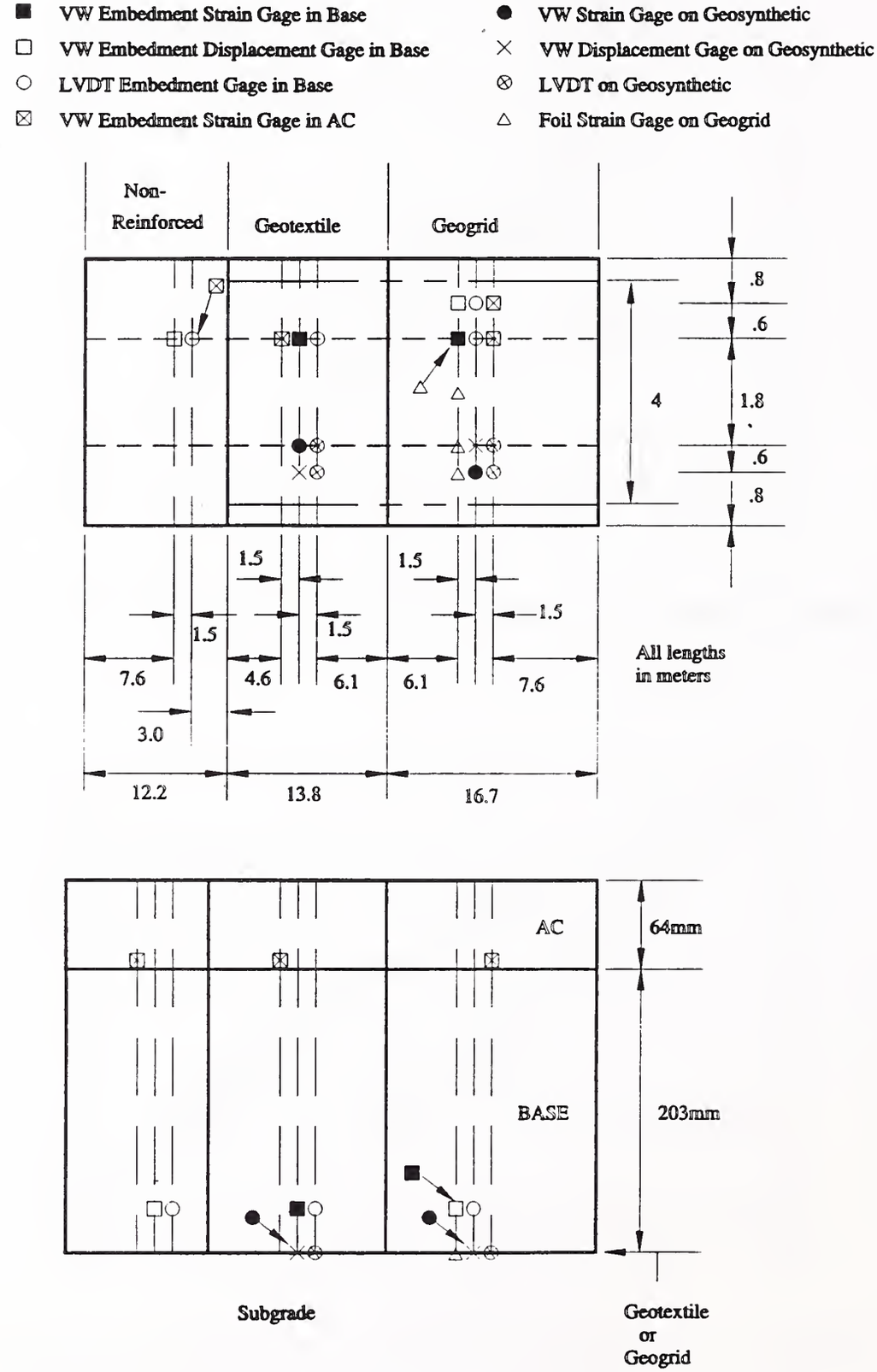

Figure C1.1: Test Section Instrumentation Layout

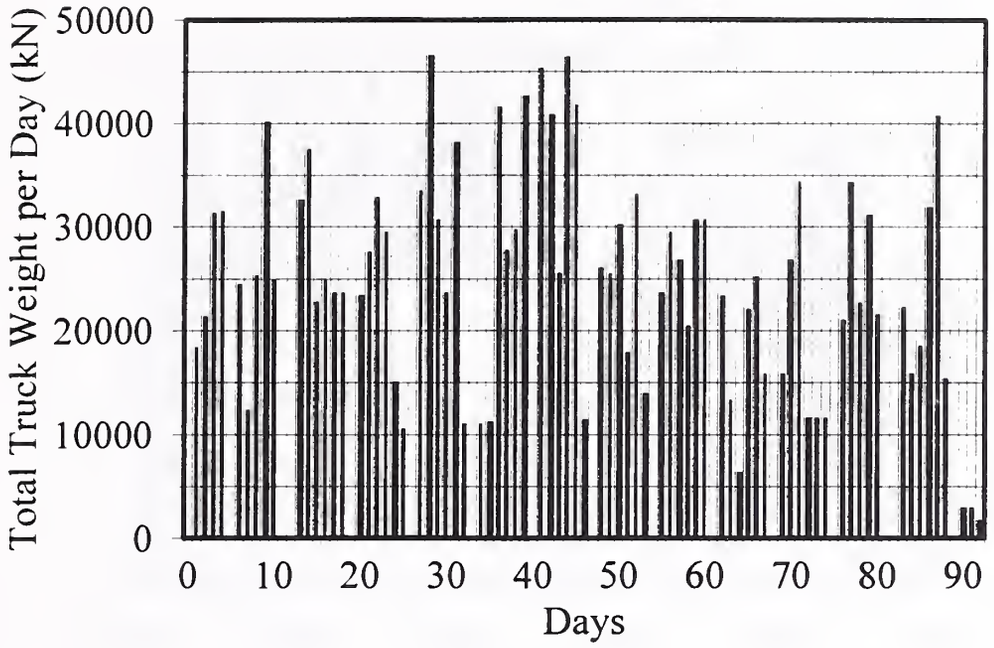

Figure C1.2A: Daily Traffic Loading History

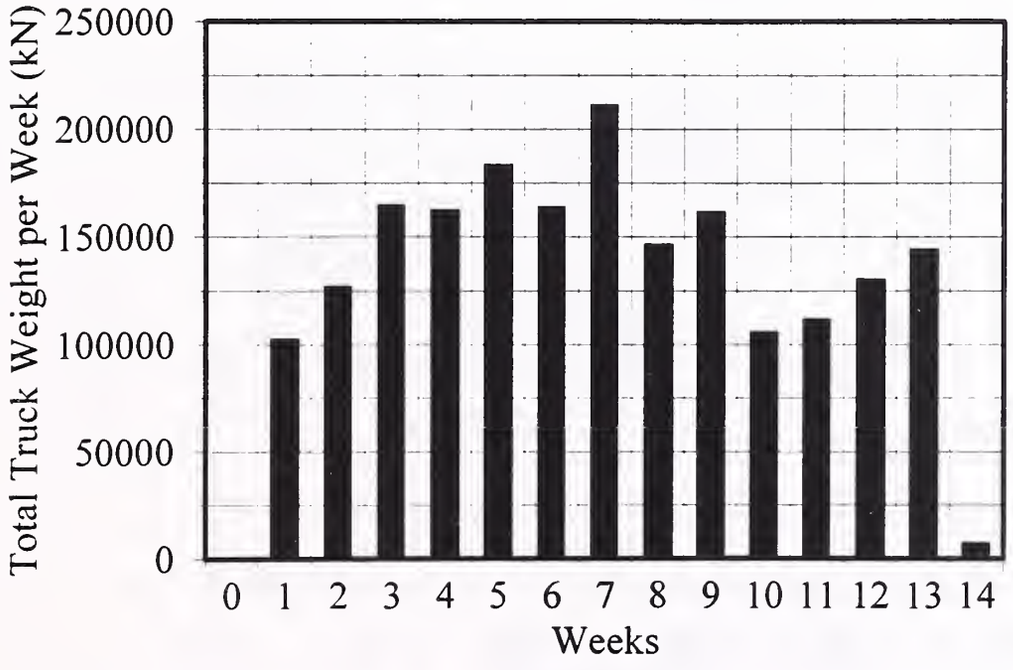

Figure C1.2B: Weekly Truck Traffic Loading History

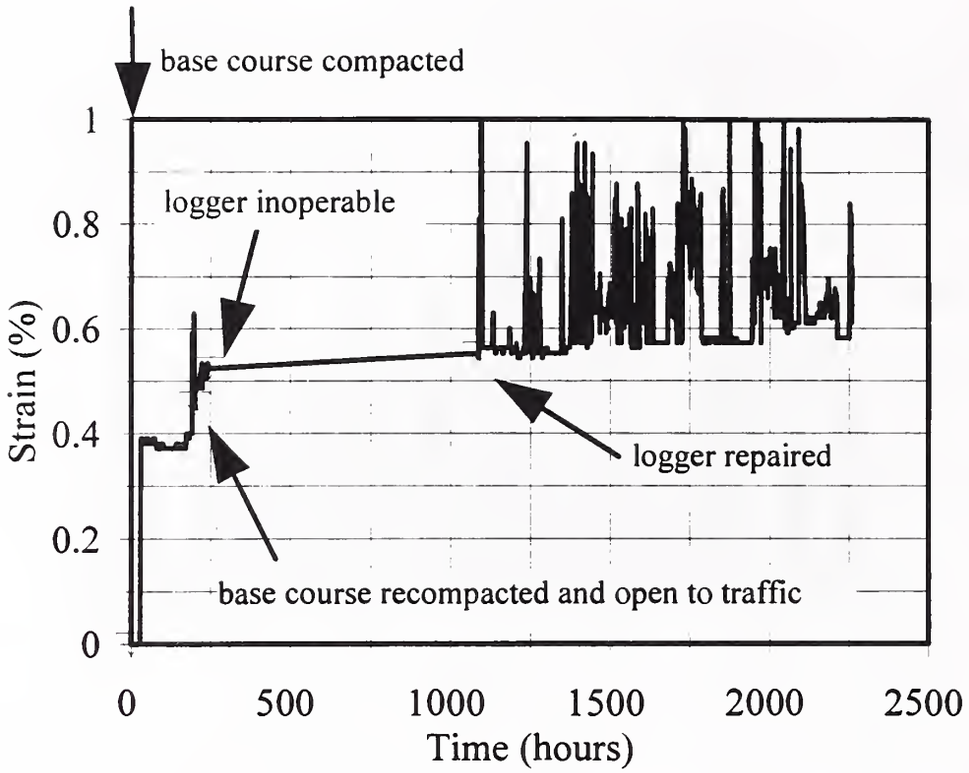

Figure C1.3: VW Displacement Gage #2 on Geogrid (on wheel-path)

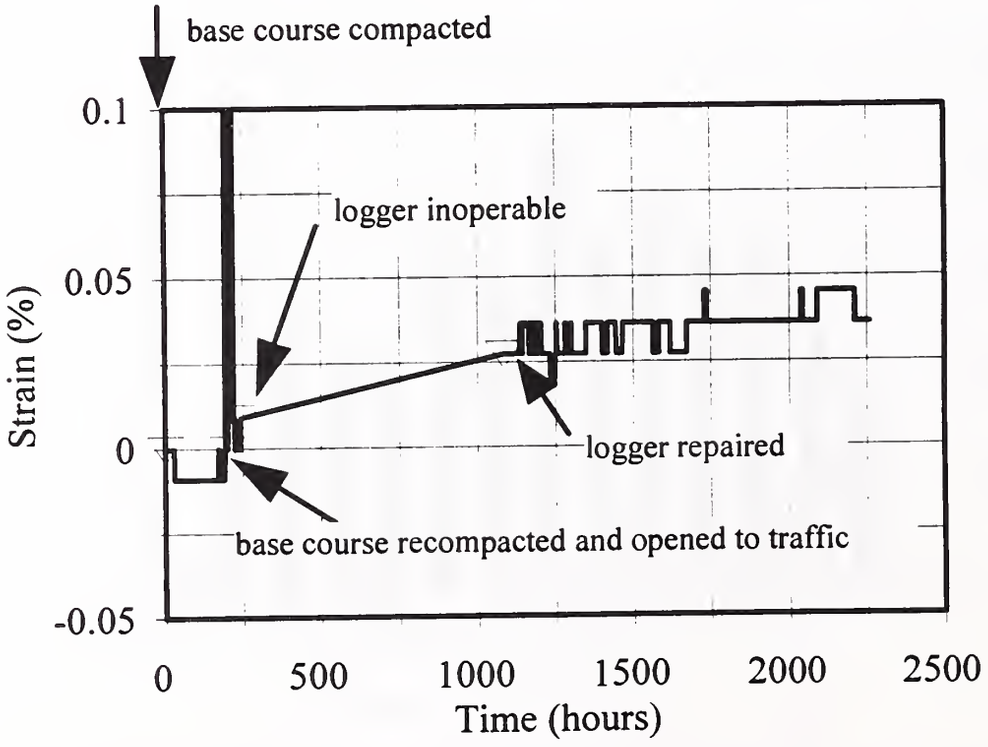

Figure C1.4: VW Displacement Gage #1 on Geotextile (off wheel-path)

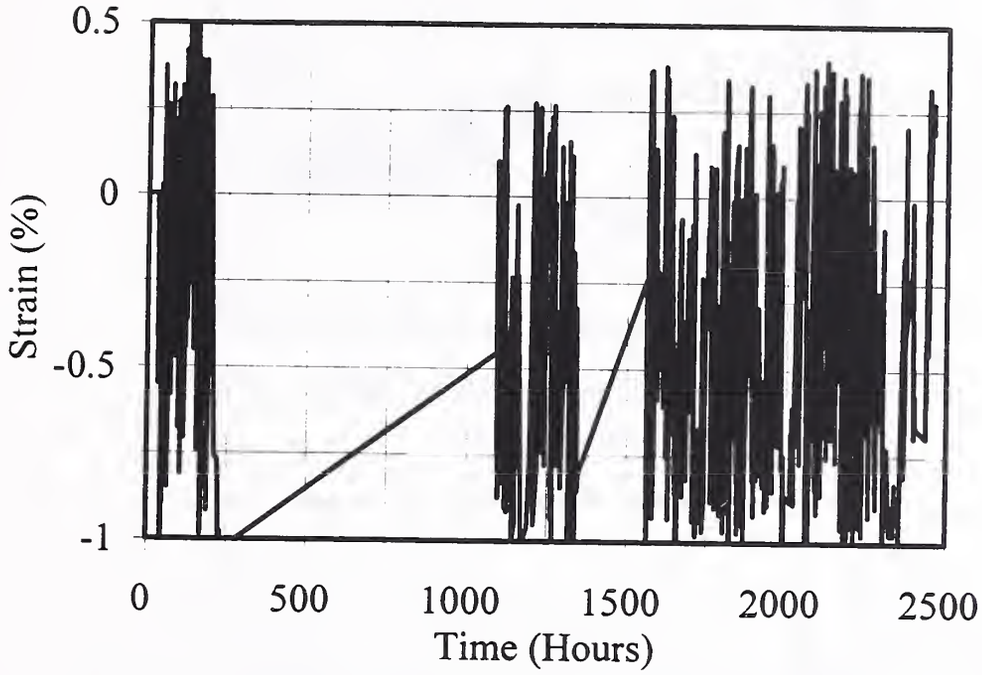

Figure C1.5: VW Strain Gage #6 on Geogrid (off wheel-path)

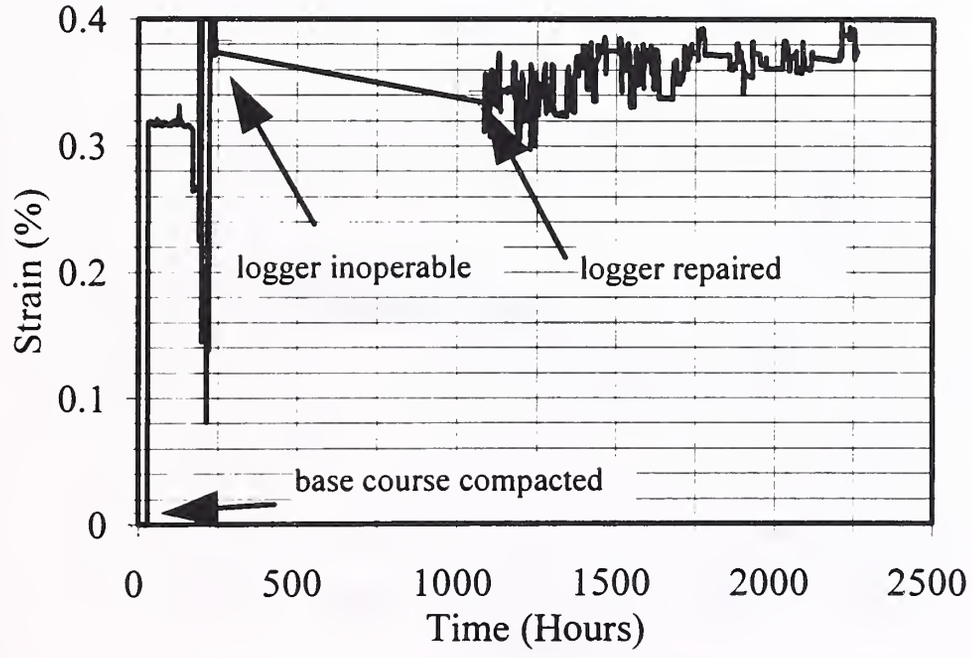

Figure C1.6: VW Strain Gage #5 on Geotextile (on wheel-path)

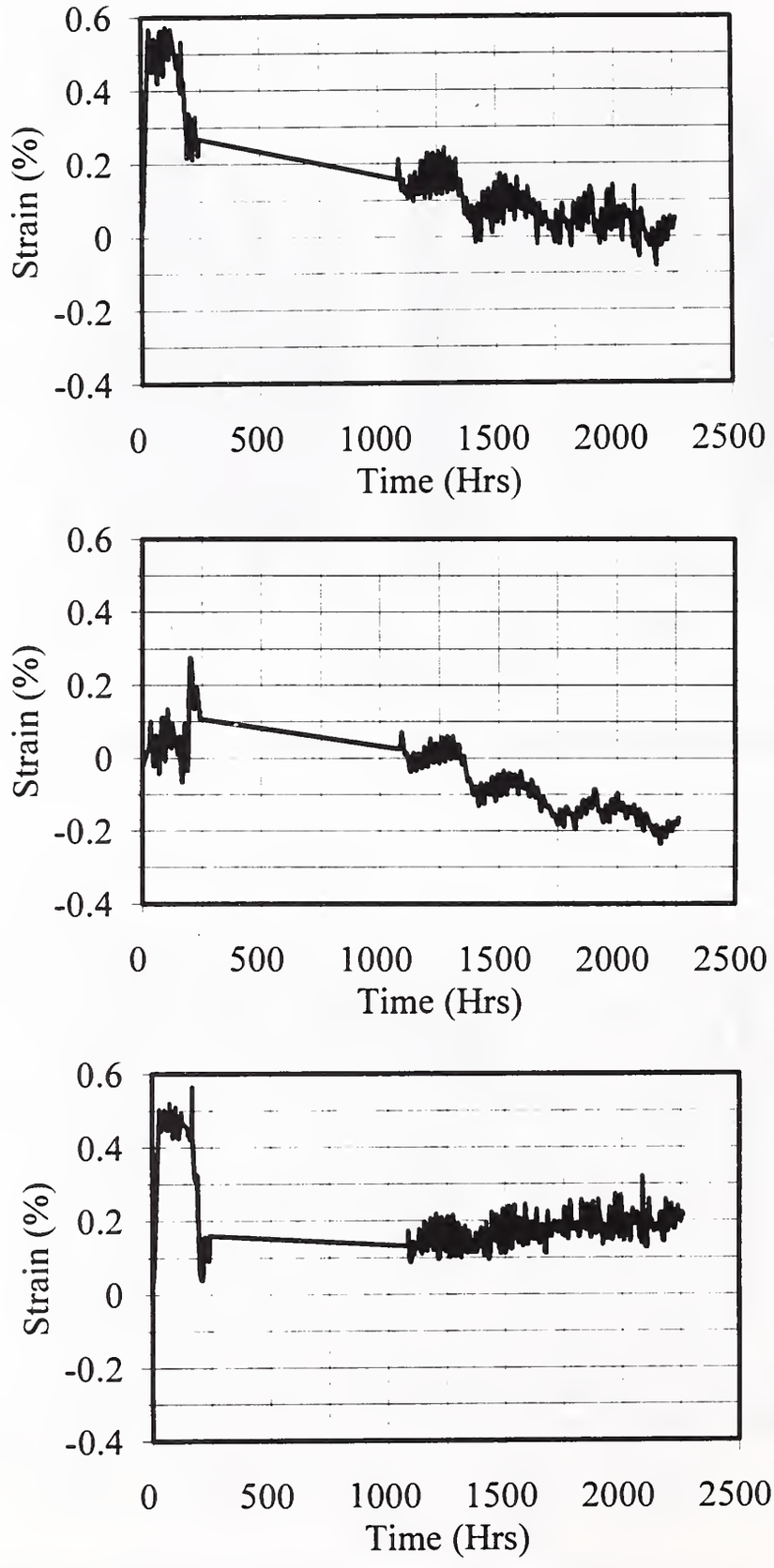

Figure C1.7: LVDT Displacement Gage #31 on Geogrid (on wheel-path)

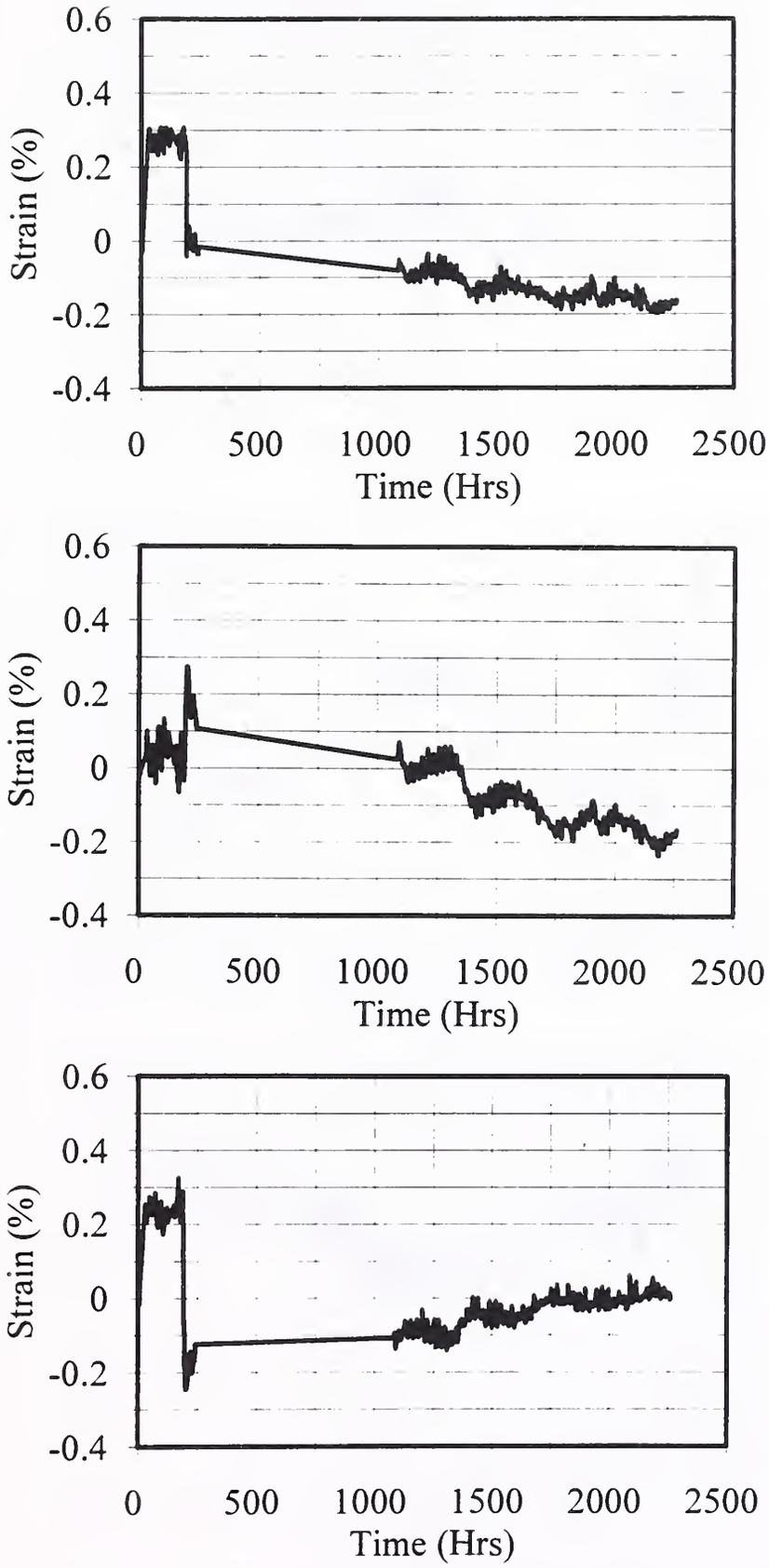

Figure C1.8: LVDT Displacement Gage #32 on Geogrid (off wheel-path)

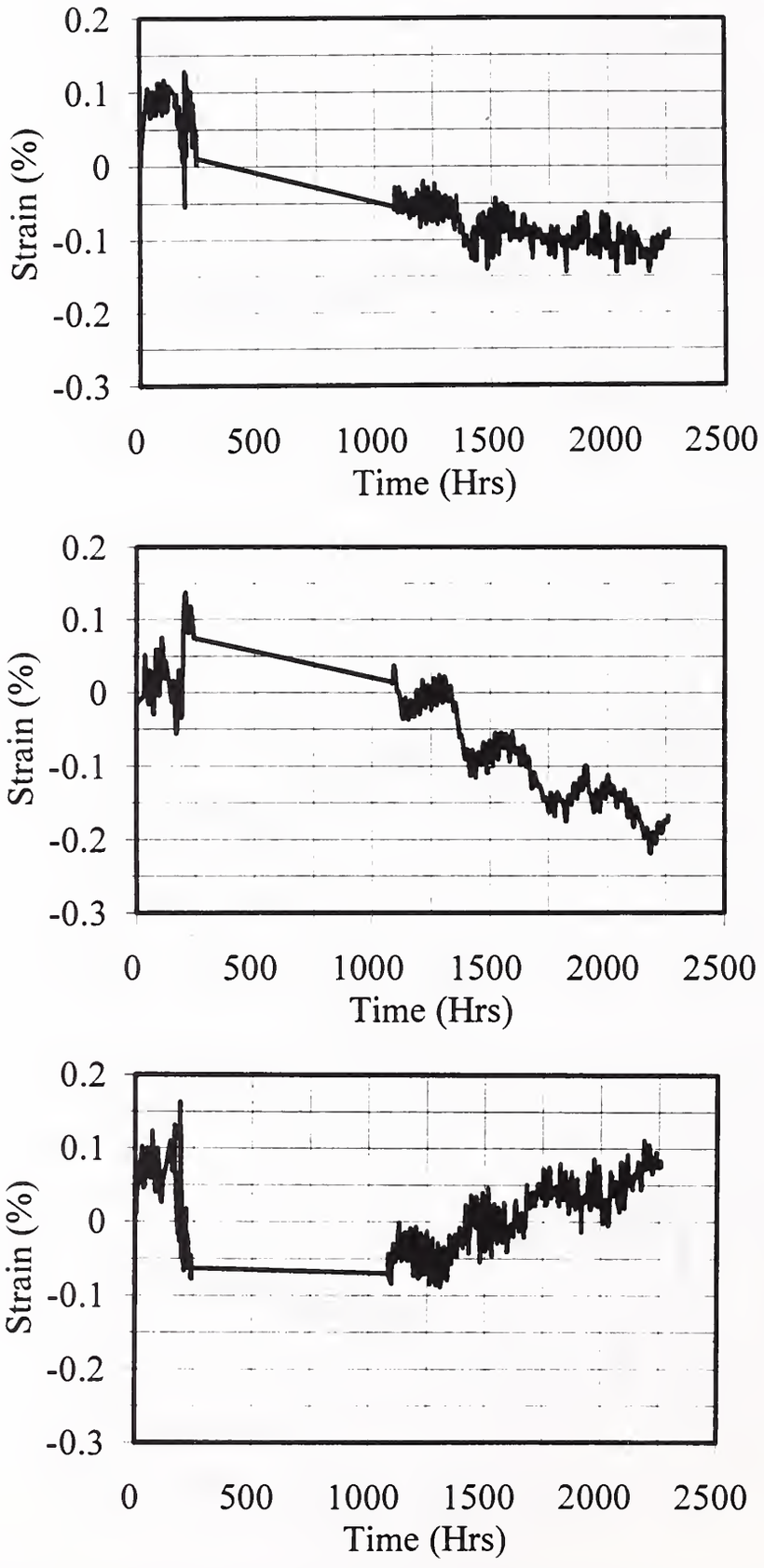

Figure C1.9: LVDT Displacement Gage #29 on Geotextile (on wheel-path)

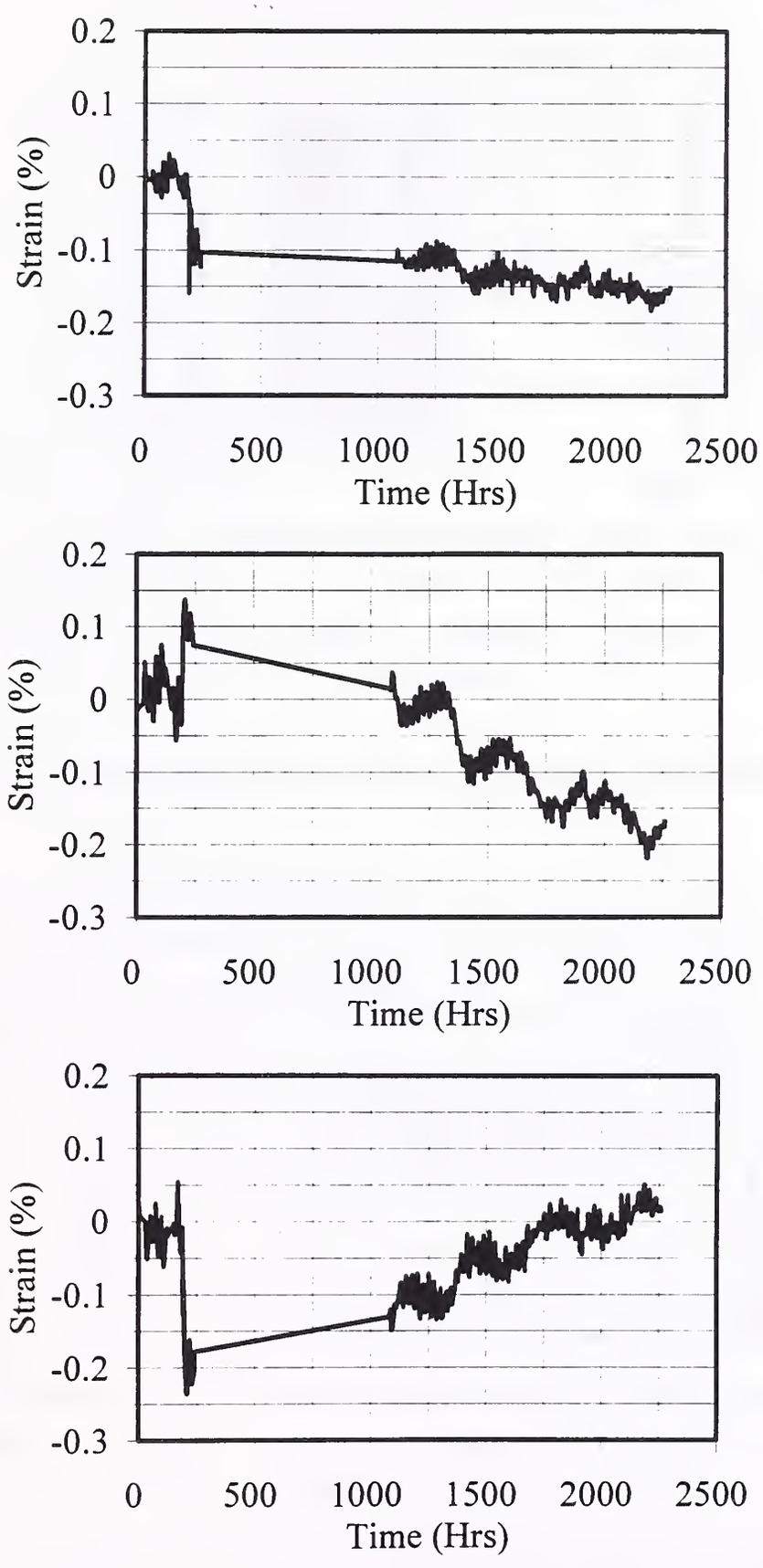

Figure C1.10: LVDT Displacement Gage #30 on Geotextile (off wheel-path)

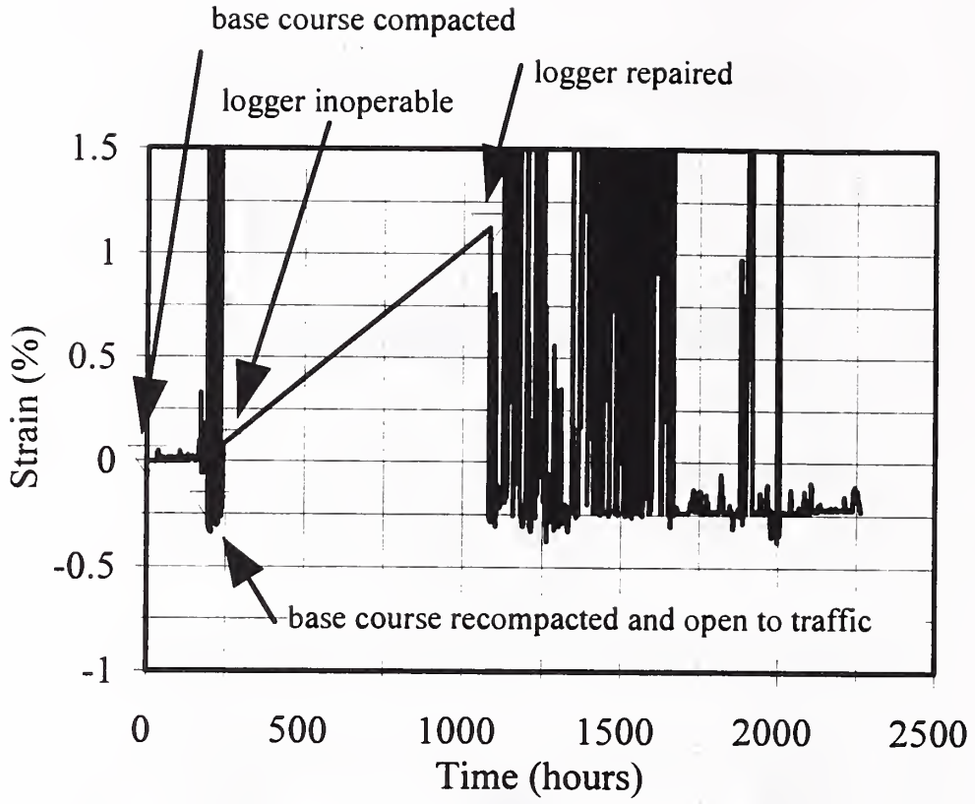

Figure C1.11: VW Embedment Displacement Gage #3 in Base Above Geogrid (off wheel-path)

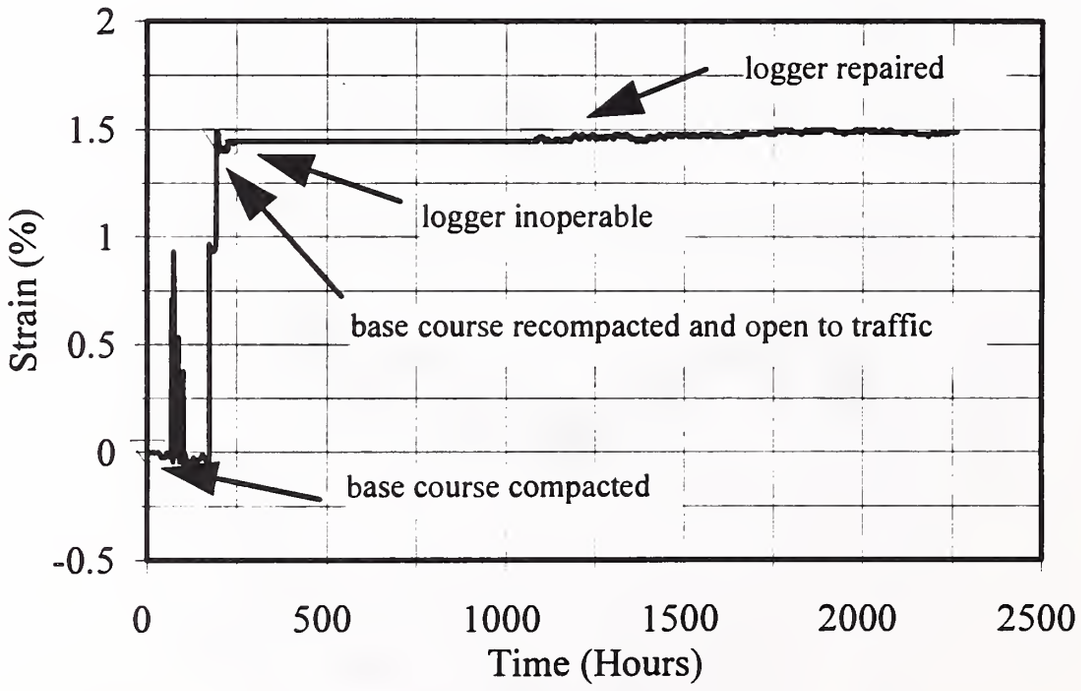

Figure C1.12: VW Embedment Displacement Gage #4 in Base in Non-Reinforced Section (on wheel-path)

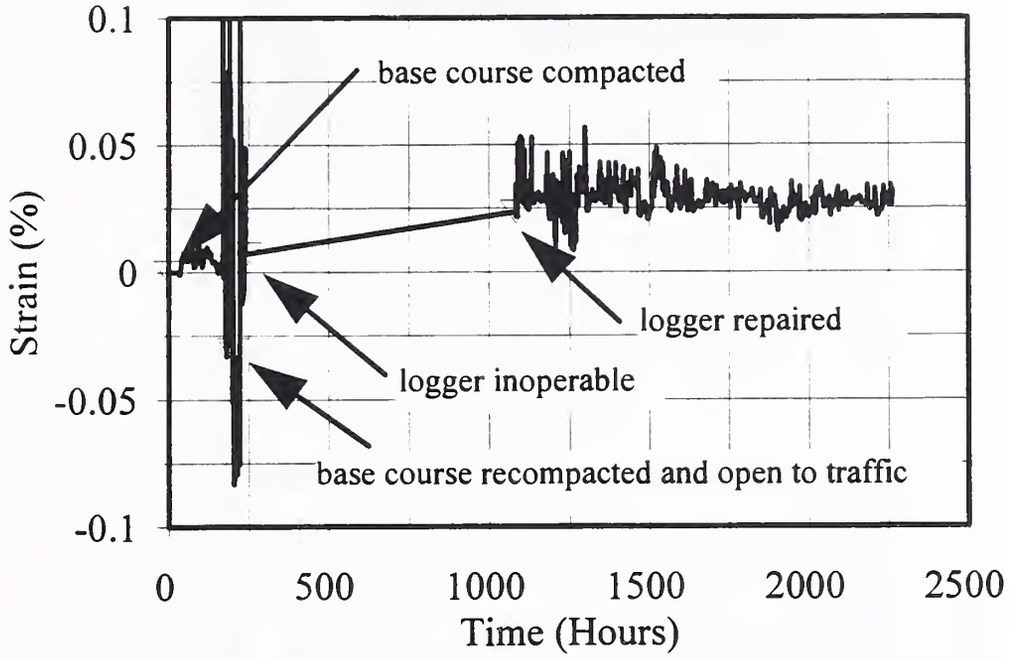

Figure C1.13: VW Embedment Strain Gage #8 in Base Above Geogrid (on wheel-path)

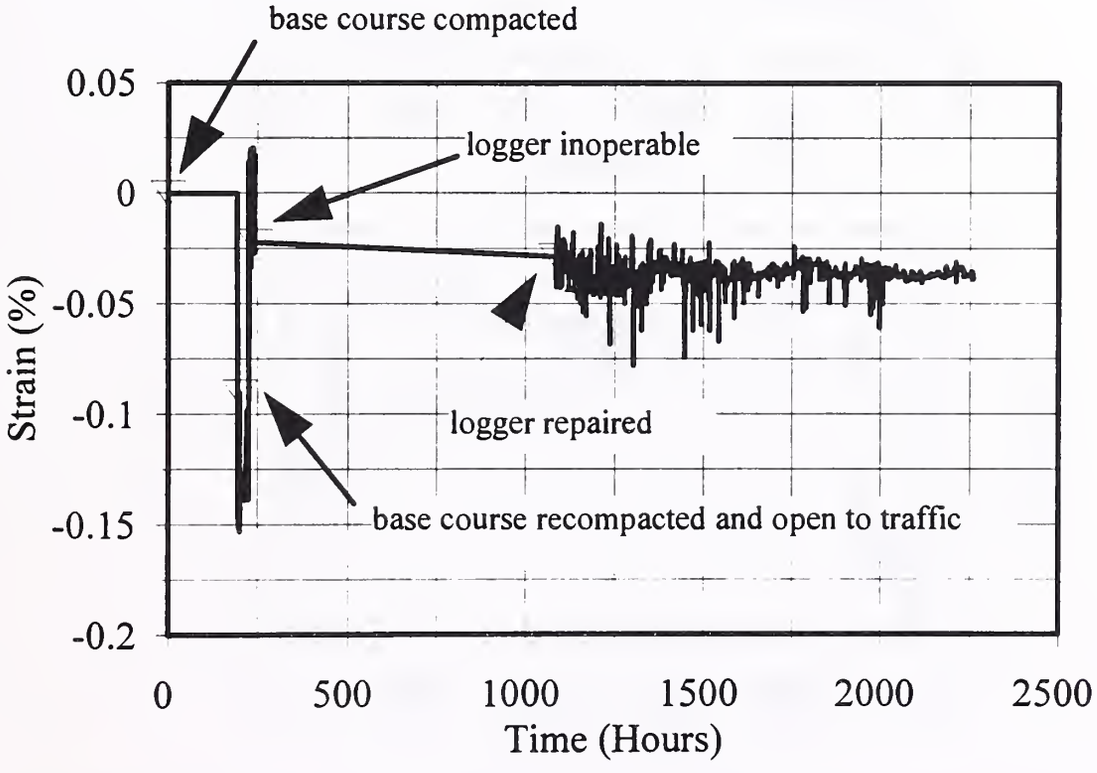

Figure C1.14: VW Embedment Strain Gage #7 in Base Above Geotextile (on wheel-path)

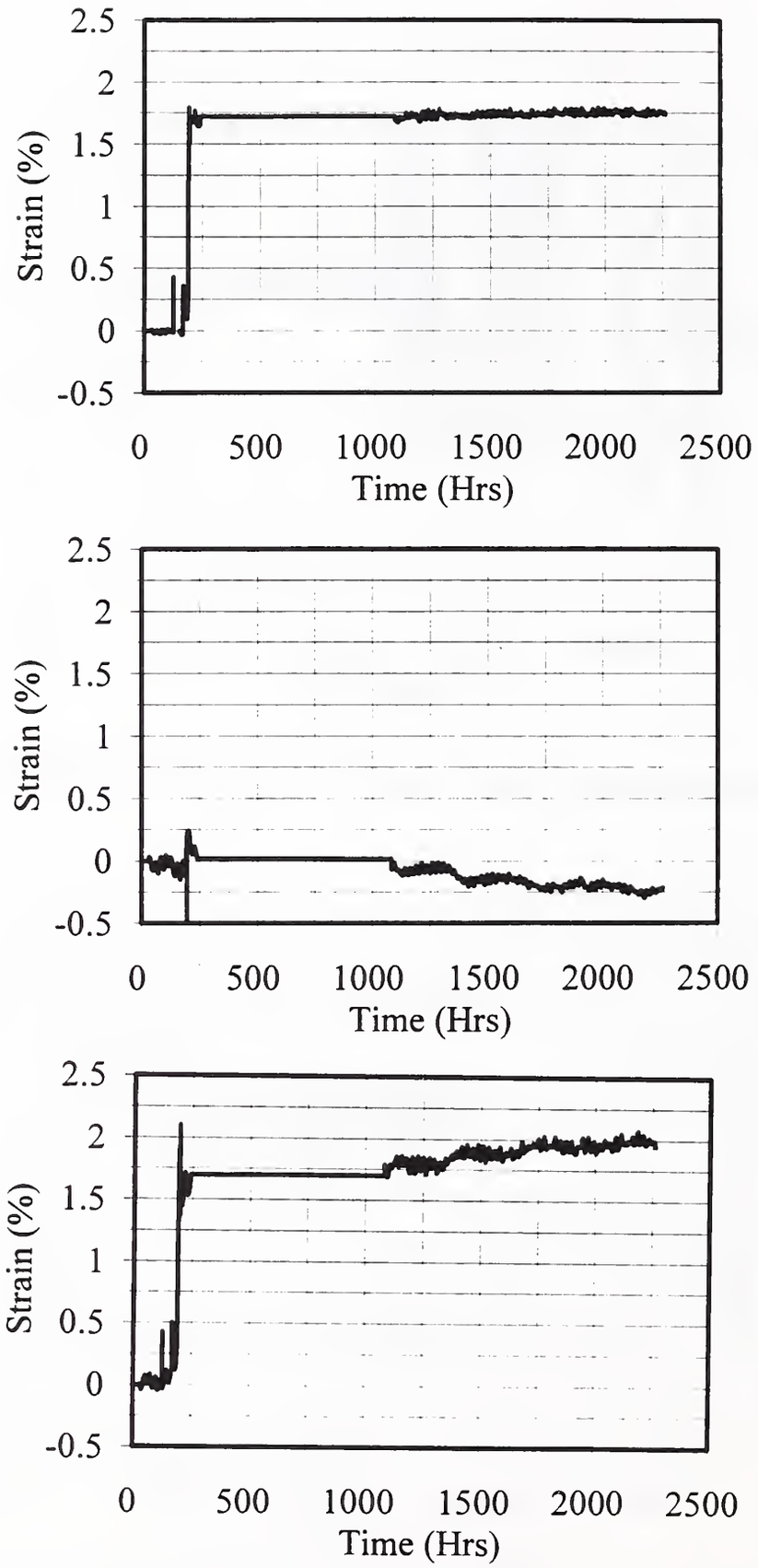

Figure C1.15: LVDT Embedment Displacement Gage #27 in Base Above Geogrid (off wheel-path)

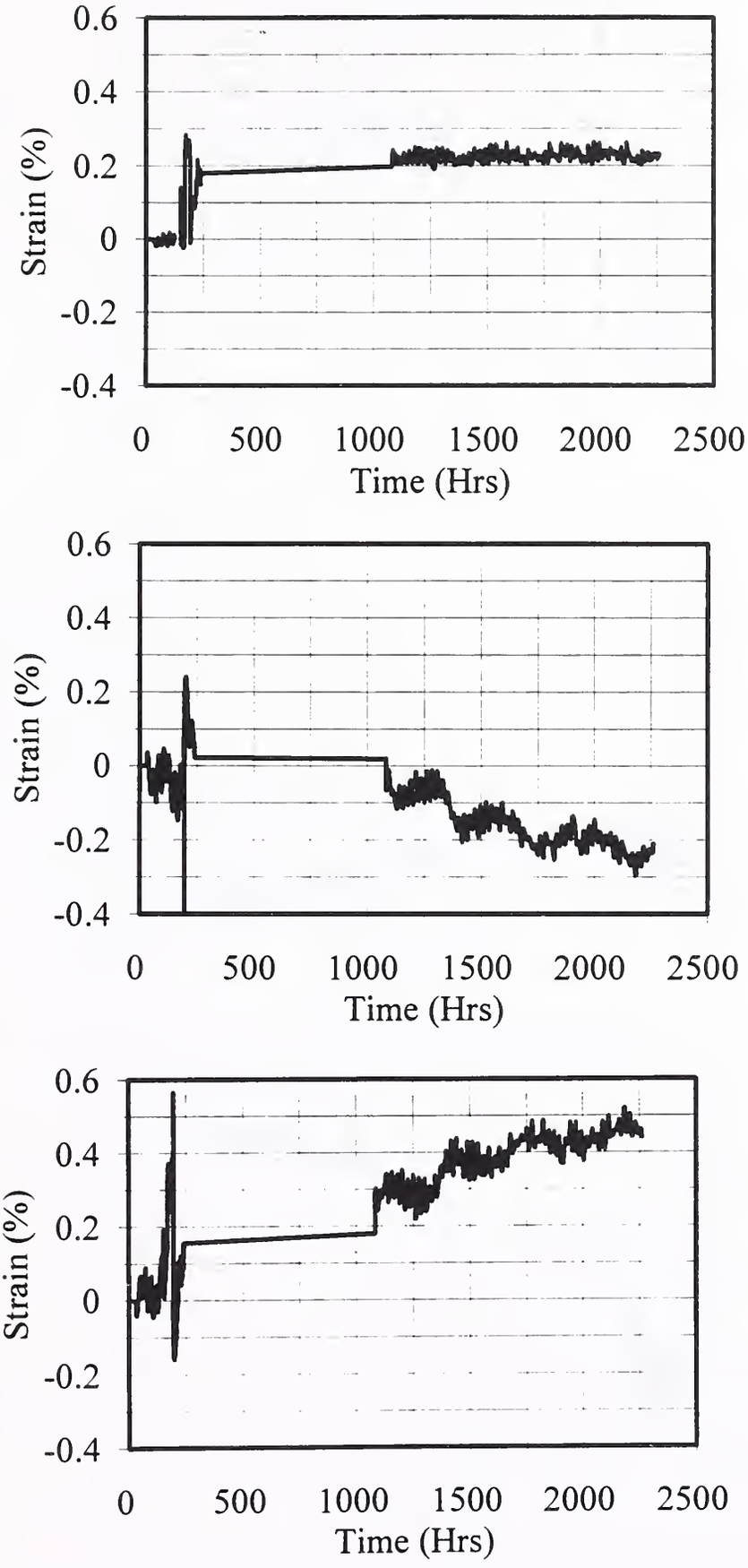

Figure C1.16: LVDT Embedment Displacement Gage #28 in Base Above Geogrid (on wheel-path)

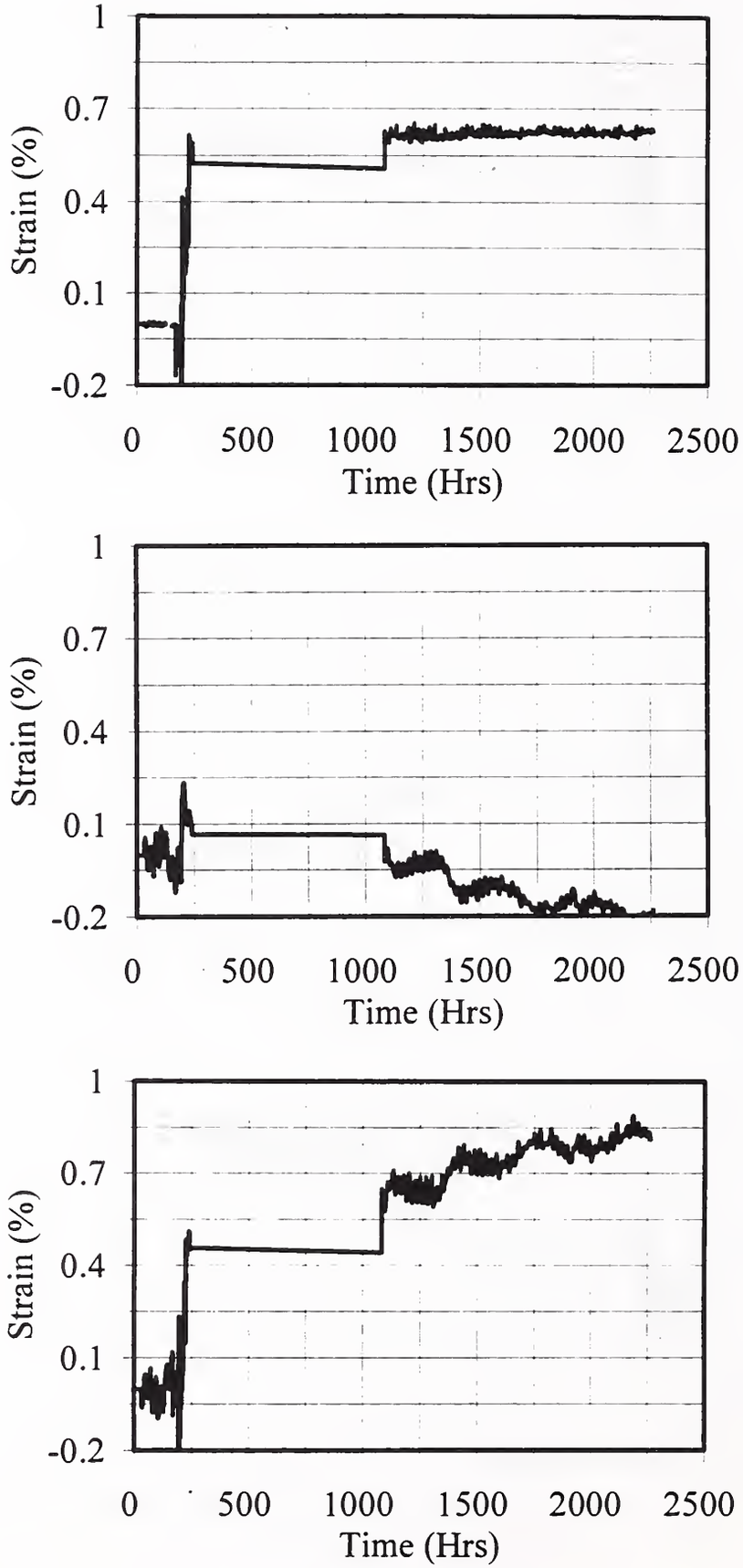

Figure C1.17: LVDT Embedment Displacement Gage #25 in Base Above Geotextile (on wheel-path)

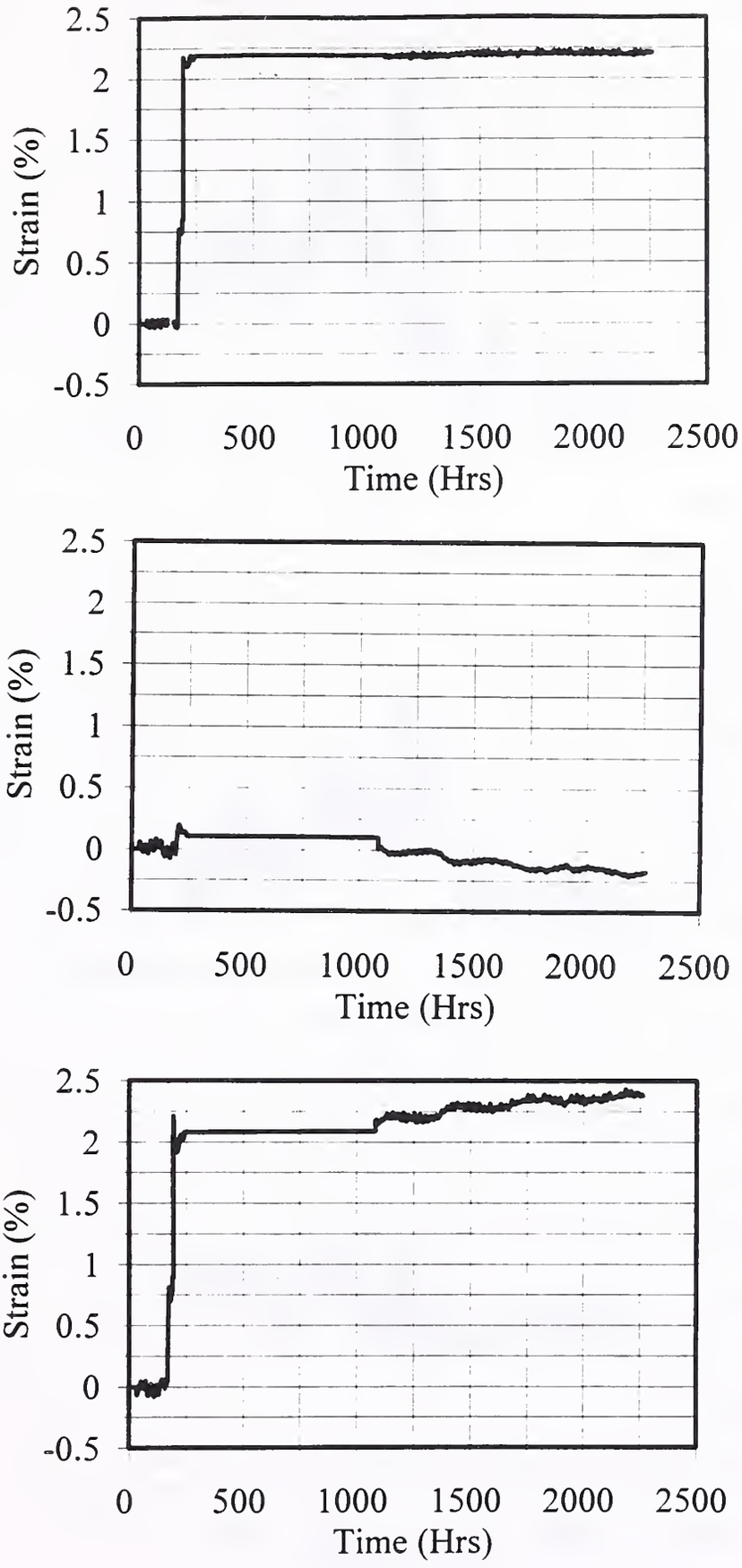

Figure C1.18: LVDT Embedment Displacement Gage #26 in Base in Non-Reinforced Section (on wheel-path)

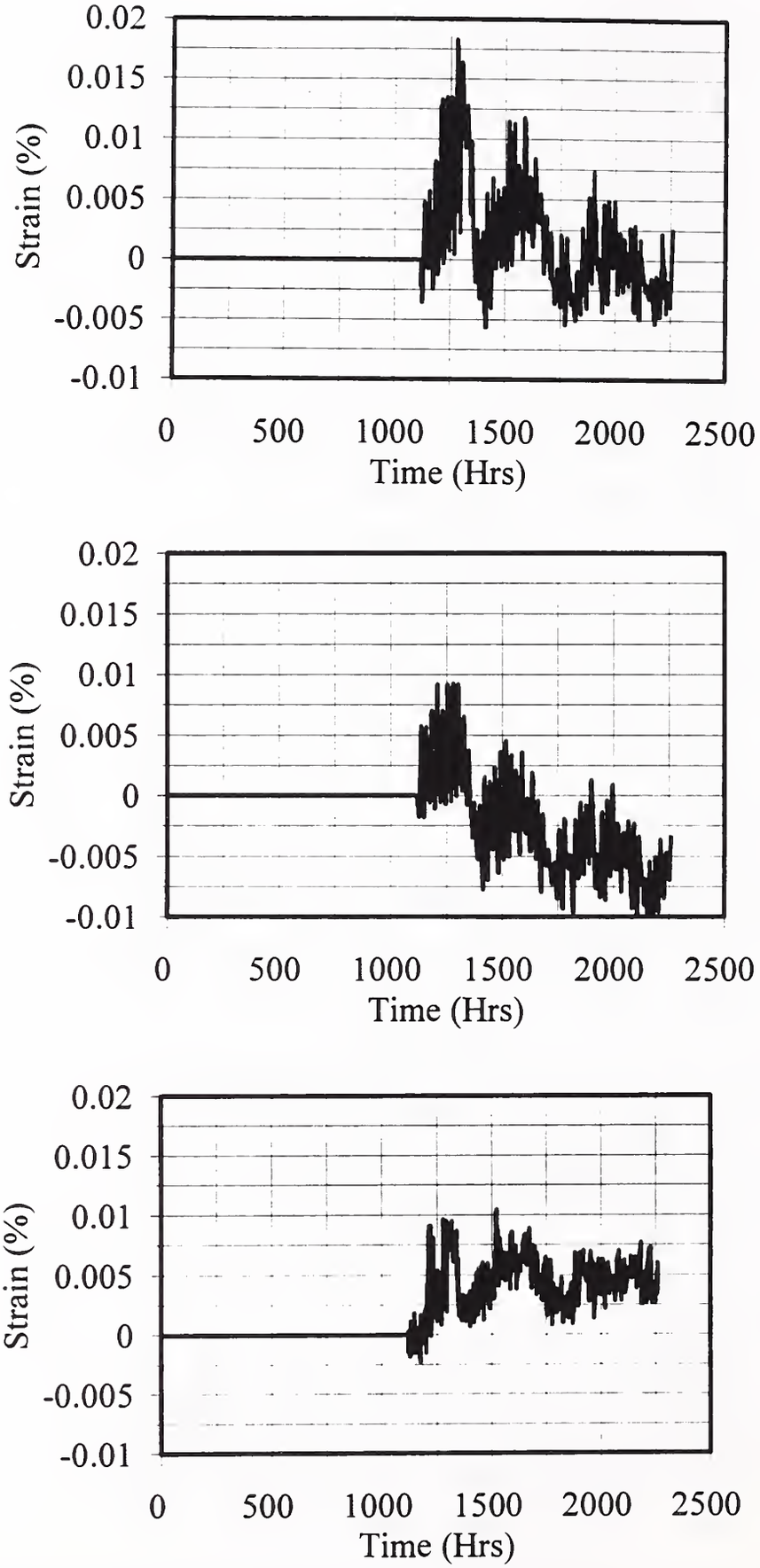

Figure C1.19: VW Embedment Strain Gage #10 in AC Above Geogrid (on wheel-path)

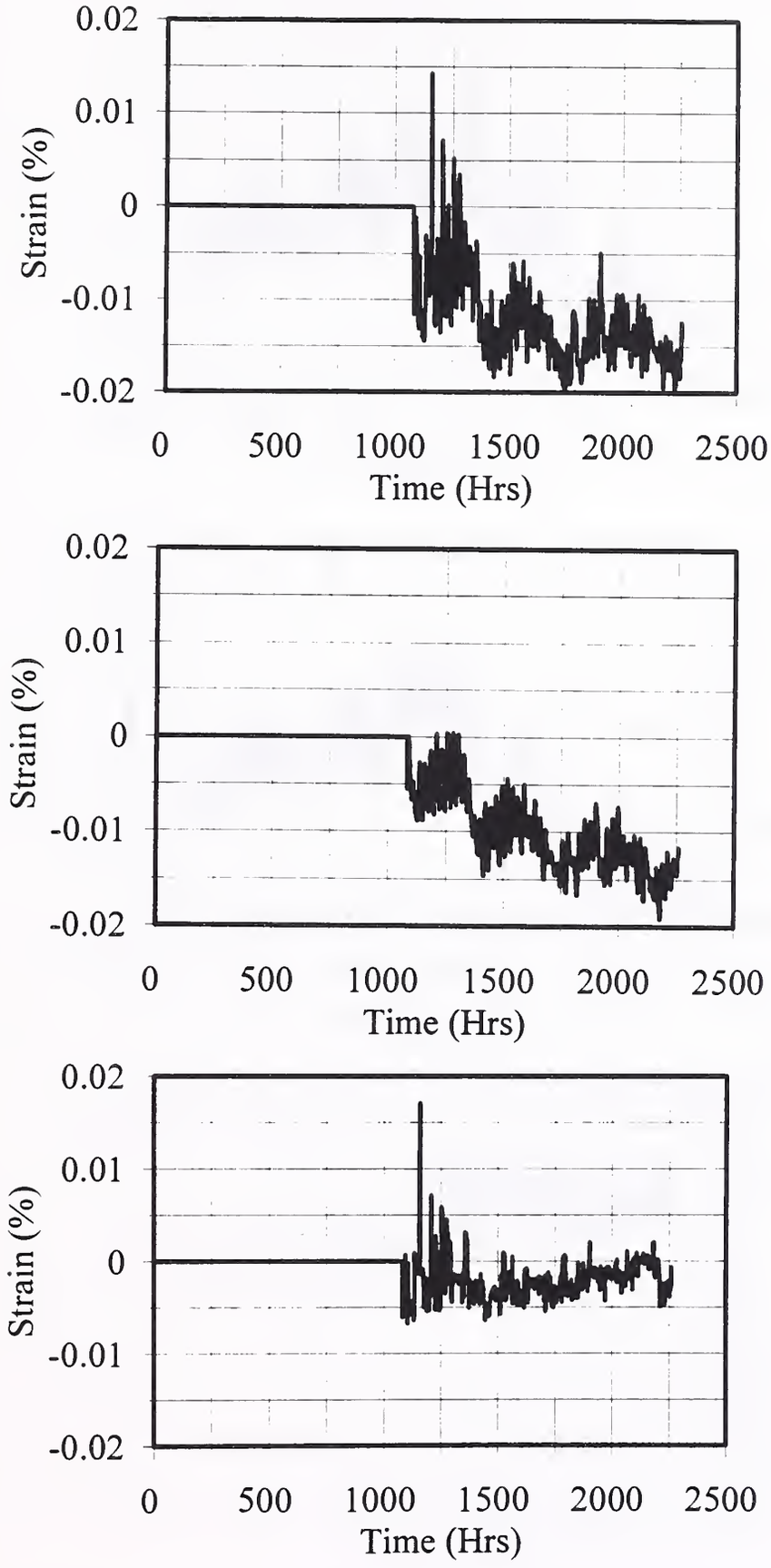

Figure C1.20: VW Embedment Strain Gage #11 in AC Above Geogrid (off wheel-path)

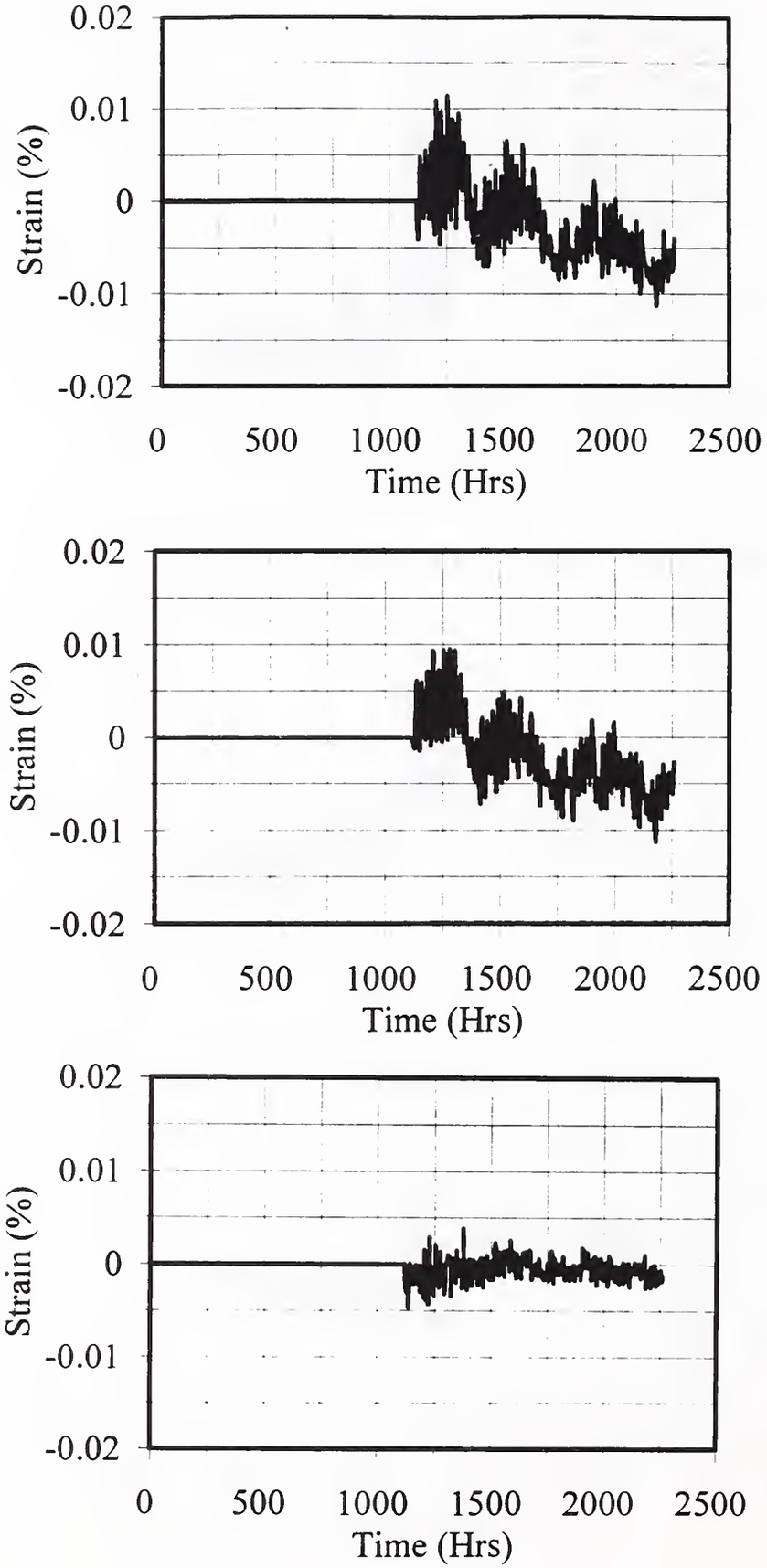

Figure C1.21: VW Embedment Strain Gage #9 in AC Above Geotextile (on wheel-path)

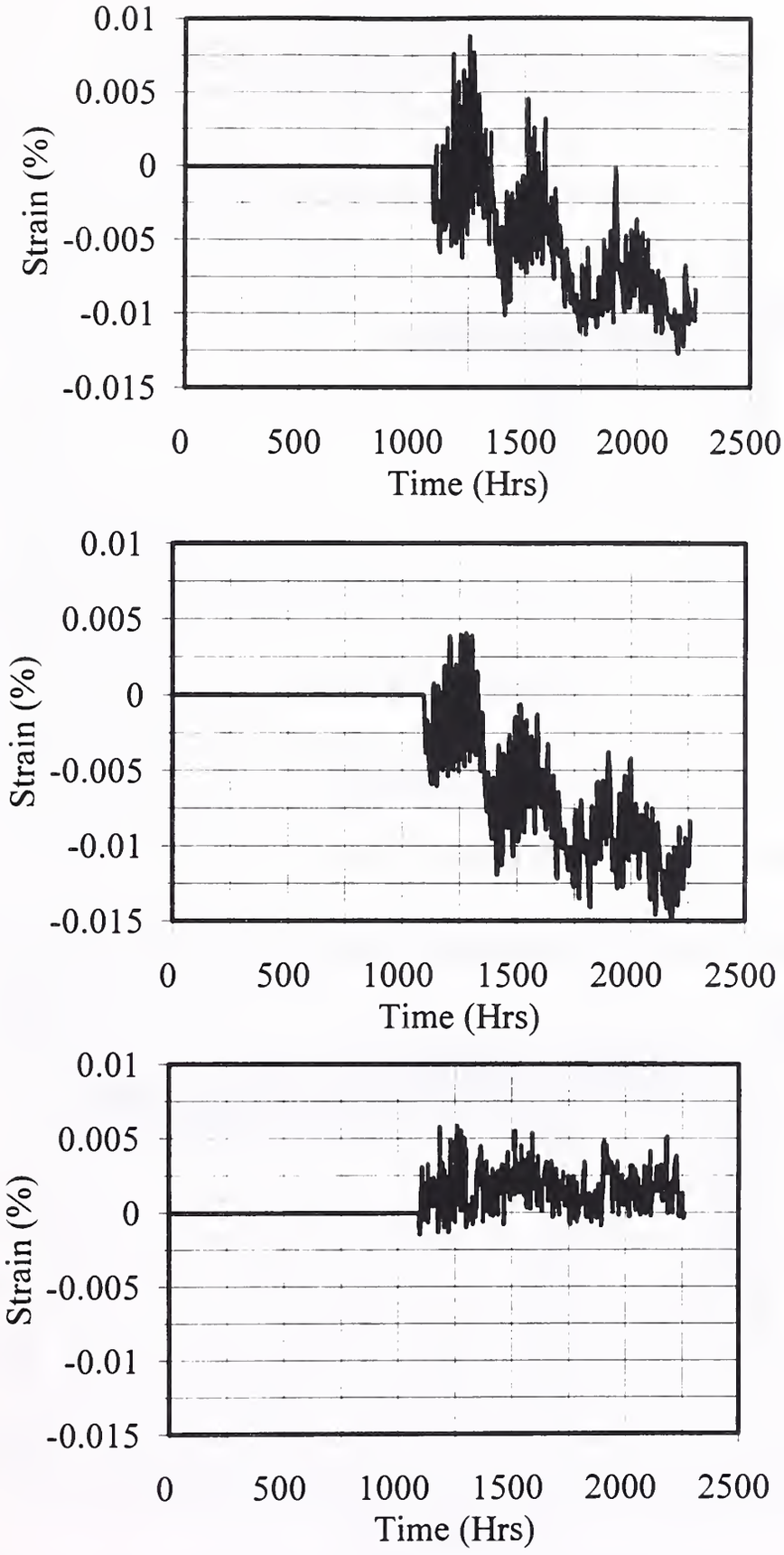

Figure C1.22: VW Embedment Strain Gage #12 in AC in Non-Reinforced Section (on wheel-path)

APPENDIX C2
DYNAMIC TRUCK PASS TEST DATA

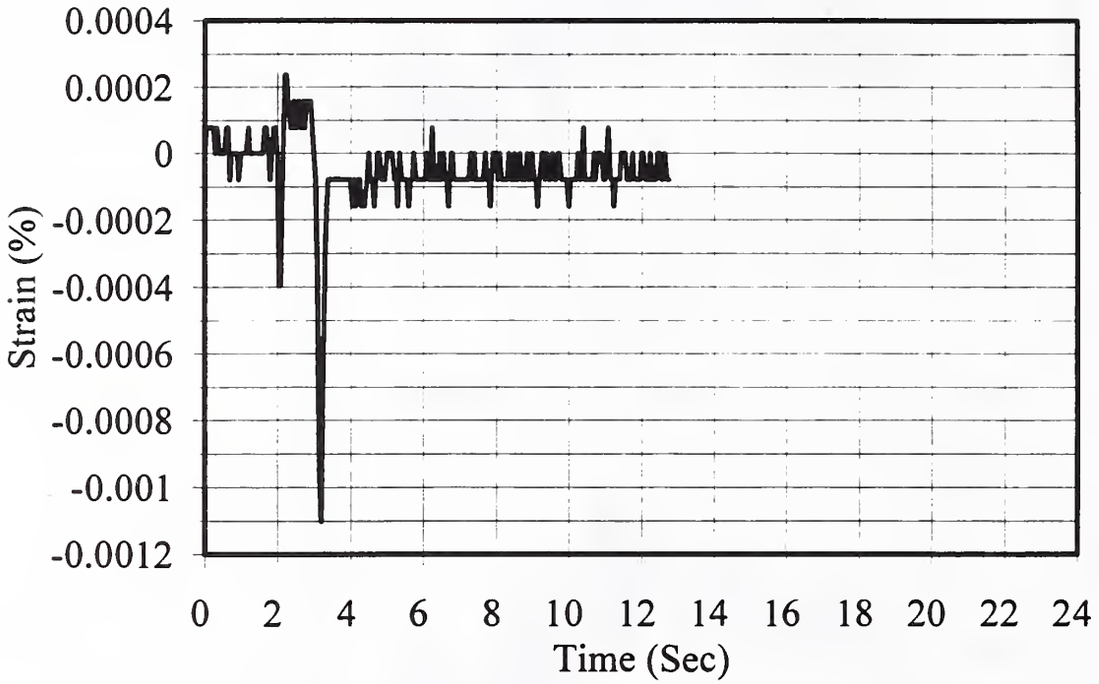

Figure C2.1: Foil Strain Gage #36 on Geogrid (on wheel path): Truck Pass Test 1

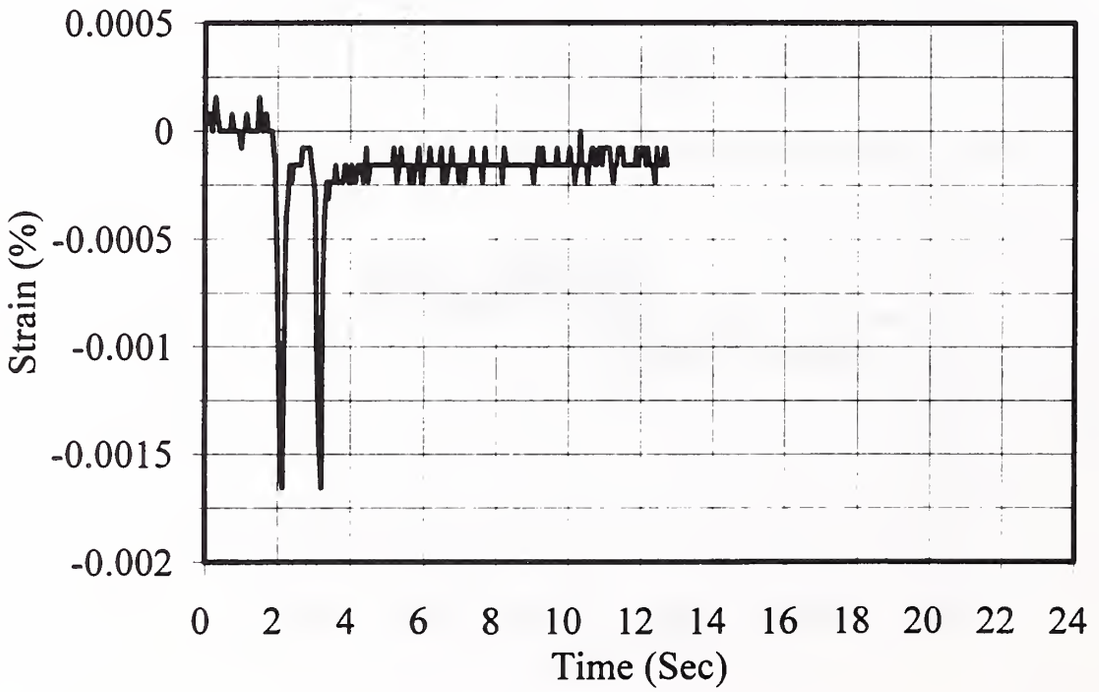

Figure C2.2: Foil Strain Gage #35 on Geogrid (below centerline): Truck Pass Test 1

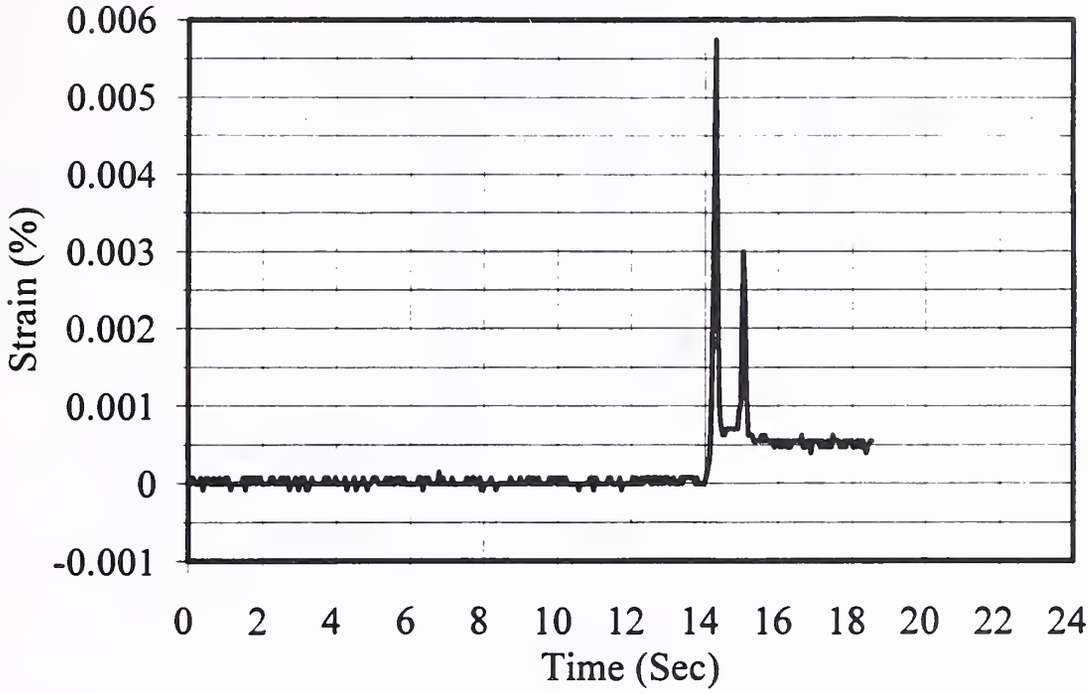

Figure C2.3: Foil Strain Gage #36 on Geogrid (on wheel path): Truck Pass Test 2

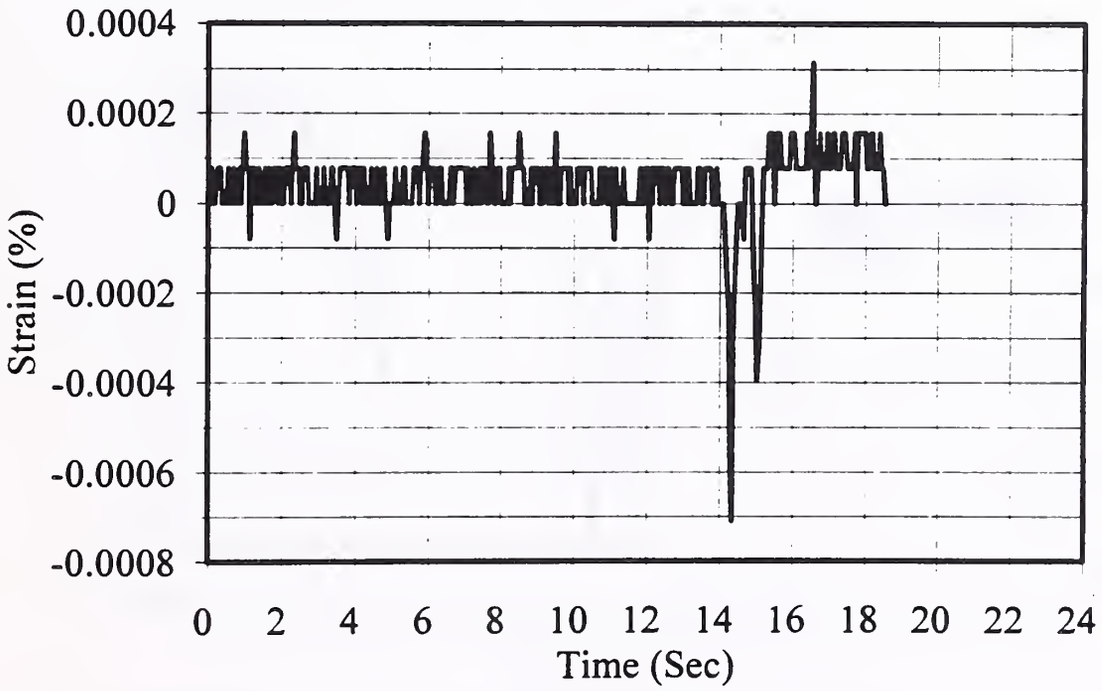

Figure C2.4: Foil Strain Gage #35 on Geogrid (below centerline): Truck Pass Test 2

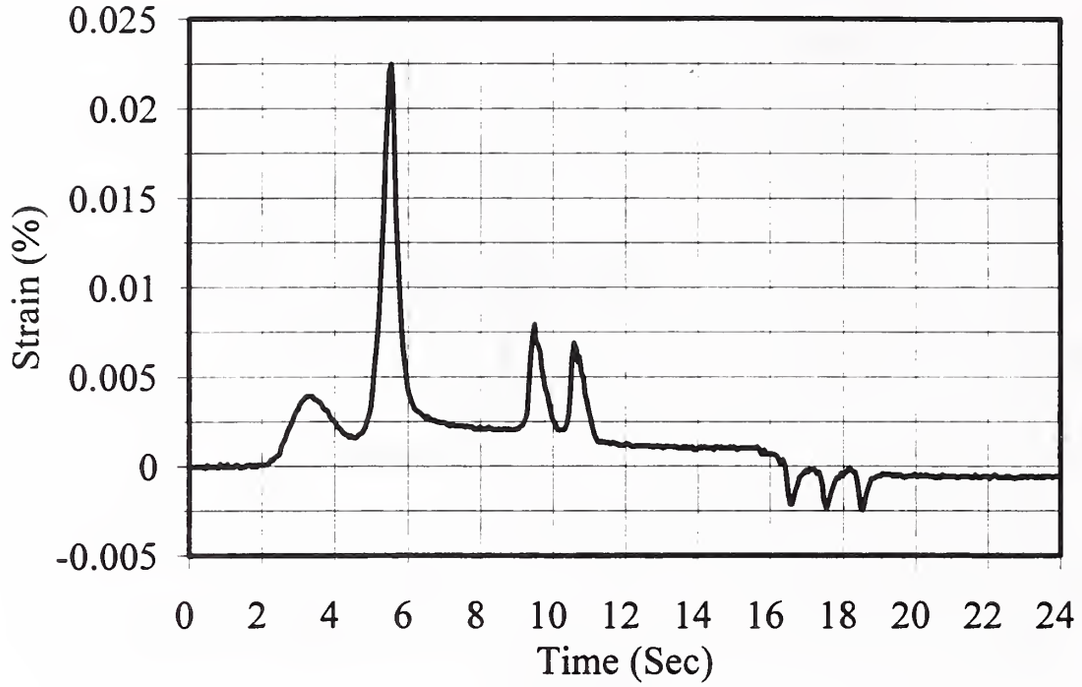

Figure C2.5: Foil Strain Gage #36 on Geogrid (on wheel path): Truck Pass Test 3

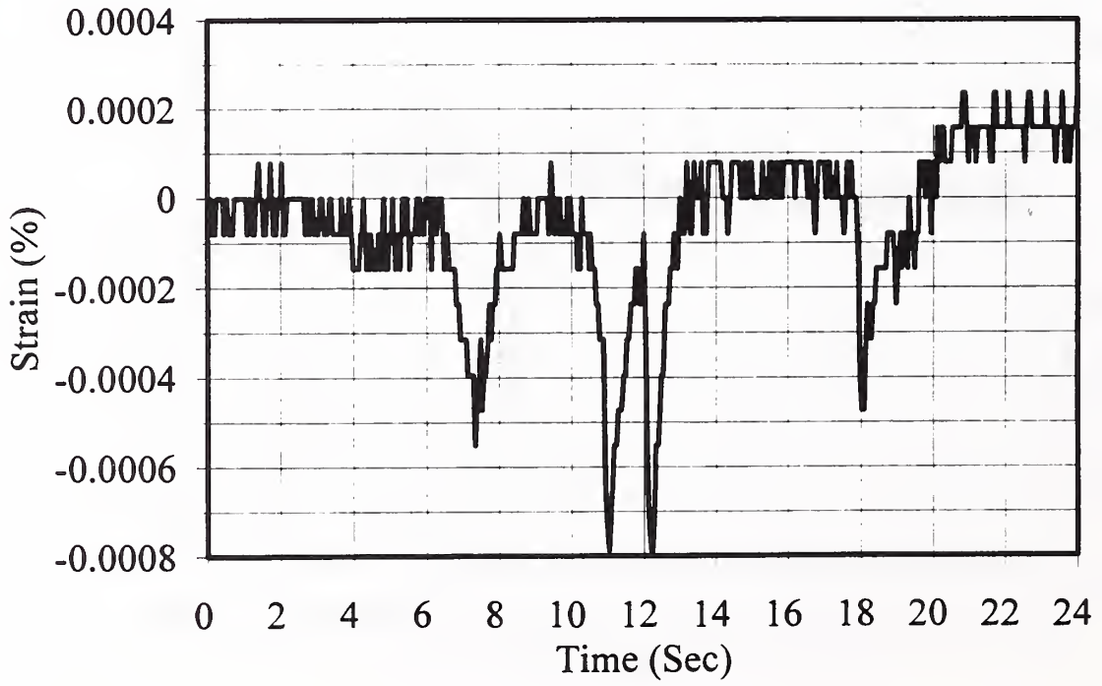

Figure C2.6: Foil Strain Gage #35 on Geogrid (below centerline): Truck Pass Test 3

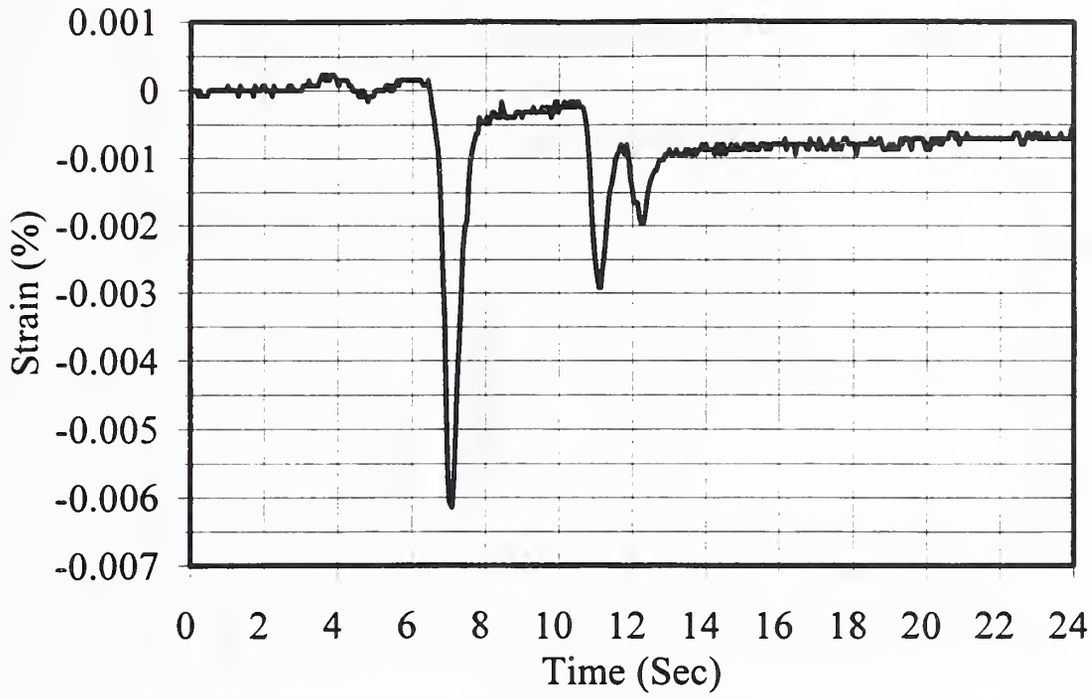

Figure C2.7: Foil Strain Gage #34 on Geogrid (on wheel path): Truck Pass Test 3

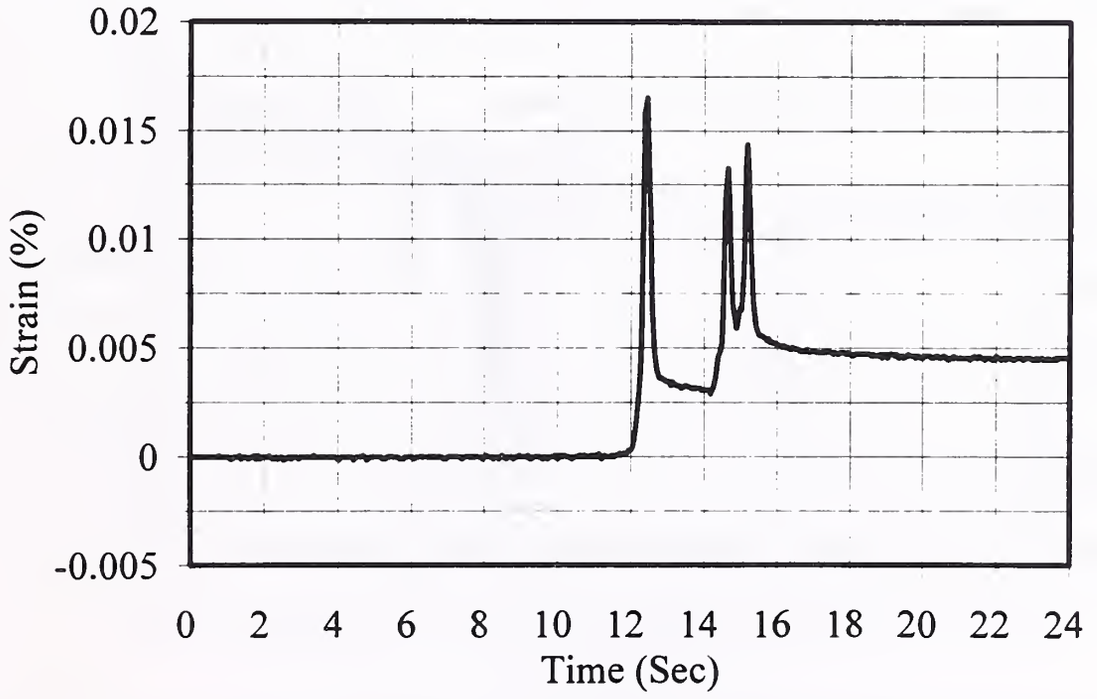

Figure C2.8: Foil Strain Gage #36 on Geogrid (on wheel path): Truck Pass Test 4

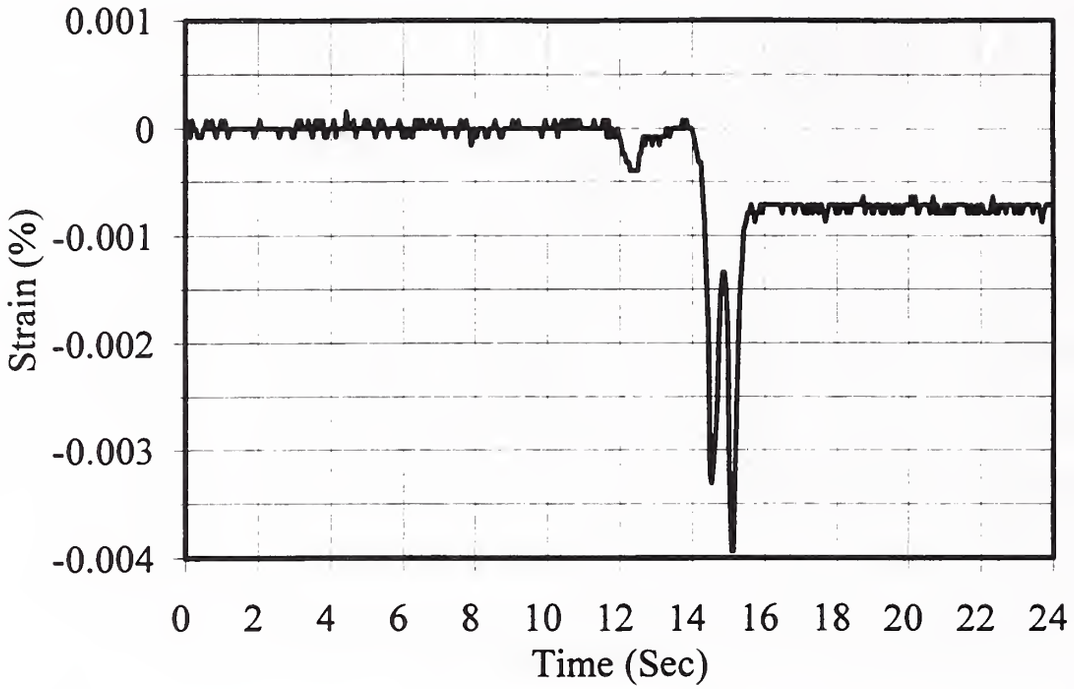

Figure C2.9: Foil Strain Gage #35 on Geogrid (below centerline): Truck Pass Test 4

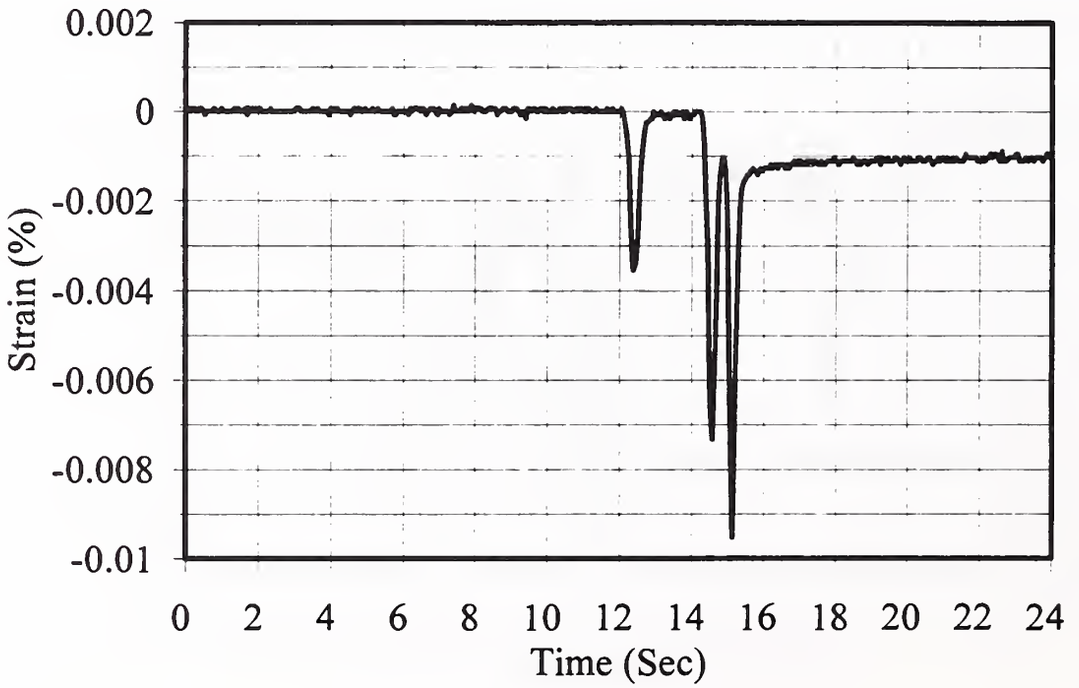

Figure C2.10: Foil Strain Gage #34 on Geogrid (on wheel path): Truck Pass Test 4

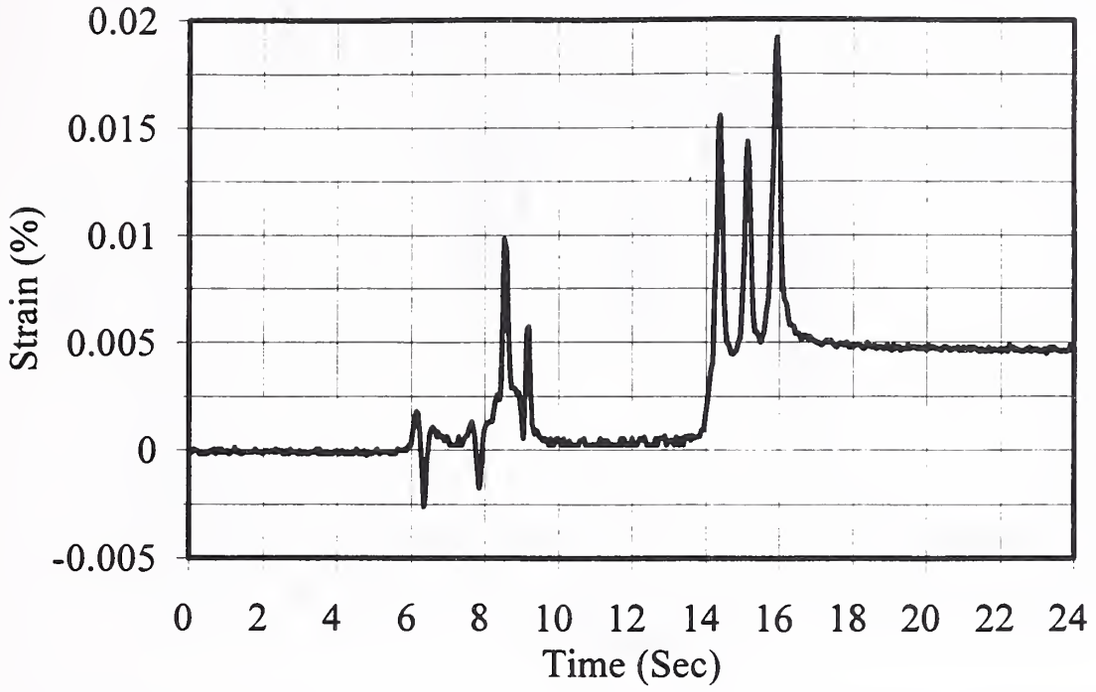

Figure C2.11: Foil Strain Gage #36 on Geogrid (on wheel path): Truck Pass Test 5

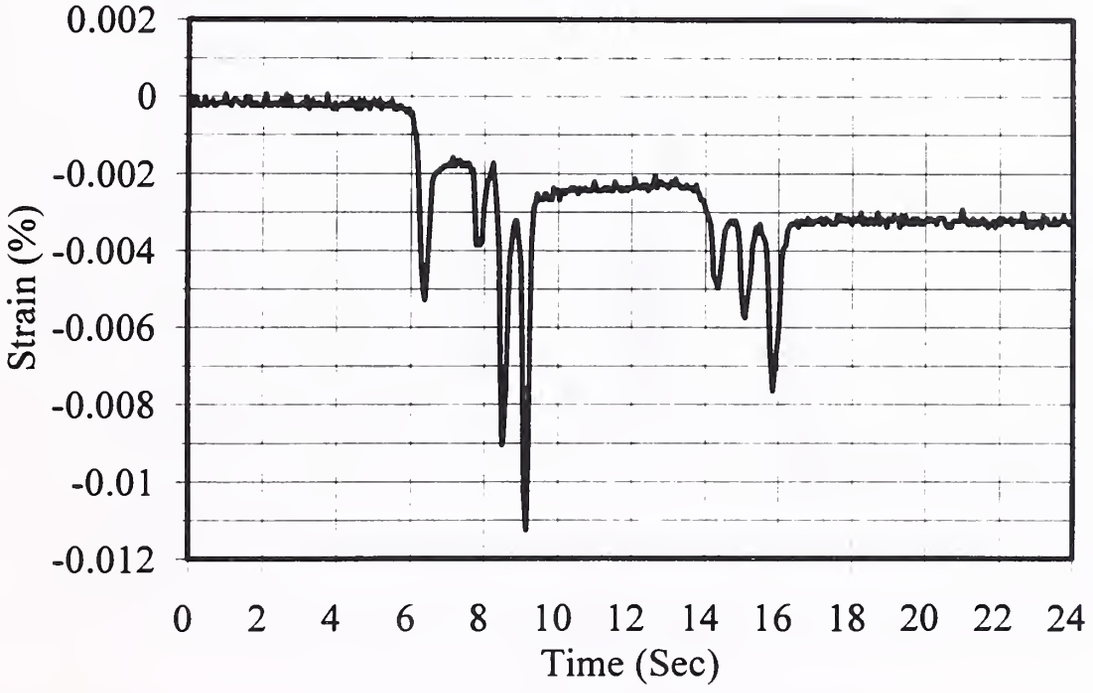

Figure C2.12: Foil Strain Gage #35 on Geogrid (below centerline): Truck Pass Test 5

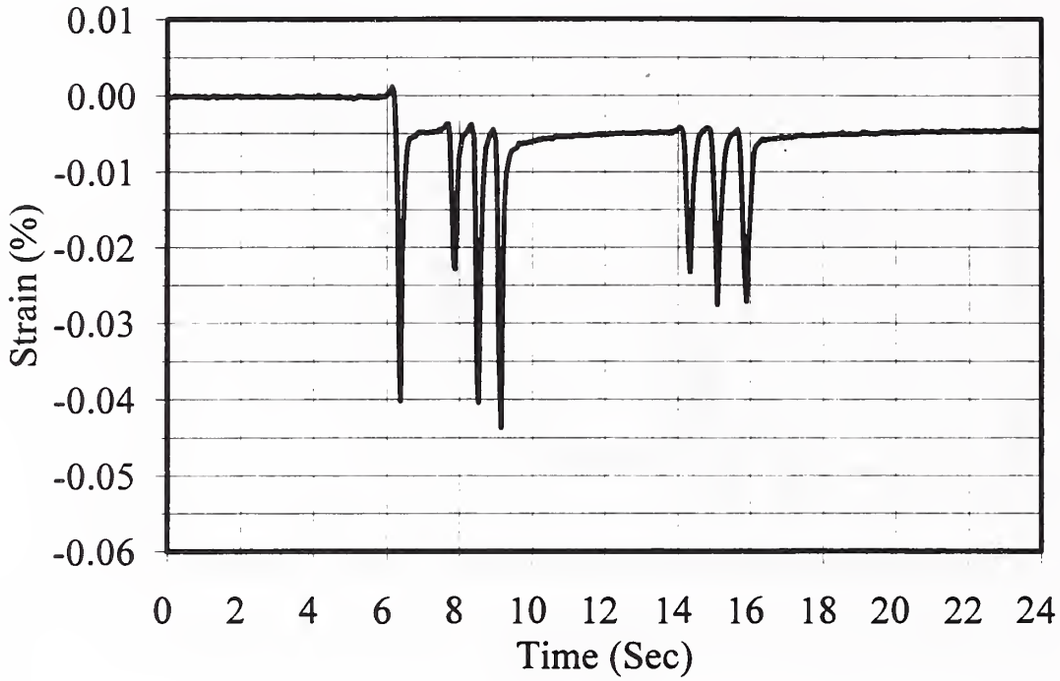

Figure C2.13: Foil Strain Gage #34 on Geogrid (on wheel path): Truck Pass Test 5

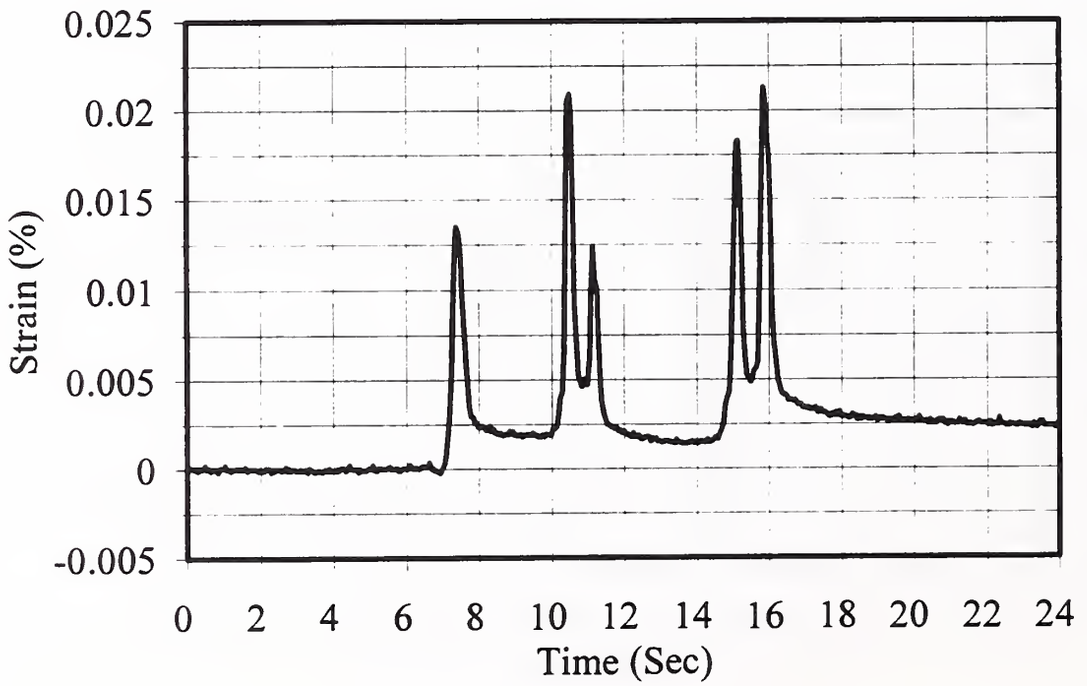

Figure C2.14: Foil Strain Gage #36 on Geogrid (on wheel path): Truck Pass Test 6

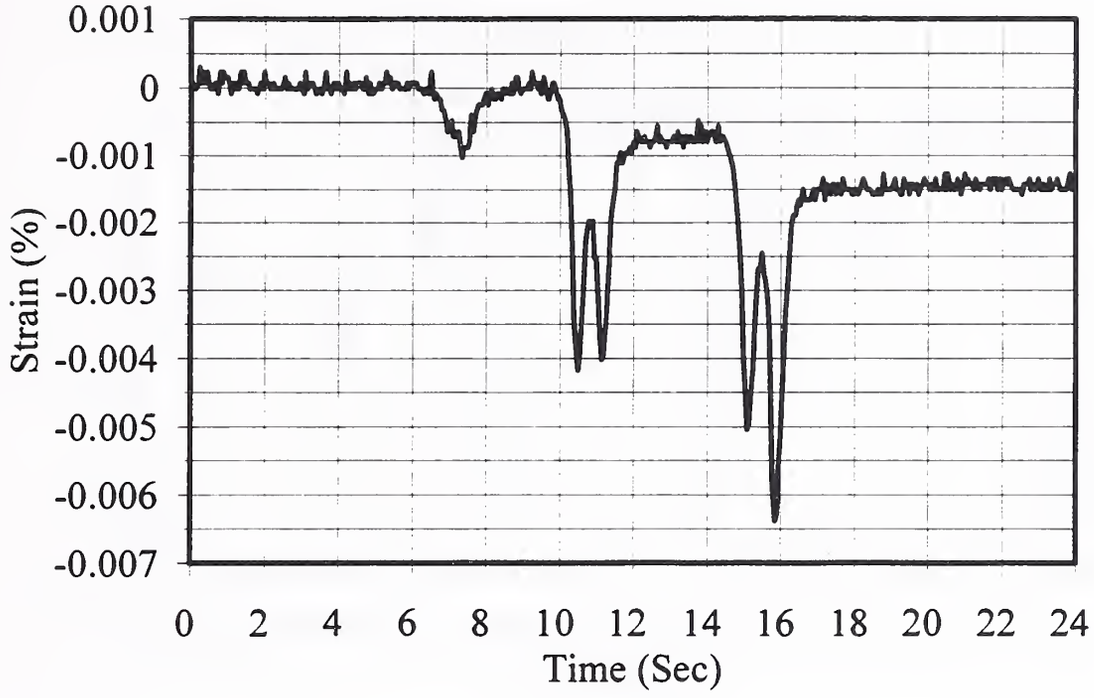

Figure C2.15: Foil Strain Gage #35 on Geogrid (below centerline): Truck Pass Test 6

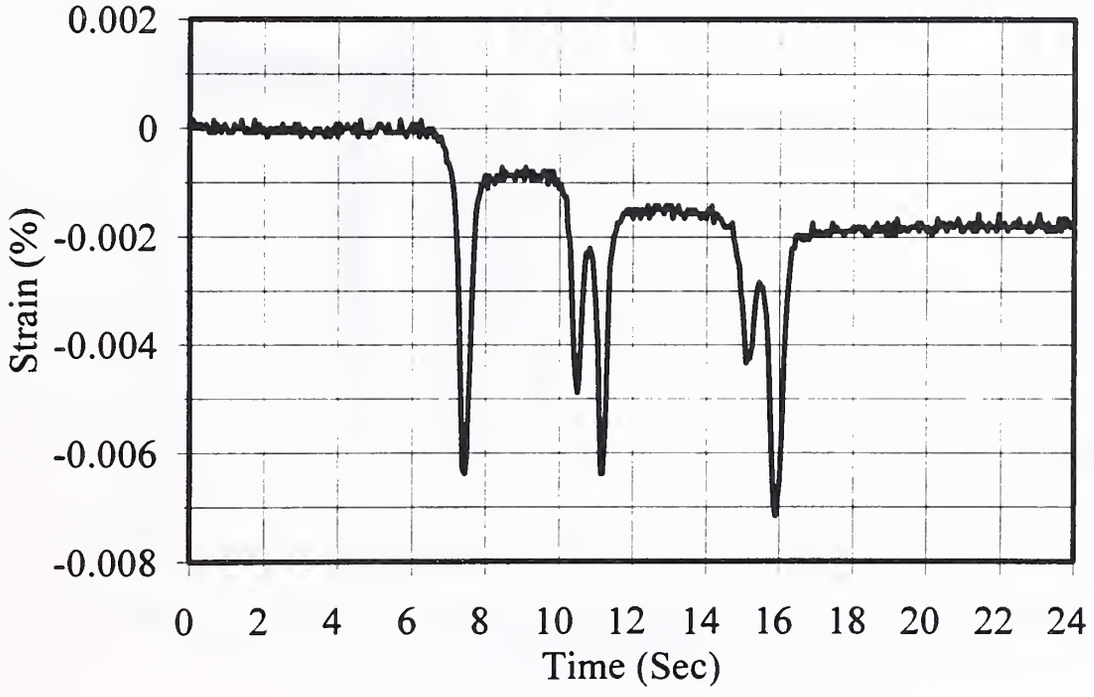

Figure C2.16: Foil Strain Gage #34 on Geogrid (on wheel path): Truck Pass Test 6

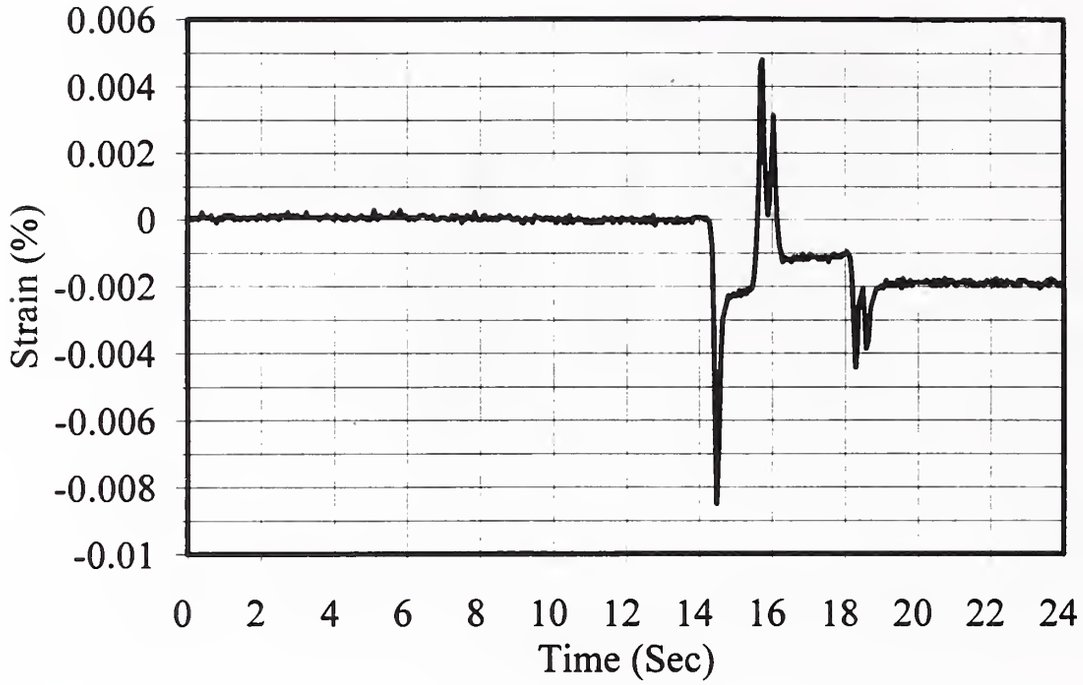

Figure C2.17: Foil Strain Gage #36 on Geogrid (on wheel path): Truck Pass Test 7

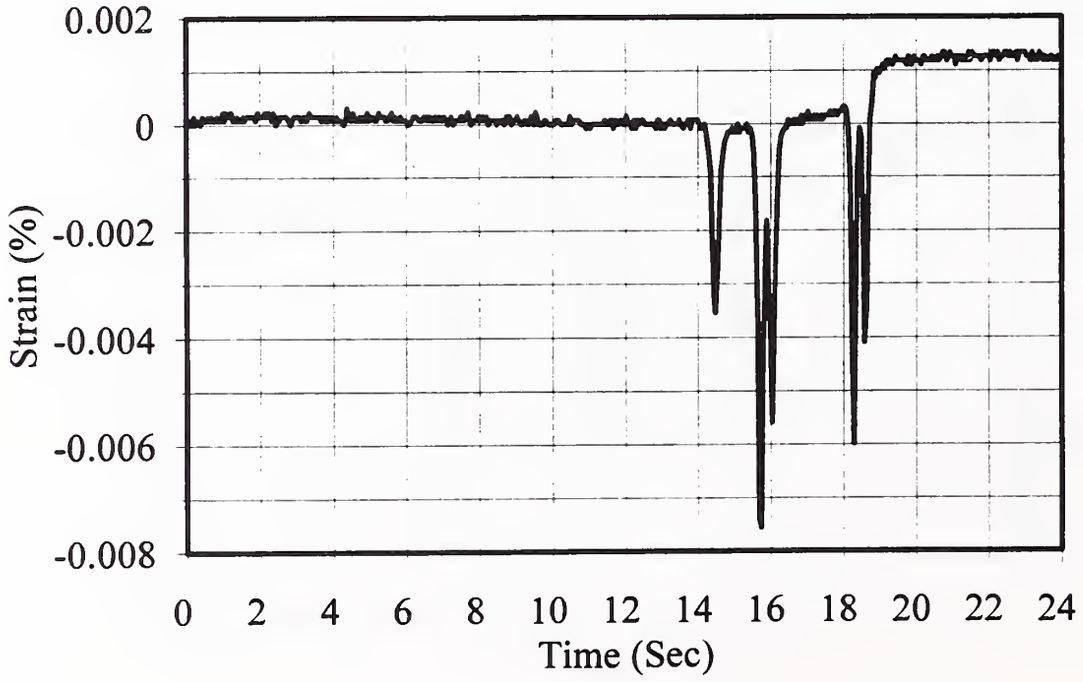

Figure C2.18: Foil Strain Gage #35 on Geogrid (below centerline): Truck Pass Test 7

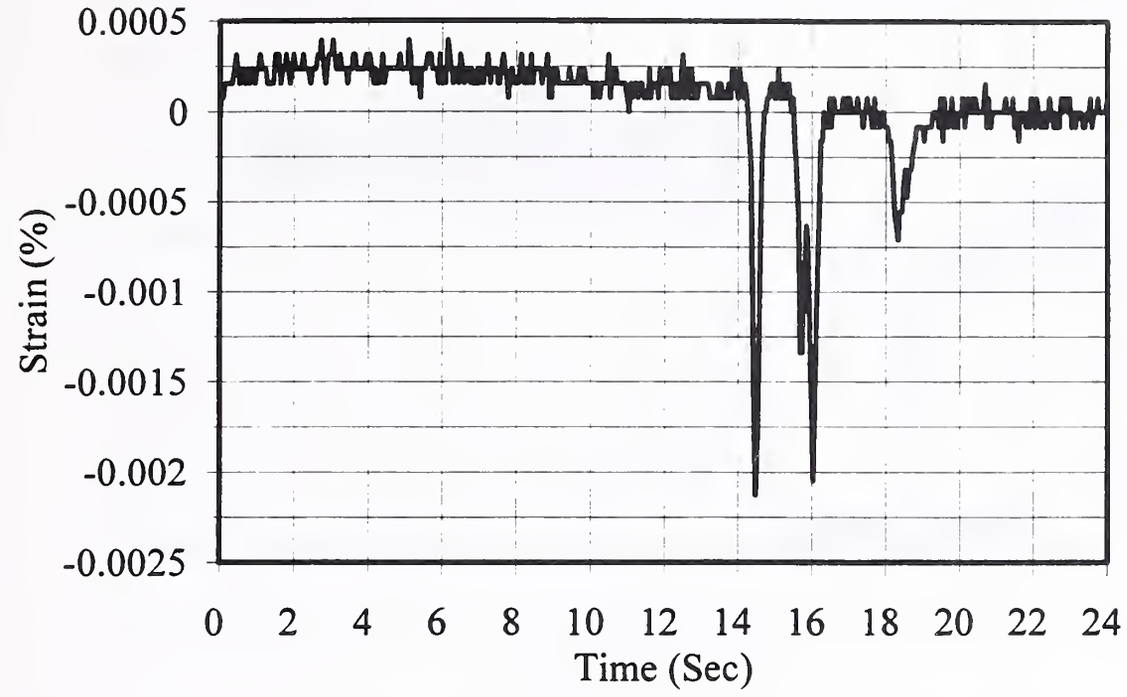

Figure C2.19: Foil Strain Gage #34 on Geogrid (on wheel path): Truck Pass Test 7

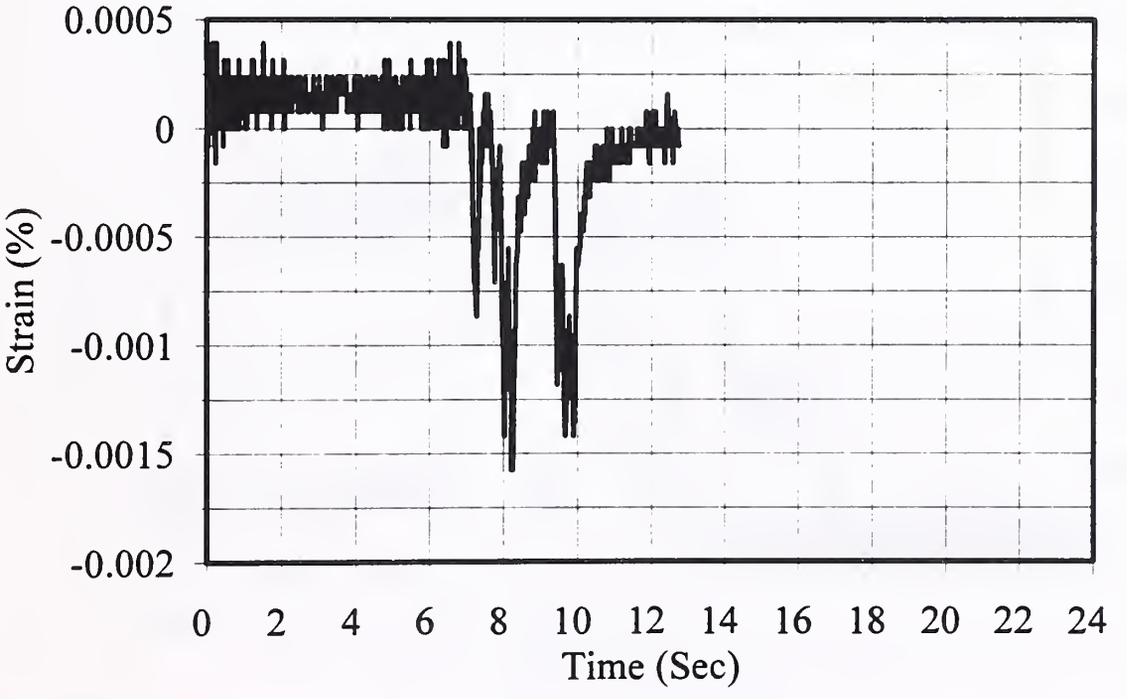

Figure C2.20: Foil Strain Gage #36 on Geogrid (on wheel path): Truck Pass Test 8

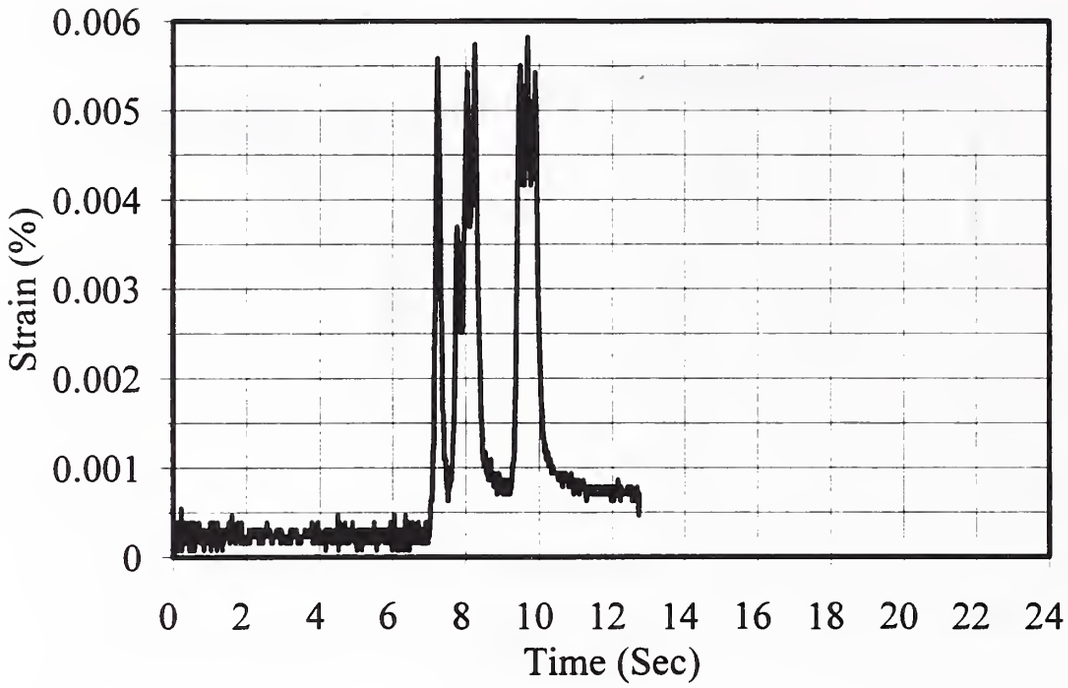

Figure C2.21: Foil Strain Gage #35 on Geogrid (below centerline): Truck Pass Test 8

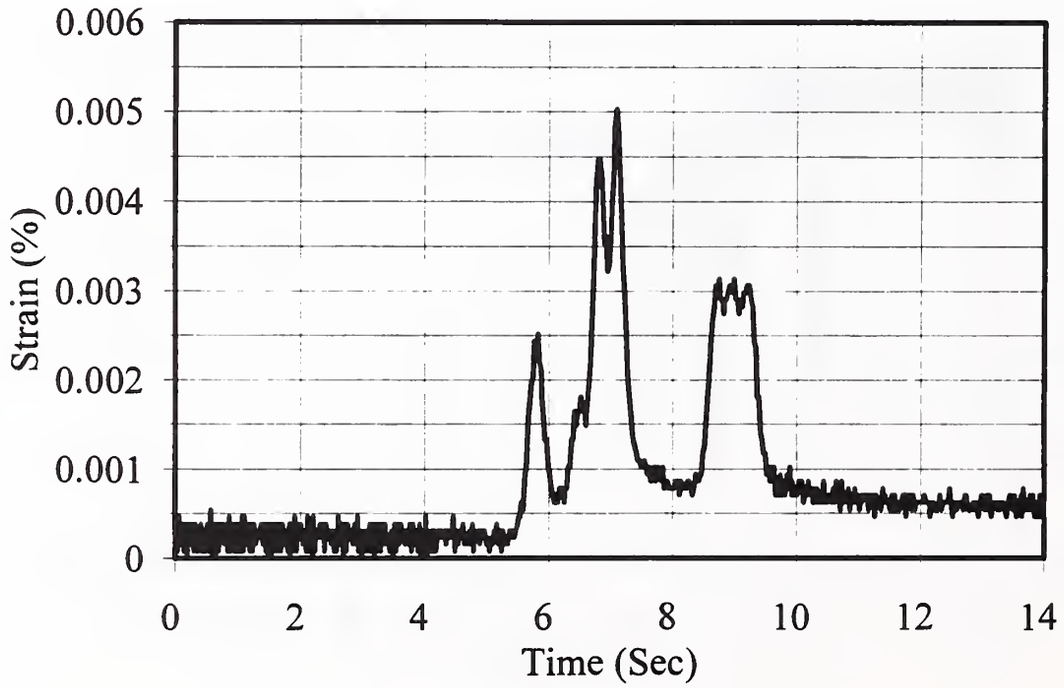

Figure C2.22: Foil Strain Gage #36 on Geogrid (on wheel path): Truck Pass Test 9

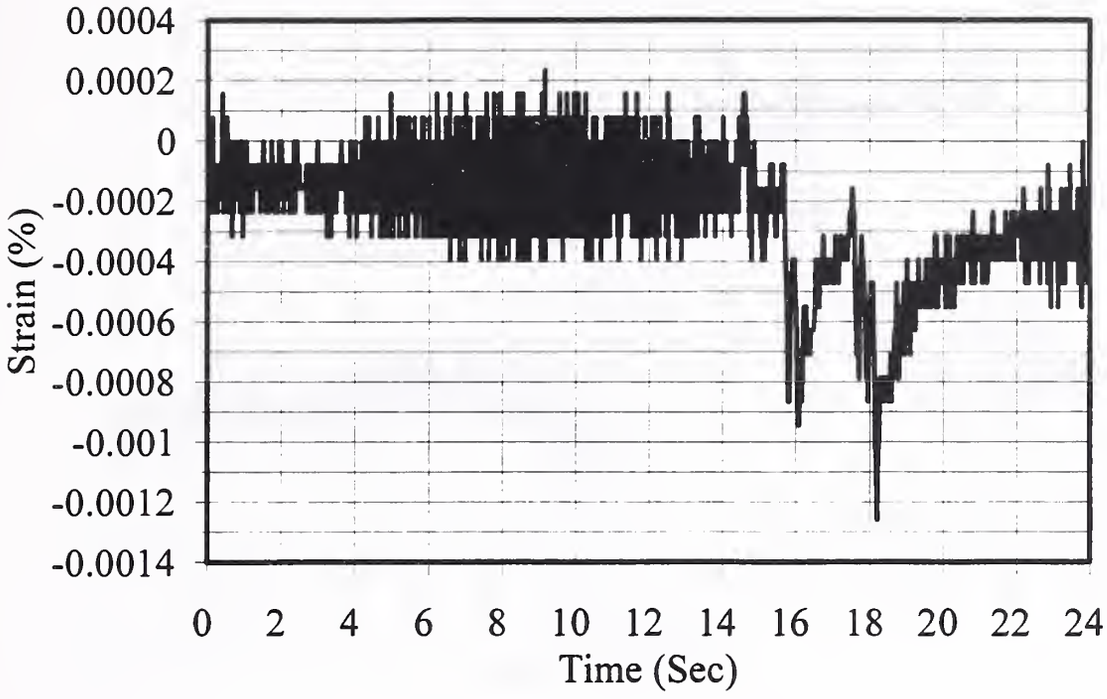

Figure C2.23: Foil Strain Gage #35 on Geogrid (below centerline): Truck Pass Test 9

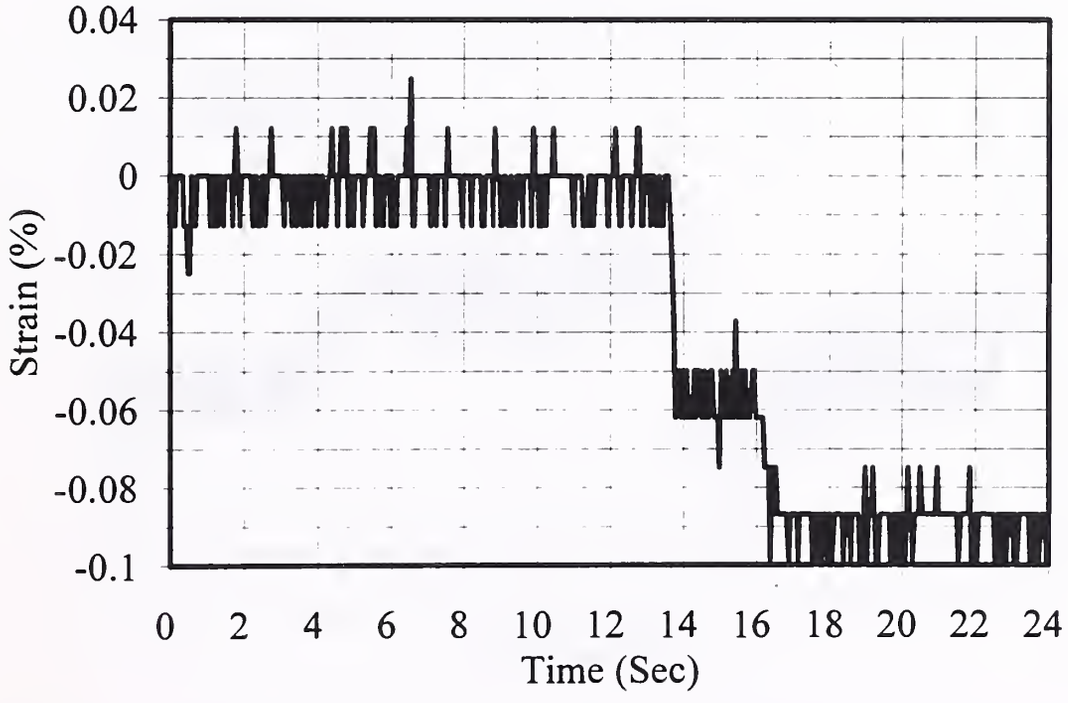

Figure C2.24: LVDT Displacement Gage #31 on Geogrid (on wheel path): Truck Pass Test 4

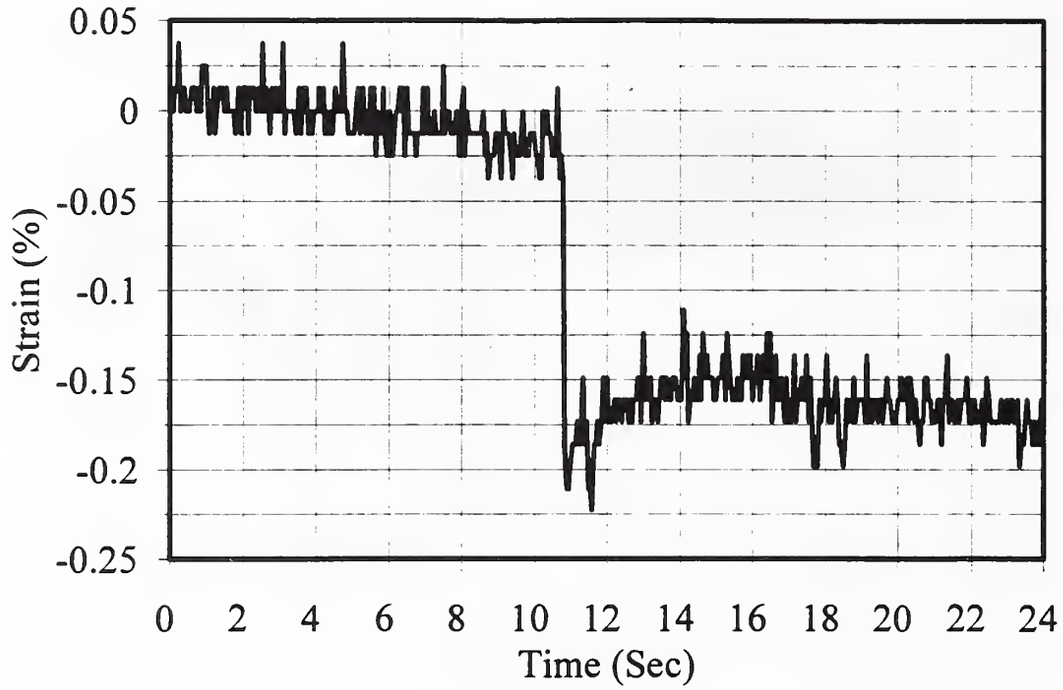

Figure C2.25: LVDT Displacement Gage #31 on Geogrid (on wheel path): Truck Pass Test 5

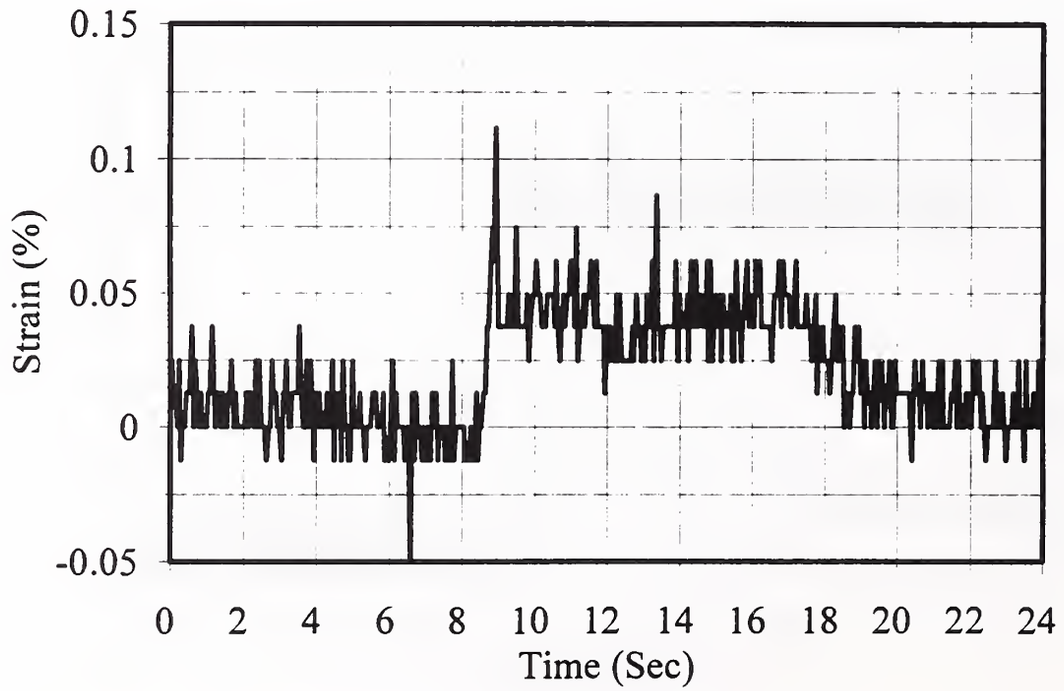

Figure C2.26: LVDT Displacement Gage #32 on Geogrid (off wheel path): Truck Pass Test 5

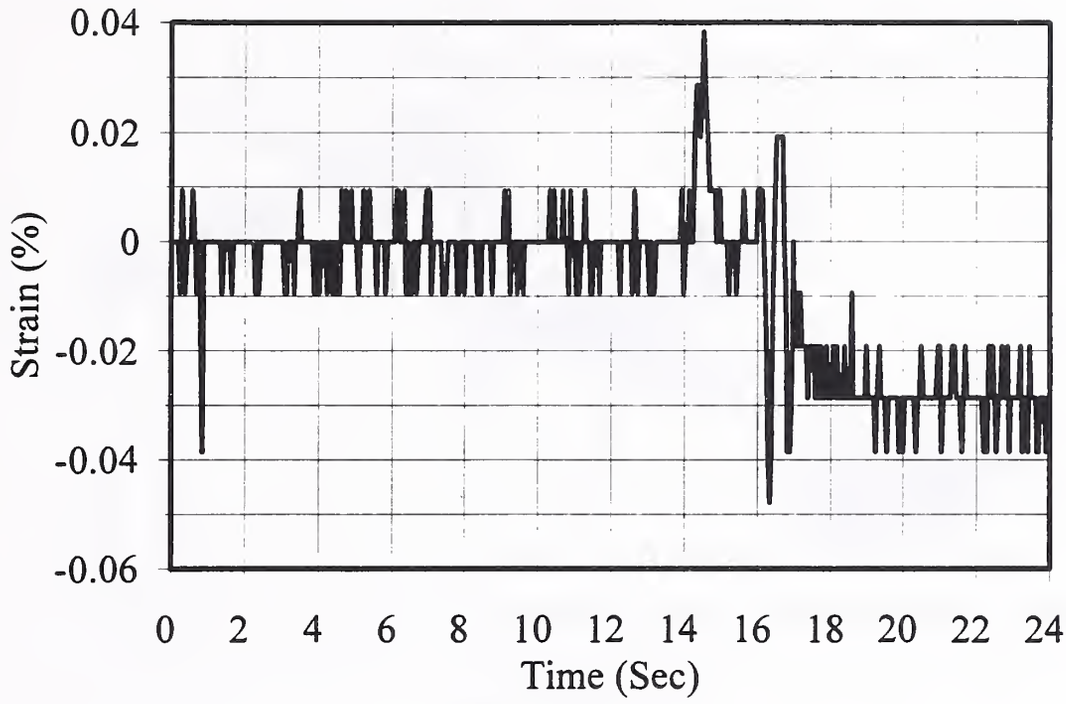

Figure C2.27: LVDT Displacement Gage #29 on Geotextile (on wheel path): Truck Pass Test 4

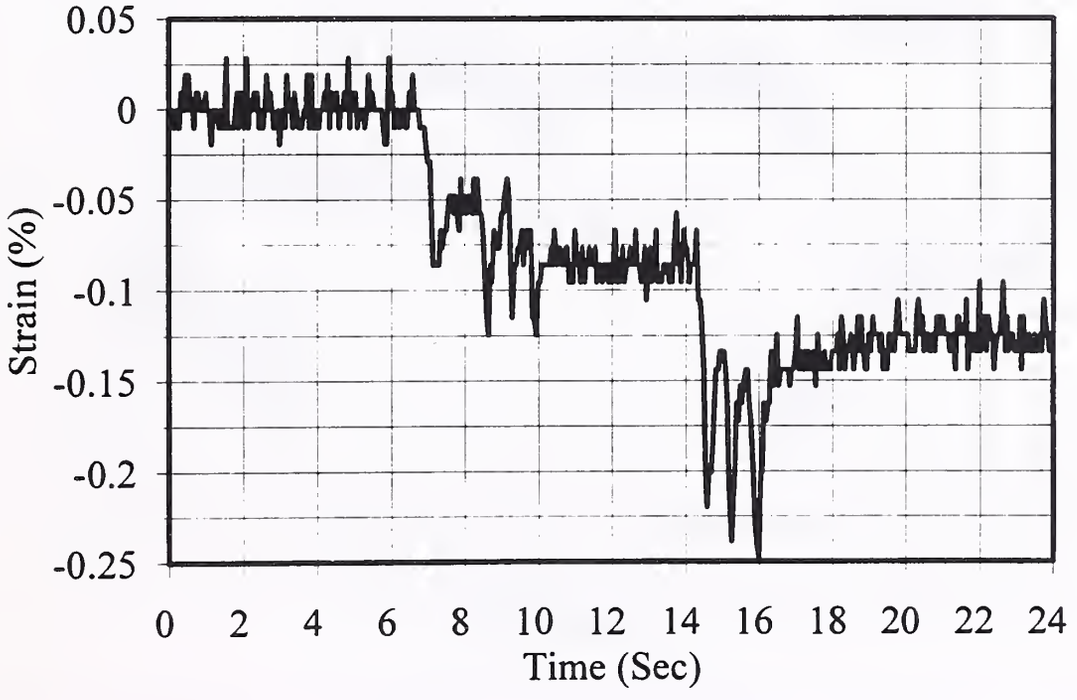

Figure C2.28: LVDT Displacement Gage #29 on Geotextile (on wheel path): Truck Pass Test 5

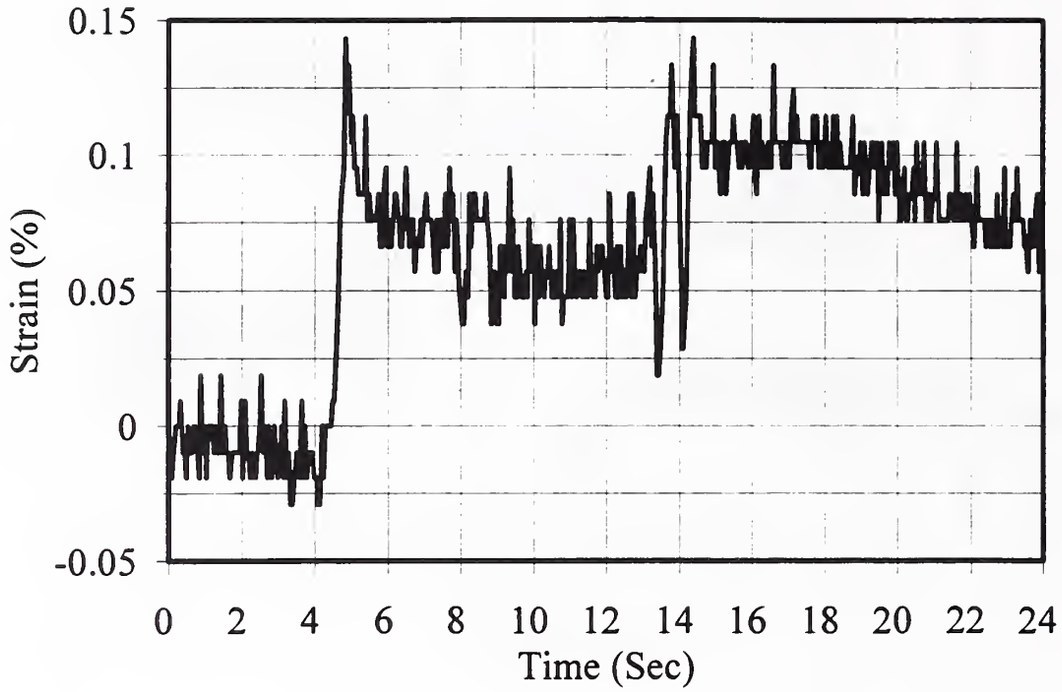

Figure C2.29: LVDT Displacement Gage #29 on Geotextile (on wheel path): Truck Pass Test 6

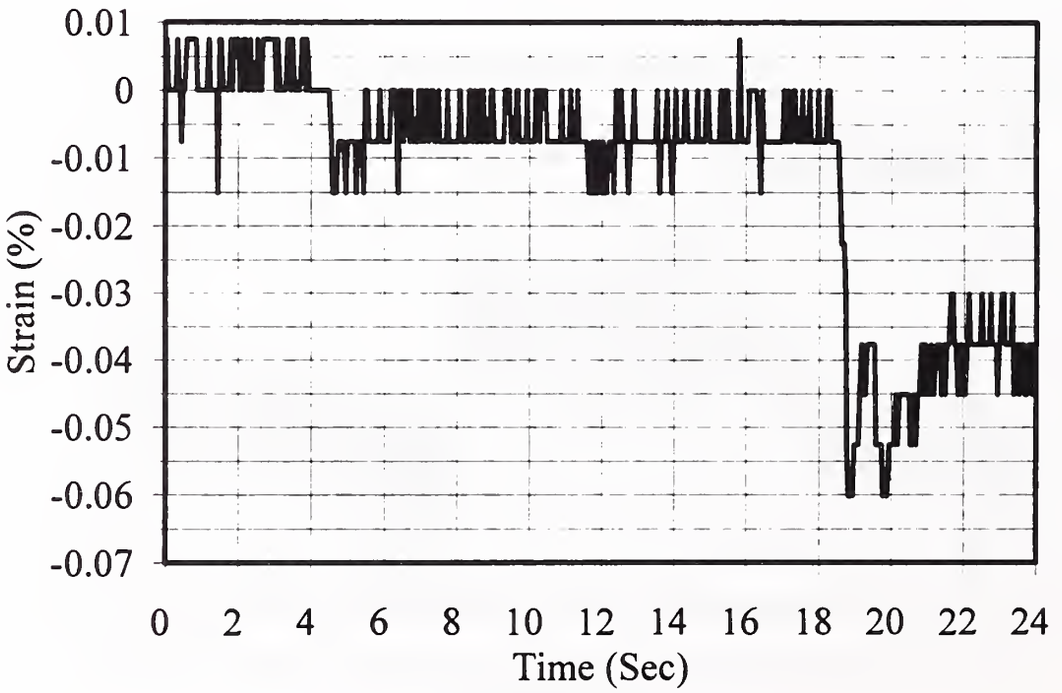

Figure C2.30: LVDT Embedment Displacement Gage #27 in Base Above Geogrid (off wheel path): Truck Pass Test 3

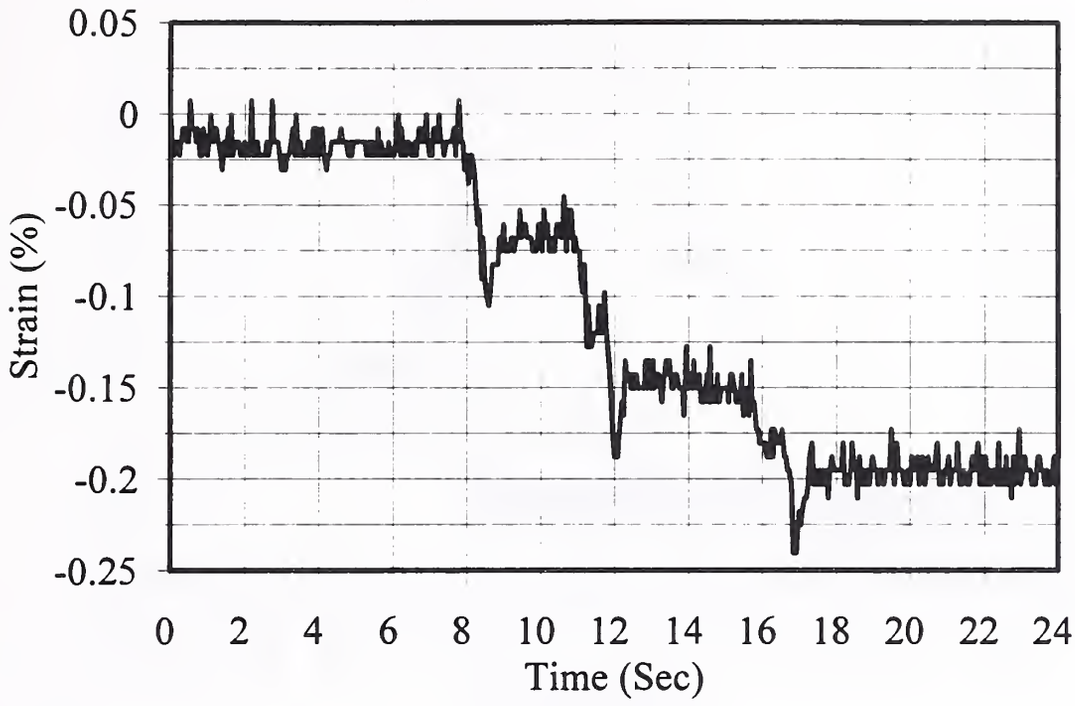

Figure C2.31: LVDT Embedment Displacement Gage #27 in Base Above Geogrid (off wheel path): Truck Pass Test 6

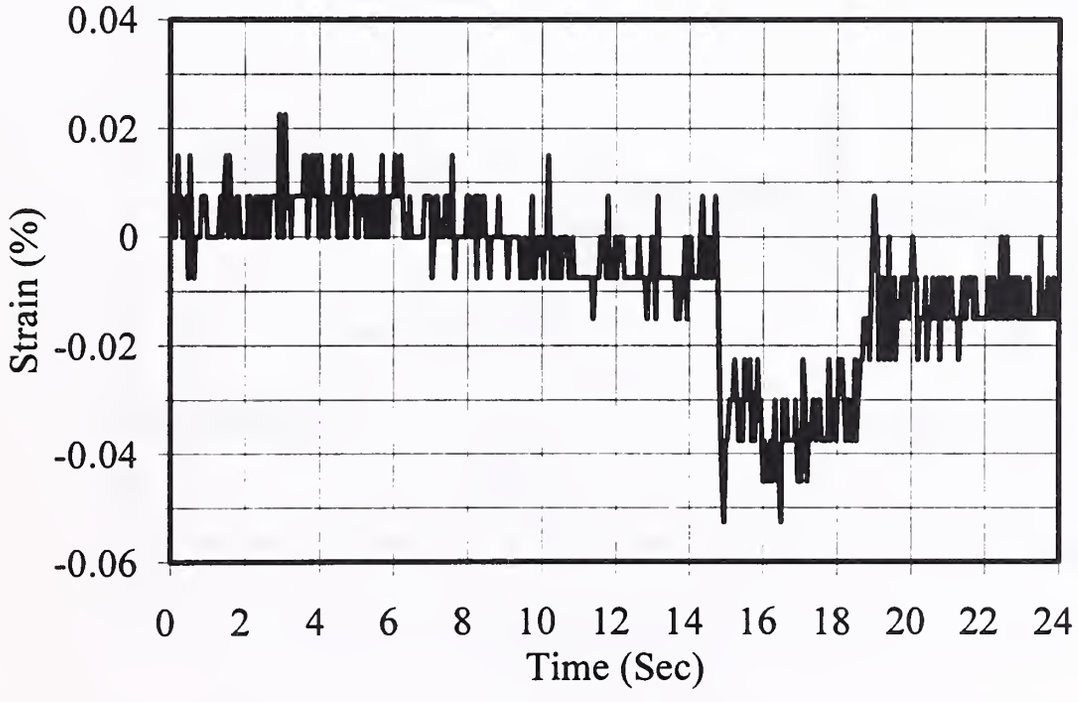

Figure C2.32: LVDT Embedment Displacement Gage #27 in Base Above Geogrid (off wheel path): Truck Pass Test 7.

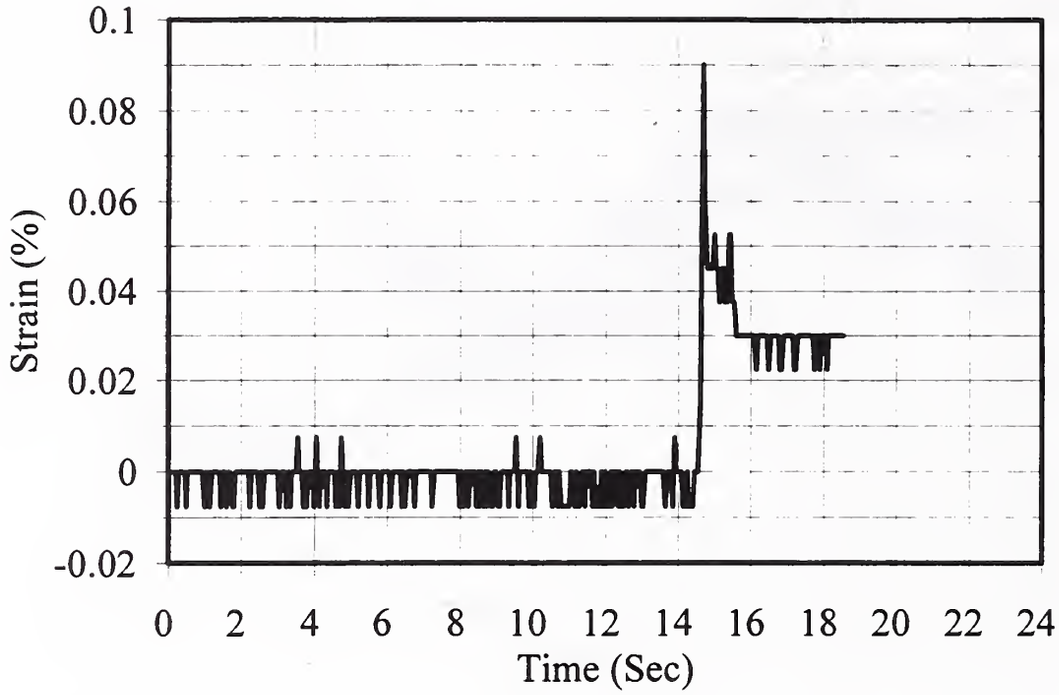

Figure C2.33: LVDT Embedment Displacement Gage #28 in Base Above Geogrid (on wheel path): Truck Pass Test 2

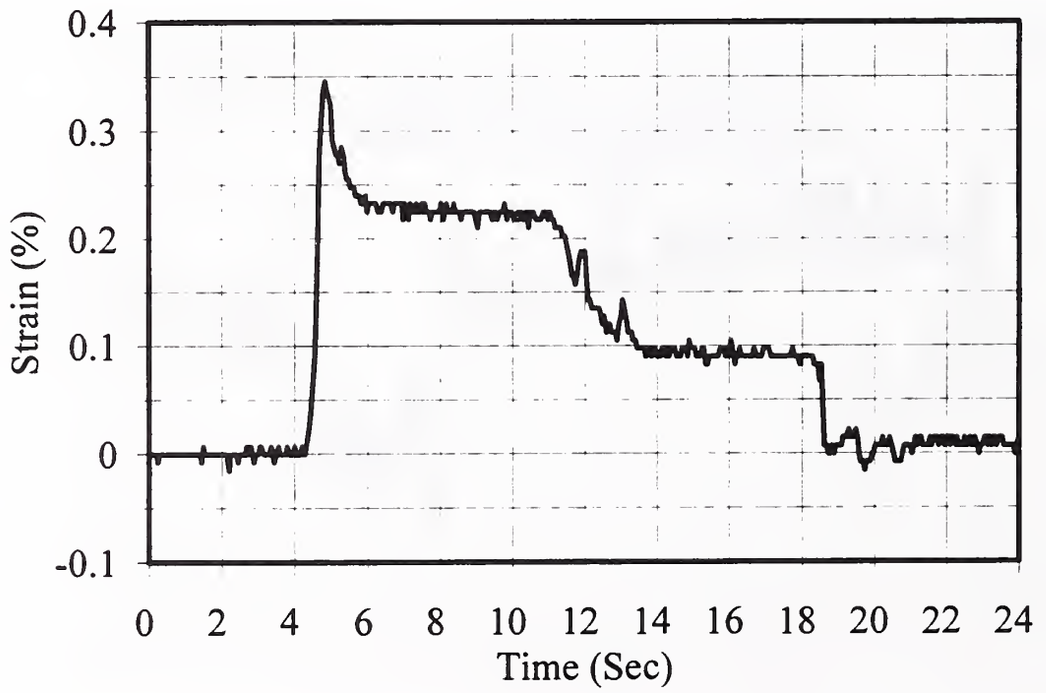

Figure C2.34: LVDT Embedment Displacement Gage #28 in Base Above Geogrid (on wheel path): Truck Pass Test 3

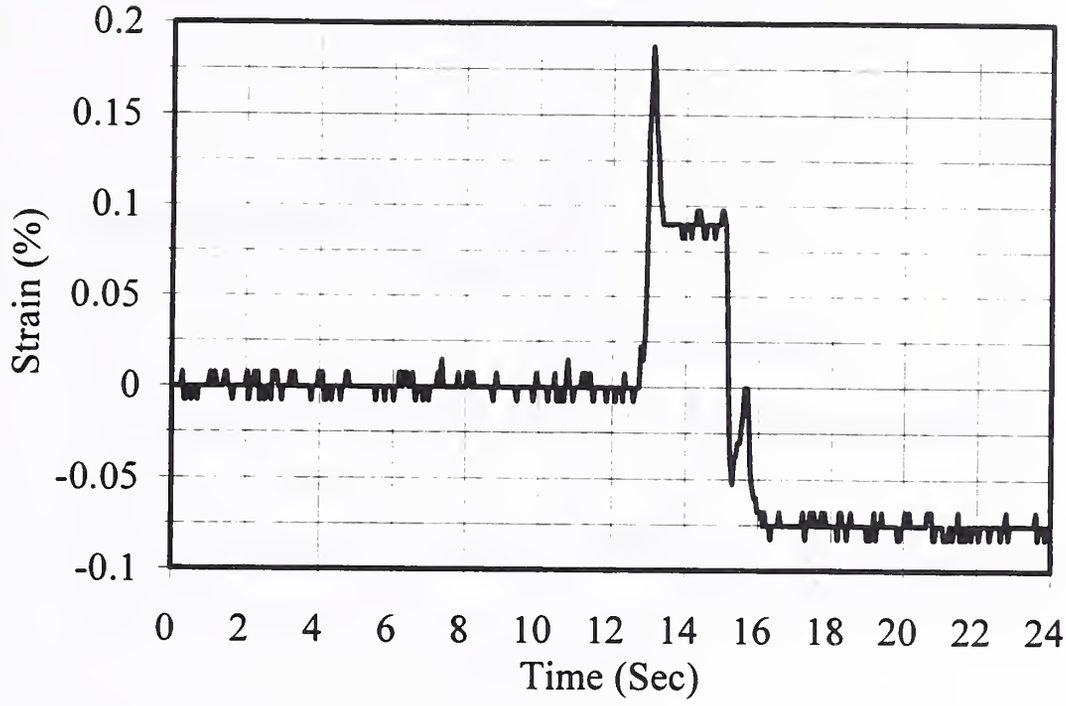

Figure C2.35: LVDT Embedment Displacement Gage #28 in Base Above Geogrid (on wheel path): Truck Pass Test 4

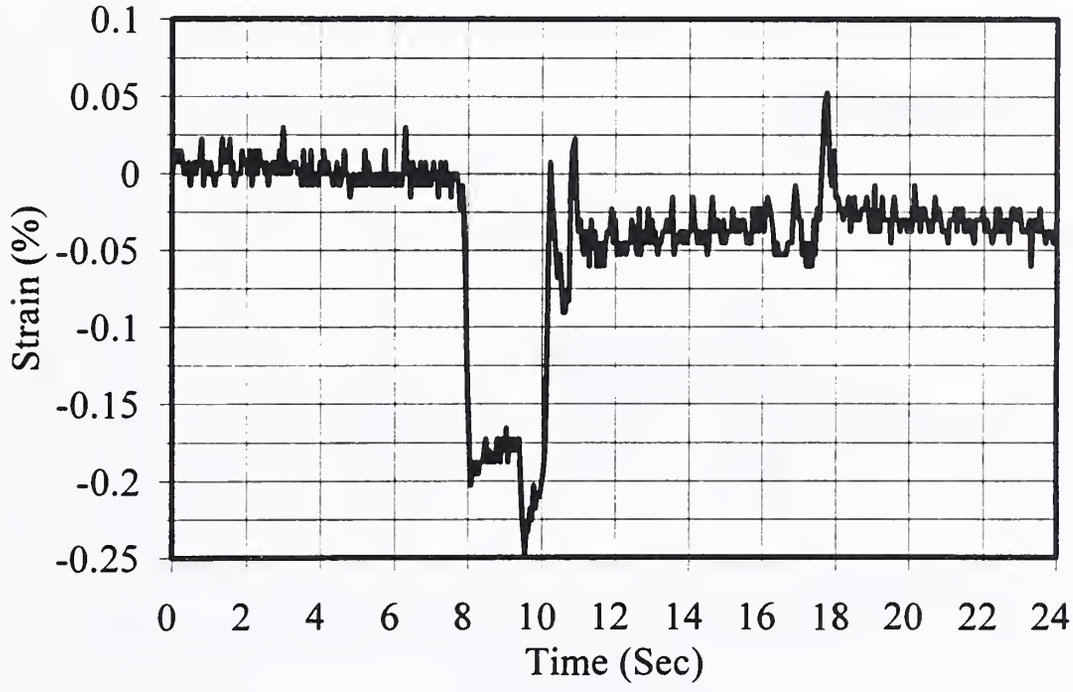

Figure C2.36: LVDT Embedment Displacement Gage #28 in Base Above Geogrid (on wheel path): Truck Pass Test 5

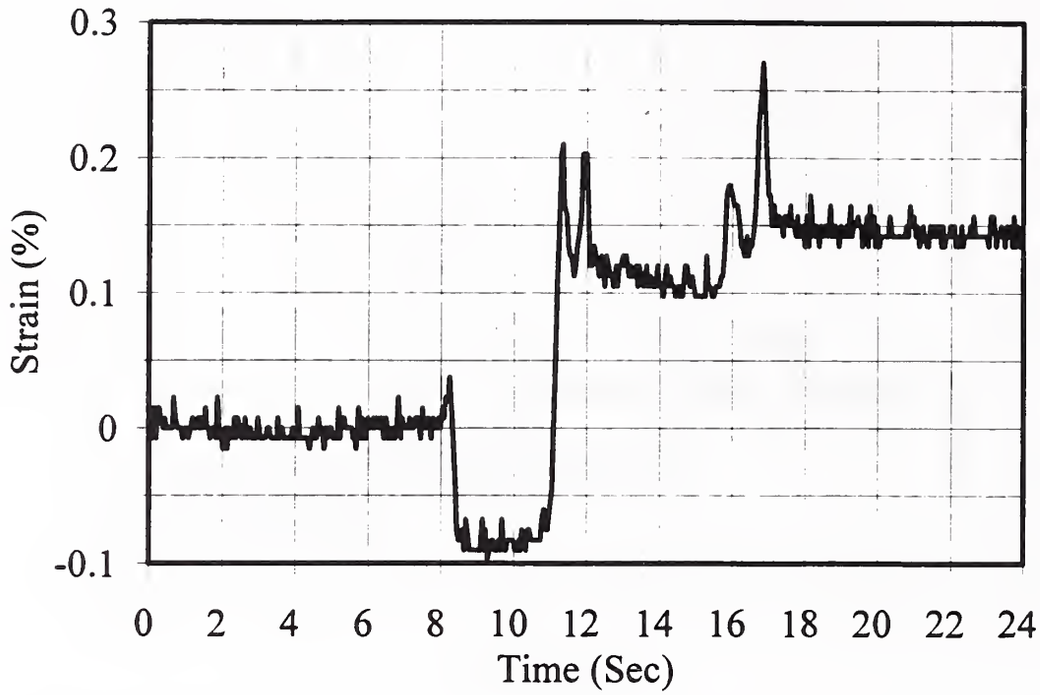

Figure C2.37: LVDT Embedment Displacement Gage #28 in Base Above Geogrid (on wheel path): Truck Pass Test 6

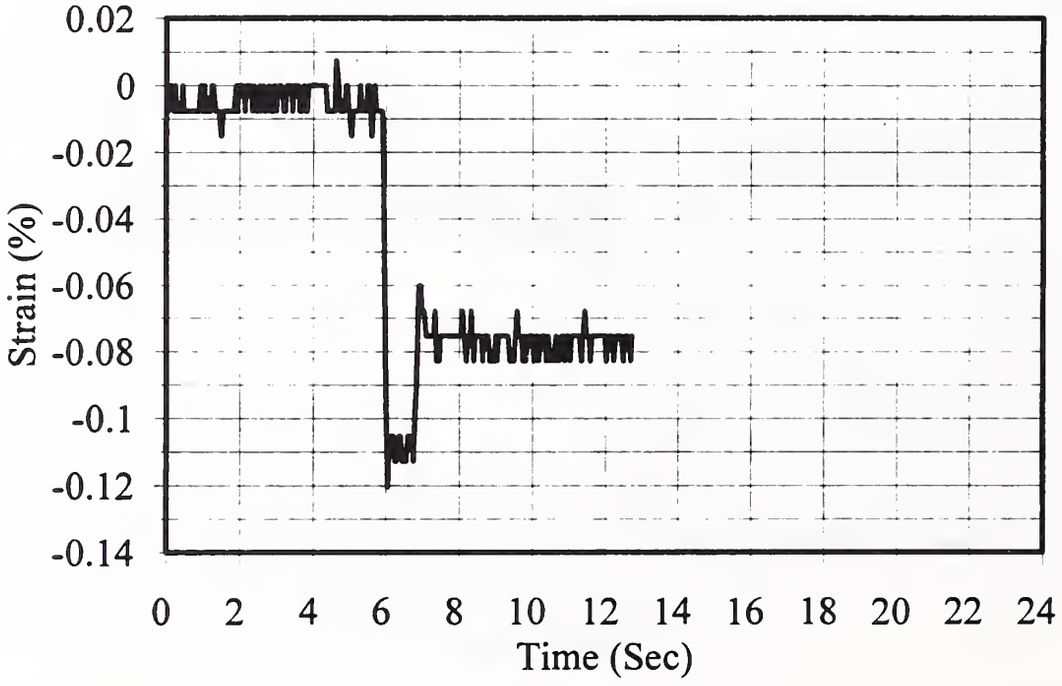

Figure C2.38: LVDT Embedment Displacement Gage #25 in Base Above Geotextile (on wheel path): Truck Pass Test 1

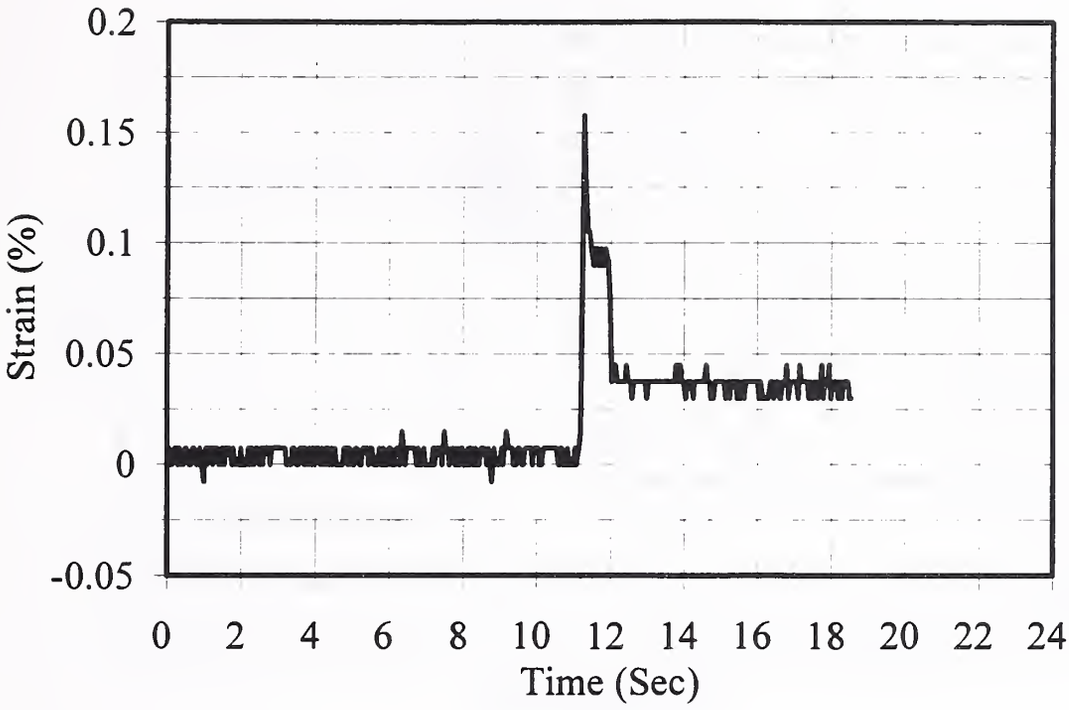

Figure C2.39: LVDT Embedment Displacement Gage #25 in Base Above Geotextile (on wheel path): Truck Pass Test 2

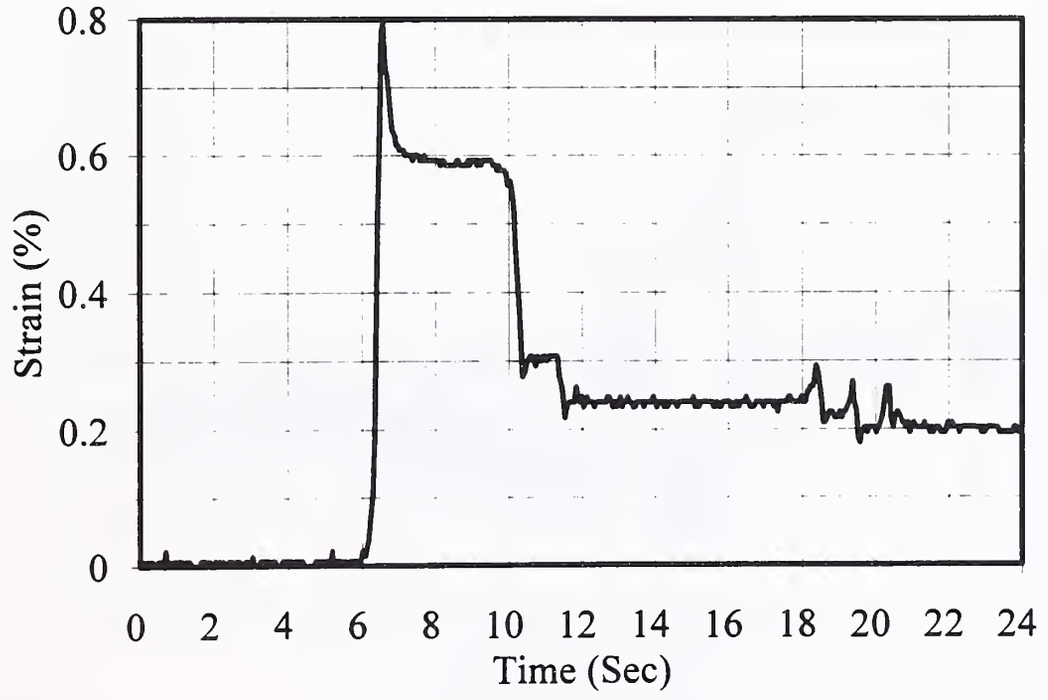

Figure C2.40: LVDT Embedment Displacement Gage #25 in Base Above Geotextile (on wheel path): Truck Pass Test 3

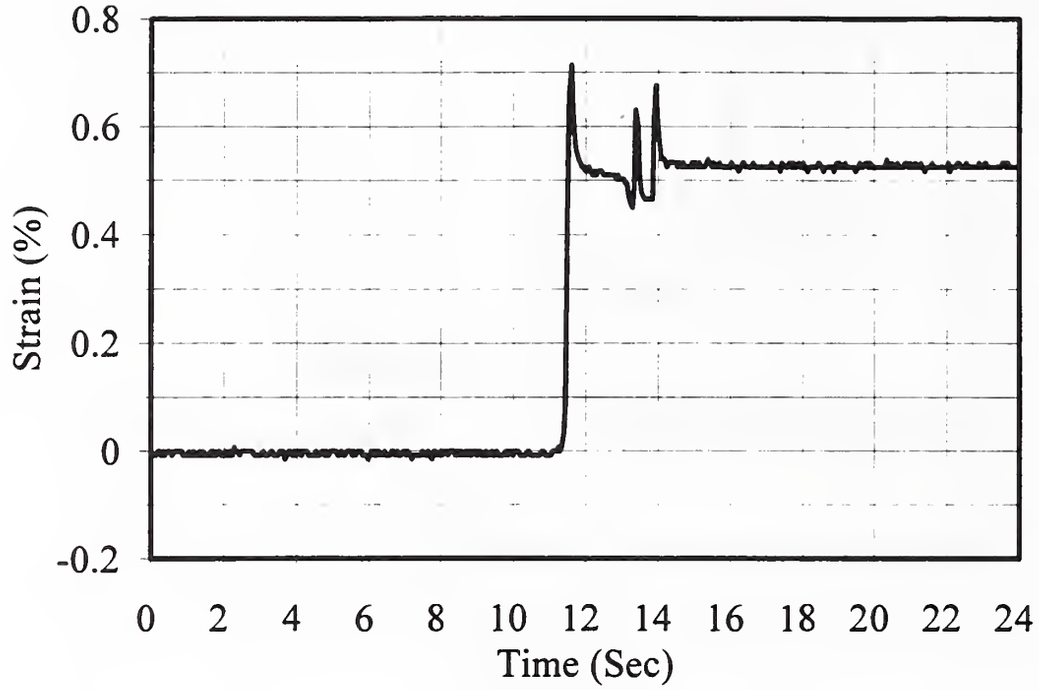

Figure C2.41: LVDT Embedment Displacement Gage #25 in Base Above Geotextile (on wheel path): Truck Pass Test 4

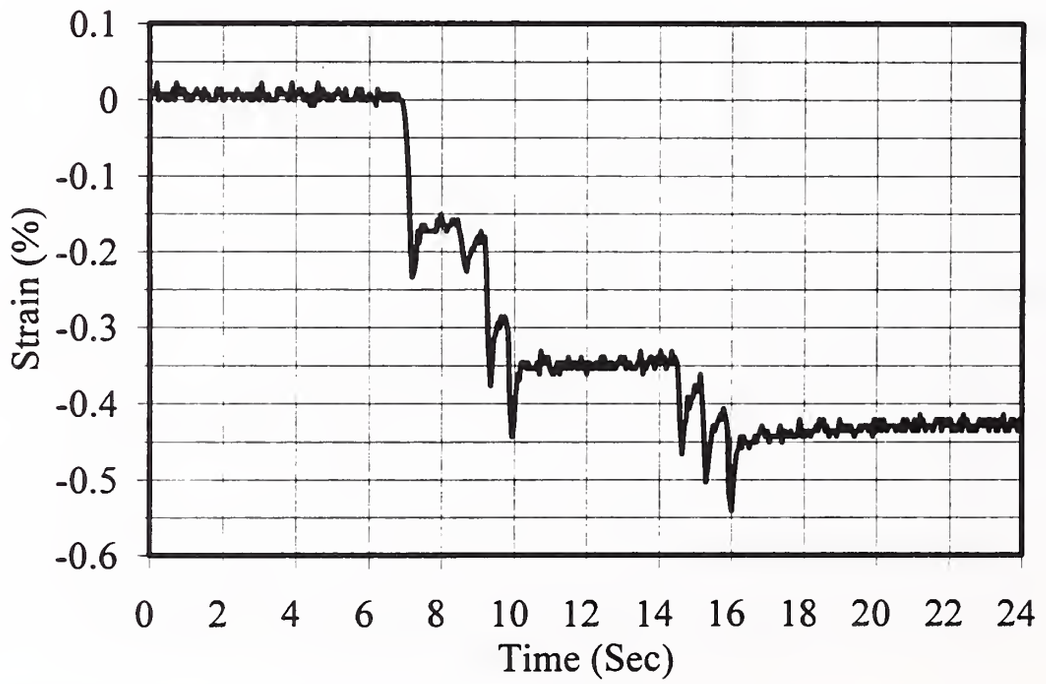

Figure C2.42: LVDT Embedment Displacement Gage #25 in Base Above Geotextile (on wheel path): Truck Pass Test 5

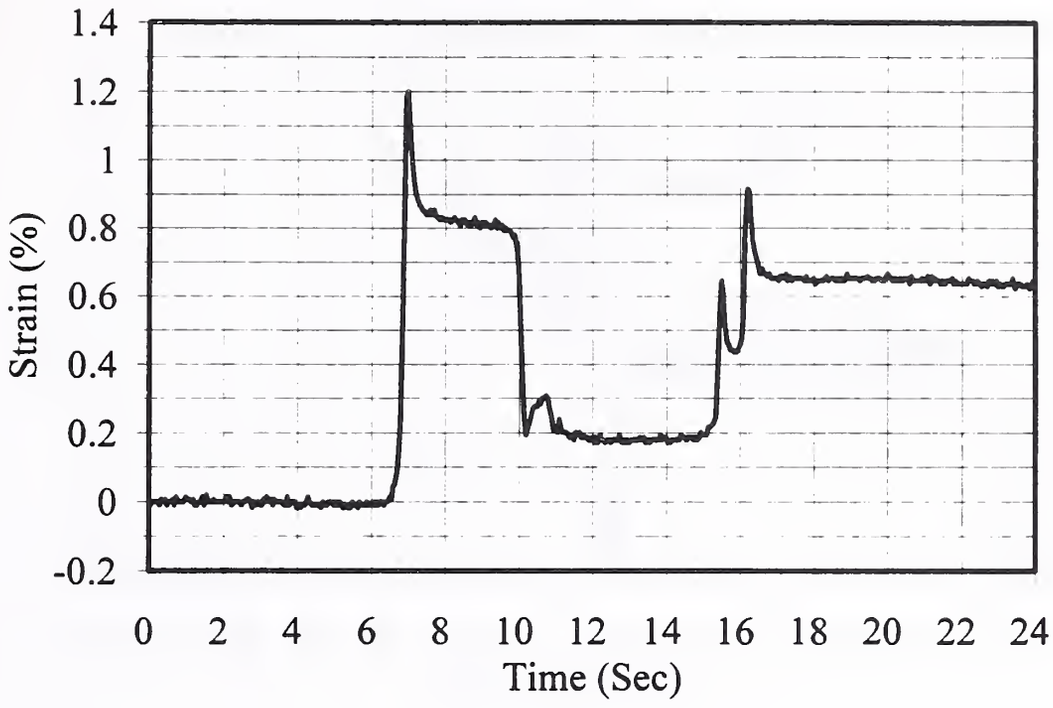

Figure C2.43: LVDT Embedment Displacement Gage #25 in Base Above Geotextile (on wheel path): Truck Pass Test 6

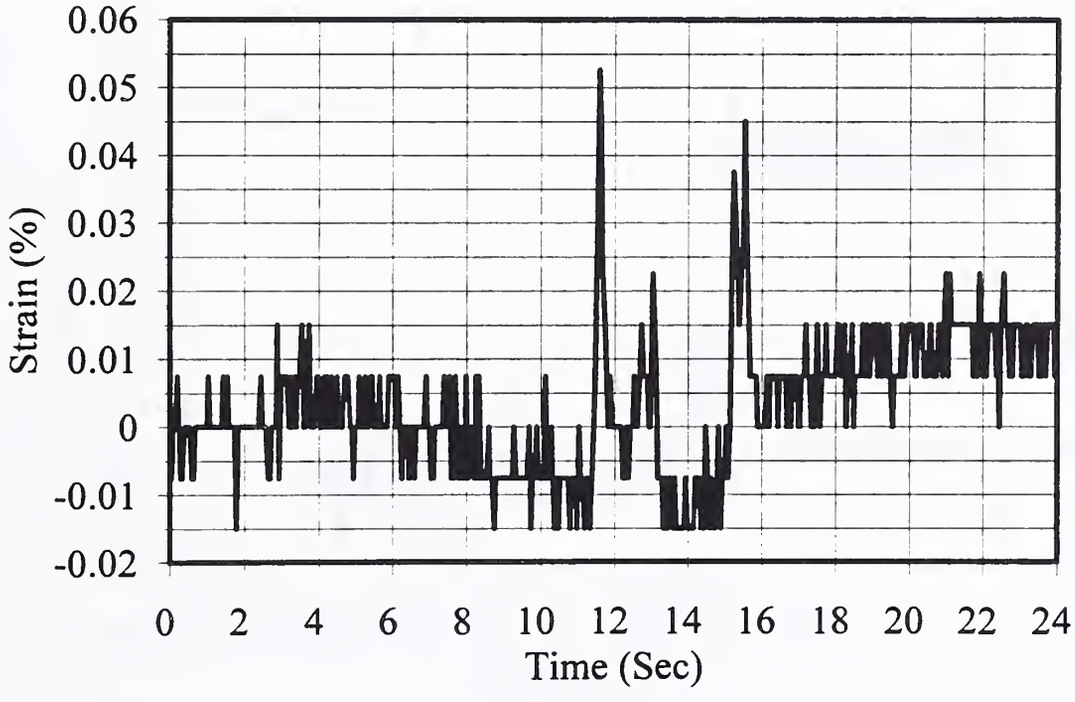

Figure C2.44: LVDT Embedment Displacement Gage #25 in Base Above Geotextile (on wheel path): Truck Pass Test 7

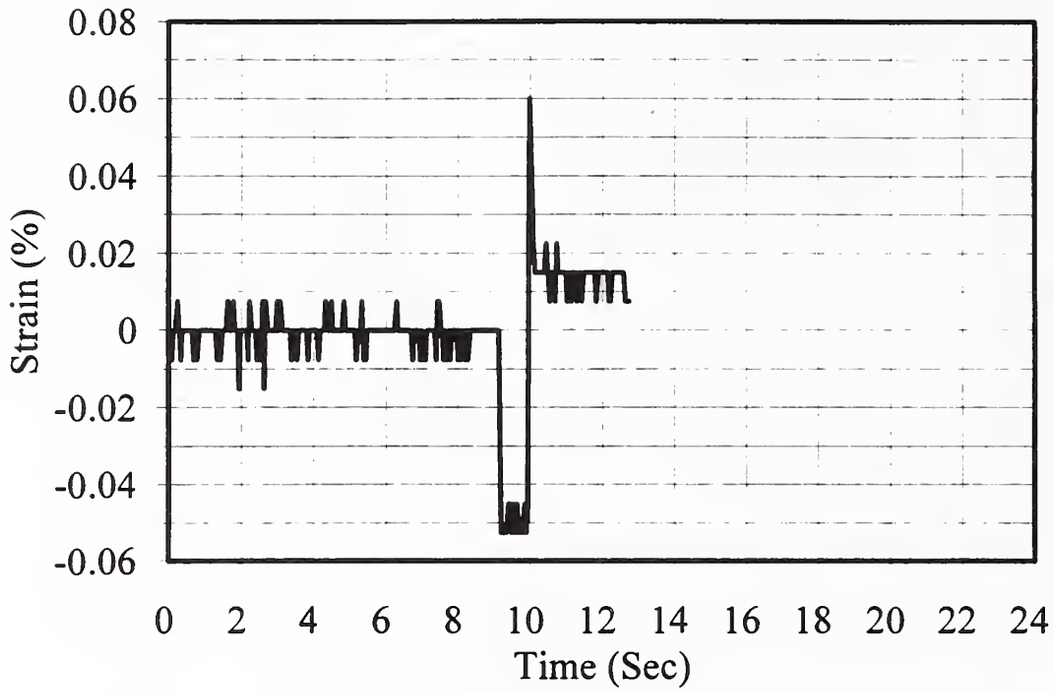

Figure C2.45: LVDT Embedment Displacement Gage #26 in Base of Non-Reinforced Section (on wheel path): Truck Pass Test 1

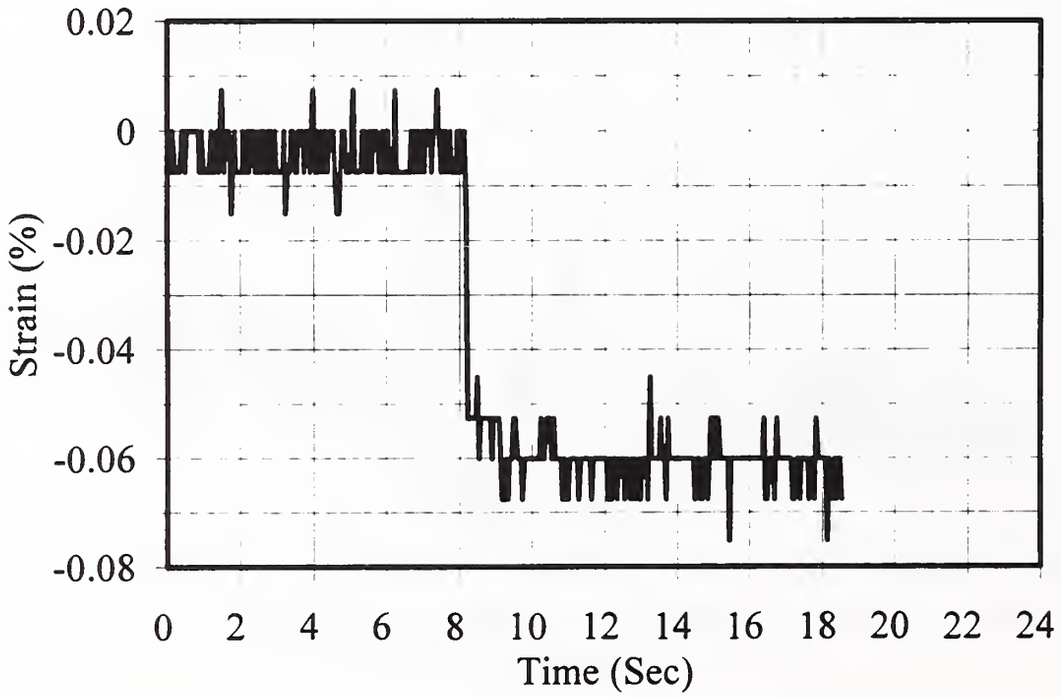

Figure C2.46: LVDT Embedment Displacement Gage #26 in Base of Non-Reinforced Section (on wheel path): Truck Pass Test 2

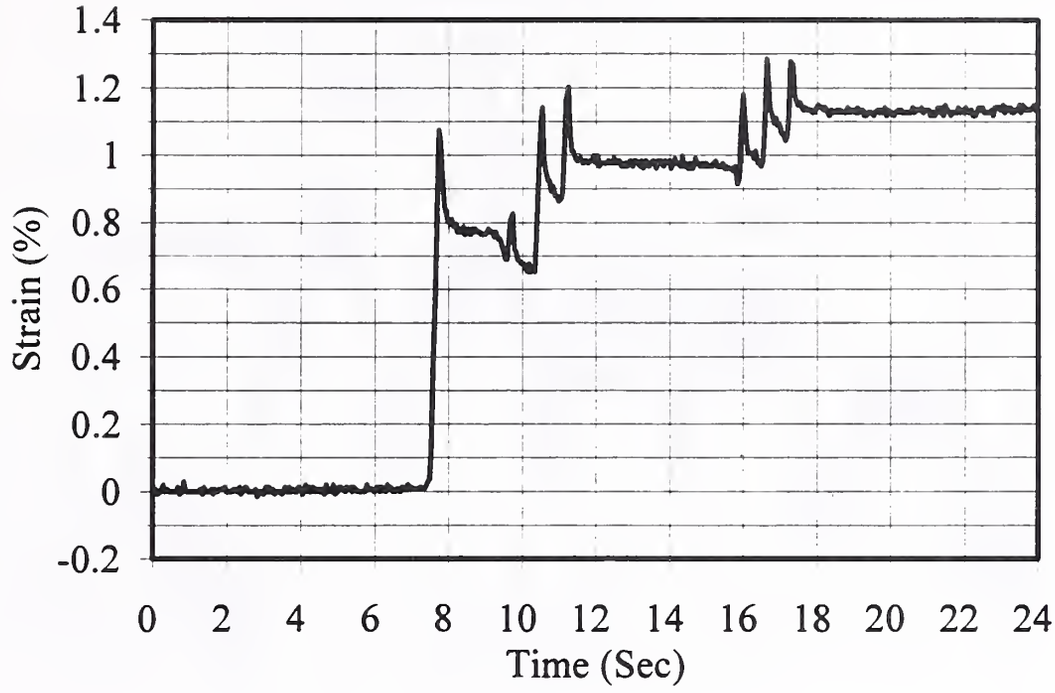

Figure C2.49: LVDT Embedment Displacement Gage #26 in Base of Non-Reinforced Section (on wheel path): Truck Pass Test 5

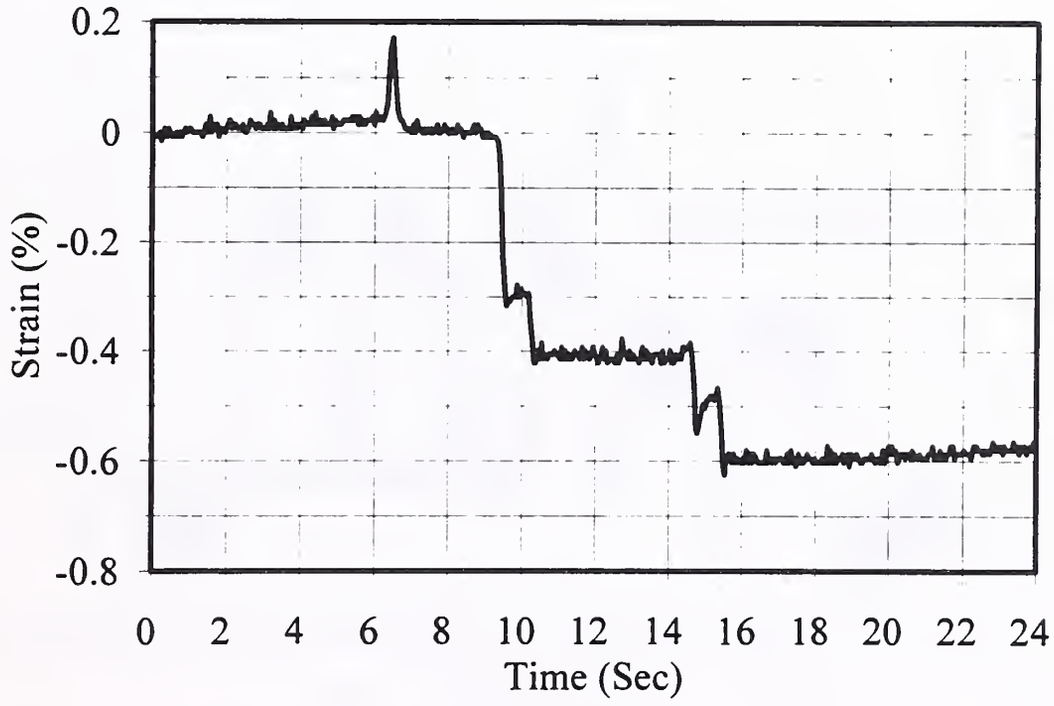

Figure C2.50: LVDT Embedment Displacement Gage #26 in Base of Non-Reinforced Section (on wheel path): Truck Pass Test 6

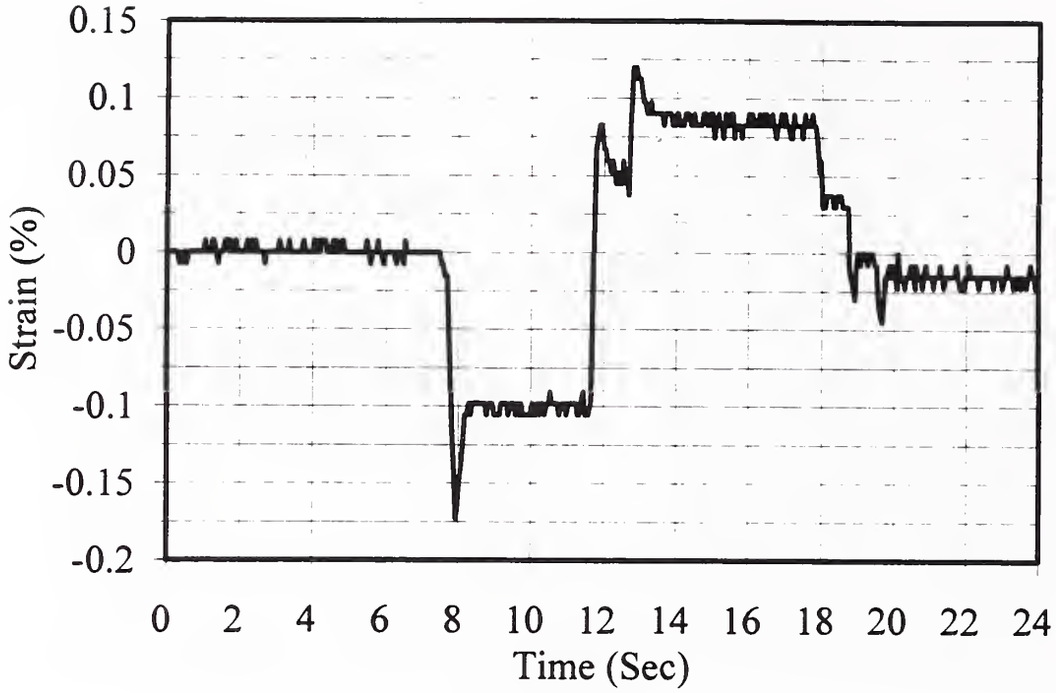

Figure C2.47: LVDT Embedment Displacement Gage #26 in Base of Non-Reinforced Section (on wheel path): Truck Pass Test 3

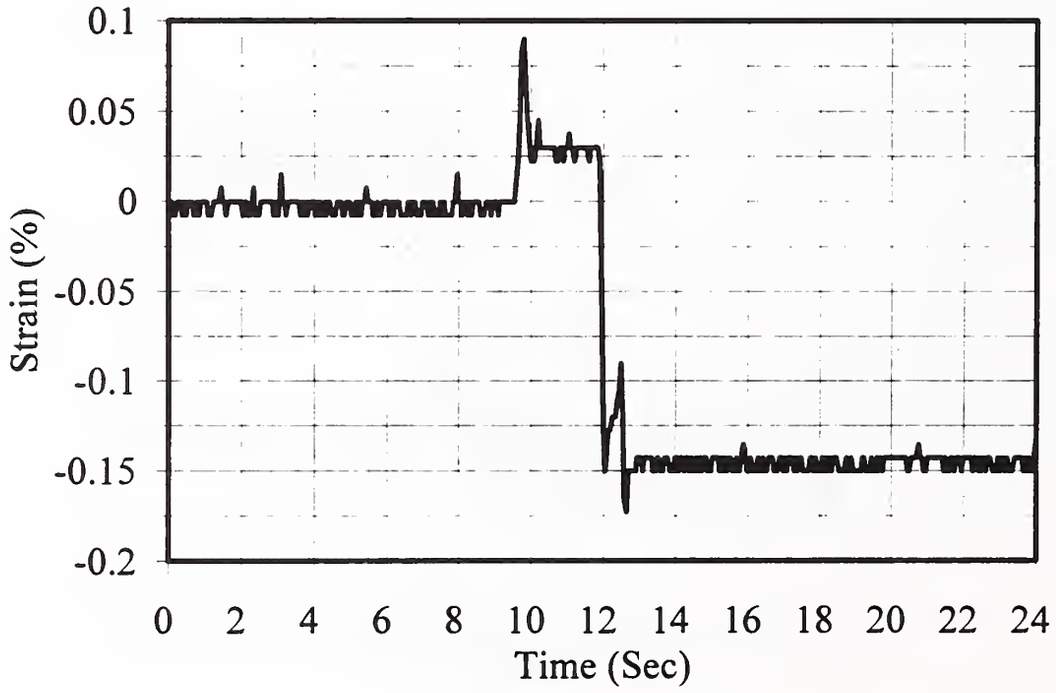

Figure C2.48: LVDT Embedment Displacement Gage #26 in Base of Non-Reinforced Section (on wheel path): Truck Pass Test 4

APPENDIX C3
DYNAMIC ROAD RATER DATA

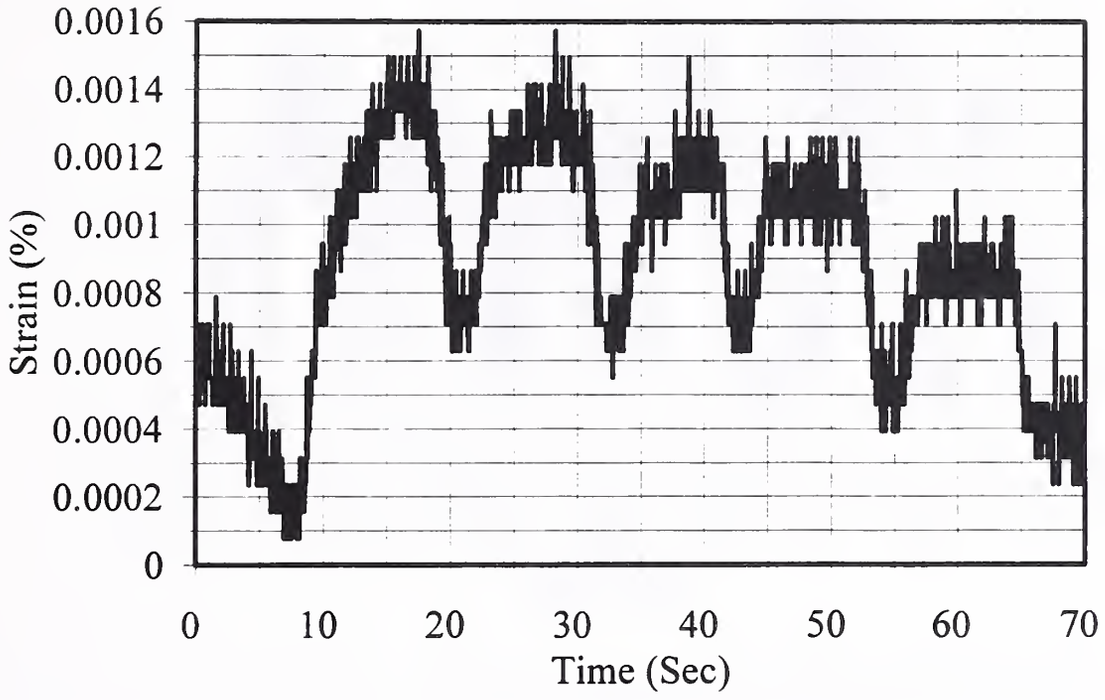

Figure C3.1: Foil Strain Gage #34 on Geogrid, July 31st Test

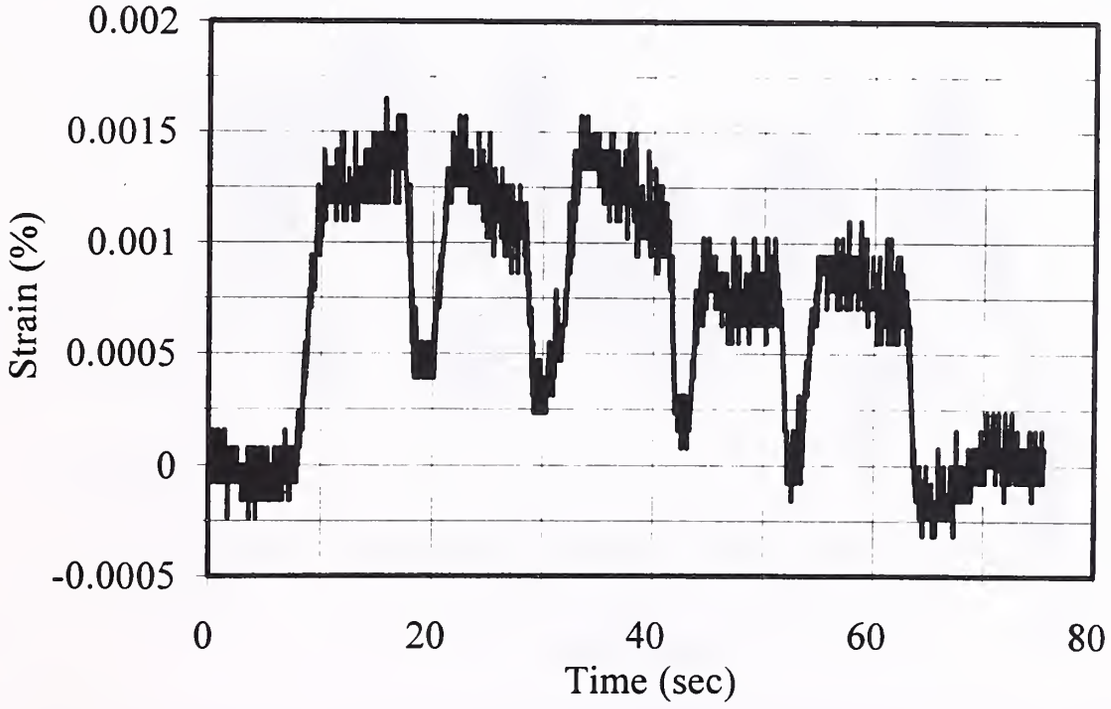

Figure C3.2: Foil Strain Gage #35 on Geogrid, July 31st Test

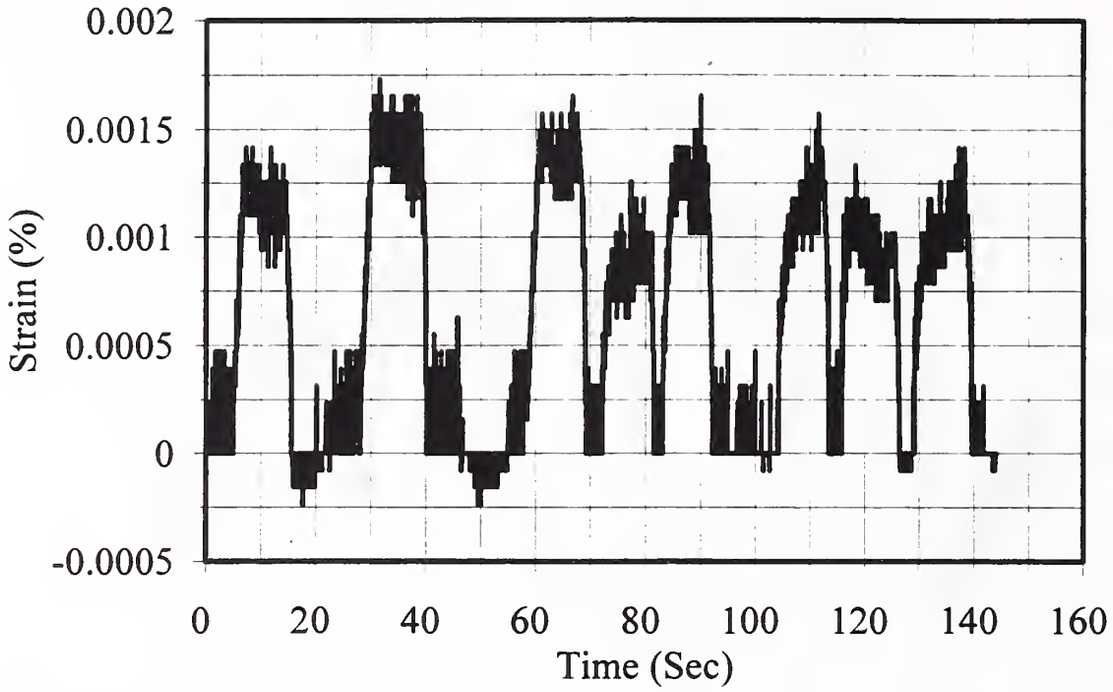

Figure C3.3: Foil Strain Gage #36 on Geogrid, July 31st Test

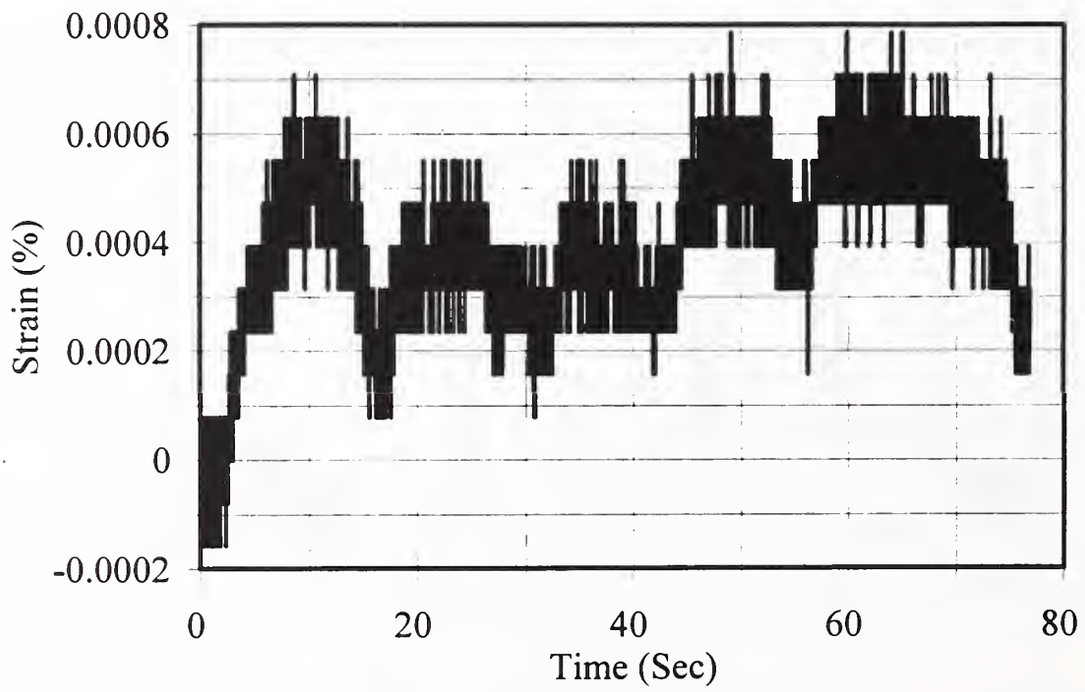

Figure C3.4: Foil Strain Gage #34 on Geogrid, September 21st Test

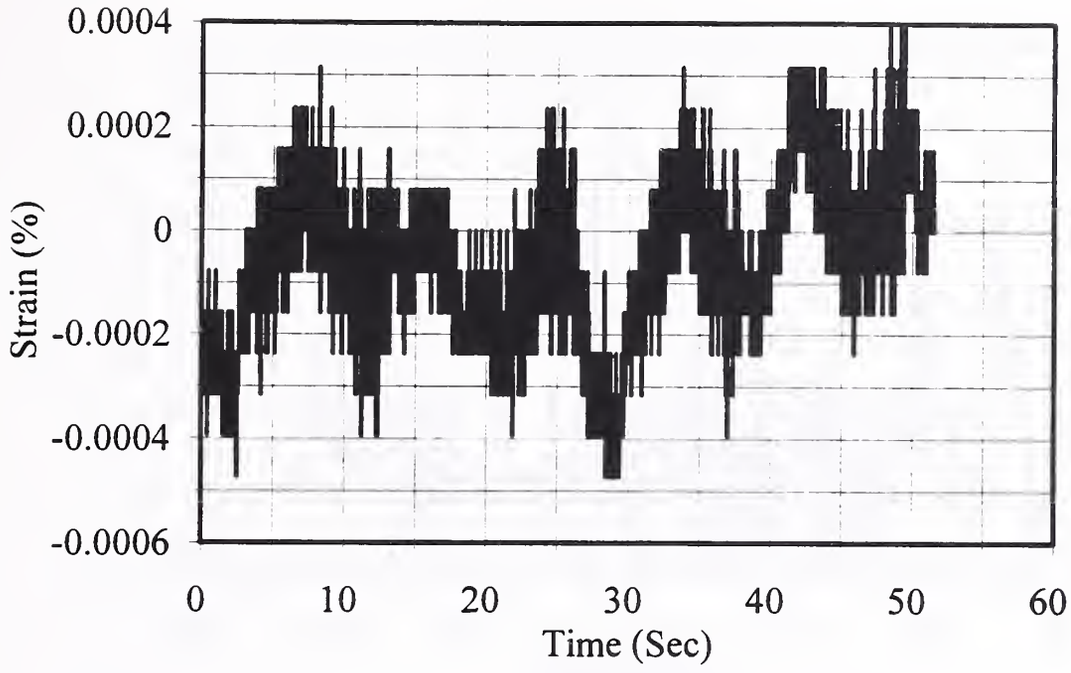

Figure C3.5: Foil Strain Gage #35 on Geogrid, September 21st Test

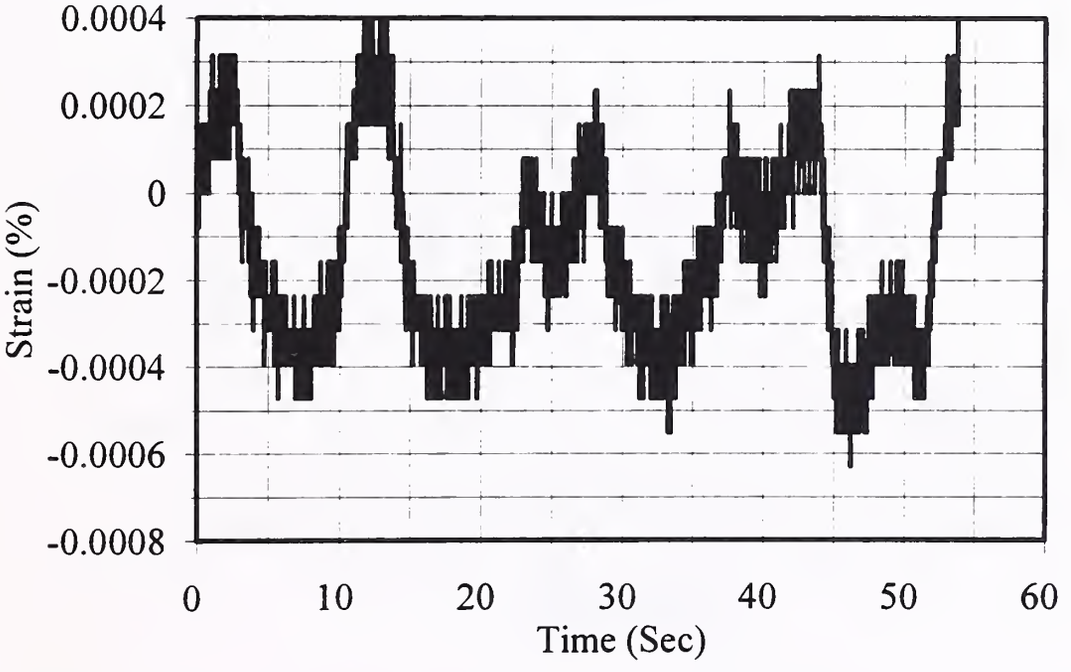

Figure C3.6: Foil Strain Gage #36 on Geogrid, September 21st Test

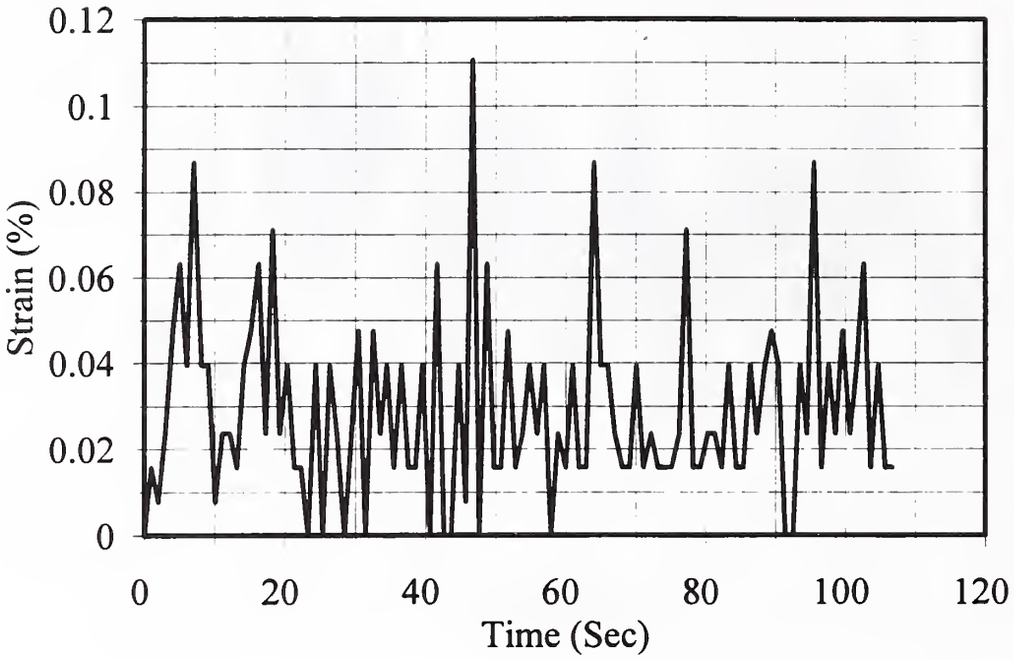

Figure C3.7: VW Displacement Gage #2 on Geogrid, September 21st Test

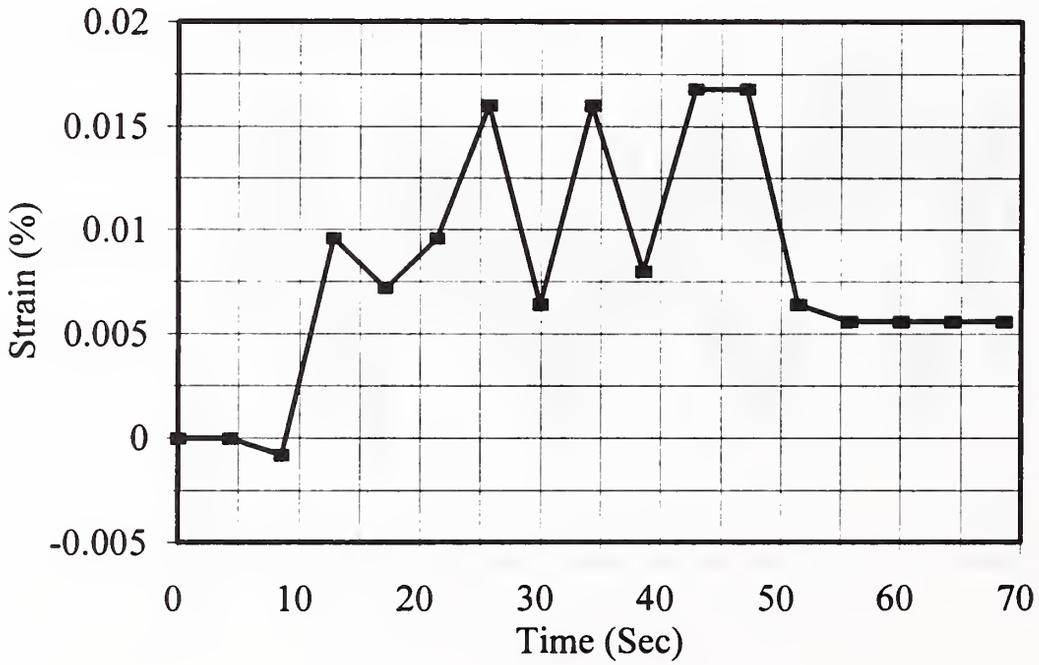

Figure C3.8: VW Strain Gage #5 on Geotextile, September 21st Test

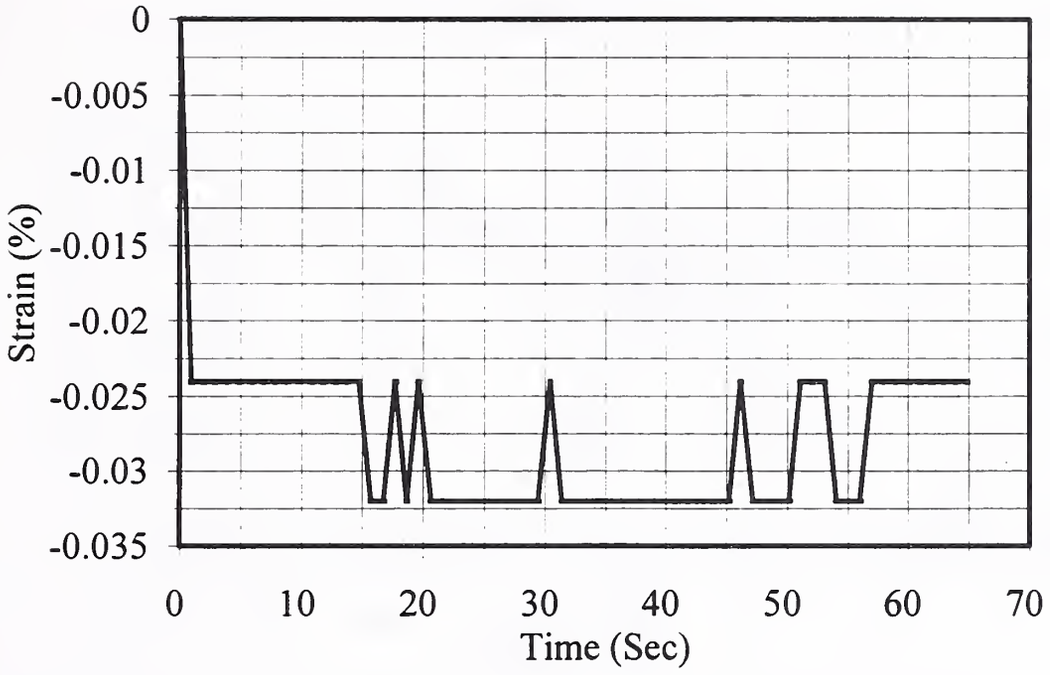

Figure C3.9: VW Embedment Displacement Gage #3 in Base Above Geogrid, September 21st Test

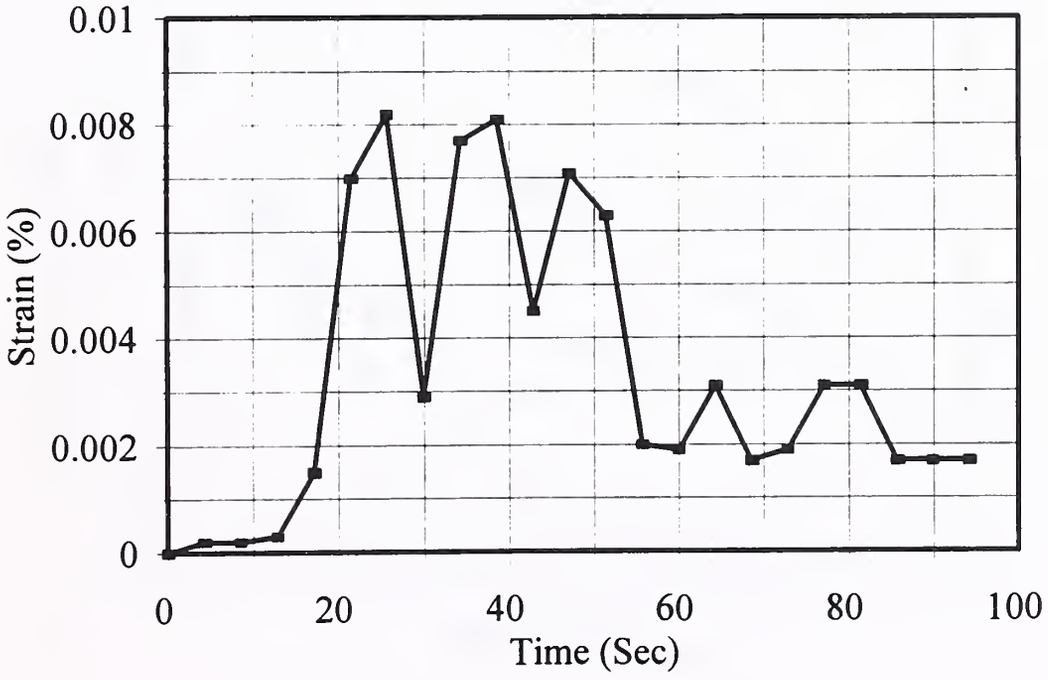

Figure C3.10: VW Embedment Strain Gage #7 in Base Above Geotextile, September 21st Test

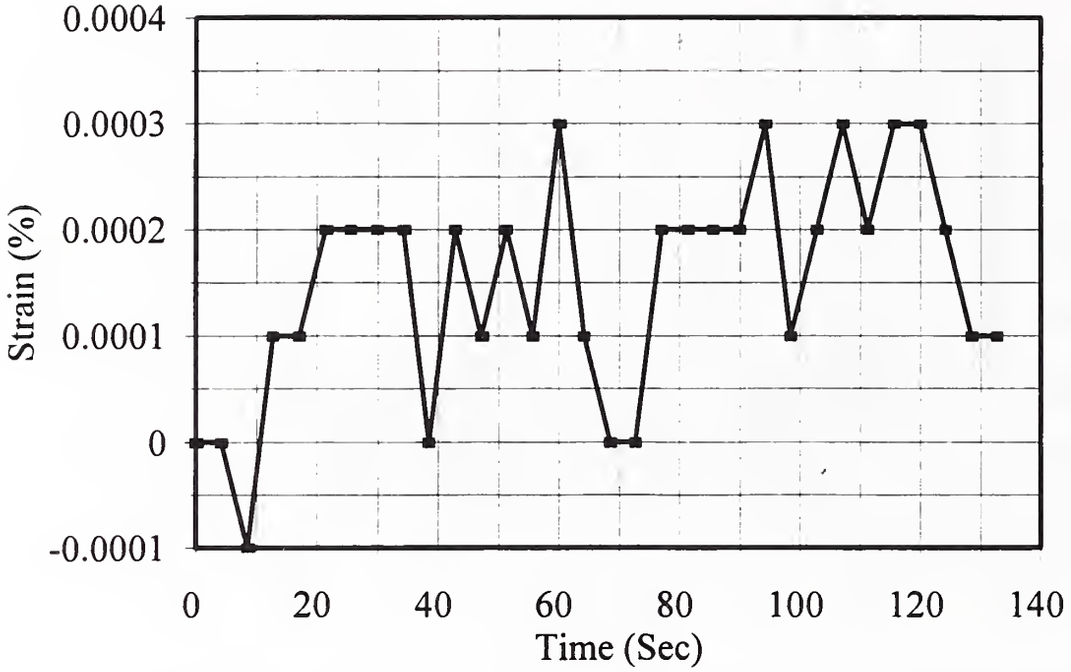

Figure C3.11: VW Embedment Strain Gage #9 in AC Above Geotextile, September 21st Test

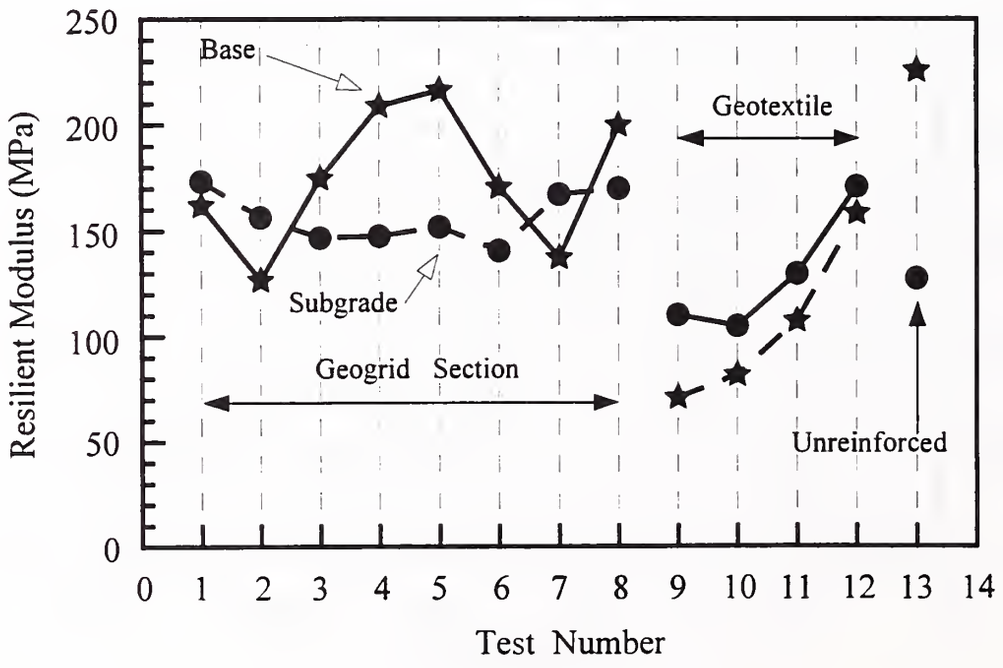

Figure C3.12: Resilient Modulus Values From July 21 Road Rater Test

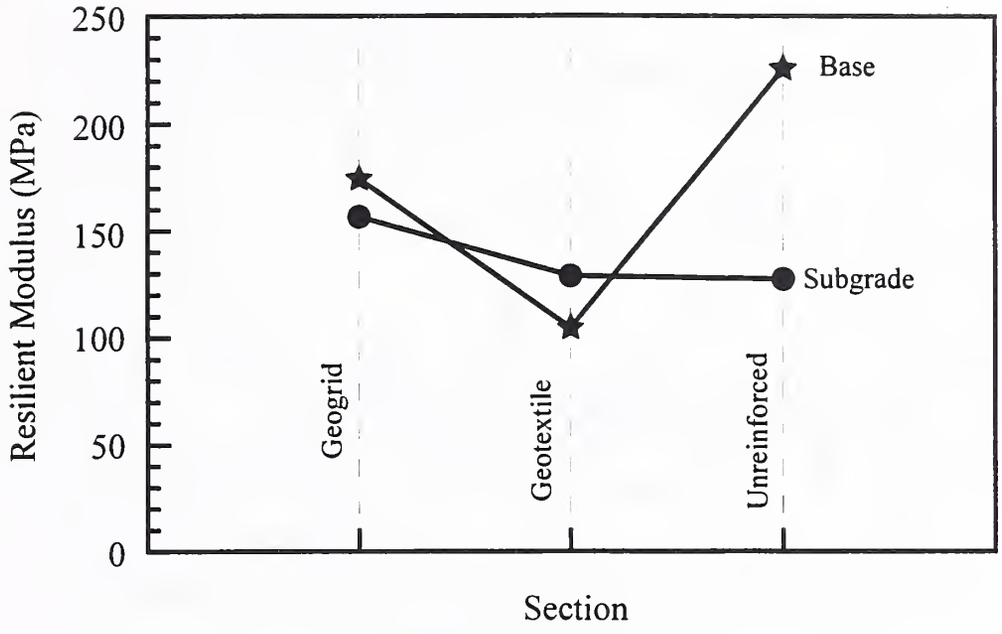

Figure C3.13: Average Resilient Modulus Values From July 21 Road Rater Test

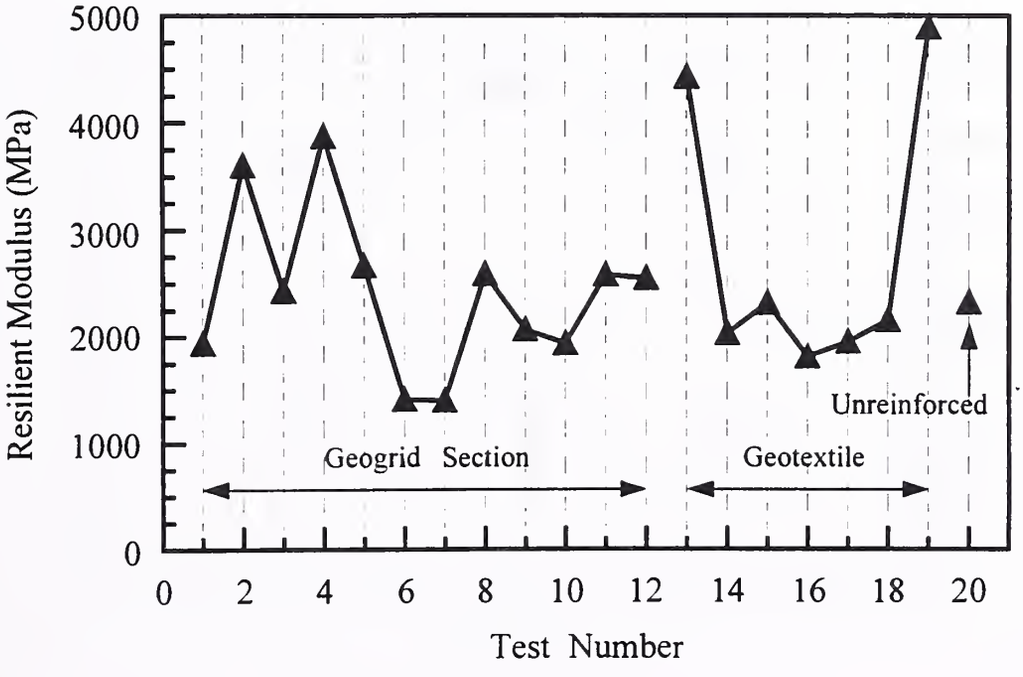

Figure C3.14: Resilient Modulus of AC Layer From September 21 Road Rater Test

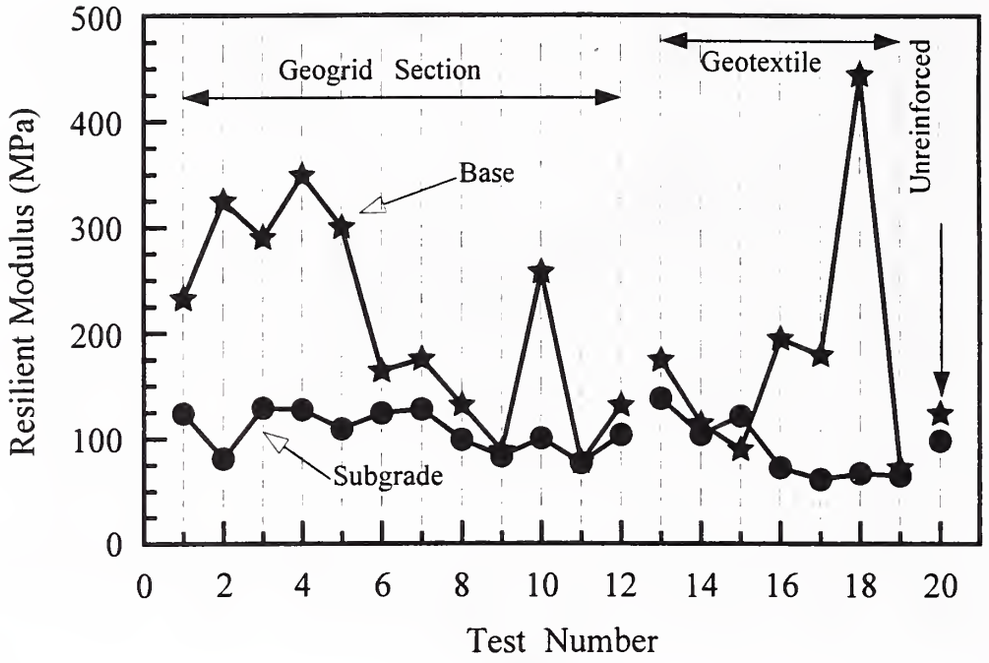

Figure C3.15: Resilient Modulus of Base and Subgrade Layers From September 21 Road Rater Test

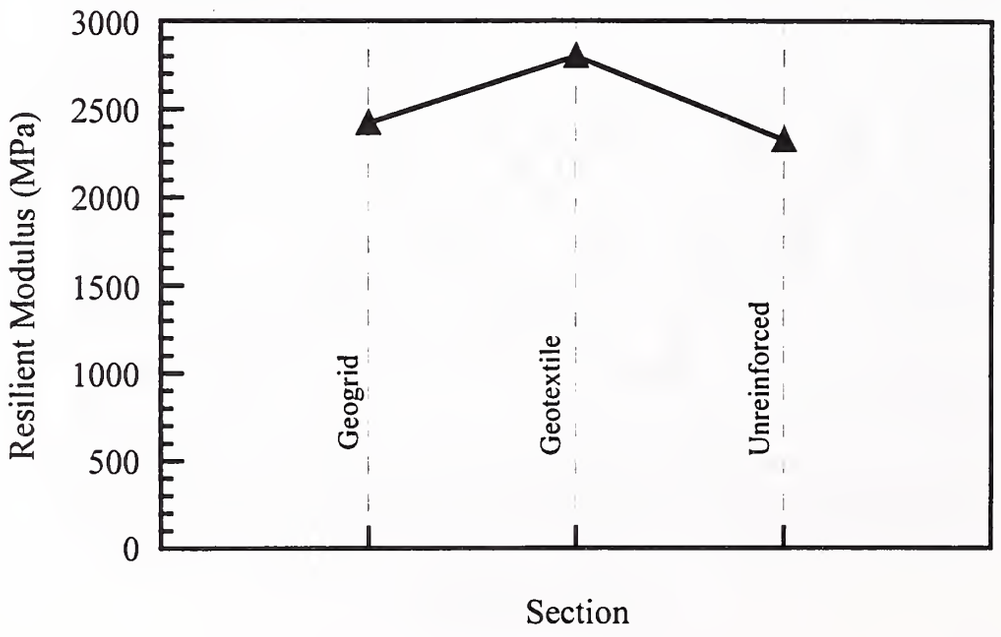

Figure C3.16: Average Resilient Modulus of AC Layer From September 21 Road Rater Test

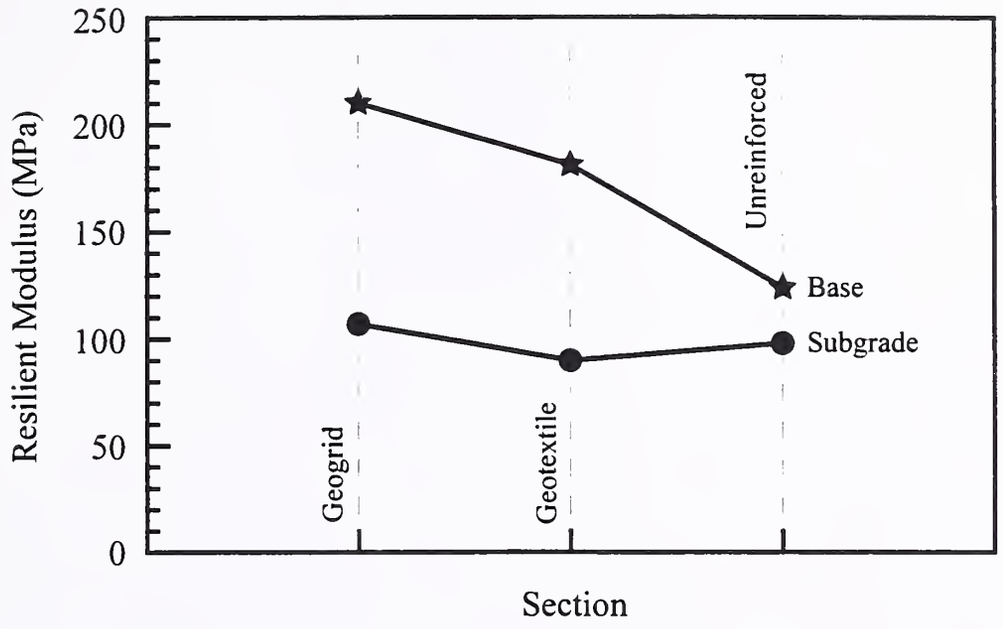

Figure C3.17:Average Resilient Modulus of Base and Subgrade Layers From September 21 Road Rater Test